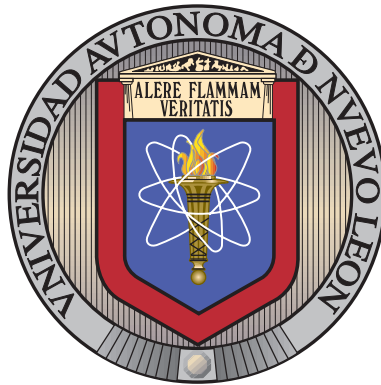


UNIVERSIDAD AUTÓNOMA DE NUEVO LEÓN

FACULTAD DE INGENIERÍA MECÁNICA Y ELÉCTRICA

SUBDIRECCIÓN DE ESTUDIOS DE POSGRADO



CONTROL STRATEGIES FOR PERMANENT
MAGNET SYNCHRONOUS MACHINES WITHOUT
MECHANICAL SENSORS BY SLIDING MODES

POR

CARLOS ENRIQUE ALVARO MENDOZA

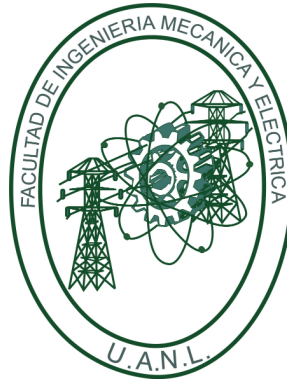
COMO REQUISITO PARCIAL PARA OBTENER EL GRADO DE
DOCTORADO EN INGENIERÍA ELÉCTRICA

FEBRERO 2023

UNIVERSIDAD AUTÓNOMA DE NUEVO LEÓN

FACULTAD DE INGENIERÍA MECÁNICA Y ELÉCTRICA

SUBDIRECCIÓN DE ESTUDIOS DE POSGRADO



CONTROL STRATEGIES FOR PERMANENT
MAGNET SYNCHRONOUS MACHINES WITHOUT
MECHANICAL SENSORS BY SLIDING MODES

POR

CARLOS ENRIQUE ALVARO MENDOZA

COMO REQUISITO PARCIAL PARA OBTENER EL GRADO DE
DOCTORADO EN INGENIERÍA ELÉCTRICA

FEBRERO 2023

UNIVERSIDAD AUTÓNOMA DE NUEVO LEÓN
Facultad de Ingeniería Mecánica y Eléctrica
Posgrado

Los miembros del Comité de Evaluación de Tesis recomendamos que la Tesis "Control strategies for permanent magnet synchronous machines without mechanical sensors by sliding modes", realizada por el estudiante Carlos Enrique Alvaro Mendoza, con número de matrícula 1887242, sea aceptada para su defensa como requisito parcial para obtener el grado de Doctorado en Ingeniería Eléctrica..

El Comité de Evaluación de Tesis

Dr. Jesús De León Morales
Director

Dr. Alberto Cavazos González
Revisor


Dr. Marco Tulio Mata Jiménez
Revisor

Dr. Fernando Salinas Salinas
Revisor

Dr. Herman Castañeda Cuevas
Revisor

Dra. Dulce Citlalli Martínez Peón
Revisor

Vo.Bo.


Dr. Simon Martínez Martínez
Subdirector de Estudios de Posgrado



Institución 190001

Programa 514601

Acta Núm. 316

Ciudad Universitaria, a 16 de enero de 2023.

Acknowledgement

I want to thank my family for all the support they have given me during my studies, in the same way I want to thank Claudia Luna in a very special way, who has been with me unconditionally throughout the process.

I respectfully thank Professor Jesús de León Morales for providing me with the necessary guidance, training, and support during my master's and doctoral studies.

Also, I want to thank Professor Mohamed Hamida and Professor Malek Ghanes for thesis supervision and support during my stay in France.

I also want to thank the reviewers Professors: Dulce Maria, Herman Castañeda, Marco Tulio, Miguel Escalante, Alberto Cavazos and Fernando Salinas for their comments and the time spent reviewing my thesis.

And last and most importantly, I want to thank Universidad Autonoma De Nuevo Leon and CONACYT for the financial support, which facilitated my doctoral studies as well as the stay in France during my thesis.

ABSTRACT

Publicación No. _____

Carlos Enrique Alvaro Mendoza, Doctorado en Ingeniería Eléctrica
Universidad Autónoma de Nuevo León, 2023

Advisor professor: Dr. Jesús De León Morales

This thesis proposes two adaptive sensorless controls based on sliding mode approach for interior permanent magnet synchronous motor (IPMSM). The proposed strategies are composed of an Adaptive High-Order Sliding Mode Observer (AHOSMO) in closed-loop with an Adaptive Super-Twisting Control (ASTWC), where the control and observer gains of the proposed strategy are reparameterized in terms of a single parameter. Then, the main advantage of this strategy is the adaptive laws are easy to implement, avoiding overestimates of gains that increases chattering, reducing the time to tune the gains, and reducing the damage of the actuators. Furthermore, a strategy for angular position estimation error extraction is proposed, without high frequency signal injection. Then, from this information and using a parameter-free virtual system, AHOSMO is designed for estimating the angular position and speed in a wide speed range, where the estimated variables provided by this observer are obtained with greater precision, despite the variations of the parameters, achieving greater robustness. These estimated states are used in the proposed robust control to track a desired reference of speed and direct-axis current. A stability analysis of the closed-loop system is presented, using a Lyapunov approach. In addition, the proposed strategy is validated through an experimental and simulation setup in order to show its effectiveness.

Table of contents

Abstract	v
List of Figures	ix
List of Tables	xiii
Nomenclature	xiii
Introduction	1
State of the art	1
Model-based method for the sensorless control	3
Saliency-based method for the sensorless control	6
Control techniques for speed regulation	7
Problem statement	8
Contributions in this work	10
Thesis organization	10
Publications	12
1 Dynamical model of interior permanent magnet synchronous machine	14
1.1 Permanent magnet synchronous motor	14
1.2 Concordia and Park transformations	18
1.3 Electrical equations of the Permanent Magnet Synchronous Motor	20
1.3.1 Dynamical model of the Interior Permanent Magnet Synchronous Motor in dq synchronous reference frame	22

1.3.2	Dynamical model of the Interior Permanent Magnet Synchronous Motor in $\alpha\beta$ stationary reference frame	26
1.4	Parameter free virtual system	27
1.5	Benchmark	29
1.5.1	Hardware description	30
1.6	Conclusion	32
2	New strategy for the rotor position and speed estimation of Interior Permanent Magnet Synchronous Motor	33
2.1	Extraction of angular position estimation error	33
2.2	Observer design based on a sliding modes approach: Proposal 1	38
2.2.1	Adaptive observer design	39
2.2.2	Adaptive observer design for the IPMSM	45
2.2.3	Simulation results	46
2.3	Observer design based on a sliding modes approach: Proposal 2	49
2.3.1	Adaptive observer design	50
2.3.2	Adaptive observer design for the IPMSM	57
2.3.3	Simulation results	59
2.4	Comparative study	61
2.5	Proposed observer analysis	66
2.6	Conclusion	68
3	Controller design for the Interior Permanent Magnet Synchronous motor	69
3.1	Control design based on Super-Twisting approach:	
	Proposal-1	69
3.1.1	Adaptive super-twisting control design	70
3.1.2	Control design for IPMSM	77
3.1.3	Simulation results	78
3.2	Control design based on Super-Twisting approach:	
	Proposal-2	80

3.2.1	Adaptive super-twisting control design	81
3.2.2	Control design for IPMSM	88
3.2.3	Simulation results	90
3.3	Comparative study	92
3.3.1	Comparative study with constant gains	93
3.3.2	Comparative study with adaptive strategies	99
3.4	Conclusion	104
4	Sensorless control of the Interior Permanent Synchronous Motor	105
4.1	Closed-loop analysis: Scheme 1	105
4.2	Simulation and experimental results: Scheme 1	110
4.2.1	Simulation tests	111
4.2.2	Experimental test	114
4.3	Closed-loop analysis: Scheme 2	119
4.4	Simulation and experimental results: Scheme 2	125
4.4.1	Simulation test	125
4.4.2	Experimental test	128
4.5	Conclusion	133
	Conclusion	136
	Bibliography	148
A	Reparameterized gains	149
A.1	Reparameterized gains for the proposed observers	149
A.1.1	Adaptive observer: Proposal 1	150
A.1.2	Adaptive observer: Proposal 2	153
A.2	Reparameterized gains for the proposed controllers	155
A.2.1	Adaptive control: Proposal 1	156
A.2.2	Adaptive control: Proposal 2	158

List of Figures

1	Main differences between an induction motor and a PMSM	3
1.1	PMSM rotor permanent magnets layout: a) Surface permanent magnets.	16
1.2	PMSM rotor permanent magnets layout: b) Inset permanent magnets.	16
1.3	PMSM rotor permanent magnets layout: c) Flux concentrating.	17
1.4	PMSM rotor permanent magnets layout: d) Interior permanent magnets.	18
1.5	Concordia transformation	19
1.6	Park transformation	20
1.7	Load torque and speed profiles used during experimental and simulation tests . .	29
1.8	Parameter variations in simulation tests	30
1.9	Load torque and speed profiles considering a low-speed region with a very small load torque.	31
1.10	Experimental setup	31
2.1	Different scenarios to see the behavior of speed, electromagnetic torque and current- i_q	36
2.2	Scheme of the proposed AHOSMO-1.	46
2.3	Flowchart for the proposed strategy.	47
2.4	AHOSMO-1. Rotor angular position estimation and its estimation error	48
2.5	AHOSMO-1. Rotor speed estimation and speed estimation error	48
2.6	AHOSMO-1. Estimation of acceleration (a) and behaviour of the adaptive law (b)	49
2.7	Scheme of the proposed AHOSMO-2.	58
2.8	AHOSMO-2. Rotor angular position estimation and its angular error	59

2.9	AHOSMO-2. Rotor speed estimation and speed estimation error	60
2.10	AHOSMO-2. Estimation of the acceleration (a) and behaviour of the adaptive law (b)	60
2.11	Simulation test: Observer based on back-electromotive force	61
2.12	Simulation test: Observer based on mechanical system by using first-order sliding modes	62
2.13	Simulation test: Observer based on high frequency signal injection	62
2.14	Performance index for the angular position estimation error	63
2.15	Performance index for speed estimation error	63
2.16	Simulation test: Initial condition for the speed (Top) and initial condition for the angular position (Bottom)	64
2.17	AHOSMO-1. State estimation using different constant gains	65
2.18	AHOSMO-1. State estimation using adaptive gains	65
2.19	Simulation test: Convergence of proposed adaptive observer and behaviour of current i_q , applying different profiles of small load Torque and low-speed.	67
2.20	Experimental test: Convergence of proposed adaptive observer and behaviour of current i_q , applying different profiles of small load Torque and low-speed.	67
3.1	ASTWC-1. Behaviour of adaptive law for the speed and current- i_d controllers	79
3.2	ASTWC-1. Speed tracking and speed tracking error	79
3.3	ASTWC-1. Behaviour of the currents i_{dq}	80
3.4	ASTWC-2. Behaviour of adaptive law for the speed and current- i_d controllers	91
3.6	ASTWC-2. Behaviour of the currents- i_{dq}	91
3.5	ASTWC-2. Speed tracking and speed tracking error	92
3.7	Speed tracking. Comparative study among Levant strategy and proposed strategies	94
3.8	Speed tracking. Comparative study among Moreno strategy and proposed strategies	95
3.9	Currents- i_{dq} . Comparative study among Levant strategy and proposed strategies	95
3.10	Currents- i_{dq} . Comparative study among Moreno strategy and proposed strategies	96

3.11	Voltages— v_{dq} . Comparative study among Levant strategy and proposed strategies	96
3.12	Voltages— v_{dq} . Comparative study among Moreno strategy and proposed strategies	97
3.13	Performance index: Comparative study using constant gains	97
3.14	Proposal 1. Performance using different constant gain values	98
3.15	Proposal 1 (ASTWC-1). Performance using adaptive gains	99
3.16	Control performance using ASMC strategy	101
3.17	Control performance using ASTW strategy	101
3.18	Control performance using SAST strategy	102
3.19	Control performance using proposed ASTWC-1 strategy	102
3.20	Control performance using proposed ASTWC-2 strategy	103
3.21	Performance index: Comparative study using adaptive gains	103
4.1	Proposed sensorless control: Scheme-1.	111
4.2	Simulation test: Behaviour of the adaptive gains, observer and control	111
4.3	Simulation test: Speed estimation and estimation error	112
4.4	Simulation test: Angular position estimation and angular position error	113
4.5	Simulation test: Estimation of acceleration	113
4.6	Simulation test: Speed tracking and tracking error	114
4.7	Simulation test: Behaviour of the currents— i_{dq}	114
4.8	Experimental test. Adaptive laws: Control ($L_{c_{i_d}}(t)$, $L_{c_{\Omega}}(t)$) and observer ($L_o(t)$).	115
4.9	Experimental test: Speed estimation and estimation error.	116
4.10	Experimental test: Angular position estimation and estimation error.	117
4.11	Performance index for the estimation and tracking of states during experiments	118
4.12	Experimental test: Estimation of the acceleration.	118
4.13	Experimental test: Speed tracking and tracking error	119
4.14	Experimental test: Profiles of the currents— i_{dq}	120
4.15	Experimental test: Profiles of the voltages— v_{dq} with adaptive laws.	121
4.16	Proposed sensorless control: Scheme-2.	126

4.17 Simulation test: Behaviour of adaptive gains for the observer ($L_{o_2}(t)$) and controllers ($L_{\Omega_2}(t), L_{i_{d_2}}(t)$)	126
4.18 Simulation test: Speed estimation and estimation error	127
4.19 Simulation test: Angular position estimation and angular position error	127
4.20 Simulation test: Estimation of acceleration	128
4.21 Simulation test: Speed tracking and tracking error	128
4.22 Simulation test: Behaviour of the currents $-i_{dq}$	129
4.23 Experimental test: Behaviour of adaptive gains for the observer and controllers .	130
4.24 Experimental test: Speed estimation and estimation error	130
4.25 Experimental test: Angular position estimation and angular position estimation error	131
4.26 Experimental test: Estimation of acceleration	131
4.27 Experimental test: Speed tracking and tracking error	132
4.28 Experimental test: Behaviour of the currents $-i_{dq}$	132
4.29 Experimental test: Profiles of the voltages $-v_{dq}$ with adaptive laws.	133

List of Tables

1.1	IPMSM nominal parameters	29
2.1	Parameters for AHOSMO-1	47
2.2	Parameters for the AHOSMO-2	59
2.3	Value for the gains of both adaptive observers at 5 seconds	66
3.1	Parameters for the ASTWCs-1	79
3.2	Parameters for ASTWCs-2	90
3.3	Value for the gains of both adaptive controllers at 5 seconds	92
4.1	Parameters for the sensorless control-1 in simulation test.	112
4.2	Parameters for the sensorless control-1 in experimental test.	115
4.3	Parameters for the sensorless control-2 in simulation test	126
4.4	Parameters for the sensorless control-2 in experimental test	129

Nomenclature

e_{θ_e} Angular position estimation error

f_v Viscous friction coefficient

i_{abc} abc -axes stator currents

i_{dq} dq -axes stator currents

i_d^* Current $-i_d$ reference

$i_{\alpha\beta}$ $\alpha\beta$ -axes stator currents

$k_o, k_{o2}, L_o, L_{o2}, \gamma_o, \gamma_{o2}$ Constant parameters (Observer)

$k_{c_{i_d}}, k_{c_{i_{d2}}}, k_{c_{\Omega}}, k_{c_{\Omega_2}}, L_c, L_{c2}, \gamma_{c_{i_d}}, \gamma_{c_{i_{d2}}}, \gamma_{c_{\Omega}}, \gamma_{c_{\Omega_2}}, \vartheta_{1i}, \vartheta_{2i}; i = 1, 2, 3.$ Constant parameters (Controller)

p Number of poles

v_{abc} abc -axes stator voltages

v_{dq} dq -axes stator voltages

$v_{\alpha\beta}$ $\alpha\beta$ -axes stator voltages

$\omega = p\Omega$ Electrical speed

$\hat{\omega}$ Estimated electrical speed

$\begin{bmatrix} x_a & x_b & x_c \end{bmatrix}^T$ Vector: x represents voltages, currents or fluxs

$\begin{bmatrix} x_d & x_q \end{bmatrix}^T$ Vector: x represents voltages, currents or fluxs

$\begin{bmatrix} x_\alpha & x_\beta & x_0 \end{bmatrix}^T$ Vector: x represents voltages, currents or fluxs

AC Alternative Current

AHOSMO Adaptive High-Order Sliding Mode Observer

ASTWC Adaptive Super-Twisting Control

DC	Direct Current
EKF	Extended Kalman Filter
EMF	Electromotive Force
HF	High Frequency
IGBT	Insulates Gate Bipolar Transistor
IPMSM	Interior Permanent Magnet Synchronous Motor
J	Inertia
Kw	Kilowatt
LTI	Linear Time Invariant
L_d, L_q	dq -axes winding inductance
L_{so}, L_{sv}	Own inductances
$L_o(t), L_{o_2}(t)$	Adaptive parameters (Observer)
$L_c(t), L_{c_2}(t), L_{c_\Omega}(t), L_{c_{\Omega_2}}(t), L_{c_{i_d}}(t), L_{c_{i_{d_2}}}(t)$	Adaptive parameters (Controller)
M_{so}	Mutual inductances
R_s	Stator resistance
PMSM	Permanent Magnet Synchronous Motor
PWM	Pulse width modulated
\mathbb{Q}^T	Matrix for simplified Concordia transformation
\mathbb{Q}_o^T	Matrix for Concordia transformation
T_e	Electromagnetic torque
T_l	Load Torque
\mathbb{T}^T	Matrix for Park transformation
$\hat{\alpha}$	Estimated acceleration
ψ_{abc}	abc -axes stator fluxes
ψ_r	Permanent-magnet flux linkage
θ	Mechanical angular position
$\hat{\theta}$	Estimated angular position
$\theta_e = p\theta$	Electrical angular position
Ω	Mechanical speed

$\hat{\Omega}$	Estimated mechanical speed
Ω^*	Speed reference

Introduction

In this section there is a brief introduction to electrical machines according to their use. In the same way, a brief introduction of synchronous and asynchronous motors, their advantages and disadvantages is made. Also, considering that the speed of the motors can be controlled, the following are the different types of methods used to control them. Finally, the approach to the problem of this thesis is presented, as well as the objectives and hypotheses.

State of the art

Electrical machines are designed to transform electrical energy into mechanical energy, mechanical energy into electrical energy or modify the level of the same electrical energy according to the required use, so that electrical machines can be classified into three groups: Generators, transformers and motors. Generators transform mechanical energy into electrical energy. Transformers use electrical energy and have the ability to change the dimension of this energy and motors are used to transform electrical energy into mechanical energy, in such a way that, since the electrical machine was invented, they have been used in domestic products, industrial process, electricity production, robotics, electric vehicles, etc.

Regarding to the motors, these can be mainly classified into two groups: Direct Current (DC) motors and Alternating Current (AC) motors. DC motors have been traditionally used for decades in different applications. However, their commutators, brushes, and required maintenance are the main disadvantages. On the other hand, AC motors can be classified into two groups: Asynchronous or induction motors and synchronous motors. The main difference between these machines is that the rotor speed of the synchronous motor has the same fre-

quency as the magnetic field, unlike induction motors, where the rotor speed is slower than the magnetic field generated in the stator, *i.e.*, the speed is asynchronous. The predominant motor technology for many years has been cage induction motors. Their superior dynamic behavior coupled with their brushless nature, which allows operation without the presence of commutators or slip rings, makes them suitable for high performance controlled operation in electric drive applications. Advances in the area of power electronics and automatic control technologies have contributed significantly to their establishment as standard motors in electric drives. However, induction motor technology also has numerous disadvantages, both in construction and in operation. For example, its relatively small air gap length and its inferiority to synchronous motors in terms of overall efficiency and power factor are the main drawbacks. Also, induction motors have windings on the rotor, which increases the temperature of the machine. Nevertheless, a clear indication towards the possible limitation in the use of induction motors and their eventual replacement has not yet been established [1].

Consequently, permanent magnet synchronous motors (PMSM) have attracted increasing interest within the scientific community, especially for high power density applications, highlighting the need for their investigation. The most important advantages of permanent magnet synchronous motor lie in the fact that permanent magnets constitute a strong and independent excitation system, *i.e.*, field current needed for induction machine is not necessary (see Figure x), and secondary copper loss does not occur, therefore high efficiency can be achieved [2]. This feature allows substantial overloading of the motor while providing higher torque density values. The fact that no electromagnetic drive system is employed further improves its transient behaviour, while small size and maintenance are also two significant benefit factors. The above advantages have led PMSM to be considered a viable and attractive solution for control drives [3, 4].

Interior permanent magnet synchronous motor (IPMSM) is the most popular in the fields of electric drive application due to torque capability, power density, simple structure, efficiency and can operate in high speeds [5]. In variable speed motor drives, conventionally, it is necessary to use an encoder [6] to measure angular position and apply speed controllers [7–10]. However, implementing encoders to control the electric motor requires additional electronics,

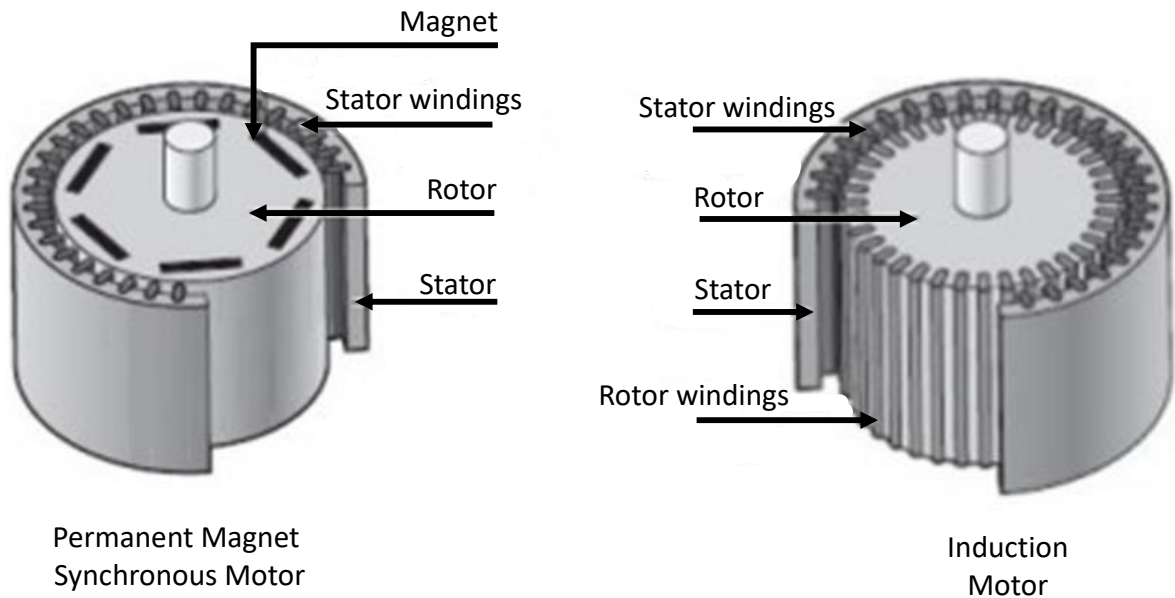


Figure 1: Main differences between an induction motor and a PMSM

preventative maintenance, and additional wiring. For these reasons, this technique has become less attractive due to high cost and lower reliability, encouraging researchers to avoid its implementation and study the sensorless strategy. Nowadays, sensorless strategy is an indirect technique under development to estimate angular position from measurable currents and voltages of the IPMSM, increasing robustness and reliability, eliminating wiring, and reducing signal noise [11–13]. In the literature, various approaches to the sensorless technique have been addressed. Among sensorless control methods, model-based method and saliency-based method are the most popular.

Model-based method for sensorless control

According to model-based method, this method is applied in high and medium speed regions; and rotor position is acquired from the stator voltages and currents without requiring additional high frequency signal injection. Back-electromotive force (EMF)-based technique [14–17] is commonly applied in this method. Considering that back-EMF induced in motor is directly

proportional to rotor speed, with this information is possible effectively estimate the rotor position [18]. Several observers based on the dynamical model of the electrical motor have been used for estimating angular position, for example, Luenberger observer [19,20], extended Kalman filter (EKF) [21,22] and sliding mode observer [23,24]. However, being that the model-based approach has a direct dependency on the dynamical model, parametric uncertainties can lead to performance degradation of control systems. It is known that parameters vary depending on operation conditions, e.g., mechanical parameters, viscous coefficient and inertia, could vary according to the applied load torque, weight, road type and tires quality in automotive applications; and electrical parameters, inductance and resistance, could vary depending on the temperature variations or magnetic circuit saturation.

An alternative to overcome this challenge is the development of algorithms for online or offline parameter identification. Among offline algorithms for parameter estimation can be found the DC Current Decay Test [25,26] and the AC standstill method [27,28] to measure inductances. However, there are disadvantages with these strategies due to the fact that it requires additional equipment and the measurement errors are caused by the estimation at a single operating point. Now, among online parameter estimation techniques, recursive least square is a technique that uses known variables as currents and voltages to estimate unknown parameters, for instance, in [29] has been proposed a strategy to identify stator resistance, machine torque and inductances. Similarly, EKF is an optimal recursive estimator that considers the effects of the measurement noise, for instance, in [30] has been proposed a permanent magnet flux identification technique of the IPMSM. Other methods for online parameter estimation are given in [31–33] in order to constantly update the machine parameters. However, a highly efficient microprocessor is required to handle the relatively complex procedure.

Another alternative to overcome the challenge of parametric uncertainties is the use of robust techniques. A technique that has been widely studied in recent decades is sliding modes proposed by [34]. Its main advantage is its robustness against disturbances and parametric uncertainties. This technique has found wide application in different areas such as fault reconstruction, condition monitoring and fault detection [35]. Classical sliding mode technique has been adopted in electrical machines for the angular position estimation, for instance [36].

However, the main drawback of this strategy is the chattering caused by the switching (discontinuity) of the signum function, generating high-frequency oscillation components in the estimated signal of the sliding mode observer (SMO). Then, low-pass filters are often used, causing phase delay, such that classical sliding mode is not a good alternative. One option to reduce the chattering phenomenon is to replace the signum function by a sigmoid function [37,38], showing relatively a good performance. Similarly, the popular super twisting [39] and high-order sliding mode techniques [40] have achieved a clear improvement in the chattering reduction as well as good performance and finite-time convergence in presence of disturbances and uncertainties. In [41], a high order terminal SMO is proposed in order to achieve finite time convergence of the estimated states and chattering suppression. In [42], a third order super-twisting extended state observer is designed to improve the estimation of angular position, speed and disturbance of IPMSM; achieving a fast convergence. On the other side, in [14], a super-twisting sliding-mode observer with online stator resistance, position and speed estimation for sensorless control is proposed. However, during observer tuning, choosing constant gains in the observer sometimes results in an overestimation of gains that causes chattering, increasing the error in the estimates. Adaptive observers have been proposed in order to avoid this overestimation and reduce the chattering. For instance, in [43] is addressed an adaptive super twisting for online tuning according to the perturbation value, such that, angular position error is reduced in a wide-speed range. In [44], an adaptive super-twisting sliding mode observer with time-varying gains is introduced, to minimize the chattering and estimate back-EMF that is required for the angular position estimation. Another strategies are addressed in [45,46]. However, these approaches need to choose several parameters to tune the system, increasing the tuning time.

In summary, the main drawback of the model-based methods is the loss of observability at low speeds due to the fact that there is a direct dependency of the back-EMF with speed rotor, *i.e.*, the magnitude of the back-EMF decreases proportionally with the speed.

Saliency-based method for sensorless control

As previously mentioned, model-based angular position estimation is possible at high and medium speed. However, it can fail at low and zero speed. Therefore, saliency-based methods are an alternative to achieve this challenge. In saliency-based methods a sufficient excitation, either by high frequency (HF) voltage or current signal injection or by using pulsewidth-modulated (PWM) inverter switching, is mandatory in order to maintain a persistent excitation in the system to extract angular position information and estimate the angular position at low and zero speed [47–50].

Voltage injection techniques can be classified according to the shape of the test signal: sine or square wave injection techniques. In addition, one can distinguish between rotating and pulsing test signal injection. For the HF rotary signal injection scheme, a balanced voltage signal is injected into the stationary reference frame to form a rotary excitation that is superimposed on the fundamental excitation. Then, by applying a synchronous reference frame filter, the negative sequence carrier current containing the position information can be derived and used to estimate the rotor position. For pulsed signal injection methods, a pulsed HF carrier signal is injected on the d-axis or q-axis in the estimated synchronous reference frame, such that, the angular position can be estimated by minimizing the amplitude modulated carrier current response that is measured along the orthogonal axis to the injection axis [51–55]. However, the performance of sensorless control with the conventional HF pulsed or rotating sinusoidal signal is still insufficient for some applications, as the filtering process limits the dynamic bandwidths.

To overcome the limitations of sensorless control with conventional sinusoidal signal injection, square wave injection in the stationary reference frame or in the estimated rotor reference frame has been developed. The injection frequency can be increased to the PWM switching frequency, and thus the filtering process can be eliminated and the dynamic performance can be improved [56–61].

Nevertheless, in saliency-based methods, additional losses and audible noise are negative effects caused by injected signal reducing the system performance. Reducing the amplitude of the signal could be an option to remove the disadvantages. However, this would cause a

degradation in the estimation of the angular position. Moreover, this technique can present magnetic saturation at high speed, such that its use is still limited.

Control techniques for speed regulation

Now, regarding speed controls used in electrical machines, several nonlinear control methods have been applied to enhance the control performance in presence of uncertainties and disturbances, for instance, in [45,62] were proposed robust backstepping controllers with integral and sliding mode actions to achieve speed regulation despite uncertainties and disturbances. A robust control has been proposed in [63], and sliding mode controls in [64–66].

As previously mentioned, sliding mode technique is one of the most studied techniques in recent years due to robustness against disturbances and uncertainties. Nevertheless, just like observers, controllers based on sliding mode have chattering problems and overestimation of gains. Therefore, adaptive laws for sliding mode controllers of the motor have been proposed to remove these drawbacks [67–69]. Some adaptive laws have also been proposed in a general way for the sliding mode control. For instance in [70], an adaptive super-twisting control is proposed, removing the requirement to know the upper bounds of external disturbance and reducing the chattering phenomenon without affecting the control performance. In [71], the chattering problem and its relation with the high activity of control action have been studied. In this way, an adaptive law is developed to get a minimum possible value of control. Another proposal was introduced in [72], offering continuous control signal, adaptation for dealing with unknown uncertainty/perturbations, non-overestimation of control gains, and reduced chattering. In [73], adaptive gains have been proposed for a super-twisting control in order to adapt in such a way that the gains are as small as possible, and yet large enough to sustain a sliding motion. Nonetheless, due to large number of control gain parameters, tuning these strategies could be complex.

Problem statement

In industrial applications, the control of IPMSM requires the knowledge of the angular position and speed, which usually is measured by using sensors (encoders). However, as mentioned, this conventional method has some disadvantages. Then, one solution is to estimate angular position and speed by using observers based on model. Frequently, the mathematical model used for control and observer design is given in dq synchronous reference frame [45, 74] or in a $\alpha\beta$ stationary reference frame [75, 76]. However, parametric uncertainties and external disturbances affect the estimation. Then, one solution to overcome this drawback would be to design a robust observer to estimate the angular position and speed of the IPMSM, such that the information from the estimated states can be used in the controller with more precision.

On the other hand, as mentioned in the theoretical framework, the design of observation and control strategies requires the use of robust techniques in presence of parametric uncertainties and disturbance. Frequently, the sliding modes approach is the most used technique, since it satisfies the robustness requirement. However, the design of observation and control strategies based on sliding mode requires the adjustment of several gains, which results in a greater tuning effort, and sometimes an overestimation of the gains is obtained, causing chattering in the system. Therefore, it is necessary to reduce the adjustment time, minimizing the number of parameters to be adjusted.

In order to overcome these problems, this thesis proposes the following:

Hypothesis:

From measurable currents i_α and i_β , which can be obtained from the abc triphasic components of the IPMSM, an extraction of the angular position estimation error ($\theta_e - \hat{\theta}_e = e_{\theta_e}$) can be carried out without high-frequency signal injection, defining θ_e as electrical angular position and $\hat{\theta}_e$ as estimated electrical angular position. The information of e_{θ_e} can be used by an observer based on a parameter free virtual system to estimate the angular position and speed of the IPMSM and overcome the issues caused by the parametric uncertainties present in the model of the IPMSM. The estimates can be interconnected with a controller to track desired references of speed and current. Then, considering the robustness of the sliding mode approach

under parametric uncertainties and disturbances, and its finite time convergence, the sliding mode technique can be used in the observer and control design of the IPMSM. Moreover, based on reparameterization properties, it is possible to design a controller and an observer for the IPMSM, such that the gains are reparameterized in terms of a single parameter, reducing the tuning time. This facilitates the design of adaptive laws for the observer and control, avoiding overestimations of gains that can cause an increase of chattering and damage the system.

The main objectives in this work are:

- **General objective:** Sensorless control design and development for the IPMSM based on adaptive sliding mode approach with a reduced number of tuning parameters such that speed and direct axis current $-i_d$ track desired references in presence of perturbations and parametric uncertainties, assuming that currents and voltages are the only information available of the IPMSM.
- **Observation objective:** Extract the angular error

$$\theta_e - \hat{\theta}_e = e_{\theta_e} \quad (0.0.1)$$

and design an adaptive observer with a reduced number of tuning parameters for estimating rotor position and speed by using the currents $i_{\alpha\beta}$ and a dynamical model without the machine parameters. After this, carry out a verification in simulations to analyze its performance. Finally, validate it experimentally.

- **Control objective:** Design and development of an adaptive control with a reduced number of tuning parameters to track a desired speed reference Ω^* and a reference current i_d^* of a IPMSM in presence of parametric uncertainties and bounded disturbances with unknown boundaries. After this, the adaptive control design must be verified by simulations in order to analyze its performance. Finally, validate the technique experimentally.
- **Sensorless control objective:** Interconnect the designed controller and observer to control the IPMSM without mechanical sensor. This will be verified in simulations and validated experimentally.

Assumptions:

- The initial position of the rotor is considered to be known. A result proposed in the literature is considered for the estimation of the initial condition.
- The currents $i_{\alpha,\beta}$ are available by measurement.

Contributions in this work

In this work, the main contributions are the following:

- An extraction of the angular error e_{θ_e} is made, and based on a virtual system without parameters of the IPMSM, two Adaptive High-Order Sliding Mode Observers (AHOSMOs) are designed to estimate angular position, speed and acceleration over a wide speed range. The robustness is improved, overcoming the disadvantages of other methods (model-based and saliency-based methods) that require knowledge of the machine parameters, use of filters as well as high-frequency signal injection to estimate angular position.
- Two Adaptive Super-Twisting Controllers (ASTWCs) are designed in order to track a desired speed reference and a desired d-axis current reference. These controller are interconnected with the AHOSMO achieving a sensorless control strategy.
- The gains for both, controllers and observers, are reparameterized in terms of a single parameter. The main advantage of this strategy is that adaptive laws are easy to implement, which avoids overestimation of gains that increases chattering, reduces time to adjust gains, and reduces damage to actuators.
- Closed-loop stability analysis under the action of the observer is improved thanks to it is simpler to analyse and the separation principle holds.

Thesis organization

This manuscript is organized as follows:

Chapter 1

In chapter 1, an introduction to the PMSM is given. The different configurations for PMSM according to permanent magnet position is addressed. After that, the Park and Concordia transformation are introduced. From these transformation, the electrical equations of the PMSM can be used to compute the dynamical model of the IPMSM in a $\alpha\beta$ stationary reference frame and in a dq synchronous reference frame. Moreover, the parameter free virtual system is presented. The benchmark for the observers and the controllers is addressed, this benchmark will be used in simulation and experimentation. In addition, a specific benchmark is presented and will be used to show the performance of the observer in different operation point.

Chapter 2

In chapter 2, a method for the extraction of the angular position estimation error is introduced. This information can be extracted by using α, β currents, i.e., the dynamical model of the IPMSM is not used. Then, considering the extraction of the angular error and a virtual system without parameters of the IPMSM, the design of two AHOSMO's are addressed to estimate angular position, speed and acceleration. The gains of the observers have been reparameterized in terms of a single parameter facilitating the design of an adaptive law for each observer. Simulation tests of the proposed observers and a comparative study are carried out.

Chapter 3

In the chapter 3, the design of two Adaptive Super-Twisting Controllers is introduced. These controllers have been designed considering reparameterized gains in terms of a single parameter. It has allowed to design an adaptive law for each control, which reduces time to adjust gains and avoids overestimation of gains that can increase chattering. Moreover, a stability analysis based on Lyapunov approach is given. After that, the proposed controllers are evaluated under simulation tests. In addition, a comparative study is carried out considering constant gains and adaptive gains.

Chapter 4

From the angular position estimation error extraction, the proposed observers in chapter 2 are able to estimate the angular position and speed. These estimates will be interconnected with the proposed controllers presented in chapter 3. Therefore, in chapter 4 is presented

the sensorless control scheme. The stability analysis in closed-loop under the estimates of the observer is introduced. Finally, simulation and experimental tests are carried out in order to show the performance and effectiveness of the proposed schemes.

Chapter 5

Finally, a general conclusion about the proposed work is addressed. Moreover, some perspectives for this work are introduced.

Publications

In this thesis, different publications have been accepted or submitted in indexed journals and scientific conferences.

Journal papers

- E. Alvaro-Mendoza, J. De-Leon Morales, M. A. Hamida, M. Ghanes. (2022). Angular position estimation error extraction for speed and angular position estimation of IPMSM using a parameter-free adaptive observer. *Journal of The Franklin Institute*, 359(13), 7140-7164.
- E. Alvaro-Mendoza, J. De León-Morales, O. Salas-Peña. (2021). State and parameter estimation for a class of nonlinear systems based on sliding mode approach. *ISA transactions*, 112, 99-107.
- E. Alvaro-Mendoza, O. Salas-Peña, J. De León-Morales. (2022). Sensorless control scheme based on sliding modes for interior permanent magnet synchronous motor. *Proceedings of the Institution of Mechanical Engineers, Part I: Journal of Systems and Control Engineering*, 236(2), 227-243.
- E. Alvaro-Mendoza, J. De-Leon Morales, M. A. Hamida, M. Ghanes, Adaptive sensorless control for interior permanent magnet synchronous machine based on sliding mode approach, *ISA Transactions*. (Under review: 2nd review)

Conference papers

- E. Alvaro-Mendoza, J. De León-Morales, M. A. Hamida and M. Ghanes. (2021, October). A novel approach to extract the angular position estimation error for position and speed estimation of Interior Permanent Magnet Synchronous Machine. In IECON 2021–47th Annual Conference of the IEEE Industrial Electronics Society (pp. 1-6). IEEE.
- E. Alvaro-Mendoza, J. De León-Morales, M. A. Hamida and M. Ghanes. (2022, August). Sensorless control of an interior permanent magnet synchronous motor based on an adaptive sliding mode observer using position error extraction method. In 2022 IEEE Conference on Control Technology and Applications (CCTA) (pp. 956-961). IEEE.
- E. Alvaro-Mendoza, M. A. Hamida J. De León-Morales and M. Ghanes. (2022, September). Application of a sensorless control based on sliding mode in permanent magnet synchronous machine using an angular error extraction. In 2022 16th International Workshop on Variable Structure Systems (VSS) (pp. 141-146). IEEE.

Chapter 1

Dynamical model of interior permanent magnet synchronous machine

In this chapter, a summary of the PMSM is addressed. Second, the Concordia and Park transformations are recalled. From these transformations, the dynamical model of the IPMSM in a $\alpha\beta$ stationary reference frame and a dq synchronous reference frame can be calculated. Subsequently, a parameter free virtual system is introduced and, finally, the benchmark used for simulation and experimental tests is addressed.

1.1 Permanent magnet synchronous motor

The PMSM control system has attracted much attention in the field of AC adjustable speed drives with the rapid development of automatic control technology, power electronics, high-speed microprocessors, sensors, special converters, and permanent magnetic materials. Until recently, the widespread use of PMSM was in some cases restrained by relatively high prices for magnetic materials with high specific magnetic energy values. However, in recent years, prices for such materials have significantly decreased. This may imply the future growth of PMSM drive systems in the industry and technology. The reason is their indisputable advantages, such as a high-efficiency factor, low noise emissions, simple construction, easy maintenance and low rotor inertia. Then, they are widely used in household appliances, transportation, aviation and

robotics [12, 13, 77].

Now, according to the operation and configuration of the PMSM, it has a speed of rotation directly proportional to the frequency of the alternating current network that feeds it. The stator has a three-phase wound, represented by the axes a, b and c with 120° degree phase difference between them. The rotor produces a magnetic field with the permanent magnets, this removes the need for a DC source to generate it. Then, according to the configuration of permanent magnets in the rotor, there exists a classification of PMSM and this is given as follows.

a) Surface permanent magnet synchronous motor

In these types of motors, the magnets are placed on the surface of the rotor, as shown in Figure 1.1. The inductances of this type of motor do not depend on the position of the rotor. This type of motor has d -axis inductance equal to the q -axis inductance, such that the reluctance torque generated by the motor is zero. In this motor, the magnets are on the surface and are exposed to a demagnetizing field. Furthermore, the relative permeability of permanent magnets is similar to that of air, which leads to a low inductance of the machine, since the effective length of the air gap is large. The air gap reluctance is theoretically constant for the different positions of the rotor, then, the starting torque of the surface permanent magnet machine is low. In addition, the magnets are subject to centrifugal forces, which can cause the magnets in the rotor to detach.

b) Inset permanent-magnet synchronous motor

In this type of motor, the magnets are inserted on the surface of the rotor as shown in Figure 1.2, and d -axis inductance is slightly different from q -axis inductance. The iron parts between the permanent magnets have interpolar spaces that add saliency. The value of this saliency depends on the height of the magnets relative to the iron and the aperture of the magnets.

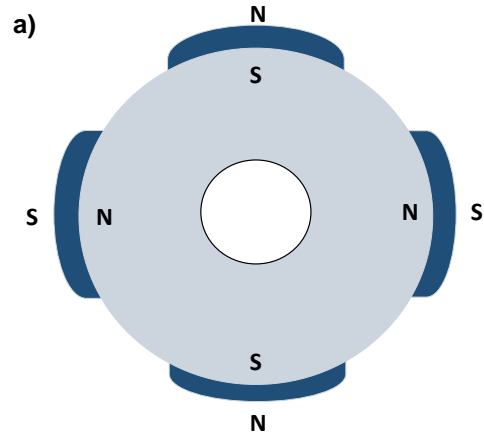


Figure 1.1: PMSM rotor permanent magnets layout: a) Surface permanent magnets.

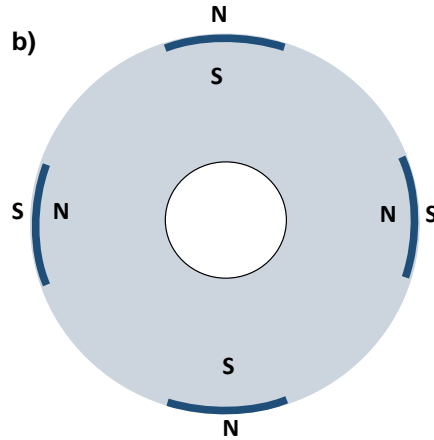


Figure 1.2: PMSM rotor permanent magnets layout: b) Inset permanent magnets.

c) Permanent magnet synchronous motor with flux concentration

In this type of motor, the magnets are located inside the rotor as can be seen in Figure 1.3. The magnets are placed radially into the rotor and buried deep inside the rotor. In this configuration, the magnets are in the direction of the circumference. The magnetic poles are then formed at the level of the ferromagnetic parts of the rotor by concentrating the flux coming from the permanent magnets. One of the main advantages of this type of PMSM is the concentration of the flux generated by the magnets and a higher inductance is obtained. Just like interior magnet machines, in this machine, the magnets are also well protected against demagnetization and mechanical stress. The synchronous reactance on the q axis is greater than on the d axis.

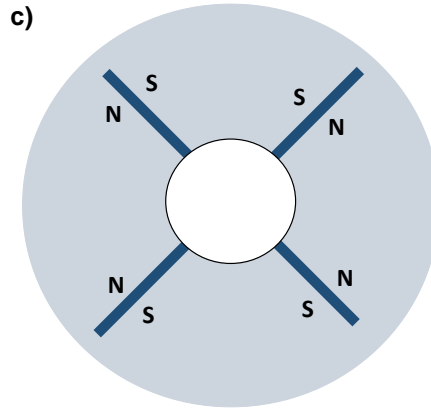


Figure 1.3: PMSM rotor permanent magnets layout: c) Flux concentrating.

d) Interior permanent-magnet synchronous motor

The IPMSM has the magnets integrated inside the rotor as can be seen in Figure 1.4, to protect the permanent magnets in deflux mode or in case of short circuit and improve the mechanical resistance. With interior magnets, the active air gap space is less than that of the equivalent machine with surface magnets. The dq-axes inductances of the IPMSM are different, $L_d < L_q$. Therefore, there is the reluctance torque, and the torque density can be higher than the equivalent surface permanent magnet machine. Due to that the magnets are internal and effectively shielded from the armature reaction field, the interior magnet machine is suitable for applications with constant power over a wide speed range. Moreover, the IPMSM inductances values change according to the rotor position and create a geometric saliency which is an important feature for low-speed control.

The work carried out in this document addresses the case of the IPMSM, since its configuration is recommended due to its torque capacity, power density, simple structure, efficiency and can operate at high speeds. Moreover, considering that the values of the inductances change according to the position of the rotor and create geometric saliency, this is an important feature for low-speed operation.

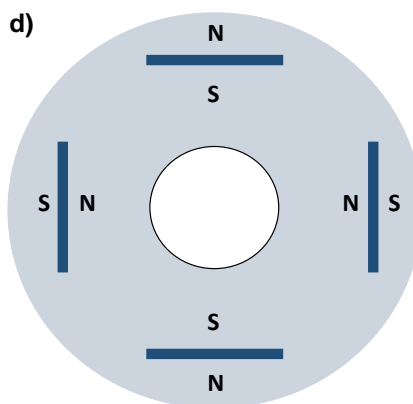


Figure 1.4: PMSM rotor permanent magnets layout: d) Interior permanent magnets.

1.2 Concordia and Park transformations

Concordia and Park transformations are coordinate changes used to change a balanced three-phase system to an equivalent system with two orthogonal axes. It can be used to simplify the study of electric motors.

Concordia transformation

The Concordia transformation is employed to simplify the analysis of three-phase system (a, b, c) in a coordinates system (α, β) as follows.

$$\begin{bmatrix} x_\alpha \\ x_\beta \\ x_o \end{bmatrix} = \mathbb{Q}_o^T \begin{bmatrix} x_a \\ x_b \\ x_c \end{bmatrix} \quad (1.2.1)$$

where \mathbb{Q}_o is given by

$$\mathbb{Q}_o = \sqrt{\frac{2}{3}} \begin{bmatrix} 1 & 0 & \frac{1}{\sqrt{2}} \\ -\frac{1}{2} & \frac{\sqrt{3}}{2} & \frac{1}{\sqrt{2}} \\ \frac{1}{2} & -\frac{\sqrt{3}}{2} & \frac{1}{\sqrt{2}} \end{bmatrix} \quad (1.2.2)$$

Moreover, this transformation has direct and inverse transform symmetry and can preserve the active and reactive powers. Since in a balanced system $x_a + x_b + x_c = 0$ and thus $x_o = 0$, then

one can also consider the simplified transformation

$$\begin{bmatrix} x_\alpha \\ x_\beta \end{bmatrix} = \mathbb{Q}^T \begin{bmatrix} x_a \\ x_b \\ x_c \end{bmatrix} \quad (1.2.3)$$

which is simply the original Concordia transformation with the 3rd equation excluded, where \mathbb{Q} is expressed as follows

$$\mathbb{Q} = \sqrt{\frac{2}{3}} \begin{bmatrix} 1 & 0 \\ -\frac{1}{2} & \frac{\sqrt{3}}{2} \\ -\frac{1}{2} & -\frac{\sqrt{3}}{2} \end{bmatrix} \quad (1.2.4)$$

In Figure 1.5, the representation of the concordia transformation is illustrated, where θ_e represents the angular position and x_α and x_β components represent the coordinates of the rotating space vector x_R in a fixed reference frame whose α -axis is aligned with phase x_a axis.

Park transformation

The Park transformation transforms the components $-\alpha\beta$ to reference system $-dq$, the objective of this transformation is to convert the variables sinusoidally in time to constant values dq, in permanent regime.

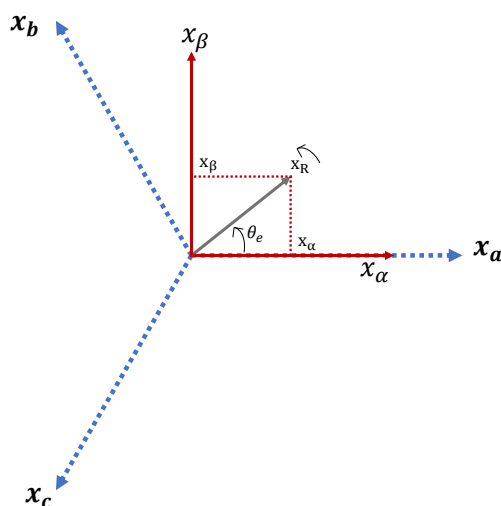


Figure 1.5: Concordia transformation

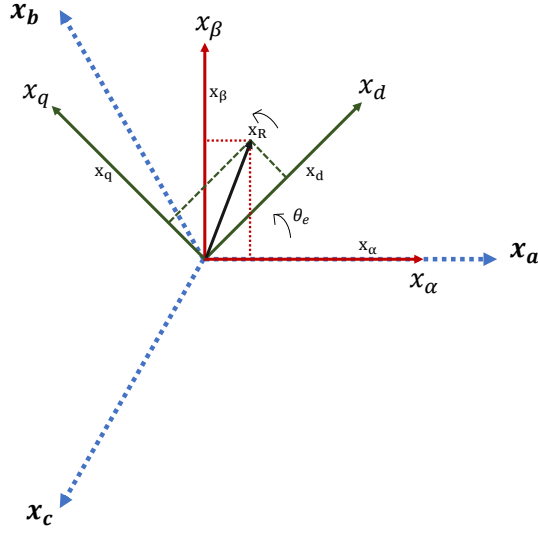


Figure 1.6: Park transformation

$$\begin{bmatrix} x_d \\ x_q \end{bmatrix} = \mathbb{T}^T \begin{bmatrix} x_\alpha \\ x_\beta \end{bmatrix} \quad (1.2.5)$$

where \mathbb{T} is given by

$$\mathbb{T} = \begin{bmatrix} \cos(\theta_e) & -\sin(\theta_e) \\ \sin(\theta_e) & \cos(\theta_e) \end{bmatrix} = e^{j\theta_e} \quad (1.2.6)$$

In Figure 1.6, the representation of the Park transformation is illustrated.

1.3 Electrical equations of the Permanent Magnet Synchronous Motor

The three-phase stator voltage equations, represented in the three-phase stationary frame (*abc*-axes), can be expressed as follows

$$v_{abc} = R_s i_{abc} + \frac{d\psi_{abc}}{dt} \quad (1.3.1)$$

where $v_{abc} = [v_a \ v_b \ v_c]^T$ represents stator voltages, R_s is stator resistance, $i_{abc} = [i_a \ i_b \ i_c]^T$ corresponds the stator currents and $\psi_{abc} = [\psi_a \ \psi_b \ \psi_c]^T$ are the stator fluxes. Moreover, ψ_{abc}

is defined as follows

$$\psi_{abc} = \mathbb{L}_{ss} \begin{bmatrix} i_a \\ i_b \\ i_c \end{bmatrix} + \begin{bmatrix} \psi_{af} \\ \psi_{bf} \\ \psi_{cf} \end{bmatrix} \quad (1.3.2)$$

where

$$\begin{bmatrix} \psi_{af} \\ \psi_{bf} \\ \psi_{cf} \end{bmatrix} = \psi_r \begin{bmatrix} \cos(p\theta) \\ \cos(p\theta - \frac{2\pi}{3}) \\ \cos(p\theta + \frac{2\pi}{3}) \end{bmatrix} \quad (1.3.3)$$

and p represents the number of poles, θ the mechanical angular position, ψ_r is the permanent-magnet flux linkage and \mathbb{L}_{ss} is expressed as follows

$$\mathbb{L}_{ss} = \mathbb{L}_{so} + \mathbb{L}_{sv} \quad (1.3.4)$$

where

$$\mathbb{L}_{so} = \begin{bmatrix} L_{so} & M_{so} & M_{so} \\ M_{so} & L_{so} & M_{so} \\ M_{so} & M_{so} & L_{so} \end{bmatrix} \quad (1.3.5)$$

and

$$\mathbb{L}_{sv} = L_{sv} \begin{bmatrix} \cos(2p\theta) & \cos(2p\theta - \frac{2\pi}{3}) & \cos(2p\theta + \frac{2\pi}{3}) \\ \cos(2p\theta - \frac{2\pi}{3}) & \cos(2p\theta + \frac{2\pi}{3}) & \cos(2p\theta) \\ \cos(2p\theta + \frac{2\pi}{3}) & \cos(2p\theta) & \cos(2p\theta - \frac{2\pi}{3}) \end{bmatrix} \quad (1.3.6)$$

defining M_{so} , L_{so} and L_{sv} as the mutual and own inductances, respectively; for $M_{so} = -\frac{1}{2}L_{so}$. Moreover, L_{so} and L_{sv} are positive parameters depending on the machine.

Now, the system (1.3.1) can be written as follow

$$\begin{bmatrix} v_a \\ v_b \\ v_c \end{bmatrix} = R_s \begin{bmatrix} i_a \\ i_b \\ i_c \end{bmatrix} + \frac{d}{dt} \left\{ \mathbb{L}_{ss} \begin{bmatrix} i_a \\ i_b \\ i_c \end{bmatrix} + \begin{bmatrix} \psi_{af} \\ \psi_{bf} \\ \psi_{cf} \end{bmatrix} \right\} \quad (1.3.7)$$

and considering the Concordia transformation (1.2.3), the system (1.3.1) expressed in $\alpha\beta$ sta-

tionary reference frame is the following

$$\begin{bmatrix} v_\alpha \\ v_\beta \end{bmatrix} = R_s \begin{bmatrix} i_\alpha \\ i_\beta \end{bmatrix} + \frac{d}{dt} \begin{bmatrix} \psi_\alpha \\ \psi_\beta \end{bmatrix} \quad (1.3.8)$$

1.3.1 Dynamical model of the Interior Permanent Magnet Synchronous Motor in dq synchronous reference frame

In this section, the dynamical model of the IPMSM is introduced. Then, from the three-phase stator voltage equations in a three-phase stationary frame ($abc - axes$) given by

$$v_{abc} = R_s i_{abc} + \frac{d}{dt} \{ \mathbb{L}_{ss} i_{abc} + \psi_{afbfcf} \} \quad (1.3.9)$$

the following equation can be written

$$v_{abc} = R_s i_{abc} + \frac{d}{dt} \{ \mathbb{L}_{ss} i_{abc} \} + \frac{d}{dt} \{ \psi_{afbfcf} \} \quad (1.3.10)$$

where

$$\frac{d}{dt} \{ \psi_{afbfcf} \} = \frac{d}{dt} \begin{bmatrix} \psi_{af} \\ \psi_{bf} \\ \psi_{cf} \end{bmatrix} = -\psi_r p \Omega \begin{bmatrix} \sin(p\theta) \\ \sin(p\theta - \frac{2\pi}{3}) \\ \sin(p\theta + \frac{2\pi}{3}) \end{bmatrix} \quad (1.3.11)$$

and Ω represents the mechanical speed. Then, replacing (1.3.11) in (1.3.10), the following equation is obtained

$$\begin{bmatrix} v_a \\ v_b \\ v_c \end{bmatrix} = R_s \begin{bmatrix} i_a \\ i_b \\ i_c \end{bmatrix} + \frac{d}{dt} \left\{ \mathbb{L}_{ss} \begin{bmatrix} i_a \\ i_b \\ i_c \end{bmatrix} \right\} - \psi_r p \Omega \begin{bmatrix} \sin(p\theta) \\ \sin(p\theta - \frac{2\pi}{3}) \\ \sin(p\theta + \frac{2\pi}{3}) \end{bmatrix} \quad (1.3.12)$$

Now, taking into account the following transformation

$$\begin{bmatrix} x_d \\ x_q \end{bmatrix} = \mathbb{T}^T \mathbb{Q}^T \begin{bmatrix} x_a \\ x_b \\ x_c \end{bmatrix} \quad (1.3.13)$$

where x represents a variable (voltage, current or flux). Then, combining (1.3.13) with (1.3.12) and multiplying the left side of (1.3.13) by $\mathbb{Q}\mathbb{T}$, the following system is obtained

$$\begin{aligned} \mathbb{Q}\mathbb{T}\mathbb{T}^T\mathbb{Q}^T \begin{bmatrix} v_a \\ v_b \\ v_c \end{bmatrix} &= R_s \mathbb{Q}\mathbb{T}\mathbb{T}^T\mathbb{Q}^T \begin{bmatrix} i_a \\ i_b \\ i_c \end{bmatrix} + \frac{d}{dt} \left\{ \mathbb{L}_{ss} \mathbb{Q}\mathbb{T}\mathbb{T}^T\mathbb{Q}^T \begin{bmatrix} i_a \\ i_b \\ i_c \end{bmatrix} \right\} \\ &\quad - \psi_r p \Omega \mathbb{Q}\mathbb{T}\mathbb{T}^T\mathbb{Q}^T \begin{bmatrix} \sin(p\theta) \\ \sin(p\theta - \frac{2\pi}{3}) \\ \sin(p\theta + \frac{2\pi}{3}) \end{bmatrix} \end{aligned} \quad (1.3.14)$$

such that

$$\mathbb{Q}\mathbb{T} \begin{bmatrix} v_d \\ v_q \end{bmatrix} = R_s \mathbb{Q}\mathbb{T} \begin{bmatrix} i_d \\ i_q \end{bmatrix} + \frac{d}{dt} \left\{ \mathbb{L}_{ss} \mathbb{Q}\mathbb{T} \begin{bmatrix} i_d \\ i_q \end{bmatrix} \right\} + \mathbb{Q}\mathbb{T} \begin{bmatrix} 0 \\ \psi_r p \Omega \end{bmatrix} \quad (1.3.15)$$

Consider that $\mathbb{Q}^T\mathbb{Q} = I_{2 \times 2}$ and $\mathbb{T}^T\mathbb{T} = I_{2 \times 2}$, where $I_{2 \times 2}$ is a identity. Then, multiplying the left side of above equation by $\mathbb{T}^T\mathbb{Q}^T$, it follows that

$$\begin{bmatrix} v_d \\ v_q \end{bmatrix} = R_s \begin{bmatrix} i_d \\ i_q \end{bmatrix} + \mathbb{T}^T \mathbb{Q}^T \frac{d}{dt} \left\{ \mathbb{L}_{ss} \mathbb{Q}\mathbb{T} \begin{bmatrix} i_d \\ i_q \end{bmatrix} \right\} + \begin{bmatrix} 0 \\ \psi_r p \Omega \end{bmatrix} \quad (1.3.16)$$

and can be rewritten as follows

$$\begin{bmatrix} v_d \\ v_q \end{bmatrix} = R_s \begin{bmatrix} i_d \\ i_q \end{bmatrix} + \mathbb{T}^T \frac{d}{dt} \{ \Gamma_{ss} \mathbb{T} \} \begin{bmatrix} i_d \\ i_q \end{bmatrix} + \mathbb{T}^T \Gamma_{ss} \mathbb{T} \frac{d}{dt} \begin{bmatrix} i_d \\ i_q \end{bmatrix} + \begin{bmatrix} 0 \\ \psi_r p \Omega \end{bmatrix} \quad (1.3.17)$$

where

$$\Gamma_{ss} = \mathbb{Q}\mathbb{L}_{ss}\mathbb{Q} = \frac{3}{2}L_{sv} \begin{bmatrix} \cos(2p\theta) & \sin(2p\theta) \\ \sin(2p\theta) & -\cos(2p\theta) \end{bmatrix} + \frac{3}{2}L_{so} \begin{bmatrix} 1 & 0 \\ 0 & 1 \end{bmatrix} \quad (1.3.18)$$

Now, L_{so} and L_{sv} are defined as follows

$$L_{so} = \frac{L_d + L_q}{3} \quad L_{sv} = \frac{L_d - L_q}{3} \quad (1.3.19)$$

where L_d and L_q are the dq -axes winding inductance. Therefore, Γ_{ss} given by (1.3.18) can be expressed by

$$\Gamma_{ss} = \frac{L_d - L_q}{2} \begin{bmatrix} \cos(2p\theta) & \sin(2p\theta) \\ \sin(2p\theta) & -\cos(2p\theta) \end{bmatrix} + \frac{L_d + L_q}{2} \begin{bmatrix} 1 & 0 \\ 0 & 1 \end{bmatrix} = \begin{bmatrix} L_\alpha & L_{\alpha\beta} \\ L_{\alpha\beta} & L_\beta \end{bmatrix} \quad (1.3.20)$$

Then, the solution for $\mathbb{T} \frac{d}{dt} \{\Gamma_{ss}\mathbb{T}\}$ in (1.3.17) is given by

$$\mathbb{T} \frac{d}{dt} \{\Gamma_{ss}\mathbb{T}\} = p\Omega \begin{bmatrix} 0 & -L_q \\ L_d & 0 \end{bmatrix} \quad (1.3.21)$$

and the solution for $\mathbb{T}^T \Gamma_{ss} \mathbb{T}$ is given by

$$\mathbb{T}^T \Gamma_{ss} \mathbb{T} = \begin{bmatrix} L_d & 0 \\ 0 & L_q \end{bmatrix} \quad (1.3.22)$$

Therefore, the system (1.3.17) expressed in a dq reference frame is given by

$$\begin{bmatrix} v_d \\ v_q \end{bmatrix} = R_s \begin{bmatrix} i_d \\ i_q \end{bmatrix} + p\Omega \begin{bmatrix} 0 & -L_q \\ L_d & 0 \end{bmatrix} \begin{bmatrix} i_d \\ i_q \end{bmatrix} + \begin{bmatrix} L_d & 0 \\ 0 & L_q \end{bmatrix} \frac{d}{dt} \begin{bmatrix} i_d \\ i_q \end{bmatrix} + \begin{bmatrix} 0 \\ \psi_r p\Omega \end{bmatrix} \quad (1.3.23)$$

Mechanical equations

The equation for the mechanical model is given by

$$\frac{d\theta}{dt} = \Omega \quad (1.3.24)$$

where θ is mechanical angular position and Ω mechanical speed. Moreover, the following equality is defined as follows

$$J \frac{d\Omega}{dt} + f_v \Omega = T_e - T_l \quad (1.3.25)$$

where J represents the inertia, f_v the viscous friction coefficient, T_l the load torque and T_e the electromagnetic torque. The electromagnetic torque T_e is defined as follows

$$T_e = p(\psi_\alpha i_\beta - \psi_\beta i_\alpha) = p(\psi_d i_q - \psi_q i_d) \quad (1.3.26)$$

where the terms ψ_d and ψ_q are defined by

$$\psi_d = L_d i_d + \psi_r, \quad \psi_q = L_q i_q \quad (1.3.27)$$

Then, the electromagnetic torque can be expressed as follows

$$T_e = p(L_d - L_q) i_d i_q + p\psi_r i_q \quad (1.3.28)$$

Therefore, the mechanical system for the IPMSM is given by

$$\begin{aligned} \frac{d\theta}{dt} &= \Omega \\ \frac{d\Omega}{dt} &= \frac{p}{J}(L_d - L_q) i_d i_q + \frac{p}{J} \psi_r i_q - \frac{T_l}{J} - \frac{f_v \Omega}{J} \end{aligned} \quad (1.3.29)$$

Dynamic model of the Interior Permanent Magnet Synchronous Motor: Electrical and mechanical equations

The dynamical model of the IPMSM with electrical and mechanical equations is the following

$$\Sigma_{elec} : \begin{cases} \frac{di_d}{dt} &= -\frac{R_s}{L_d} i_d + p\Omega \frac{L_q}{L_d} i_q + \frac{v_d}{L_d} \\ \frac{di_q}{dt} &= -\frac{R_s}{L_q} i_q - p\Omega \frac{L_d}{L_q} i_d + \frac{v_q}{L_q} - p\Omega \frac{\psi_r}{L_q} \end{cases} \quad (1.3.30)$$

$$\Sigma_{mech} : \begin{cases} \frac{d\theta}{dt} &= \Omega \\ \frac{d\Omega}{dt} &= \frac{p}{J} (L_d - L_q) i_d i_q + \frac{p}{J} \psi_r i_q - \frac{f_v}{J} \Omega - \frac{1}{J} T_l \end{cases} \quad (1.3.31)$$

1.3.2 Dynamical model of the Interior Permanent Magnet Synchronous Motor in $\alpha\beta$ stationary reference frame

In this section the dynamical model of the IPMSM in a $\alpha\beta$ stationary reference frame is addressed. Then, transforming (1.3.23) into $\alpha\beta$ stationary reference frame, the following system is obtained

$$\begin{bmatrix} v_\alpha \\ v_\beta \end{bmatrix} = \begin{bmatrix} R + \frac{d}{dt} L_\alpha & \frac{d}{dt} L_{\alpha\beta} \\ \frac{d}{dt} L_{\alpha\beta} & R + \frac{d}{dt} L_\beta \end{bmatrix} \begin{bmatrix} i_\alpha \\ i_\beta \end{bmatrix} + p\Omega \begin{bmatrix} -\sin(\theta_e) \\ \cos(\theta_e) \end{bmatrix} \quad (1.3.32)$$

where $\theta_e = p\theta$ is the electrical angular position and $L_\alpha = L_o + L_1 \cos(2\theta_e)$, $L_\beta = L_o - L_1 \cos(2\theta_e)$, $L_{\alpha,\beta} = L_1 \sin(2\theta_e)$, $L_o = \frac{(L_d + L_q)}{2}$ and $L_1 = \frac{(L_d - L_q)}{2}$. The system (1.3.32) can be written in a compact form as follows

$$v_{\alpha\beta} = A_{\alpha\beta} + B_{\alpha\beta} + C_{\alpha\beta} + D_{\alpha\beta} \quad (1.3.33)$$

where $v_{\alpha\beta} = [v_\alpha \ v_\beta]^T$, $A_{\alpha\beta} = R_s [i_\alpha \ i_\beta]^T$

$$B_{\alpha\beta} = \frac{d}{dt} \left\{ L_o \begin{bmatrix} i_\alpha \\ i_\beta \end{bmatrix} \right\}, C_{\alpha\beta} = p\Omega \psi_r \begin{bmatrix} -\sin(\theta_e) \\ \cos(\theta_e) \end{bmatrix}, D_{\alpha\beta} = \frac{d}{dt} \left\{ L_1 \begin{bmatrix} \cos(2\theta_e) & \sin(2\theta_e) \\ \sin(2\theta_e) & -\cos(2\theta_e) \end{bmatrix} \begin{bmatrix} i_\alpha \\ i_\beta \end{bmatrix} \right\}$$

The system structure (1.3.33) is not easy for mathematical processing, having functions of rotor position θ_e , which makes the equation difficult to solve. An easy way to solve this issue is to use the estimated position $\hat{\theta}_e$ instead of θ_e . This is possible if the amplitude of $D_{\alpha\beta}$ is smaller enough than $C_{\alpha\beta}$, i.e., $|L_1 i_{\alpha,\beta}| \ll \psi_r$. In fact, the approximation made in (1.3.32) and (1.3.33) is based on the assumption that this condition is valid. Then, it is true for motors with relatively small reluctance torque. However, if the motor reluctance torque cannot be neglected, such as the permanent magnet torque, the sensorless estimation could be unstable. On the other side, in (1.3.33), the system contains the terms $2\theta_e$. The reason why term $2\theta_e$ appears in (1.3.33) is

due to that impedance matrix is asymmetric. Therefore, if the impedance matrix is rewritten symmetrically as

$$\begin{bmatrix} v_d \\ v_q \end{bmatrix} = \begin{bmatrix} R_s + pL_d & -p\Omega L_q \\ p\Omega L_q & R + pL_d \end{bmatrix} \begin{bmatrix} i_d \\ i_q \end{bmatrix} + \begin{bmatrix} 0 \\ (L_d - L_q)(p\Omega i_d - \dot{i}_q) + p\Omega\psi_r \end{bmatrix} \quad (1.3.34)$$

then, the $\alpha\beta$ stationary reference frame can be written as follows

$$\begin{bmatrix} v_\alpha \\ v_\beta \end{bmatrix} = \begin{bmatrix} R_s + pL_d & p\Omega(L_d - L_q) \\ -p\Omega(L_d - L_q) & R + pL_d \end{bmatrix} \begin{bmatrix} i_\alpha \\ i_\beta \end{bmatrix} + [(L_d - L_q)(p\Omega i_d - \dot{i}_q) + p\Omega\psi_r] \begin{bmatrix} -\sin(\theta_e) \\ \cos(\theta_e) \end{bmatrix} \quad (1.3.35)$$

The system (1.3.35) is a transformation of (1.3.32) without any approximation. It is a general form of the mathematical model of IPMSM. Moreover, if $L_d = L_q$, the model of the surface permanent magnet synchronous motor is obtained and if $\psi = 0$, it is possible to obtain the synchronous reluctance motor.

1.4 Parameter free virtual system

In order to analyse the system that will be used for the observer design and considering that during the machine operation, some machine parameters can change its nominal value, the uncertain system for system (1.3.31) is given by

$$\begin{cases} \dot{\theta}_e = p\Omega \\ \dot{\Omega} = \frac{p}{J'} [(L_d + \Delta L_d) - (L_q + \Delta L_q)] i_d i_q + \frac{p}{J'} \psi_r i_q - \frac{(f_v + \Delta f_v)}{J'} \Omega - \frac{1}{J'} T_l \end{cases} \quad (1.4.1)$$

where $J' = (J + \Delta J)$ and θ_e is the electrical angular position. The uncertain term can be defined as follows

$$f_1 + \Delta f_1 = \frac{p}{J'} [(L_d + \Delta L_d) - (L_q + \Delta L_q)] i_d i_q + \frac{p}{J'} \psi_r i_q - \frac{(f_v + \Delta f_v)}{J'} \omega - \frac{1}{J'} T_l$$

Consequently, the uncertain system is represented in a compact form as follows

$$\begin{cases} \dot{\theta}_e &= p\Omega \\ \dot{\Omega} &= f_1 + \Delta f_1 \end{cases} \quad (1.4.2)$$

Defining $\alpha = f_1 + \Delta f_1$ and assuming that Δf_1 is differentiable, the following extended system is obtained

$$\begin{cases} \dot{\theta}_e &= p\Omega \\ \dot{\Omega} &= \alpha \\ \dot{\alpha} &= \dot{f}_1 + \Delta \dot{f}_1 = \rho(t) \end{cases} \quad (1.4.3)$$

Finally, we obtain the auxiliary system that will be used in the observer design, which does not depend on the machine parameters

$$\begin{cases} \dot{\theta}_e &= \omega \\ \dot{\omega} &= \alpha \\ \dot{\alpha} &= \rho(t) \end{cases} \quad (1.4.4)$$

where $\theta_e = p\theta$ is the electrical angular position, $\omega = p\Omega$ is the electrical speed, p the pole pair number and α is the acceleration, where the time derivative of the acceleration is equal $\rho(t)$, which is a function containing the nonlinear terms and uncertainties, bounded with unknown bound. Therefore, from the information of θ_e and ω , it is possible to compute the mechanical angular position $\left(\theta = \frac{\theta_e}{p}\right)$ and the mechanical speed $\left(\Omega = \frac{\omega}{p}\right)$.

It is clear that the mechanical sub-system (1.3.31) of the IPMSM does not depend on the acceleration, however, to estimate the position and the speed, the mechanical sub-system has been extended including the acceleration in order to improve the estimation of those variables. In other words, the first two equations of (1.4.4) are enough to have a good estimation with low transient modes. However, with fast dynamics, speed estimation errors could increase due to that its derivative is supposed to be equal to zero. To overcome this problem, the machine acceleration— α is also estimated to achieve a more precise estimation in fast transient

modes. Therefore, the virtual system (1.4.4) will be used to estimate angular position, speed and acceleration by using an extraction of the angular position estimation error e_{θ_e} that is presented later.

1.5 Benchmark

In this section, the benchmark for the IPMSM is introduced. Simulation and experimental tests are going to be evaluated in order to show the performance of the proposed strategies. The parameters of the IPMSM are presented in Table 1.1. The simulation and experimentation are

Table 1.1: IPMSM nominal parameters

Symbol	Parameter	Value	Unit
R_s	Stator resistance	1.4	ohms
J	Moment of inertia	$7.3e^{-3}$	kg.m ²
p	Number of pole pairs	5	
T_l	Torque	4	N-m
ψ_r	Permanent-magnet flux linkage	0.18	Wb
L_d	d-axis winding inductance	0.0057	H
L_q	q-axis winding inductance	0.0099	H
f_v	Viscous friction coefficient	0.0034	kg-m ² /s

carried out at low, medium and high speed of operation. Similarly, a load torque with sudden changes is considered to show the robustness of the proposal. It can be shown in Figure 1.7.

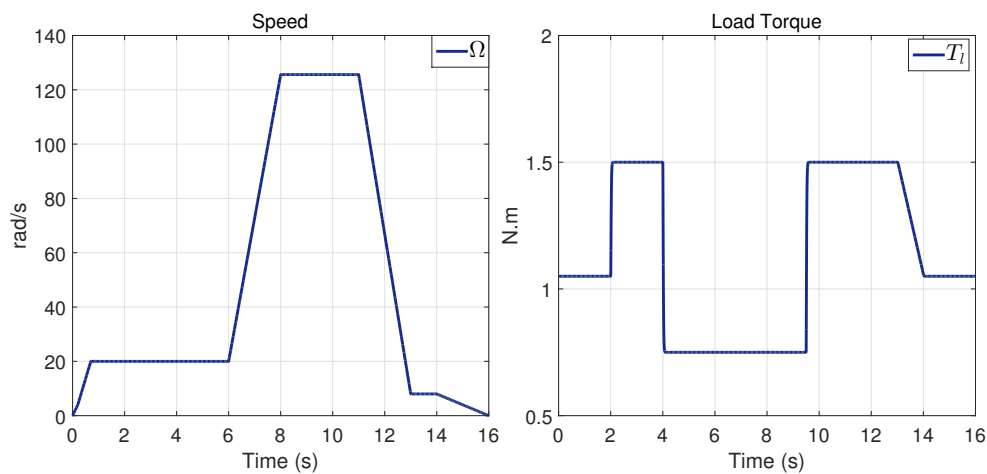


Figure 1.7: Load torque and speed profiles used during experimental and simulation tests

As mentioned in the introduction, electrical parameters could vary during the operation of the motor due to magnetic saturation or temperature variations; mechanical parameters could vary depending on the load torque, weight and so on. However, during the experimental tests, it is not possible to have access to the motor parameters to vary their values. Then, the experimental tests are carried out over a large time interval to see the effect of the parameters on the estimation based on a virtual system without parameters. In addition, a simulation test is carried out under resistance, inertia and inductance variations, as shown in Figure 1.8 to show the robustness of the proposed strategy. On the other hand, from simulation, the

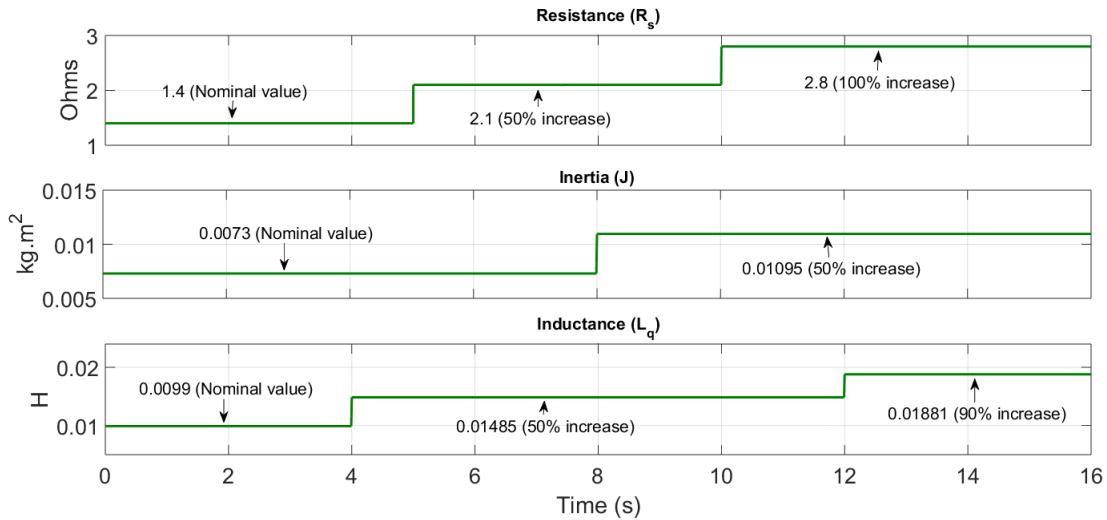


Figure 1.8: Parameter variations in simulation tests

performance and effectiveness of the proposed observer based on the extraction of the angular error e_θ during a time interval of 16 s will be shown by using the profiles of Figure 1.9, at high, low and zero speed, and under different load torque values.

1.5.1 Hardware description

The experimental setup is shown in Figure 1.10 which is composed of an IPMSM rated at 3 kW supplied by a three-phase voltages source inverter. The inverter is powered by 400 V DC voltage. The pulse width modulation (PWM) technique is generated by a dSPACE DS1103

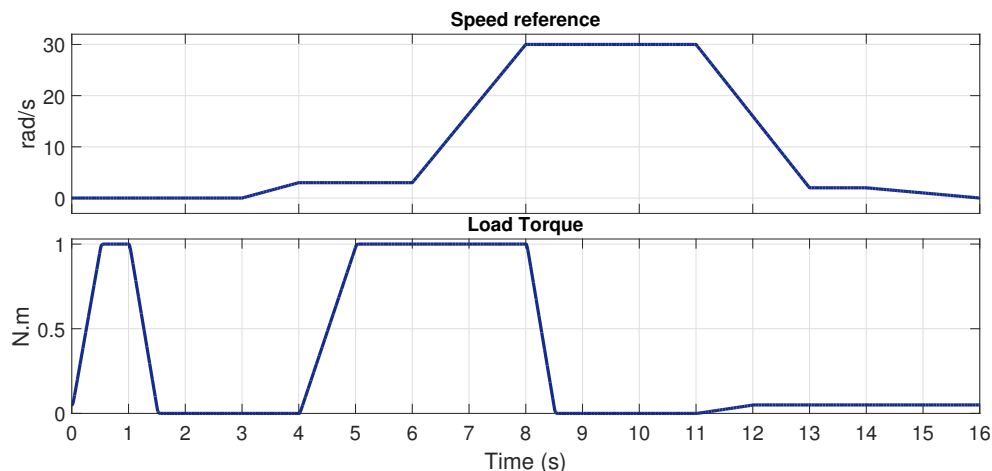


Figure 1.9: Load torque and speed profiles considering a low-speed region with a very small load torque.

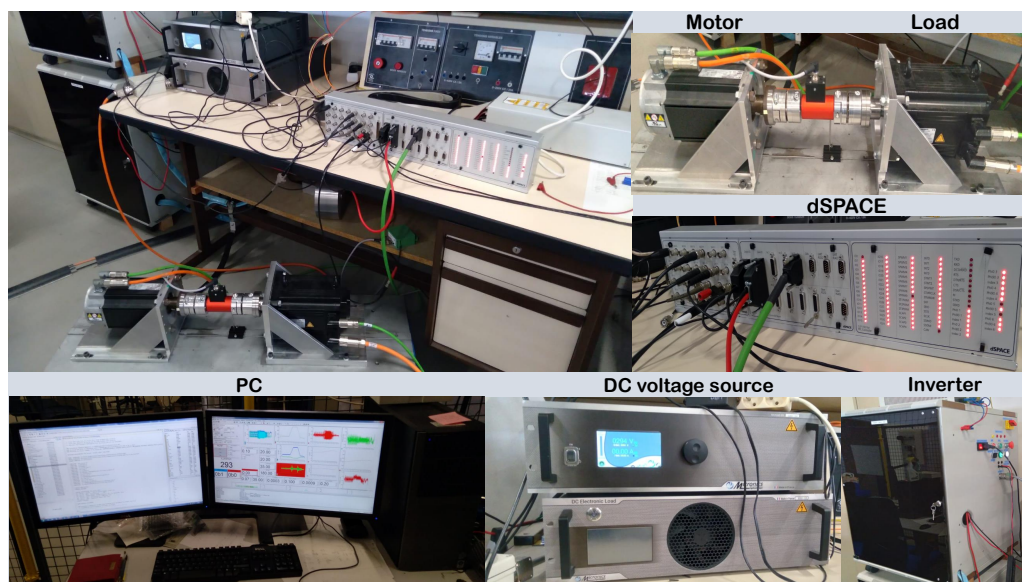


Figure 1.10: Experimental setup

with a switching frequency of 10 kHz. The digital board of dSPACE receives the stator currents and the dc link voltages data with a 10 kHz frequency and the measured torque data with a 2 kHz frequency. The load torque is generated by a PMSM mechanically coupled with the shaft of the IPMSM, while the angular position is measured by the encoder. Moreover, a Kalman-filter applied to the measured position is used to calculate the rotor speed.

1.6 Conclusion

The basics of permanent magnet synchronous motors, including their main dynamical models, have been addressed in this chapter. It is well known that this dynamical model depends on parameters as stator resistance, inductances and so on. Therefore, the use of dynamic models in the observer design represents a problem, since the motor parameters vary during operation. For this reason, a parameter-free virtual system has been introduced to avoid the parametric uncertainties. The virtual system will be used in the observer design in the following chapter, taking into account the benchmark presented in this chapter.

Chapter 2

New strategy for the rotor position and speed estimation of Interior Permanent Magnet Synchronous Motor

In this chapter, a strategy to extract the angular position estimation error of the IPMSM is addressed. After this, two adaptive observers based on the sliding mode approach will be introduced. These observers use the information of the angular position estimation error extraction in order to estimate the angular position, speed and acceleration. Furthermore, the observer gains are reparameterized based on a single parameter to simplify the tuning procedure. Some tests are addressed for each observer and a comparative study is carried out.

2.1 Extraction of angular position estimation error

A methodology to extract the angular position estimation error (0.0.1) of IPMSM, from an $\alpha\beta$ stationary reference frame, is addressed. Then, considering that the currents $i_{\alpha\beta}$ are measurable and in order to extract e_{θ_e} , consider Park transformation, such that the currents i_d and i_q are expressed as

$$i_{dq} = \mathbb{T}^T(\theta_e) i_{\alpha\beta} \quad (2.1.1)$$

with

$$i_{dq} = \begin{bmatrix} i_d \\ i_q \end{bmatrix}, \quad \mathbb{T}^T(\theta_e) = \begin{bmatrix} \cos(\theta_e) & \sin(\theta_e) \\ -\sin(\theta_e) & \cos(\theta_e) \end{bmatrix}, \quad i_{\alpha\beta} = \begin{bmatrix} i_\alpha \\ i_\beta \end{bmatrix}, \quad (2.1.2)$$

where currents i_{dq} and angular position θ_e are not measurable. Therefore, considering that there exists a control law for current- i_d and current- i_q tracks a reference current- i_d^* . Then, in order to extract e_θ , the following equation is introduced

$$\Lambda_{\theta_1} = \mathbb{I}_{qn} - \mathbb{I}_{dn} + i_d^* \sqrt{2} \quad (2.1.3)$$

and the terms \mathbb{I}_{dn} and \mathbb{I}_{qn} are defined as follows,

$$\mathbb{I}_{dnqn} = \mathbb{M}(\hat{\theta}_e + \phi) \quad \mathbb{T}^{-T}(\theta) \quad i_{dq} \quad (2.1.4)$$

with $\mathbb{I}_{dnqn} = [\mathbb{I}_{dn} \quad \mathbb{I}_{qn}]^T$ and the transformation matrix $\mathbb{M}(\hat{\theta}_e + \phi)$ expressed as follows

$$\mathbb{M}(\hat{\theta}_e + \phi) = \begin{bmatrix} \cos(\hat{\theta}_e + \phi) & \sin(\hat{\theta}_e + \phi) \\ -\sin(\hat{\theta}_e + \phi) & \cos(\hat{\theta}_e + \phi) \end{bmatrix}, \quad (2.1.5)$$

defining $\hat{\theta}_e$ as the estimated angular position and ϕ is an offset angle that must be chosen appropriately to extract e_{θ_e} . In addition, notice that $(i_d^*, i_{\alpha\beta}, \phi)$ are known values and $\hat{\theta}$ will be computed by using the observer presented later, then

$$\Lambda_{\theta_1} = \Lambda_{\theta_1}(\hat{\theta}_e, i_{\alpha\beta}, i_d^*, \phi) \quad (2.1.6)$$

can be computed taking into account that

$$\mathbb{T}^{-T}(\theta_e) \quad i_{dq} \quad = \quad i_{\alpha\beta} \quad = \quad \begin{bmatrix} i_\alpha \\ i_\beta \end{bmatrix} \quad = \quad \begin{bmatrix} \cos(\theta_e)i_d - \sin(\theta_e)i_q \\ \sin(\theta_e)i_d + \cos(\theta_e)i_q \end{bmatrix} \quad (2.1.7)$$

Now, from transformation matrix $\mathbb{M}(\hat{\theta}_e + \phi)$, the currents $i_{\alpha\beta}$ can be transformed into alternate synchronous reference frame. Then, the terms \mathbb{I}_{dn} and \mathbb{I}_{qn} are defined as follows

$$\mathbb{I}_{dn} = \cos(e_{\theta_e} - \phi)i_d - \sin(e_{\theta_e} - \phi)i_q, \quad \mathbb{I}_{qn} = \sin(e_{\theta_e} - \phi)i_d + \cos(e_{\theta_e} - \phi)i_q \quad (2.1.8)$$

where \mathbb{I}_{dn} and \mathbb{I}_{qn} depends explicitly on e_{θ_e} . Nonetheless, extraction of e_{θ_e} in this structure is not possible. Therefore, selecting $\phi = \frac{\pi}{4}$, it is possible to factor and simplify (2.1.8) in terms of e_{θ_e} in order to compute (2.1.3), otherwise it is not easy to handle nor extract easily the angular position error. In consequence, (2.1.3) is expressed in terms of e_{θ_e} as follows

$$\Lambda_{\theta_1} = i_q\sqrt{2} \sin(e_{\theta_e}) - i_d\sqrt{2} \cos(e_{\theta_e}) + i_d^*\sqrt{2} \quad (2.1.9)$$

Considering that Λ_{θ_1} is calculated by using measurable currents $i_{\alpha\beta}$; and assuming i_d tracks a desired reference i_d^* . Then, the above equation can be rewritten as follows

$$\Lambda_{\theta_1} = i_q\sqrt{2} \sin(e_{\theta_e}) + i_d^*\sqrt{2} [1 - \cos(e_{\theta_e})] \quad (2.1.10)$$

and using a trigonometric identity, the following equation is obtained

$$\Lambda_{\theta_1} = i_q\sqrt{2} \sin(e_{\theta_e}) + i_d^*\sqrt{2} \left[2\left(\sin\left(\frac{e_{\theta_e}}{2}\right)\right)^2 \right] \quad (2.1.11)$$

Therefore, for a small angular error e_{θ_e} , an approximation for Λ_{θ_1} is stated as

$$\Lambda_{\theta_1} \approx i_q e_{\theta_e} \sqrt{2} + \frac{i_d^*}{\sqrt{2}} e_{\theta_e}^2. \quad (2.1.12)$$

Moreover, consider that quadratic term is smaller than the linear term. Then, Λ_{θ_1} is given by

$$\Lambda_{\theta_1} \approx i_q e_{\theta_e} \sqrt{2} \quad (2.1.13)$$

Notice that (2.1.13) depends of the current i_q . It is worth mentioning that the changes in the current i_q are directly proportional to the electromagnetic torque T_e [78]. As can be seen

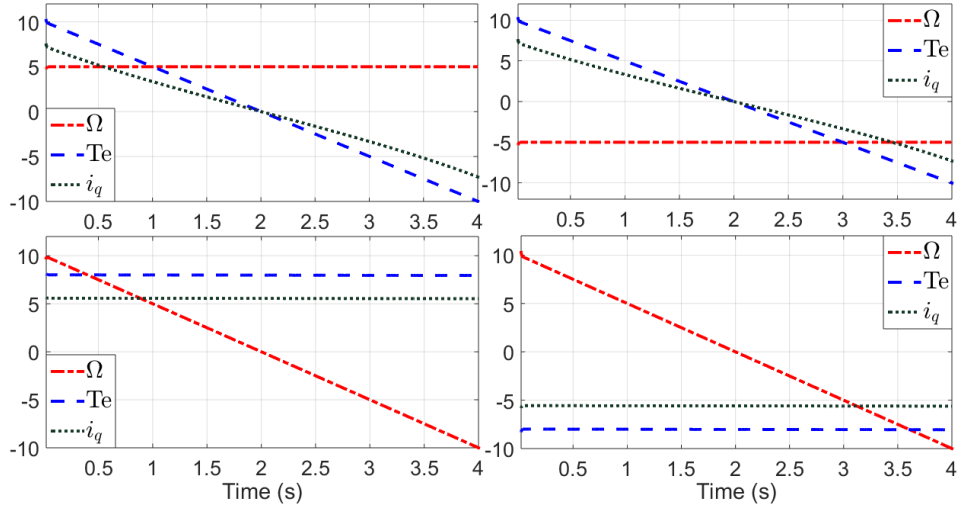


Figure 2.1: Different scenarios to see the behavior of speed, electromagnetic torque and current- i_q .

in Figure 2.1, different profiles of speed and electromagnetic torque have been plotted and the behavior of the current i_q is shown. Then, from Figure 2.1, current i_q can be positive or negative depending on the electrical machine operation. Then, multiplying $sign(i_q)$ in both side of the equation, it follows that

$$\begin{aligned} \Lambda_{\theta_1} sign(i_q) &\approx i_q sign(i_q) \sqrt{2} (e_{\theta_e}) \\ &\approx \sqrt{2} |i_q| e_{\theta_e} \end{aligned} \quad (2.1.14)$$

Taking into account that $i_{q_{max}} > |i_q|$. Finally, it follows that

$$\Lambda_{\theta} \approx \mu e_{\theta_e} \quad (2.1.15)$$

with $\Lambda_{\theta} = \Lambda_{\theta_1} sign(i_q)$, and $\mu = i_{q_{max}} \sqrt{2}$, where $i_{q_{max}}$ is the maximum value of i_q , according to the nominal current of the machine.

Nevertheless, i_q is not available for measurement. Then, in (2.1.15), i_q will be replaced by the estimated current \hat{i}_q . In fact, \hat{i}_q is obtained from the transformation of the measured currents i_{α} and i_{β} from the stator reference frame to synchronous reference frame as shown by these

equations

$$\begin{bmatrix} \hat{i}_d \\ \hat{i}_q \end{bmatrix} = \mathbb{T}^T(\hat{\theta}_e) \begin{bmatrix} i_\alpha \\ i_\beta \end{bmatrix} \quad (2.1.16)$$

where $\mathbb{T}^T(\hat{\theta}_e) = \begin{bmatrix} \cos(\hat{\theta}_e) & \sin(\hat{\theta}_e) \\ -\sin(\hat{\theta}_e) & \cos(\hat{\theta}_e) \end{bmatrix}$ and since $\hat{\theta}_e$ will be calculated by the proposed observer, then,

$$\hat{i}_q = -\sin(\hat{\theta}_e)i_\alpha + \cos(\hat{\theta}_e)i_\beta \quad (2.1.17)$$

The initial rotor position information is needed for practical implementation to obtain \hat{i}_q . This problem is addressed in the literature by several research works [79–81] and is supposed to be solved. In the experimental implementation, the rotor is moved very slightly by applying short voltage in order to detect the initial rotor position information. Once this information is obtained, the current \hat{i}_q could be calculated using equation (2.1.17). Based on the calculated \hat{i}_q , the rotor position estimation error could be extracted by

$$e_{\theta_e} \approx \frac{\Lambda_\theta}{\mu} = \frac{\Lambda_{\theta_1} \text{sign}(\hat{i}_q)}{\mu} \quad (2.1.18)$$

where Λ_{θ_1} is computed from (2.1.3). In the sequel, (2.1.18) will be used in the observer for estimating the angular position, speed and acceleration.

2.2 Observer design based on a sliding modes approach:

Proposal 1

In this section, an observer is designed by using the sliding mode approach. Consider the following class of nonlinear system given by

$$\begin{aligned}
 \dot{x}_1 &= x_2 \\
 \dot{x}_2 &= x_3 \\
 \dot{x}_3 &= \rho(t) \\
 y &= x_1
 \end{aligned} \tag{2.2.1}$$

where x_1 , x_2 and x_3 are the states, $\rho(t)$ is an unknown and bounded term and $y \in \Re$ the output of the system.

Assumption 2.1. *The term $\rho(t)$ is bounded and unknown, i.e., $|\rho(t)| \leq \varrho_1$ for $\varrho_1 > 0$.*

Now, an observer based on sliding mode for the system (2.2.1) is expressed as follows

$$\begin{aligned}
 \dot{\hat{x}}_1 &= \hat{x}_2 + K_{1,1}|e_1|^{\frac{2}{3}}\text{sign}(e_1) \\
 \dot{\hat{x}}_2 &= \hat{x}_3 + K_{2,1}|e_1|^{\frac{1}{3}}\text{sign}(e_1) \\
 \dot{\hat{x}}_3 &= K_{3,1}\text{sign}(e_1) \\
 \hat{y} &= \hat{x}_1
 \end{aligned} \tag{2.2.2}$$

where \hat{x}_1 , \hat{x}_2 and \hat{x}_3 are the estimated states and \hat{y} is the estimated output. Moreover, the gains for the observer are reparameterized based on a single parameter L_o as follows

$$K_{1,1} = 3L_o^{\frac{5}{3}}, \quad K_{2,1} = 2L_o^{\frac{10}{3}}, \quad K_{3,1} = \left(\frac{4}{9}\right)L_o^5 \tag{2.2.3}$$

where $L_o > 0$ is a constant positive parameter. However, if L_o is too large, it could cause an overestimation and increase the chattering amplitude, causing damage to the actuator. Currently, the design of an adaptive law for the gains is the best alternative to mitigate this

problem.

2.2.1 Adaptive observer design

Now, an adaptive observer will be designed for the system (2.2.1). Then, the following observer

$$\begin{aligned}
 \dot{\hat{x}}_1 &= \hat{x}_2 + \tilde{K}_{1,1}|e_1|^{\frac{2}{3}}\text{sign}(e_1) \\
 \dot{\hat{x}}_2 &= \hat{x}_3 + \tilde{K}_{2,1}|e_1|^{\frac{1}{3}}\text{sign}(e_1) \\
 \dot{\hat{x}}_3 &= \tilde{K}_{3,1}\text{sign}(e_1) \\
 \hat{y} &= \hat{x}_1
 \end{aligned} \tag{2.2.4}$$

is an AHOSMO-1 and its gains are defined as follows

$$\tilde{K}_{1,1} = 3L_o^{\frac{5}{3}}(t), \quad \tilde{K}_{2,1} = 2L_o^{\frac{10}{3}}(t), \quad \tilde{K}_{3,1} = \left(\frac{4}{9}\right)L_o^5(t) \tag{2.2.5}$$

where $L_o(t) > 0$ is an adaptive parameter that will be introduced later.

Remark 2.1: *The demonstration to calculate the proposed gains has been introduced in Appendix A (see A.1.1).*

Taking into account the observer (2.2.4), an analysis of convergence will be introduced and an adaptive law for $L_o(t)$ will be designed. Then, defining the following estimation errors

$$\begin{aligned}
 e_1 &= x_1 - \hat{x}_1 \\
 e_2 &= x_2 - \hat{x}_2 \\
 e_3 &= x_3 - \hat{x}_3
 \end{aligned} \tag{2.2.6}$$

the following dynamics can be calculated

$$\begin{aligned}
 \dot{e}_1 &= e_2 - 3L_o^{\frac{5}{3}}(t)|e_1|^{\frac{2}{3}}\text{sign}(e_1) \\
 \dot{e}_2 &= e_3 - 2L_o^{\frac{10}{3}}(t)|e_1|^{\frac{1}{3}}\text{sign}(e_1) \\
 \dot{e}_3 &= \rho(t) - \left(\frac{2}{3}\right)^2 L_o^5(t)\text{sign}(e_1)
 \end{aligned} \tag{2.2.7}$$

Now, taking into account the dynamics of the estimation errors, the following change of variable is established as follows

$$\zeta_1 = \frac{e_1}{L_o^2(t)}, \quad \zeta_2 = \frac{e_2}{L_o^2(t)}, \quad \zeta_3 = \frac{e_3}{L_o^2(t)} \quad (2.2.8)$$

and taking the first derivative in time, the dynamical system in terms of the new variables is given by

$$\begin{aligned} \dot{\zeta}_1 &= -3L_o(t)|\zeta_1|^{\frac{2}{3}}\text{sign}(\zeta_1) + \zeta_2 - 2\zeta_1 \frac{\dot{L}_o(t)}{L_o(t)} \\ \dot{\zeta}_2 &= -2L_o^2(t)|\zeta_1|^{\frac{1}{3}}\text{sign}(\zeta_1) + \zeta_3 - 2\zeta_2 \frac{\dot{L}_o(t)}{L_o(t)} \\ \dot{\zeta}_3 &= -\left(\frac{2}{3}\right)^2 L_o^3(t)\text{sign}(\zeta_1) + \frac{\rho(t)}{L_o^2(t)} - 2\zeta_3 \frac{\dot{L}_o(t)}{L_o(t)} \end{aligned} \quad (2.2.9)$$

On the other side, the following new change of variable is introduced

$$\xi_1 = |\zeta_1|^{\frac{2}{3}}\text{sign}(\zeta_1), \quad \xi_2 = \frac{\zeta_2}{L_o(t)}, \quad \xi_3 = \frac{3\zeta_3|\zeta_1|^{\frac{1}{3}}}{2L_o^2(t)} \quad (2.2.10)$$

and the dynamical system can be expressed by using the new variables as follows

$$\begin{aligned} \dot{\xi}_1 &= \frac{2L_o(t)}{3|\zeta_1|^{\frac{1}{3}}} [-3\xi_1 + \xi_2] - \frac{4\dot{L}_o(t)}{3L_o(t)}\xi_1 \\ \dot{\xi}_2 &= \frac{2L_o(t)}{3|\zeta_1|^{\frac{1}{3}}} [-3\xi_1 + \xi_3] - \frac{3\dot{L}_o(t)}{L_o(t)}\xi_2 \\ \dot{\xi}_3 &= \frac{2L_o(t)}{3|\zeta_1|^{\frac{1}{3}}} \left[-\xi_1 + \left(\frac{3}{2}\right)^2 \frac{|\zeta_1|^{\frac{2}{3}}\rho(t)}{L_o^5(t)} + \frac{\xi_3}{2|\zeta_1|^{\frac{2}{3}}} (-3\xi_1 + \xi_2) \right] - \frac{14\dot{L}_o(t)}{3L_o(t)}\xi_3 \end{aligned} \quad (2.2.11)$$

The resulting system (2.2.11) can be expressed in the following compact form

$$\dot{\xi} = \alpha_o [(A_o - P_o^{-1}C_o^T C_o) \xi + \Phi_o] - N_o \xi \frac{\dot{L}_o(t)}{L_o(t)} \quad (2.2.12)$$

where $\alpha_o = \frac{2L_o(t)}{3|\zeta_1|^{\frac{1}{3}}}$ and

$$\xi = \begin{bmatrix} \xi_1 \\ \xi_2 \\ \xi_3 \end{bmatrix}, \quad A_o = \begin{bmatrix} 0 & 1 & 0 \\ 0 & 0 & 1 \\ 0 & 0 & 0 \end{bmatrix}, \quad C_o = [1 \ 0 \ 0], \quad P_o = \begin{bmatrix} 1 & -1 & 1 \\ -1 & 2 & -3 \\ 1 & -3 & 6 \end{bmatrix},$$

$$N_o = \begin{bmatrix} \frac{4}{3} & 0 & 0 \\ 0 & 3 & 0 \\ 0 & 0 & \frac{14}{3} \end{bmatrix}, \quad \Phi_o = \begin{bmatrix} 0 \\ 0 \\ \left(\frac{3}{2}\right)^2 \frac{|\zeta_1|^{\frac{2}{3}} \rho(t)}{L_o^5(t)} + \frac{\xi_3}{2|\zeta_1|^{\frac{2}{3}}} (-3\xi_1 + \xi_2) \end{bmatrix}.$$

Assumption 2.2. *The terms in vector Φ_o are locally Lipschitz with respect to ξ [82], i.e., $\|\Phi_o\| \leq \hbar\|\xi\|$, for $\hbar > 0$.*

Moreover, P_o is a symmetric positive-definite matrix, whose solution is given by

$$P_o + A_o^T P_o + P_o A_o - C_o^T C_o = 0$$

Theorem 2.1. *Consider the dynamic system (2.2.1) and the Assumptions 2.1 and 2.2 are satisfied. Furthermore,*

$$\dot{L}_o(t) = \begin{bmatrix} k_o^{\frac{1}{2}} \frac{|e_1|^{\frac{2}{3}}}{L_o^{\frac{1}{3}}(t)} - \gamma_o^{\frac{1}{2}} L_o^2(t) \end{bmatrix} \quad (2.2.13)$$

is an adaptive law-1 of $L_o(t)$, for $\gamma_o > 0$ and $k_o > 0$ chosen appropriately, where $k_o > \gamma_o > 0$. Then, the system (2.2.4) is an Adaptive High Order Sliding Mode Observer (AHOSMO-1) for the dynamic system (2.2.1) such that estimation errors e_i , for $i = 1, 2, 3$; converge to zero in finite time.

Proof

A Lyapunov candidate function is considered as follows

$$V_{(\xi, L_o(t))} = V_{(\xi)} + V_{(L_o(t))} \quad (2.2.14)$$

defining $V_{(\xi)} = \xi^T P_o \xi$ and $V_{(L_o(t))} = \frac{\gamma_o}{2} L_o(t)^2$. Then, considering the Lyapunov candidate function, it is possible to take its first derivative in time and replace the suitable expressions, it follows that

$$\begin{aligned} \dot{V}_{(\xi, L_o)} = & \alpha_o \xi^T [A_o^T P_o + P_o A_o] \xi - 2\alpha_o \xi^T C_o^T C_o \xi - \frac{\dot{L}_o(t)}{L_o(t)} \xi^T [P_o N_o + N_o P_o] \xi \\ & + \gamma_o \dot{L}_o(t) L_o(t) + 2\alpha_o \xi^T P_o \Phi_o \end{aligned} \quad (2.2.15)$$

Taking into account that $A_o^T P_o + P_o A_o = -P_o + C_o^T C_o$. Then, equation (2.2.15) can be rewritten as follows

$$\dot{V}_{(\xi, L_o(t))} = -\alpha_o \xi^T P_o \xi - \alpha_o \xi^T C_o^T C_o \xi - \frac{\dot{L}_o(t)}{L_o(t)} \xi^T [P_o N_o + N_o P_o] \xi + \gamma_o \dot{L}_o(t) L_o(t) + 2\alpha_o \xi^T P_o \Phi_o \quad (2.2.16)$$

Now, taking into account that $P_o N_o + N_o P_o = R_o$, and defining R_o as a symmetric positive-definite matrix. Then, $\xi^T R_o \xi \geq \frac{\lambda_{\min}(R_o)}{\lambda_{\max}(P_o)} V_{(\xi)} = k_o V_{(\xi)}$, where $\lambda_{\min}(R_o)$ and $\lambda_{\max}(P_o)$ are the minimum and maximum singular values of R_o and P_o , respectively. Moreover, $-\alpha_o \xi^T C_o^T C_o \xi < 0$, for $L_o(t) > 0$. Then,

$$\dot{V}_{(\xi, L_o(t))} \leq -\alpha_o V_{(\xi)} - \frac{\dot{L}_o(t)}{L_o(t)} [k_o V_{(\xi)} - \gamma_o L_o^2(t)] + 2\alpha_o \xi^T P_o \Phi_o \quad (2.2.17)$$

Considering that

$$[k_o V_{(\xi)} - \gamma_o L_o^2(t)] = \left[k_o^{\frac{1}{2}} V_{(\xi)}^{\frac{1}{2}} + \gamma_o^{\frac{1}{2}} L_o(t) \right] \left[k_o^{\frac{1}{2}} V_{(\xi)}^{\frac{1}{2}} - \gamma_o^{\frac{1}{2}} L_o(t) \right]$$

and $f_{(V_{(\xi)}, L_o(t))} = \left[k_o^{\frac{1}{2}} V_{(\xi)}^{\frac{1}{2}} + \gamma_o^{\frac{1}{2}} L_o(t) \right] > 0$. Then, equation (2.2.17) is written as

$$\dot{V}_{(\xi, L_o(t))} \leq -\alpha_o V_{(\xi)} - f_{(V_{(\xi)}, L_o(t))} \frac{\dot{L}_o(t)}{L_o(t)} \left[k_o^{\frac{1}{2}} V_{(\xi)}^{\frac{1}{2}} - \gamma_o^{\frac{1}{2}} L_o(t) \right] + 2\alpha_o \xi^T P_o \Phi_o \quad (2.2.18)$$

On the other side, using the following inequalities

$$|\zeta_1|^{\frac{4}{3}} = |\xi_1|^2 \leq \|\xi\|^2 \quad (2.2.19)$$

and

$$\lambda_{\min}(P_o)\|\xi\|^2 \leq V(\xi) \leq \lambda_{\max}(P_o)\|\xi\|^2 \quad (2.2.20)$$

where $\lambda_{\min}(P_o)$ and $\lambda_{\max}(P_o)$ are the minimum and maximum singular values of P_o . Then, the following inequality is satisfied

$$|\zeta_1|^{\frac{2}{3}} \leq \|\xi\| \leq \left(\frac{V(\xi)}{\lambda_{\min}(P_o)} \right)^{\frac{1}{2}} \quad (2.2.21)$$

Therefore, from above inequality, it follows that

$$\dot{V}_{(\xi, L_o(t))} \leq -\alpha_o V(\xi) - f_{(V(\xi), L_o(t))} \frac{\dot{L}_o(t)}{L_o(t)} \left[k_o^{\frac{1}{2}} \frac{|e_1|^{\frac{2}{3}}}{L_o^{\frac{4}{3}}(t)} - \gamma_o^{\frac{1}{2}} L_o(t) \right] + 2\alpha_o \xi^T P_o \Phi_o \quad (2.2.22)$$

Choosing an adaptive law as follows $\dot{L}_o(t) = \left[k_o^{\frac{1}{2}} \frac{|e_1|^{\frac{2}{3}}}{L_o^{\frac{4}{3}}(t)} - \gamma_o^{\frac{1}{2}} L_o(t) \right] L_o(t)$. Then,

$$\dot{V}_{(\xi, L_o(t))} \leq -\alpha_o V(\xi) - f_{(V(\xi), L_o(t))} \left[k_o^{\frac{1}{2}} \frac{|e_1|^{\frac{2}{3}}}{L_o^{\frac{4}{3}}(t)} - \gamma_o^{\frac{1}{2}} L_o(t) \right]^2 + 2\alpha_o \xi^T P_o \Phi_o \quad (2.2.23)$$

Assuming that e_1 tend to zero faster than $L_o(t)$. Equation (2.2.23) is given by

$$\dot{V}_{(\xi, L_o(t))} \leq -\alpha_o V(\xi) - f_{(V(\xi), L_o(t))} [\gamma_o L_o^2(t)] + 2\alpha_o \xi^T P_o \Phi_o \quad (2.2.24)$$

From Assumption 2.2, taking the norm to the nonlinear term $2\alpha_o \xi^T P_o \Phi_o$ and the inequality (2.2.20), then, it follows that

$$\dot{V}_{(\xi, L_o(t))} \leq -\frac{2L_o(t)}{3|\zeta_1|^{\frac{1}{3}}} [1 - \sigma_o] V(\xi) - f_{(V(\xi), L_o(t))} [\gamma_o L_o^2(t)] \quad (2.2.25)$$

where $\sigma_o = \frac{2\|P_o\|\hbar}{\lambda_{\min}(P_o)}$. Furthermore, from $|\zeta_1|^{\frac{2}{3}} = |\xi_1| \leq |\xi|^2 \leq \|\xi\|^2$, the following inequality is satisfied,

$$|\zeta_1|^{\frac{1}{3}} \leq \|\xi\| \leq \left(\frac{V(\xi)}{\lambda_{\min}(P_o)} \right)^{\frac{1}{2}} \quad (2.2.26)$$

Then,

$$\dot{V}_{(\xi, L_o(t))} \leq -L_o(t)\Gamma_o V_{(\xi)}^{\frac{1}{2}} - f_{(V_{(\xi)}, L_o(t))} [\gamma_o L_o^2(t)] \quad (2.2.27)$$

where $\Gamma_o = \frac{2[1 - \sigma_o] \lambda_{\min}^{\frac{1}{2}}(P_o)}{3}$. Rewritten (2.2.27) as follows

$$\dot{V}_{(\xi, L_o(t))} \leq -L_o(t)\sqrt{2}\gamma_o^{\frac{1}{2}} \left[\frac{\Gamma_o}{\sqrt{2}\gamma_o^{\frac{1}{2}}} V_{(\xi)}^{\frac{1}{2}} + f_{(V_{(\xi)}, L_o)} \frac{\gamma_o^{\frac{1}{2}}}{\sqrt{2}} L_o(t) \right] \quad (2.2.28)$$

and defining $\eta_0 = L_o(t)\sqrt{2}\gamma_o^{\frac{1}{2}}$ and $\varphi = \min \left[\frac{\Gamma_o}{\sqrt{2}\gamma_o^{\frac{1}{2}}}, f_{(V_{(\xi)}, L_o(t))} \right]$. It follows that

$$\dot{V}_{(\xi, L_o(t))} \leq -\eta \left[V_{(\xi)}^{\frac{1}{2}} + \frac{\gamma_o^{\frac{1}{2}}}{\sqrt{2}} L_o(t) \right] \quad (2.2.29)$$

where $\eta = \eta_0\varphi$. On the other hand, considering that Jensen's inequality [83] is expressed as follows

$$[|a|^q + |b|^q]^{\frac{1}{q}} \leq |a| + |b| \quad (2.2.30)$$

and defining $a = V_{(\xi)}^{\frac{1}{2}}$, $b = V_{(L_o(t))}^{\frac{1}{2}}$ and $q = 2$. Then, the following inequality is satisfied

$$\left[|V_{(\xi)}^{\frac{1}{2}}|^2 + |V_{(L_o(t))}^{\frac{1}{2}}|^2 \right]^{\frac{1}{2}} \leq |V_{(\xi)}^{\frac{1}{2}}| + \left| \frac{\gamma_o^{\frac{1}{2}}}{\sqrt{2}} L_o(t) \right| \quad (2.2.31)$$

and

$$V_{(\xi, L_o(t))}^{\frac{1}{2}} \leq V_{(\xi)}^{\frac{1}{2}} + \frac{\gamma_o^{\frac{1}{2}}}{\sqrt{2}} L_o(t). \quad (2.2.32)$$

Finally, the Lyapunov dynamic equation is satisfied as follows

$$\dot{V}_{(\xi, L_o(t))} \leq -\eta V_{(\xi, L_o(t))}^{\frac{1}{2}} \quad (2.2.33)$$

As mentioned before, $\dot{V}_{(\xi, L_o(t))}$ is a Lyapunov function, with $L_o(t)$ sufficiently large, satisfying $\eta > 0$. Then, $\dot{V}_{(\xi, L_o(t))}$ is negative definite and can guarantee the convergence of the observer in finite time. On the other side, taking into account the equation $\dot{v} = -\eta v^{\frac{1}{2}}$, whose solution

is defined by $v(t) = (v(0)^{\frac{1}{2}} - \frac{1}{2}\eta t)^2$. Then, the comparison principle can be applied in order to estimate the convergence time T_1 . Therefore, $V_{(\xi, L_o(t))} < v(t)$ when $V_{(\xi(0), L_o(0))} < v(0)$, then ξ has a finite-time convergence in an estimated time defined by $T_1 = \frac{2V_{(\xi(0), L_o(0))}^{\frac{1}{2}}}{\eta}$ for $L_o(t)$ sufficiently large. Thus, $V_{(\xi, L_o(t))}$ tends to zero in finite-time, which involves that the estimation errors e_i , for $i = 1, 2, 3$; tend to zero in finite time.

Remark 2.2. *As can be seen, the system (2.2.12) has a singularity when $e_1 = 0$. The singularity arise due to the change of variable $\xi_1 = |\zeta_1|^{\frac{2}{3}} \text{sign}(\zeta_1)$, $\xi_2 = \frac{\zeta_2}{L_o(t)}$, $\xi_3 = \frac{3\zeta_3|\zeta_1|^{\frac{1}{3}}}{2L_o^2(t)}$; converting system (2.2.7) into system (2.2.12), whose domain is defined as follows $\mathcal{D} = \{(\xi_1, \xi_2, \xi_3) \in \mathbb{R}^3 \mid \xi_1 \neq 0\}$. Nonetheless, considering convergence analysis, the singularity does not appear when the system is expressed in terms of the original coordinates [84, 85].*

2.2.2 Adaptive observer design for the IPMSM

Consider the adaptive law-1 in Theorem 2.1 and the virtual system (1.4.4), then, an adaptive observer based on the virtual system (1.4.4) is designed as follows

$$\begin{aligned}\dot{\hat{\theta}}_e &= \hat{\omega} + \tilde{K}_{1,1}|e_{\theta_e}|^{\frac{2}{3}} \text{sign}(e_{\theta_e}) \\ \dot{\hat{\omega}} &= \hat{\alpha} + \tilde{K}_{2,1}|e_{\theta_e}|^{\frac{1}{3}} \text{sign}(e_{\theta_e}) \\ \dot{\hat{\alpha}} &= \tilde{K}_{3,1} \text{sign}(e_{\theta_e})\end{aligned}\tag{2.2.34}$$

where $\hat{\theta}_e$, $\hat{\omega}$ and $\hat{\alpha}$ are the estimation of electrical angular position, electrical speed and acceleration, respectively. However, θ_e is not measured directly, such that, the observer (2.2.34) cannot be implemented. Therefore, considering the methodology to extract e_{θ_e} introduced in section 2.1, then, Λ_{θ} can be expressed in terms of the estimation error e_{θ_e} as $\Lambda_{\theta} = \mu e_{\theta_e}$, with $\mu > 0$. Thus, $e_{\theta_e} = \theta_e - \hat{\theta}_e$ can be replaced by $\theta_e - \hat{\theta}_e = \frac{\Lambda_{\theta}}{\mu}$ into the observer (2.2.34), *i.e.*, the

AHOSMO-1 for the IPMSM is given by

$$\begin{aligned}
 \dot{\hat{\theta}}_e &= \hat{\omega} + \tilde{K}_{1,1} \left| \frac{\Lambda_\theta}{\mu} \right|^{\frac{2}{3}} \text{sign}\left(\frac{\Lambda_\theta}{\mu}\right) \\
 \dot{\hat{\omega}} &= \hat{\alpha} + \tilde{K}_{2,1} \left| \frac{\Lambda_\theta}{\mu} \right|^{\frac{1}{3}} \text{sign}\left(\frac{\Lambda_\theta}{\mu}\right) \\
 \dot{\hat{\alpha}} &= \tilde{K}_{3,1} \text{sign}\left(\frac{\Lambda_\theta}{\mu}\right)
 \end{aligned} \tag{2.2.35}$$

Then, the observer (2.2.35) is used to estimate the angular position, speed and acceleration. As previously mentioned, $\hat{\theta} = \frac{\hat{\theta}_e}{p}$ is the estimated mechanical angular position and $\hat{\Omega} = \frac{\hat{\omega}}{p}$ is the mechanical speed. In Figure 2.2, a scheme of the proposed AHOSMO-1 (2.2.35) is introduced. In addition, in Figure 2.3 a flowchart is presented in order to show the interconnection among

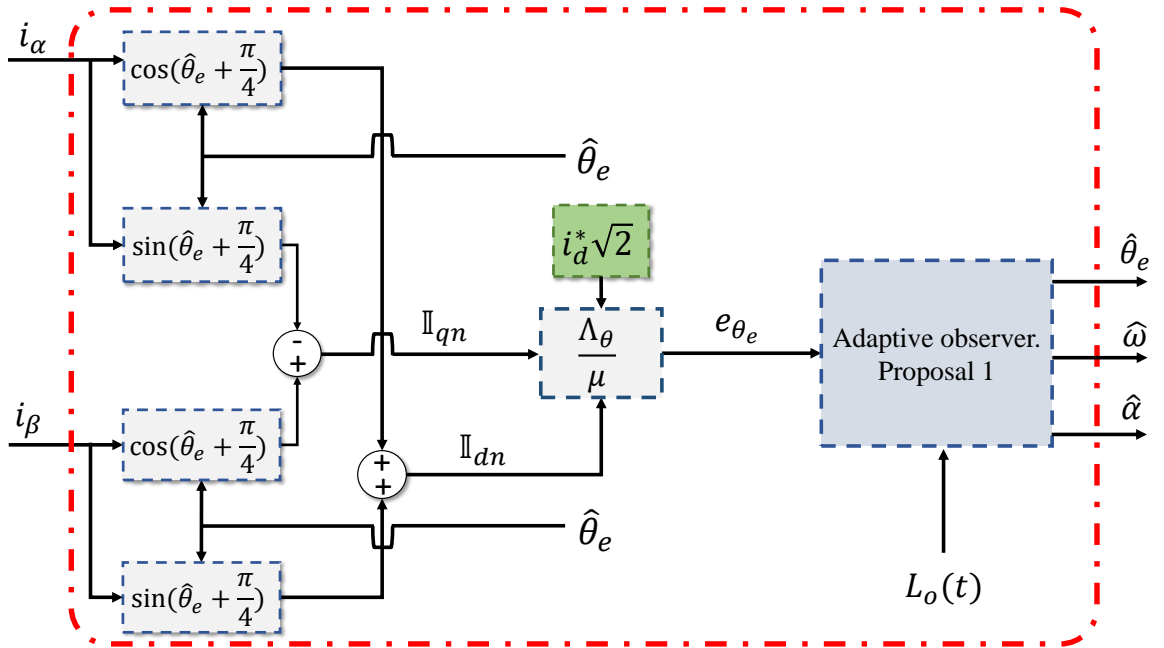


Figure 2.2: Scheme of the proposed AHOSMO-1.

the extraction of the angular error and the adaptive observer in the system.

2.2.3 Simulation results

In this section, a simulation result is presented to show the AHOSMO-1 performance in open-loop. Simulation test has been carried out in Matlab-Simulink environment, using a sampling

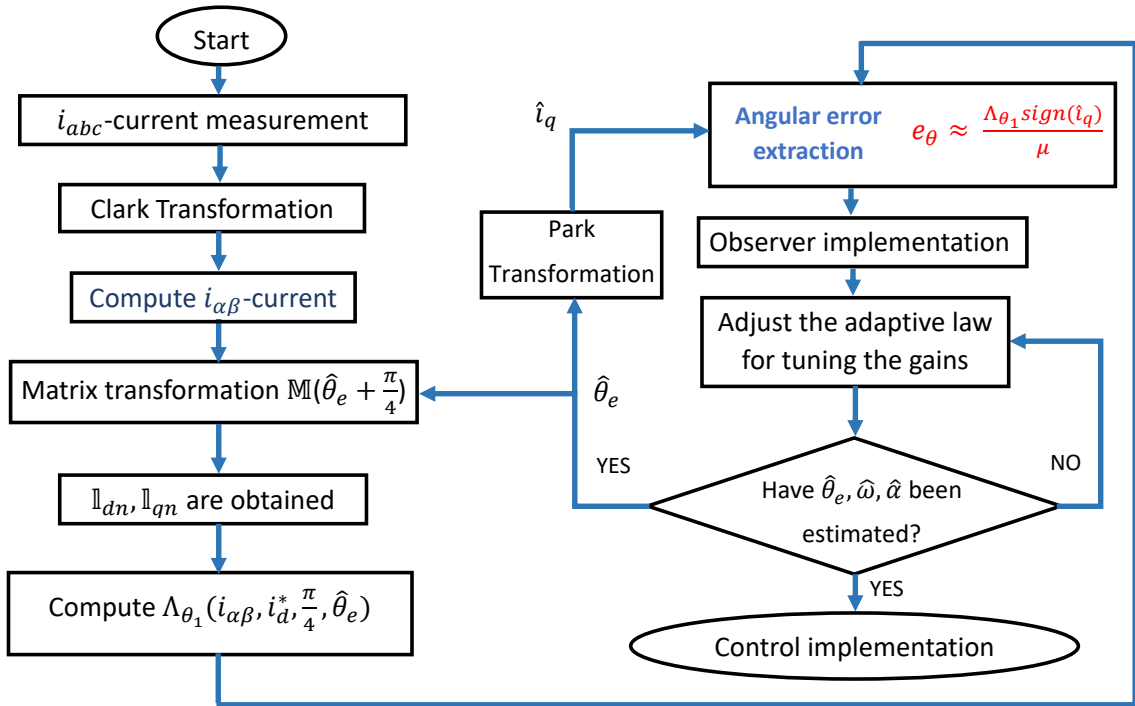


Figure 2.3: Flowchart for the proposed strategy.

time of 1×10^{-3} with a fixed-step *ode4* solver. Moreover, the test has been made by considering the profiles and parametric uncertainties given by Figure 1.7 and Figure 1.8, respectively. The parameters of the adaptive observer are given in Table 2.1. In Figure 2.4, the estimation of the

Table 2.1: Parameters for AHOSMO-1

Values		
$L_o(0)$	γ_0	k_o
1.5	0.003	120

angular position is given. It is possible to see that observer has a good performance during the estimation.

In Figure 2.5 the speed estimation and its estimation error are shown. The speed estimation error shows that the observer is not affected by parametric uncertainties. Moreover, thanks to the estimation of the acceleration [see Figure 2.6-a)], a minimum error can be seen during speed profile change. This error is caused by the fast dynamic in the speed, for this reason, the

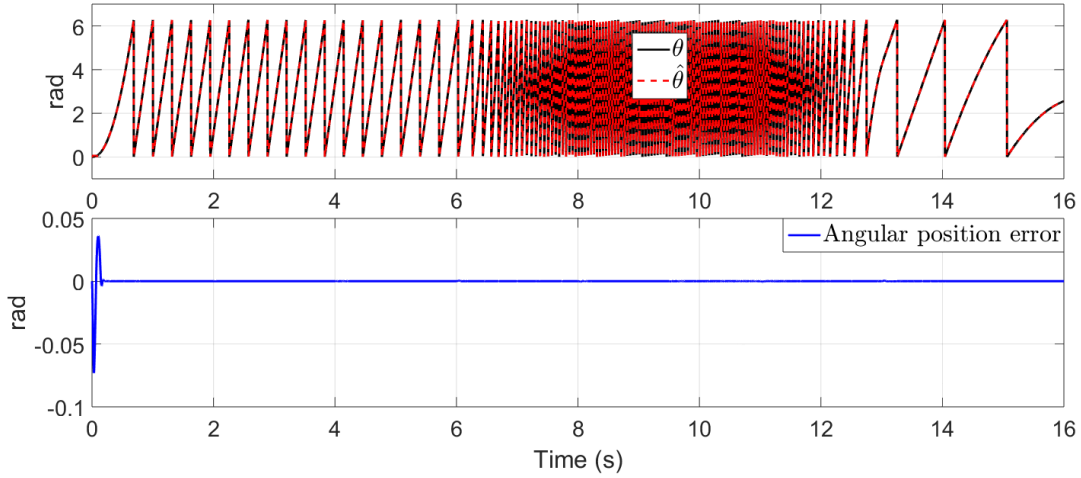


Figure 2.4: AHOSMO-1. Rotor angular position estimation and its estimation error

acceleration estimation has been included to compensate those errors in fast transient modes, minimizing the estimation error.

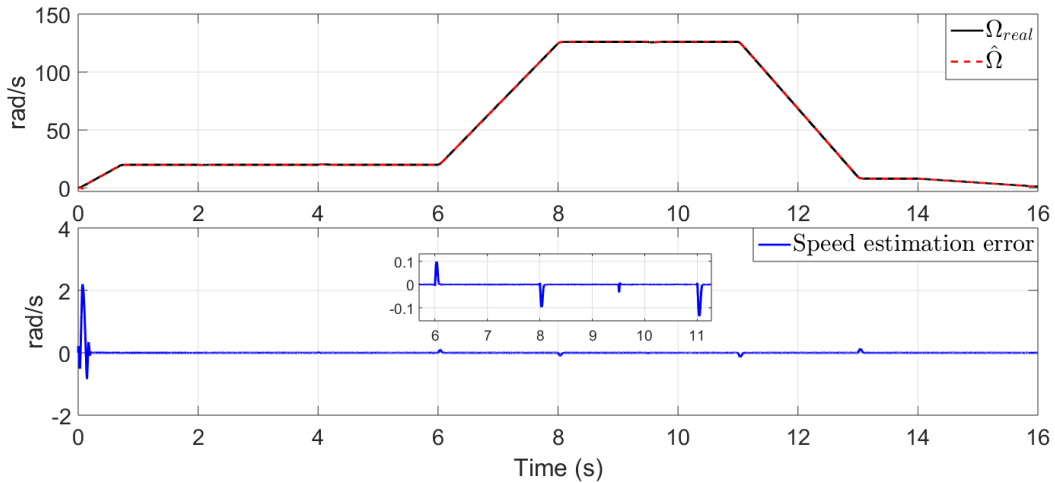


Figure 2.5: AHOSMO-1. Rotor speed estimation and speed estimation error

On the other hand, in Figure 2.6-b), the behaviour of adaptive law for the observer is shown, which takes values in order to achieve a good estimation of the observer avoiding overestimation of gain. Therefore, in this open-loop test for the first adaptive observer, good results have been obtained by simulation.

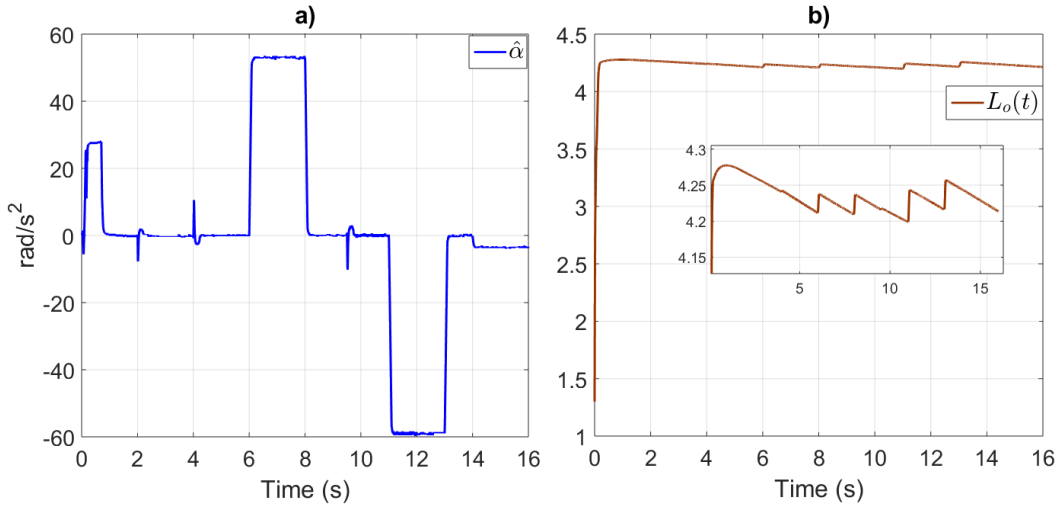


Figure 2.6: AHOSMO-1. Estimation of acceleration (a) and behaviour of the adaptive law (b)

2.3 Observer design based on a sliding modes approach:

Proposal 2

In this section, a second observer is designed for a class of nonlinear system given by (2.2.1). Then, an observer for the system (2.2.1) is expressed as follows

$$\begin{aligned}
 \dot{\hat{x}}_{1_2} &= \hat{x}_2 + K_{1,2}|e_{1_2}|^{\frac{2}{3}}\text{sign}(e_{1_2}) \\
 \dot{\hat{x}}_{2_2} &= \hat{x}_3 + K_{2,2}|e_{1_2}|^{\frac{1}{3}}\text{sign}(e_{1_2}) \\
 \dot{\hat{x}}_{3_2} &= K_{3,2}\text{sign}(e_{1_2}) \\
 \hat{y} &= \hat{x}_{1_2}
 \end{aligned} \tag{2.3.1}$$

where \hat{x}_{1_2} , \hat{x}_{2_2} and \hat{x}_{3_2} represent the estimated states and \hat{y} is the estimated output. Moreover, the gains for the observer are reparameterized in terms of L_{o_2} as follows

$$K_{1,2} = 3L_{o_2} \quad K_{2,2} = 2L_{o_2}^2 \quad K_{3,2} = \left(\frac{2}{3}\right)^2 L_{o_2}^3 \tag{2.3.2}$$

where $L_{o_2} > 0$ is a constant positive parameter. However, if L_{o_2} is too large, it could cause an overestimation and increase the chattering amplitude, causing damage to the actuator. For

this reason, in the next section, an adaptive law for the gains will be designed.

2.3.1 Adaptive observer design

Now, a second adaptive observer is proposed for the system (2.2.1). The main difference with respect to the first adaptive observer (AHOSMO-1) is the reduction of the change of coordinates during the proof, which helps to simplify the calculations during the analysis, obtaining a new adaptive law for the observer with a new gain reparameterization.

Consider the following system

$$\begin{aligned}
 \dot{\hat{x}}_{1_2} &= \hat{x}_2 + \tilde{K}_{1,2}|e_{1_2}|^{\frac{2}{3}} \text{sign}(e_{1_2}) \\
 \dot{\hat{x}}_{2_2} &= \hat{x}_3 + \tilde{K}_{2,2}|e_{1_2}|^{\frac{1}{3}} \text{sign}(e_{1_2}) \\
 \dot{\hat{x}}_{3_2} &= \tilde{K}_{3,2} \text{sign}(e_{1_2}) \\
 \hat{y} &= \hat{x}_{1_2}
 \end{aligned} \tag{2.3.3}$$

which is an AHOSMO-2 and its reparameterized gains in terms of a single parameter are defined by

$$\tilde{K}_{1,2} = 3L_{o_2}(t) \quad \tilde{K}_{2,2} = 2L_{o_2}^2(t) \quad \tilde{K}_{3,2} = \left(\frac{2}{3}\right)^2 L_{o_2}^3(t) \tag{2.3.4}$$

where $L_{o_2}(t)$ is an adaptive parameter that will be introduced later.

Remark 2.3: *The demonstration to compute the proposed gains has been introduced in Appendix A (See A.1.2).*

Now, an analysis of convergence for the observer (2.3.3) and an adaptive law for the parameter $L_{o_2}(t)$ are introduced. Then, consider the following estimation errors

$$e_{1_2} = x_1 - \hat{x}_{1_2}, \quad e_{2_2} = x_2 - \hat{x}_{2_2}, \quad e_{3_2} = x_3 - \hat{x}_{3_2} \tag{2.3.5}$$

and their dynamics as follows

$$\begin{aligned}
 \dot{e}_{12} &= e_{22} - 3L_{o2}(t)|e_{12}|^{\frac{2}{3}}\text{sign}(e_{12}) \\
 \dot{e}_{22} &= e_{32} - 2L_{o2}^2(t)|e_{12}|^{\frac{1}{3}}\text{sign}(e_{12}) \\
 \dot{e}_{32} &= \rho(t) - \left(\frac{2}{3}\right)^2 L_{o2}^3(t)\text{sign}(e_{12})
 \end{aligned} \tag{2.3.6}$$

Now, a change of variable is introduced as follows

$$\xi_{12} = \frac{|e_{12}|^{\frac{2}{3}}\text{sign}(e_{12})}{L_{o2}(t)} \quad \xi_{22} = \frac{e_{22}}{L_{o2}^2(t)} \quad \xi_{32} = \frac{3e_{32}|e_{12}|^{\frac{1}{3}}}{2L_{o2}^3(t)} \tag{2.3.7}$$

Then, it follows that the dynamical system can be expressed by using the new variables. Therefore, the following system can be obtained

$$\begin{aligned}
 \dot{\xi}_{12} &= \frac{2L_{o2}(t)}{3|e_{12}|^{\frac{1}{3}}} [-3\xi_{12} + \xi_{22}] - \frac{\dot{L}_{o2}(t)}{L_{o2}(t)} \xi_{12} \\
 \dot{\xi}_{22} &= \frac{2L_{o2}(t)}{3|e_{12}|^{\frac{1}{3}}} [-3\xi_{12} + \xi_{32}] - \frac{2\dot{L}_{o2}(t)}{L_{o2}(t)} \xi_{22} \\
 \dot{\xi}_{32} &= \frac{2L_{o2}(t)}{3|e_{12}|^{\frac{1}{3}}} \left[-\xi_{12} + \left(\frac{3}{2}\right)^2 \frac{|e_{12}|^{\frac{2}{3}}\rho(t)}{L_{o2}^4(t)} + \frac{L_{o2}(t)\xi_{32}}{2|e_{12}|^{\frac{2}{3}}} [-3\xi_{12} + \xi_{22}] \right] - \frac{3\dot{L}_{o2}(t)}{L_{o2}(t)} \xi_{32}
 \end{aligned} \tag{2.3.8}$$

and can be simplified as follows

$$\dot{\xi}_{o2} = \alpha_{o2} [(A_o - P_o^{-1}C_o^T C_o) \xi_{o2} + \Phi_{o2}] - D_{o2} \xi_{o2} \frac{\dot{L}_{o2}(t)}{L_{o2}(t)} \tag{2.3.9}$$

defining $\alpha_{o2} = \frac{2L_{o2}(t)}{3|e_{12}|^{\frac{1}{3}}}$ and the following terms as follows

$$\xi_{o2} = \begin{bmatrix} \xi_{12} \\ \xi_{22} \\ \xi_{32} \end{bmatrix}, \quad A_o = \begin{bmatrix} 0 & 1 & 0 \\ 0 & 0 & 1 \\ 0 & 0 & 0 \end{bmatrix}, \quad C_o = [1 \quad 0 \quad 0], \quad P_o = \begin{bmatrix} 1 & -1 & 1 \\ -1 & 2 & -3 \\ 1 & -3 & 6 \end{bmatrix}, \tag{2.3.10}$$

$$D_{o_2} = \begin{bmatrix} 1 & 0 & 0 \\ 0 & 2 & 0 \\ 0 & 0 & 3 \end{bmatrix}, \quad \Phi_{o_2} = \begin{bmatrix} 0 \\ 0 \\ \left(\frac{3}{2}\right)^2 \frac{|e_{1_2}|^{\frac{2}{3}} \rho(t)}{L_{o_2}^4(t)} + \frac{L_{o_2}(t) \xi_{3_2}}{2|e_{1_2}|^{\frac{2}{3}}} [-3\xi_{1_2} + \xi_{2_2}] \end{bmatrix}. \quad (2.3.11)$$

Assumption 2.3. *The term in the vector Φ_{o_2} is locally Lipschitz with respect to ξ_{o_2} [82], i.e., $\|\Phi_{o_2}\| \leq \hbar_2 \|\xi_{o_2}\|$, for $\hbar_2 > 0$.*

Moreover, P_o is a symmetric positive-definite matrix, whose solution is given by

$$P_o + A_o^T P_o + P_o A_o - C_o^T C_o = 0 \quad (2.3.12)$$

Theorem 2.2. *Consider the dynamic system (2.2.1) and the Assumptions 2.1 and 2.3 are satisfied. Furthermore,*

$$\dot{L}_{o_2}(t) = \left[k_{o_2}^{\frac{1}{2}} |e_{1_2}|^{\frac{2}{3}} - \gamma_{o_2}^{\frac{1}{2}} L_{o_2}^2(t) \right] \quad (2.3.13)$$

is an adaptive law-2 of $L_{o_2}(t)$, for $\gamma_{o_2} > 0$ and $k_{o_2} > 0$ chosen appropriately, where $k_{o_2} > \gamma_{o_2} > 0$. Then, the system (2.3.3) is an Adaptive High-Order Sliding Mode Observer (AHOSMO-2) for the dynamic system (2.2.1) such that estimation errors e_{i_2} , for $i = 1, 2, 3$; converge to zero in finite time.

Proof

A Lyapunov candidate function is considered as follows

$$V_{(\xi_{o_2}, L_{o_2}(t))} = V_{(\xi_{o_2})} + V_{(L_{o_2}(t))} \quad (2.3.14)$$

defining $V_{(\xi_{o_2})} = \xi_{o_2}^T P_o \xi_{o_2}$ and $V_{(L_{o_2}(t))} = \frac{\gamma_{o_2}}{2} L_{o_2}^2(t)$. Then, considering the Lyapunov candidate function, it is possible to take its first derivative in time and replace the suitable expressions, it follows that

$$\begin{aligned} \dot{V}_{(\xi_{o_2}, L_{o_2}(t))} &= \alpha_{o_2} \xi_{o_2}^T [A_o^T P_o + P_o A_o] \xi_{o_2} - 2\alpha_{o_2} \xi_{o_2}^T C_o^T C_o \xi_{o_2} \\ &\quad - 2 \frac{\dot{L}_{o_2}(t)}{L_{o_2}(t)} \xi_{o_2}^T P_o D_{o_2} \xi_{o_2} + \gamma_{o_2} \dot{L}_{o_2}(t) L_{o_2}(t) + 2\alpha_{o_2} \xi_{o_2}^T P_o \Phi_{o_2} \end{aligned} \quad (2.3.15)$$

Taking into account that $A_o^T P_o + P_o A_o = -P_o + C_o^T C_o$. Then, equation (2.3.15) can be rewritten as follows

$$\begin{aligned} \dot{V}_{(\xi_{o_2}, L_{o_2}(t))} = & -\alpha_{o_2} \xi_{o_2}^T P_o \xi_{o_2} - \alpha_{o_2} \xi_{o_2}^T C_o^T C_o \xi_{o_2} - 2 \frac{\dot{L}_{o_2}(t)}{L_{o_2}(t)} \xi_{o_2}^T P_o D_{o_2} \xi_{o_2} \\ & + \gamma_{o_2} \dot{L}_{o_2}(t) L_{o_2}(t) + 2\alpha_{o_2} \xi_{o_2}^T P_o \Phi_{o_2} \end{aligned} \quad (2.3.16)$$

On the other hand, using the following inequalities

$$\frac{|e_{1_2}|^{\frac{4}{3}}}{L_{o_2}^2(t)} = |\xi_{1_2}|^2 \leq \|\xi_{o_2}\|^2 \quad (2.3.17)$$

and

$$\lambda_{\min}(P_o) \|\xi_{o_2}\|^2 \leq V_{(\xi_{o_2})} \leq \lambda_{\max}(P_o) \|\xi_{o_2}\|^2 \quad (2.3.18)$$

where $\lambda_{\min}(P_o)$ and $\lambda_{\max}(P_o)$ are the minimum and maximum singular values of P_o . Moreover,

$$\lambda_{\min}(P_o D_{o_2}) \|\xi_{o_2}\|^2 \leq \xi_{o_2}^T P_o D_{o_2} \xi_{o_2} \leq \lambda_{\max}(P_o D_{o_2}) \|\xi_{o_2}\|^2 \quad (2.3.19)$$

where $\lambda_{\min}(P_o D_{o_2})$ and $\lambda_{\max}(P_o D_{o_2})$ are the minimum and maximum singular values of $P_o D_{o_2}$.

Then,

$$\begin{aligned} \dot{V}_{(\xi_{o_2}, L_{o_2}(t))} \leq & -\alpha_{o_2} \xi_{o_2}^T P_o \xi_{o_2} - \alpha_{o_2} \xi_{o_2}^T C_o^T C_o \xi_{o_2} - 2\lambda_{\min}(P_o D_{o_2}) \|\xi_{o_2}\|^2 \frac{\dot{L}_{o_2}(t)}{L_{o_2}(t)} \\ & + \gamma_{o_2} \dot{L}_{o_2}(t) L_{o_2}(t) + 2\alpha_{o_2} \xi_{o_2}^T P_o \Phi_{o_2} \end{aligned} \quad (2.3.20)$$

In this way,

$$\begin{aligned} \dot{V}_{(\xi_{o_2}, L_{o_2}(t))} \leq & -\alpha_{o_2} \xi_{o_2}^T P_o \xi_{o_2} - \alpha_{o_2} \xi_{o_2}^T C_o^T C_o \xi_{o_2} - k_{o_2} \|\xi_{o_2}\|^2 \frac{\dot{L}_{o_2}(t)}{L_{o_2}(t)} \\ & + \gamma_{o_2} \dot{L}_{o_2}(t) L_{o_2}(t) + 2\alpha_{o_2} \xi_{o_2}^T P_o \Phi_{o_2} \end{aligned} \quad (2.3.21)$$

where $k_{o_2} = 2\lambda_{\min}(P_o D_{o_2}) > 0$. The above equation can be established as follows

$$\begin{aligned} \dot{V}_{(\xi_{o_2}, L_{o_2}(t))} &\leq -\alpha_{o_2} \xi_{o_2}^T P_o \xi_{o_2} - \alpha_{o_2} \xi_{o_2}^T C_o^T C_o \xi_{o_2} + 2\alpha_{o_2} \xi_{o_2}^T P_o \Phi_{o_2} \\ &\quad - \frac{\dot{L}_{o_2}(t)}{L_{o_2}(t)} [k_{o_2} \|\xi_{o_2}\|^2 - \gamma_{o_2} L_{o_2}^2(t)] \end{aligned} \quad (2.3.22)$$

Now, the last term of the above equation can be expressed as follows

$$\frac{\dot{L}_{o_2}(t)}{L_{o_2}(t)} [k_{o_2} \|\xi_{o_2}\|^2 - \gamma_{o_2} L_{o_2}^2(t)] = \frac{\dot{L}_{o_2}(t)}{L_{o_2}(t)} \left[k_{o_2}^{\frac{1}{2}} \|\xi_{o_2}\| + \gamma_{o_2}^{\frac{1}{2}} L_{o_2}(t) \right] \left[k_{o_2}^{\frac{1}{2}} \|\xi_{o_2}\| - \gamma_{o_2}^{\frac{1}{2}} L_{o_2}(t) \right] \quad (2.3.23)$$

and $f_{(\xi_{o_2}, L_{o_2}(t))} = \left[k_{o_2}^{\frac{1}{2}} \|\xi_{o_2}\| + \gamma_{o_2}^{\frac{1}{2}} L_{o_2}(t) \right] > 0$. Then,

$$\begin{aligned} \dot{V}_{(\xi_{o_2}, L_{o_2}(t))} &\leq -\alpha_{o_2} \xi_{o_2}^T P_o \xi_{o_2} - \alpha_{o_2} \xi_{o_2}^T C_o^T C_o \xi_{o_2} + 2\alpha_{o_2} \xi_{o_2}^T P_o \Phi_{o_2} \\ &\quad - f_{(\xi_{o_2}, L_{o_2}(t))} \frac{\dot{L}_{o_2}(t)}{L_{o_2}(t)} \left[k_{o_2}^{\frac{1}{2}} \|\xi_{o_2}\| - \gamma_{o_2}^{\frac{1}{2}} L_{o_2}(t) \right] \end{aligned} \quad (2.3.24)$$

From inequalities (2.3.17) and (2.3.18), the following inequality is satisfied

$$\frac{|e_{12}|^{\frac{2}{3}}}{L_{o_2}(t)} \leq \|\xi_{o_2}\| \leq \left(\frac{V_{(\xi_{o_2})}}{\lambda_{\min}(P_o)} \right)^{\frac{1}{2}} \quad (2.3.25)$$

Then, from (2.3.25), it follows that

$$\begin{aligned} \dot{V}_{(\xi_{o_2}, L_{o_2}(t))} &\leq -\alpha_{o_2} V_{(\xi_{o_2})} - \alpha_{o_2} \xi_{o_2}^T C_o^T C_o \xi_{o_2} + 2\alpha_{o_2} \xi_{o_2}^T P_o \Phi_{o_2} \\ &\quad - f_{(\xi_{o_2}, L_{o_2}(t))} \frac{\dot{L}_{o_2}(t)}{L_{o_2}(t)} \left[k_{o_2}^{\frac{1}{2}} \frac{|e_{12}|^{\frac{2}{3}}}{L_{o_2}(t)} - \gamma_{o_2}^{\frac{1}{2}} L_{o_2}(t) \right] \end{aligned} \quad (2.3.26)$$

Choosing an adaptive law as follows

$$\dot{L}_{o_2}(t) = \left[k_{o_2}^{\frac{1}{2}} \frac{|e_{12}|^{\frac{2}{3}}}{L_{o_2}(t)} - \gamma_{o_2}^{\frac{1}{2}} L_{o_2}(t) \right] L_{o_2}(t) \quad (2.3.27)$$

Then,

$$\dot{V}_{(\xi_{o_2}, L_{o_2}(t))} \leq -\alpha_{o_2} V_{(\xi_{o_2})} - \alpha_{o_2} \xi_{o_2}^T C_o^T C_o \xi_{o_2} - f_{(\xi_{o_2}, L_{o_2}(t))} \left[k^{\frac{1}{2}} \frac{|e_{1_2}|^{\frac{2}{3}}}{L_{o_2}(t)} - \gamma_{o_2}^{\frac{1}{2}} L_{o_2}(t) \right]^2 + 2\alpha_{o_2} \xi_{o_2}^T P_o \Phi_{o_2} \quad (2.3.28)$$

and assuming that e_{1_2} tend to zero faster than $L_{o_2}(t)$, and $-\alpha_{o_2} \xi_{o_2}^T C_o^T C_o \xi_{o_2} < 0$, for $L_{o_2}(t) > 0$.

Equation (2.3.28) is given by

$$\dot{V}_{(\xi_{o_2}, L_{o_2}(t))} \leq -\alpha_{o_2} V_{(\xi_{o_2})} - f_{(\xi_{o_2}, L_{o_2}(t))} [\gamma_{o_2} L_{o_2}^2(t)] + 2\alpha_{o_2} \xi_{o_2}^T P_o \Phi_{o_2} \quad (2.3.29)$$

Taking the norm to the nonlinear term $2\alpha_{o_2} \xi_{o_2}^T P_o \Phi_{o_2}$ and from Assumption 2.3, then (2.3.29) is given by

$$\dot{V}_{(\xi_{o_2}, L_{o_2}(t))} \leq -\alpha_{o_2} V_{(\xi_{o_2})} + 2\alpha_{o_2} \|\xi_{o_2}\|^2 \|P_o\| \bar{h}_2 - f_{(\xi_{o_2}, L_{o_2}(t))} [\gamma_{o_2} L_{o_2}^2(t)] \quad (2.3.30)$$

Now, from inequality (2.3.18). Then, it follows that

$$\dot{V}_{(\xi_{o_2}, L_{o_2}(t))} \leq -\frac{2L_{o_2}(t)}{3|e_{1_2}|^{\frac{1}{3}}} [1 - \sigma_{o_2}] V_{(\xi_{o_2})} - f_{(\xi_{o_2}, L_{o_2}(t))} [\gamma_{o_2} L_{o_2}^2(t)] \quad (2.3.31)$$

where $\sigma_{o_2} = \frac{2\|P_o\|\bar{h}_2}{\lambda_{max}(P_o)}$. Furthermore, from $\frac{|e_{1_2}|^{\frac{2}{3}}}{L_{o_2}(t)} = |\xi_{1_2}| \leq |\xi_{1_2}|^2 \leq \|\xi_{o_2}\|^2$, the following inequality is satisfied

$$\frac{|e_{1_2}|^{\frac{1}{3}}}{L_{o_2}^{\frac{1}{2}}(t)} \leq \|\xi_{o_2}\| \leq \left(\frac{V_{(\xi_{o_2})}}{\lambda_{min}(P_o)} \right)^{\frac{1}{2}} \quad (2.3.32)$$

and considering that (2.3.31) can be written as follows

$$\dot{V}_{(\xi_{o_2}, L_{o_2}(t))} \leq -\frac{2L_{o_2}(t)}{\frac{3|e_{1_2}|^{\frac{1}{3}} L_{o_2}^{\frac{1}{2}}(t)}{L_{o_2}^{\frac{1}{2}}(t)}} [1 - \sigma_{o_2}] V_{(\xi_{o_2})} - f_{(\xi_{o_2}, L_{o_2}(t))} [\gamma_{o_2} L_{o_2}^2(t)] \quad (2.3.33)$$

Then,

$$\dot{V}_{(\xi_{o_2}, L_{o_2}(t))} \leq -L_{o_2}^{\frac{1}{2}}(t) \Gamma_{o_2} V_{(\xi_{o_2})}^{\frac{1}{2}} - f_{(\xi_{o_2}, L_{o_2}(t))} [\gamma_{o_2} L_{o_2}^2(t)] \quad (2.3.34)$$

where $\Gamma_{o_2} = \frac{2[1 - \sigma_{o_2}] \lambda_{\min}^{\frac{1}{2}}(P_o)}{3}$. Rewritten (2.3.34) as follows

$$\dot{V}_{(\xi_{o_2}, L_{o_2}(t))} \leq -L_{o_2}(t) \sqrt{2} \gamma_{o_2}^{\frac{1}{2}} \left[\frac{\Gamma_{o_2}}{\sqrt{2} \gamma_{o_2}^{\frac{1}{2}} L_{o_2}^{\frac{1}{2}}(t)} V_{(\xi_{o_2})}^{\frac{1}{2}} + f_{(\xi_{o_2}, L_{o_2}(t))} \frac{\gamma_{o_2}^{\frac{1}{2}}}{\sqrt{2}} L_{o_2}(t) \right] \quad (2.3.35)$$

and defining $\eta_{0_2} = L_{o_2}(t) \sqrt{2} \gamma_{o_2}^{\frac{1}{2}}$ and $\varphi_{o_2} = \min \left(\frac{\Gamma_{o_2}}{\sqrt{2} \gamma_{o_2}^{\frac{1}{2}} L_{o_2}^{\frac{1}{2}}(t)}, f_{(\xi_{o_2}, L_{o_2}(t))} \right)$. We can write the following equation

$$\dot{V}_{(\xi_{o_2}, L_{o_2}(t))} \leq -\tilde{\eta} \left[V_{(\xi_{o_2})}^{\frac{1}{2}} + \frac{\gamma_{o_2}^{\frac{1}{2}}}{\sqrt{2}} L_{o_2}(t) \right] \quad (2.3.36)$$

where $\tilde{\eta} = \eta_{0_2} \varphi_{o_2}$. On the other hand, considering that Jensen's inequality [83] is expressed as follows

$$\left[|a_{o_2}|^q + |b_{o_2}|^q \right]^{\frac{1}{q}} \leq |a_{o_2}| + |b_{o_2}| \quad (2.3.37)$$

and defining $a_{o_2} = V_{(\xi_{o_2})}^{\frac{1}{2}}$, $b_{o_2} = \frac{\gamma_{o_2}^{\frac{1}{2}}}{\sqrt{2}} L_{o_2}(t)$ and $q = 2$. Then, the following inequality is satisfied

$$\left[|V_{(\xi_{o_2})}^{\frac{1}{2}}|^2 + \left| \frac{\gamma_{o_2}^{\frac{1}{2}}}{\sqrt{2}} L_{o_2}(t) \right|^2 \right]^{\frac{1}{2}} \leq |V_{(\xi_{o_2})}^{\frac{1}{2}}| + \left| \frac{\gamma_{o_2}^{\frac{1}{2}}}{\sqrt{2}} L_{o_2}(t) \right| \quad (2.3.38)$$

such that

$$V_{(\xi_{o_2}, L_{o_2}(t))}^{\frac{1}{2}} \leq V_{(\xi_{o_2})}^{\frac{1}{2}} + \frac{\gamma_{o_2}^{\frac{1}{2}}}{\sqrt{2}} L_{o_2}(t) \quad (2.3.39)$$

Finally, the Lyapunov dynamic equation is satisfied as follows

$$\dot{V}_{(\xi_{o_2}, L_{o_2}(t))} \leq -\tilde{\eta} V_{(\xi_{o_2}, L_{o_2}(t))}^{\frac{1}{2}} \quad (2.3.40)$$

As mentioned before, $\dot{V}_{(\xi_{o_2}, L_{o_2}(t))}$ is a Lyapunov function, with $L_{o_2}(t)$ sufficiently large, satisfying $\tilde{\eta} > 0$. Then, $\dot{V}_{(\xi_{o_2}, L_{o_2}(t))}$ is negative definite and can guarantee the convergence of the observer in finite time. On the other side, taking into account the equation $\dot{v} = -\tilde{\eta} v^{\frac{1}{2}}$, whose solution is defined by $v(t) = (v(0)^{\frac{1}{2}} - \frac{1}{2} \tilde{\eta} t)^2$. Then, the comparison principle can be applied in order to estimate the convergence time T_{1_2} . Therefore, $V_{(\xi_{o_2}, L_{o_2}(t))} < v(t)$ when $V_{(\xi_{o_2}(0), L_{o_2}(0))} < v(0)$, then

ξ_{o_2} has a finite-time convergence in an estimated time defined by

$$T_{1_2} = \frac{2V_{(\xi_{o_2}(0), L_{o_2}(0))}^{\frac{1}{2}}}{\tilde{\eta}}$$

for $L_{o_2}(t)$ sufficiently large. Thus, $V_{(\xi_{o_2}, L_{o_2}(t))}$ tends to zero in finite-time, which involves that the estimation errors e_{i_2} , for $i = 1, 2, 3$; tend to zero in finite time.

Remark 2.4. *As we can see, the system (2.3.9) has a singularity when $e_1 = 0$. The singularity arise due to the change of variable*

$$\xi_{1_2} = \frac{|e_{1_2}|^{\frac{2}{3}} \text{sign}(e_{1_2})}{L_{o_2}(t)}, \quad \xi_{2_2} = \frac{e_{2_2}}{L_{o_2}^2(t)}, \quad \xi_{3_2} = \frac{3e_{3_2}|e_{1_2}|^{\frac{1}{3}}}{2L_{o_2}^3(t)}$$

converting system (2.3.6) into system (2.3.9), whose domain is defined as follows

$$\mathcal{D}_\epsilon = \{(\xi_{1_2}, \xi_{2_2}, \xi_{3_2}) \in \mathbb{R}^3 \mid \xi_{1_2} \neq 0\}.$$

Nonetheless, considering convergence analysis, the singularity does not appear when the system is expressed in terms of the original coordinates (see for more details [84, 85]).

2.3.2 Adaptive observer design for the IPMSM

Consider the adaptive law-2 in Theorem 2.2 and the virtual system (1.4.4), then, an AHOSMO-2 for the virtual system (1.4.4) is designed as follows

$$\begin{aligned} \dot{\hat{\theta}}_e &= \hat{\omega} + \tilde{K}_{1,2}|e_{\theta_e}|^{\frac{2}{3}} \text{sign}(e_{\theta_e}) \\ \dot{\hat{\omega}} &= \hat{\alpha} + \tilde{K}_{2,2}|e_{\theta_e}|^{\frac{1}{3}} \text{sign}(e_{\theta_e}) \\ \dot{\hat{\alpha}} &= \tilde{K}_{3,2} \text{sign}(e_{\theta_e}) \end{aligned} \tag{2.3.41}$$

where $\hat{\theta}_e$, $\hat{\omega}$ and $\hat{\alpha}$ are the estimation of electrical angular position, electrical speed and acceleration, respectively. However, θ_e is not measured directly, such that, the observer (2.3.41) cannot be implemented. Therefore, considering the methodology to extract e_{θ_e} introduced in

section 2.1, then, Λ_θ can be expressed in terms of the estimation error e_{θ_e} as $\Lambda_\theta = \mu e_{\theta_e}$, with $\mu > 0$. Thus, $e_{\theta_e} = \theta_e - \hat{\theta}_e$ can be replaced by $\theta_e - \hat{\theta}_e = \frac{\Lambda_\theta}{\mu}$ into the observer (2.3.41), i.e., the AHOSMO-2 for the IPMSM is given by

$$\begin{aligned}\dot{\hat{\theta}}_e &= \hat{\omega} + \tilde{K}_{1,2} \left| \frac{\Lambda_\theta}{\mu} \right|^{\frac{2}{3}} \text{sign}\left(\frac{\Lambda_\theta}{\mu}\right) \\ \dot{\hat{\omega}} &= \hat{\alpha} + \tilde{K}_{2,2} \left| \frac{\Lambda_\theta}{\mu} \right|^{\frac{1}{3}} \text{sign}\left(\frac{\Lambda_\theta}{\mu}\right) \\ \dot{\hat{\alpha}} &= \tilde{K}_{3,2} \text{sign}\left(\frac{\Lambda_\theta}{\mu}\right)\end{aligned}\quad (2.3.42)$$

Then, the observer (2.3.42) is used to estimate the angular position, speed and acceleration. In Figure 2.7, a scheme of the proposed adaptive observer-2 is introduced. Moreover, in Figure 2.3, a flowchart has been presented to show the interconnection among the extraction of the angular error and the adaptive observer. As previously mentioned, $\hat{\theta} = \frac{\hat{\theta}_e}{p}$ is the estimated mechanical angular position and $\hat{\Omega} = \frac{\hat{\omega}}{p}$ is the estimated mechanical speed.

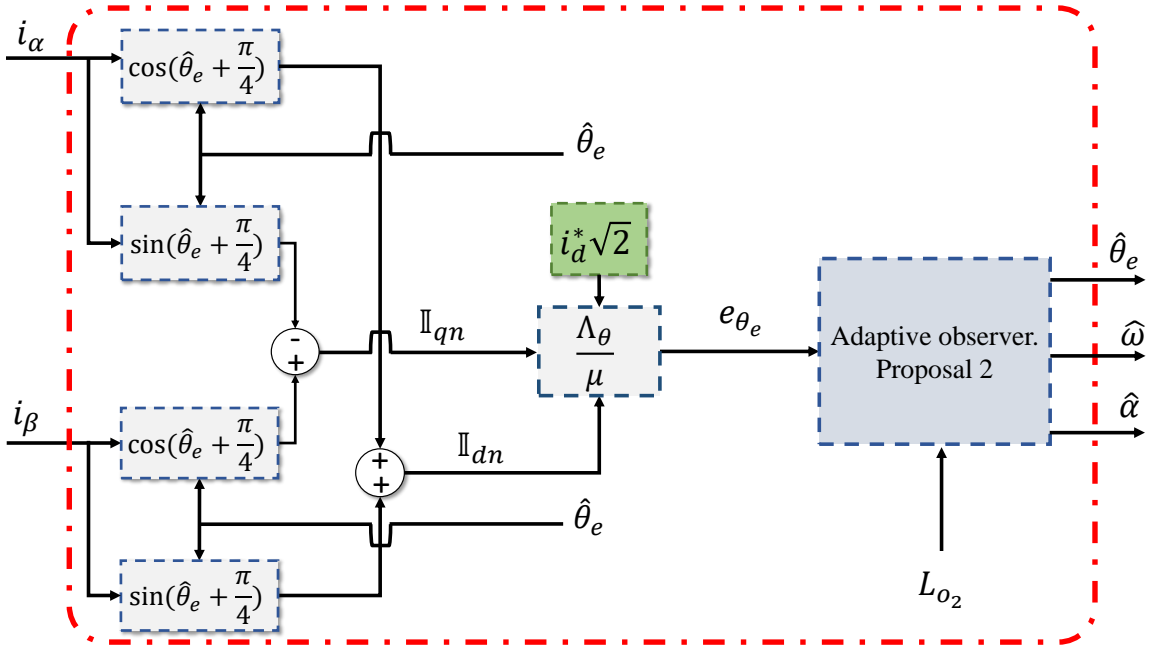


Figure 2.7: Scheme of the proposed AHOSMO-2.

2.3.3 Simulation results

Considering the second adaptive observer introduced in this section. Simulation results in open-loop are going to be introduced to estimate angular position, speed and acceleration. As previously mentioned, simulation test has been carried out in Matlab-Simulink environment, using a sampling time of 1×10^{-3} with a fixed-step *ode4* solver. The profiles in Figure 1.7 and the parameter variations in Figure 1.8 have been used. Moreover, the parameters of the adaptive observer are given in Table 2.2.

Table 2.2: Parameters for the AHOSMO-2

Values		
$L_{o2}(0)$	γ_{o2}	k_{o2}
8	0.0001	80

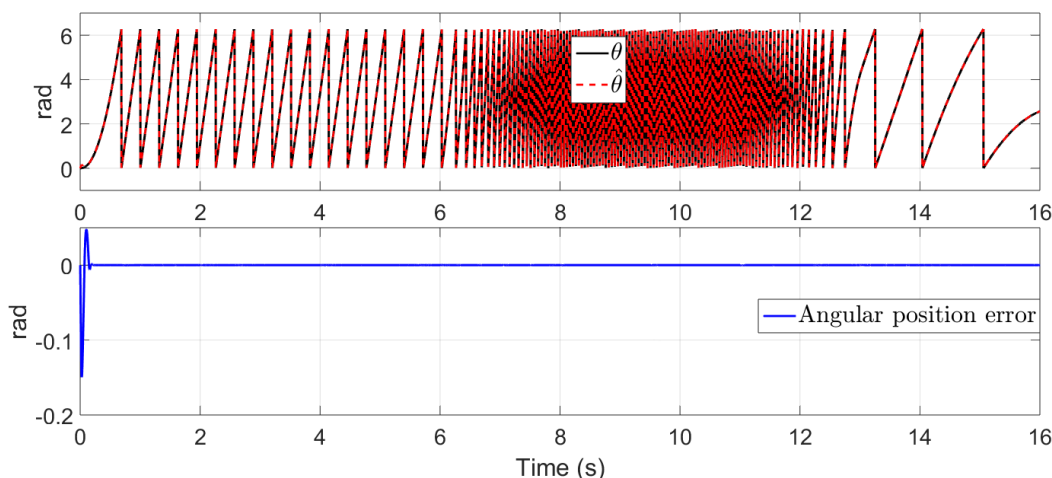


Figure 2.8: AHOSMO-2. Rotor angular position estimation and its angular error

In Figure 2.8, angular position estimation and its estimation error are illustrated, showing good effectiveness during the estimation despite parametric uncertainties. In Figure 2.9, speed estimation and its speed estimation error show that the strategy based on the virtual system without parameters has a good performance. Moreover, it is compensated with the estimation of the acceleration to avoid large estimation errors in the speed and angular position, see Figure

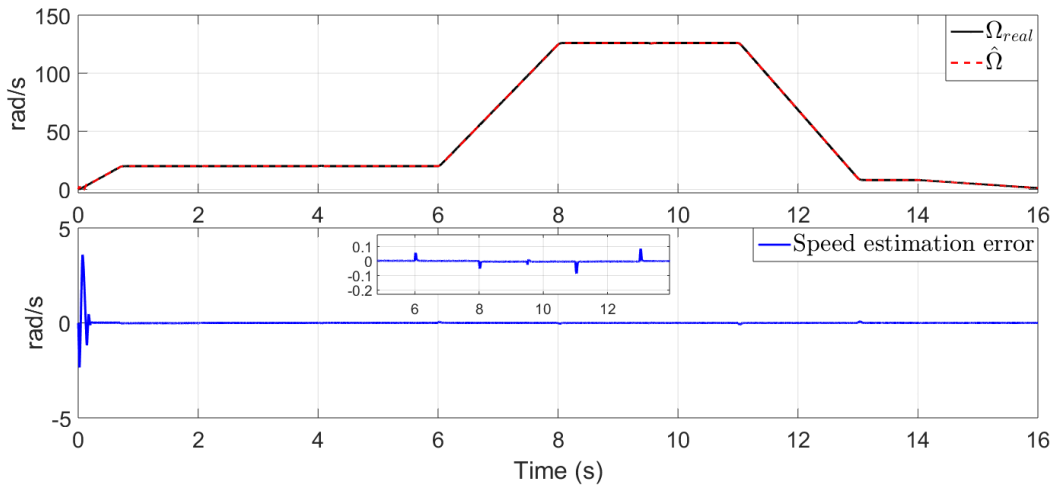


Figure 2.9: AHOSMO-2. Rotor speed estimation and speed estimation error

2.10-a). In addition, in Figure 2.10-b), the adaptive parameter $L_o(t)$ is introduced, showing the profile it takes to achieve the correct estimation of the estimates.

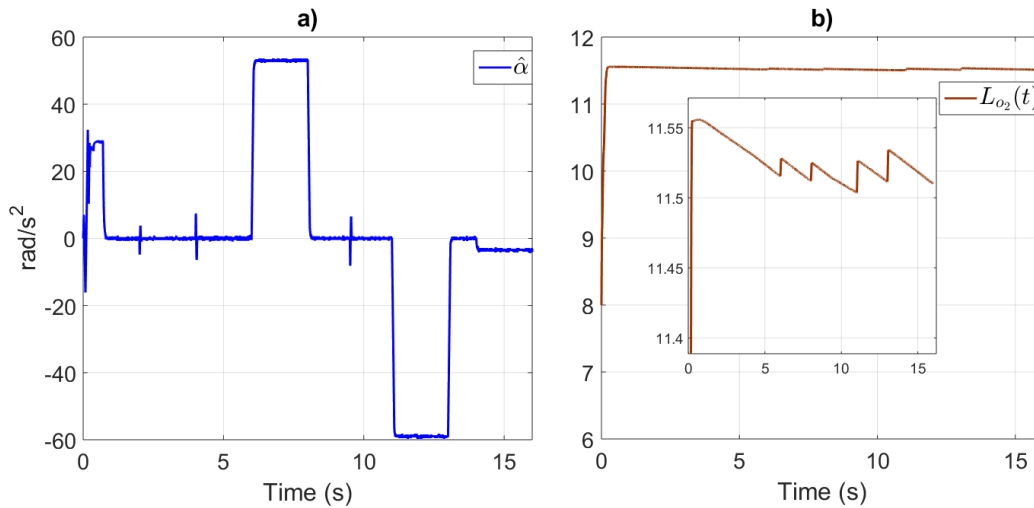


Figure 2.10: AHOSMO-2. Estimation of the acceleration (a) and behaviour of the adaptive law (b)

2.4 Comparative study

In this section, from simulations, a comparative study is presented. The comparative study is carried out by considering the following strategies: an observer based on back-electromotive force, an observer based on mechanical system by using first-order sliding modes and an observer based on high frequency signal injection. The simulation test under parameter variations (see Figure 1.8) and disturbance is carried out. First, an observer based on back-electromotive

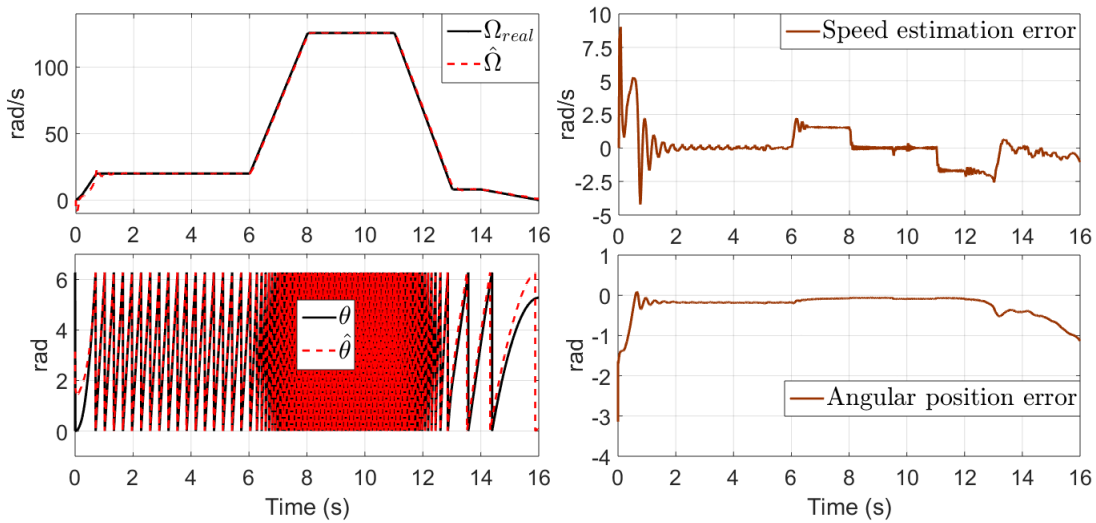


Figure 2.11: Simulation test: Observer based on back-electromotive force

force is introduced in Figure 2.11 for estimating angular position and speed. In this class of observers, the use of low pass filter generates a phase-delay in the estimation of the angular position, and the parameter variations causes an error increment. After that, an observer based on mechanical system by using first-order sliding modes is shown in Figure 2.12, estimating speed, angular position and load torque. The chattering effect can be seen in the angular error and the speed estimation error. Moreover, the effect of parameter variations causes an error increase in the estimation of the load torque. Another strategy often used in sensorless methods is the observer based on high frequency signal injection, which considers an extraction of angular error from high frequency signal injection. In Figure 2.13, this strategy is introduced in order to estimate angular position and speed. Then, from the errors in speed and angular position, it is possible to see the performance of this strategy under the variation of parameters.

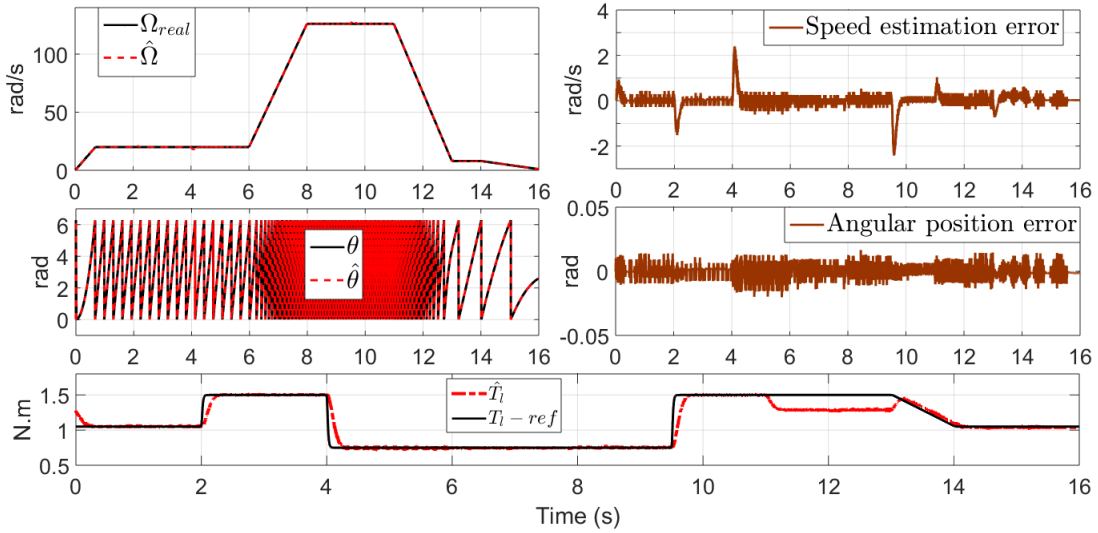


Figure 2.12: Simulation test: Observer based on mechanical system by using first-order sliding modes

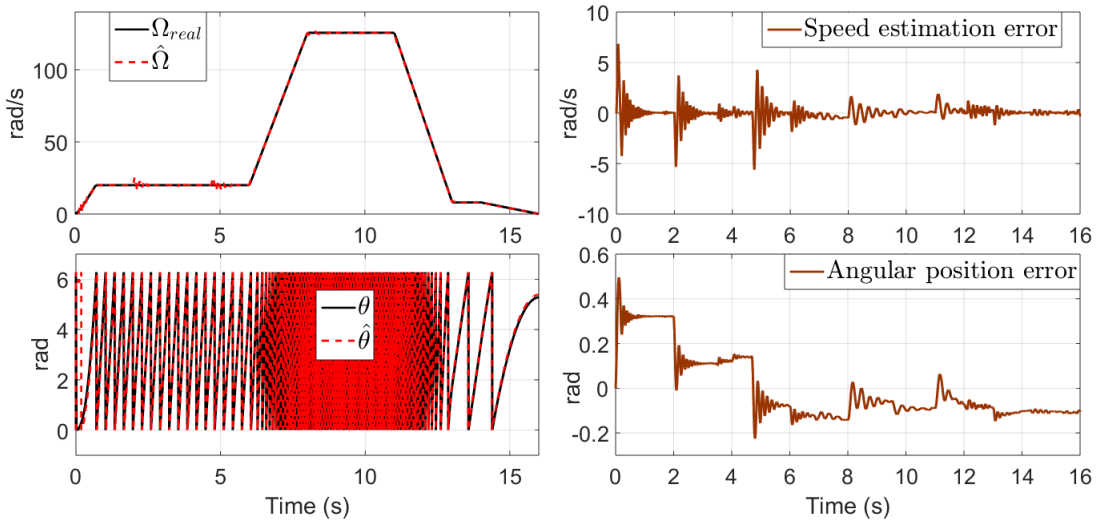


Figure 2.13: Simulation test: Observer based on high frequency signal injection

A disadvantage of this strategy is the sensitivity to variations in inductance.

A performance index, Integral Absolute Error (IAE), is computed in order to show numerically the performance of each observer for the angular position estimation error and the speed estimation error as can be illustrated in Figure 2.14 and Figure 2.15 , respectively.

The proposed observers (AHOSMO-1, AHOSMO-2) based on virtual system achieve a better performance compared with the other strategies. The improvement can be shown from

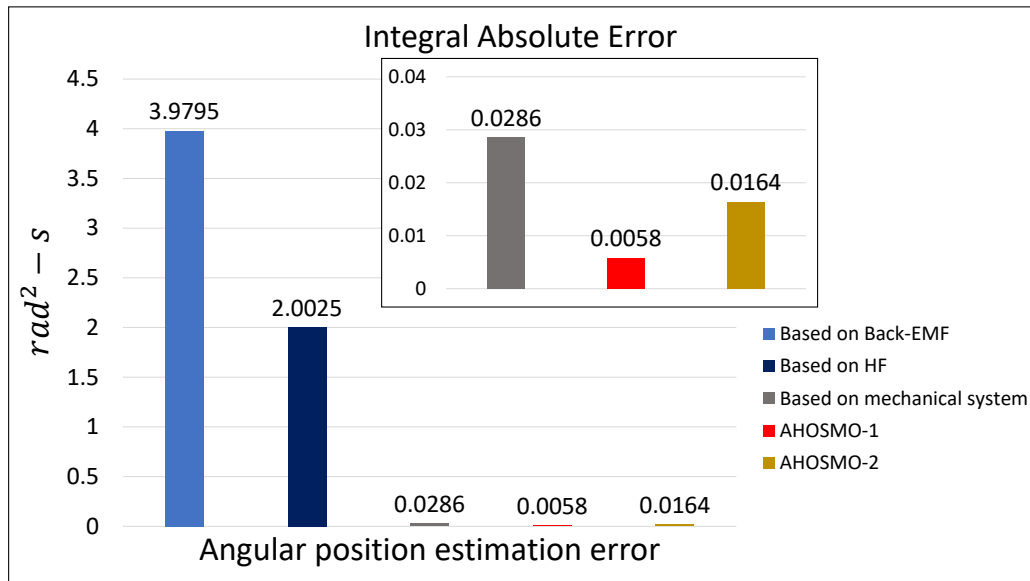


Figure 2.14: Performance index for the angular position estimation error

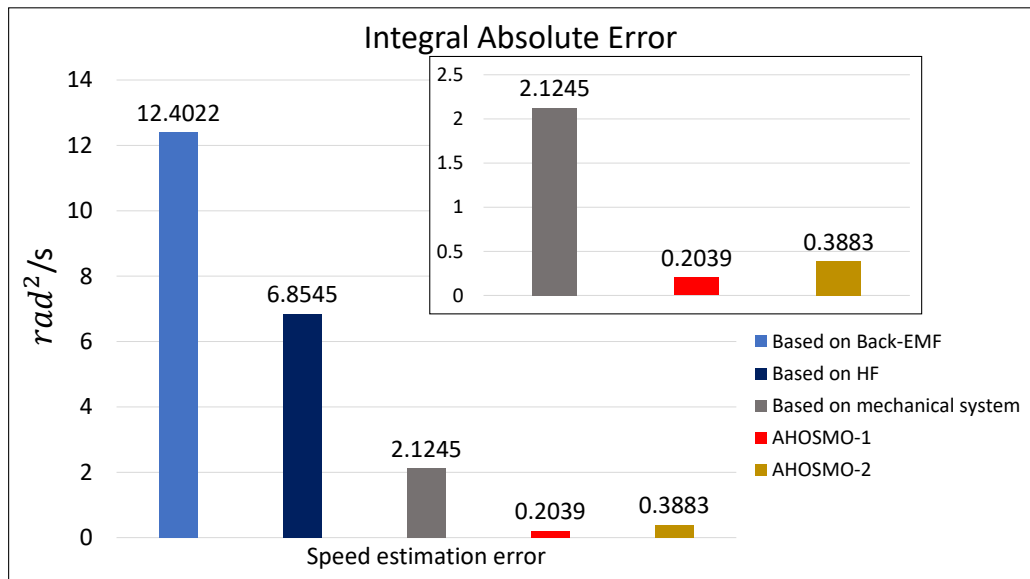


Figure 2.15: Performance index for speed estimation error

the performance index, validating the effectiveness of the proposed observers. Therefore, the extraction of the angular error e_{θ_e} introduced in section 2.1 has been achieved successfully.

In addition, a simulation test to show the convergence of the observer has been carried out, as can be seen in Figure 2.16. The initial conditions for the estimated speed and estimated angular position are $\hat{\Omega}(0) = 20$ rad/s and $\hat{\theta}(0) = 5.5$ rad, respectively. We can see as the

convergence is ensured such that convergence of the observer is achieved in finite time.

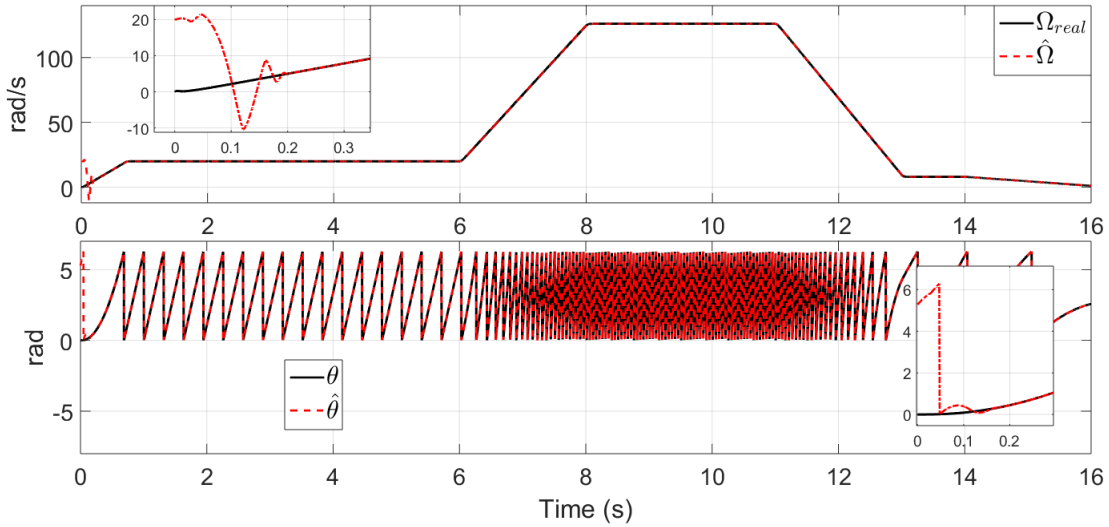


Figure 2.16: Simulation test: Initial condition for the speed (Top) and initial condition for the angular position (Bottom)

On the other hand, this work proposes adaptive observers. Therefore, two simulation tests have been carried out to show the advantages of using adaptive gain instead of constant gains. These demo tests have been applied in AHOSMO-1 taking into account that gains $K_{1,1}$, $K_{2,1}$ and $K_{3,1}$ are a function of the parameter L_o . Then, in Figure 2.17, a test is introduced by considering constant gains, i.e., L_o is constant. During this test, the gain L_o has taken 3 values; 4, 6 and 8, respectively. It is possible to see that estimation of speed, angular position and acceleration has a good performance when $L_o = 4$, avoiding the increase of chattering. However, at 5 seconds when $L_o = 6$, it is possible to see the increase of chattering in the estimation errors and estimated acceleration. Similarly occurs when $L_o = 8$ at 10 seconds. It is due to a gain overestimation, causing chattering in the estimations. Then, in order to avoid this issue, the use of adaptive gain have been an alternative, as shown in Figure 2.18, where is possible to illustrate how the gain $L_o(t)$ is adapted and finds the best value, avoiding an overestimation of gain, reducing chattering in the estimate and achieving a good estimation. Therefore, it has been shown that an adaptive gain can improve the result obtained by constant gains.

In addition, the proposed adaptive laws, for the parameters $L_o(t)$ and $L_{o_2}(t)$ of the observers AHOSMO-1 and AHOSMO-2, have been numerically evaluated at 5 seconds, as can be show

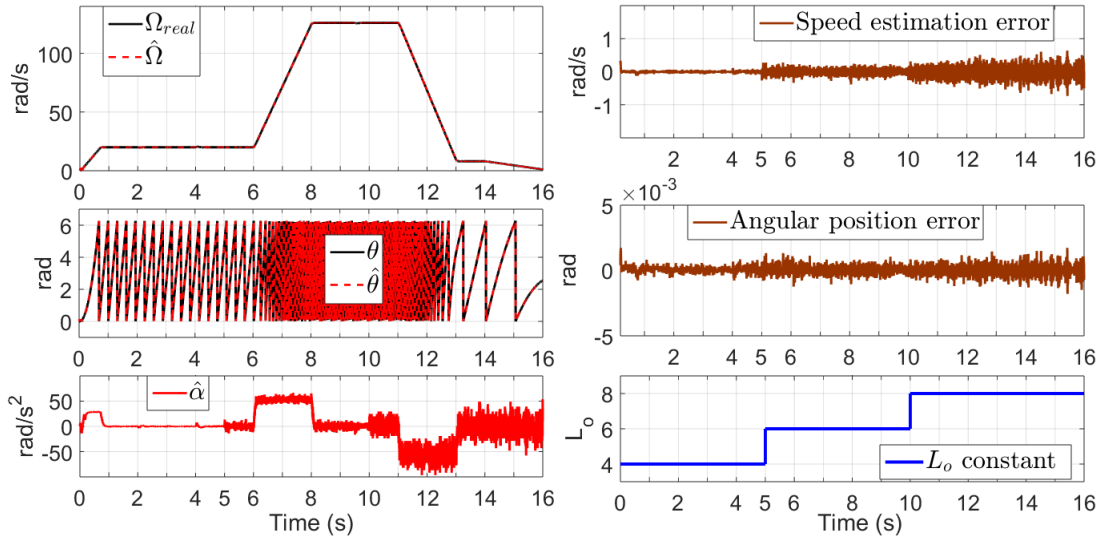


Figure 2.17: AHOSMO-1. State estimation using different constant gains

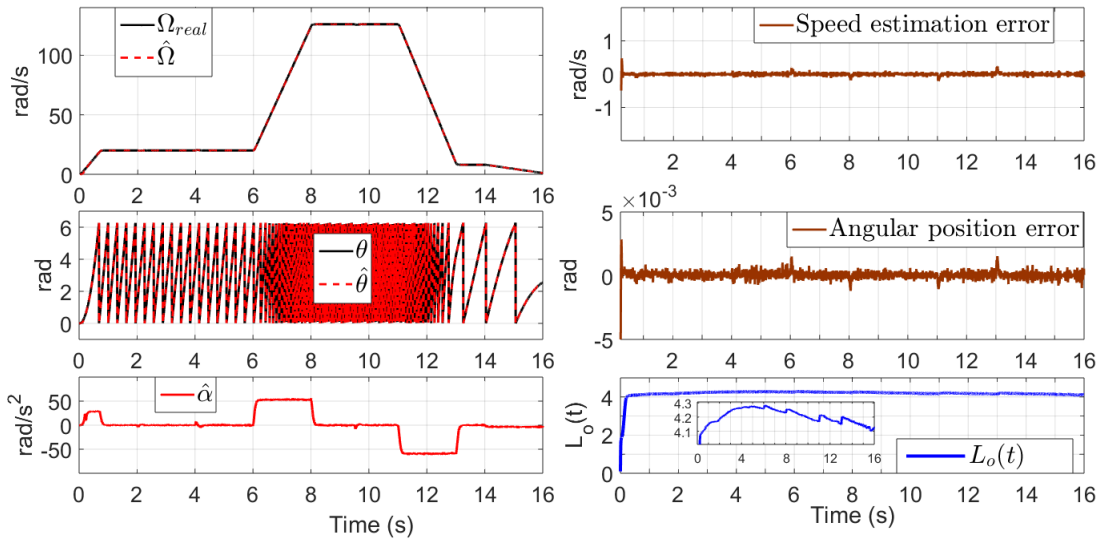


Figure 2.18: AHOSMO-1. State estimation using adaptive gains

in Table 2.3. The final value of each gain at 5 seconds can show that both adaptive laws have a similar behavior with respect to the energy used. However, the gains in terms of $L_o(t)$ has slightly higher values, such that it could be concluded that the adaptive law $L_o(t)$ is more conservative.

Table 2.3: Value for the gains of both adaptive observers at 5 seconds

AHOSMO-1			
$L_o(5)$	$\tilde{K}_{1,1}$	$\tilde{K}_{2,1}$	$\tilde{K}_{3,1}$
4.14	32.07	228.5	542.9
AHOSMO-2			
$L_{o_2}(5)$	$\tilde{K}_{1,2}$	$\tilde{K}_{2,2}$	$\tilde{K}_{3,2}$
11.53	34.58	265.8	680.9

2.5 Proposed observer analysis

The performance of the proposed observer based on the extraction of e_{θ_e} is evaluated in a simulation and experimental test considering the profiles of Figure 1.9. A low-speed and zero region is taken into account due to that in this region most of the observers present observability problems. It is well known that IPMSM is not observable when the angular speed is equal to zero. However, in the proposed strategy, the angular position estimation error e_{θ_e} extracted depends on the dynamics of the current $-i_q$ directly. Therefore, the observability is ensured for a current $-i_q$ different to zero, i.e., $i_q \neq 0$, such that this condition is satisfied when the load torque or the speed are different to zero. In this way, the load torque profile considered in the validation has values equals to zero and different to zero with small values.

A simulation test is introduced in Figure 2.19 and an experimental test is introduced in Figure 2.20. Then, from Figure 2.19 and Figure 2.20, it is shown that at the beginning, the speed is 0 rad/s with a load torque going from 0.05 N.m to 1 N.m . Then, the observer converges to real angular position and speed. After that, from 1.5 s to 4 s the load torque is 0 N.m and the speed is still 0 rad/s until 3 s . Therefore, from 1.5 s , the observer diverges, since, there exists a loss of observability when both speed and load torque are zero, since at that moment the electric machine is standstill and there is not a persistent current $-i_q$ in Λ_θ . However, from 3 s the speed increase until 2.5 rad/s , such that, the current $-i_q$ is different to 0, then the observer tends towards real speed and angular position. Therefore, from 3.5 s is possible to see the convergence in the angular position. Then, the speed stays at low-speed (2.5 rad/s) for 2 s with a load torque different to 0 N.m , such that, a good estimation is achieved

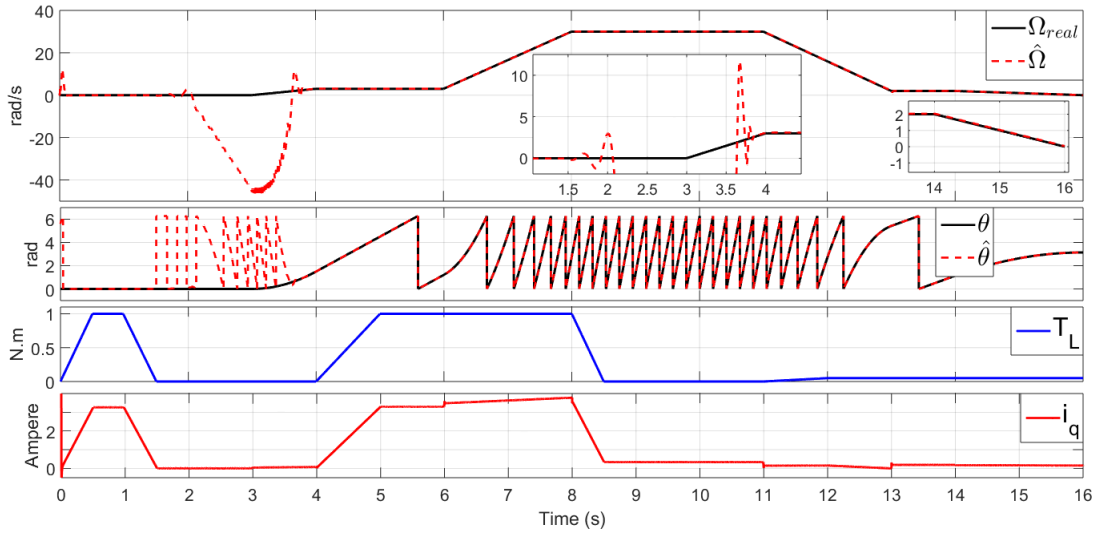


Figure 2.19: Simulation test: Convergence of proposed adaptive observer and behaviour of current i_q , applying different profiles of small load Torque and low-speed.

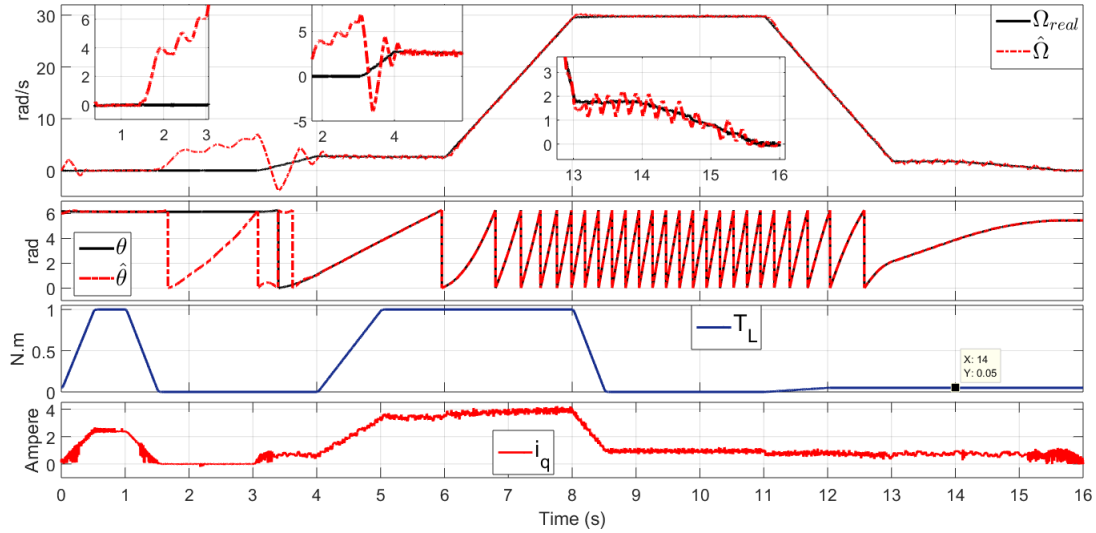


Figure 2.20: Experimental test: Convergence of proposed adaptive observer and behaviour of current i_q , applying different profiles of small load Torque and low-speed.

for the observer. After that, the speed increases until 30 rad/s and stays there for 3 s , and the load torque tends to 0 N.m and stays there from 8.5 s to 11 s , such that, the observer achieves a very accurate estimate. Finally, the speed decreases until 2 rad/s and from 13 s until 16 s , the speed continues to decrease until it reaches 0 rad/s with a small load torque of 0.05 N.m . From this test, it can be concluded that the observability depends on i_q directly, which must

be different from zero ($i_q \neq 0$) to ensure the observability. As shown in the Figure 2.19 and Figure 2.20, $i_q = 0$ when both load torque and speed are 0, otherwise, $i_q \neq 0$.

2.6 Conclusion

The extraction of the angular position estimation error has been the main challenge in this work in order to apply a sensorless technique. In this chapter, the angular error e_θ was extracted successfully. Considering that measurable currents $i_{\alpha\beta}$ can be taken from the abc triphasic components of the IPMSM, this information has been considered and represented by using the Park transformation. Moreover, taking into account some ideas of the saliency method-based, one equation was defined without considering the high-frequency signal injection characteristic. Then, after some calculations, one approximation of the angular error was obtained. It is worth mentioning that the extraction of the angular position error does not require the use of additional elements like filters and high-frequency signal injection.

A sensorless scheme requires information on the angular position and speed. Then, the extracted angular error has been a key piece to design two adaptable observers based on a virtual system without machine parameters to estimate angular position and speed. These adaptive observer have been designed by considering reparameterized gains, *i.e.*, all gains are in terms of a single parameter to reduce the tuning time and facilitate the design of adaptive laws for the observers. Simulation tests were introduced as well as a comparative study. The effectiveness and performance of the adaptive observers based on the extraction of the angular error has been illustrated.

Chapter 3

Controller design for the Interior

Permanent Magnet Synchronous motor

In this chapter, two adaptive controllers are designed. The gains of these controllers are based on a single parameter to reduce the tuning time. The controllers will be applied to track a reference of direct-axis current and speed. Some tests for the adaptive controllers are addressed and a comparative study is introduced.

3.1 Control design based on Super-Twisting approach:

Proposal-1

Consider the class of nonlinear system given by

$$\begin{aligned}\dot{\chi}_1 &= \chi_2 \\ \dot{\chi}_2 &= f(\chi) + g(\chi)u + \delta(t) \\ y &= C\chi\end{aligned}\tag{3.1.1}$$

where $\chi = [\chi_1 \ \chi_2]^T$ is a state vector, for $\chi \in \mathfrak{R}^2$; $u \in \mathfrak{R}$ is the input, $f(\chi)$ and $g(\chi)$ are nonlinear terms, $y \in \mathfrak{R}$ is the output of the system, $\delta(t)$ is a time-varying external disturbance and $C = [1 \ 0]$.

Assumption 3.1. *The nonlinear terms $f(\chi)$ and $g(\chi)$ are globally Lipschitz with respect to χ [86].*

Now, a sliding surface S is defined as follows

$$S = \vartheta_{11}e_{1\chi} + e_{2\chi} \quad (3.1.2)$$

where $e_{1\chi} = \chi_1 - \chi_{ref}$ is a tracking error, $e_{2\chi} = \dot{\chi}_1 - \dot{\chi}_{ref}$ and $\vartheta_{11} > 0$; whose dynamic is given by

$$\dot{S} = \vartheta_{11}e_{2\chi} + f(\chi) + g(\chi)u + \delta(t) - \ddot{\chi}_{ref} \quad (3.1.3)$$

A control input is chosen as follows

$$u = \frac{1}{g(\chi)} [-\vartheta_{11}e_{2\chi} - f(\chi) + \ddot{\chi}_{ref} + \mathcal{V}_{st}], \quad (3.1.4)$$

with

$$\mathcal{V}_{st} = -K_{c1}|S|^{\frac{1}{2}}\text{sign}(s) - \int K_{c2}\text{sign}(S)dt \quad (3.1.5)$$

where $K_{c1} = 2L_c^2$ and $K_{c2} = \frac{L_c^4}{2}$ are reparameterized based on a single parameter L_c , such that $L_c > 0$ is a constant positive parameter. Then, equation (3.1.4) is a super twisting control for the system (3.1.1). However, tuning with constant gains sometimes causes gain overestimation. Therefore, in the next section, an adaptive control will be presented to avoid this problem.

3.1.1 Adaptive super-twisting control design

Consider the following control

$$u = \frac{1}{g(\chi)} [-\vartheta_{11}e_{2\chi} - f(\chi) + \ddot{\chi}_{ref} + \mathcal{V}_{st}], \quad (3.1.6)$$

with

$$\mathcal{V}_{st} = -\tilde{K}_{c1}|S|^{\frac{1}{2}}\text{sign}(s) - \int_0^t \tilde{K}_{c2}\text{sign}(S)d\tau \quad (3.1.7)$$

which is an Adaptive Super-Twisting Control (ASTWC-1) for the system (3.1.1) and their reparameterized gains, in terms of a single parameter, are defined by

$$\tilde{K}_{c1} = 2L_c^2(t) \quad \tilde{K}_{c2} = \frac{L_c^4(t)}{2} \quad (3.1.8)$$

where $L_c(t)$ is an adaptive parameter that will be introduced later.

Remark 3.1. *A demonstration to compute the proposed gains has been introduced in Appendix A (See A.2.1).*

A stability analysis and the adaptive law design for the parameter $L_c(t)$ will be introduced in the sequel.

Consider that the dynamic of the sliding surface (3.1.3) in closed-loop with the control (3.1.6) is given by

$$\dot{S} = -\tilde{K}_{c1}|S|^{\frac{1}{2}}\text{sign}(S) - \int_0^t \tilde{K}_{c2}\text{sign}(S)d\tau + \delta(t) \quad (3.1.9)$$

where (3.1.9) can be expressed as follows

$$\begin{cases} \dot{S} = -\tilde{K}_{c1}|S|^{1/2}\text{sign}(S) + \nu + \delta(t) \\ \dot{\nu} = -\tilde{K}_{c2}\text{sign}(S) \end{cases} \quad (3.1.10)$$

then, sliding variable S and its time derivative \dot{S} converge to 0 in finite time.

Assumption 3.2. $\delta(t)$ and its time derivative $\dot{\delta}(t)$ are bounded for unknown positive constants, i.e., $|\delta(t)| < \delta_M$, $|\dot{\delta}(t)| \leq \Delta_M$; with $\delta_M, \Delta_M > 0$, $\forall t \geq 0$ [87].

Now, introducing the following change of variable: $\Upsilon_1 = S$ and $\Upsilon_2 = \nu + \delta(t)$. System (3.1.10) is expressed as

$$\Sigma_{STW} : \begin{cases} \dot{\Upsilon}_1 = -\tilde{K}_{c1}|\Upsilon_1|^{1/2}\text{sign}(\Upsilon_1) + \Upsilon_2, \\ \dot{\Upsilon}_2 = -\tilde{K}_{c2}\text{sign}(\Upsilon_1) + d(t) \end{cases} \quad (3.1.11)$$

with $d(t) = \dot{\delta}(t)$. Consider the following change of coordinates

$$z_1 = \frac{\Upsilon_1}{L_c^2(t)} \quad z_2 = \frac{\Upsilon_2}{L_c^2(t)} \quad (3.1.12)$$

and its first derivative in time as follows

$$\begin{aligned} \dot{z}_1 &= -2L_c(t)|z_1|^{\frac{1}{2}}\text{sign}(z_1) + z_2 - \frac{2z_1\dot{L}_c(t)}{L_c(t)} \\ \dot{z}_2 &= -\frac{L_c^2(t)}{2}\text{sign}(z_1) + \frac{d(t)}{L_c^2(t)} - \frac{2z_2\dot{L}_c(t)}{L_c(t)} \end{aligned} \quad (3.1.13)$$

After that, a new change of variable is given by

$$\mathcal{L}_1 = |z_1|^{\frac{1}{2}}\text{sign}(z_1) \quad \mathcal{L}_2 = \frac{z_2}{L_c(t)} \quad (3.1.14)$$

then the dynamics, in terms of these new variables, are given by

$$\begin{aligned} \dot{\mathcal{L}}_1 &= \frac{L_c(t)}{2|z_1|^{\frac{1}{2}}} [-2\mathcal{L}_1 + \mathcal{L}_2] - \mathcal{L}_1 \frac{\dot{L}_c(t)}{L_c(t)} \\ \dot{\mathcal{L}}_2 &= \frac{L_c(t)}{2|z_1|^{\frac{1}{2}}} \left[-\mathcal{L}_1 + \frac{2|z_1|^{\frac{1}{2}}d(t)}{L_c^4(t)} \right] - 3\mathcal{L}_2 \frac{\dot{L}_c(t)}{L_c(t)} \end{aligned} \quad (3.1.15)$$

The system (3.1.15) can be expressed in compact form as follows

$$\dot{\mathcal{L}} = \alpha_c [(A_c - P_c^{-1}C_c^T C_c) \mathcal{L} + \Phi_c] - N_c \mathcal{L} \frac{\dot{L}_c(t)}{L_c(t)} \quad (3.1.16)$$

with $\alpha_c = \frac{L_c(t)}{2|z_1|^{\frac{1}{2}}}$, and

$$\begin{aligned} \mathcal{L} &= [\mathcal{L}_1 \quad \mathcal{L}_2]^T, \quad C_c = [1 \quad 0], \\ A_c &= \begin{bmatrix} 0 & 1 \\ 0 & 0 \end{bmatrix}, \quad N_c = \begin{bmatrix} 1 & 0 \\ 0 & 3 \end{bmatrix}, \quad \Phi_c = \begin{bmatrix} 0 \\ \frac{2|z_1|^{\frac{1}{2}}}{L_c^4(t)} (d(t)) \end{bmatrix}, \quad P_c = \begin{bmatrix} 1 & -1 \\ -1 & 2 \end{bmatrix}, \end{aligned}$$

where P_c is a symmetric positive-definite matrix, solution of the following equation

$$P_c + A_c^T P_c + P_c A_c - C_c^T C_c = 0 \quad (3.1.17)$$

Assumption 3.3. *The terms in Φ_c are uniformly bounded with respect to u and locally Lipschitz with respect to \mathcal{L} , i.e., $\|\Phi_c\| \leq \wp \|\mathcal{L}\|$, for $\wp > 0$.*

Theorem 3.1. *Consider the system (3.1.11) and the Assumption 3.1, 3.2 and 3.3 are fulfilled. Furthermore,*

$$\dot{L}_c(t) = k_c^{\frac{1}{2}} |S|^{\frac{1}{2}} - \gamma_c^{\frac{1}{2}} L_c^2(t) \quad (3.1.18)$$

is an adaptive law-1 for $L_c(t)$, with $k_c > 0$ and $\gamma_c > 0$ chosen appropriately, where $k_c > \gamma_c > 0$. Then, the trajectories of Σ_{STW} converge towards a vicinity of the origin in finite time.

Proof

Consider a Lyapunov candidate function as follows

$$V_{(\mathcal{L}, L_c(t))} = V_{(\mathcal{L})} + V_{(L_c(t))} \quad (3.1.19)$$

with $V_{(\mathcal{L})} = \mathcal{L}^T P_c \mathcal{L}$ and $V_{(L_c(t))} = \frac{\gamma_c}{2} L_c^2(t)$, for $\gamma_c > 0$. Then, taking its first derivative in time and replacing the suitable expressions, it follows that

$$\begin{aligned} \dot{V}_{(\mathcal{L}, L_c(t))} = & \alpha_c \mathcal{L}^T [A_c^T P_c + P_c A_c] \mathcal{L} - 2\alpha_c \mathcal{L}^T C_c^T C_c \mathcal{L} - \frac{\dot{L}_c(t)}{L_c(t)} \mathcal{L}^T [P_c N_c + N_c P_c] \mathcal{L} \\ & + \gamma_c \dot{L}_c(t) L_c(t) + 2\alpha_c \mathcal{L}^T P_c \Phi_c \end{aligned} \quad (3.1.20)$$

From $A_c^T P_c + P_c A_c = -P_c + C_c^T C_c$, it follows that above equation can be expressed as follows

$$\begin{aligned} \dot{V}_{(\mathcal{L}, L_c(t))} = & -\alpha_c \mathcal{L}^T P_c \mathcal{L} - \alpha_c \mathcal{L}^T C_c^T C_c \mathcal{L} - \frac{\dot{L}_c(t)}{L_c(t)} \mathcal{L}^T [P_c N_c + N_c P_c] \mathcal{L} \\ & + \gamma_c \dot{L}_c(t) L_c(t) + 2\alpha_c \mathcal{L}^T P_c \Phi_c \end{aligned} \quad (3.1.21)$$

Now, considering that $P_c N_c + N_c P_c = R_c$ and defining R_c as a symmetric positive-definite matrix. Then, $\mathcal{L}^T R_c \mathcal{L} \geq \frac{\lambda_{\min}(R_c)}{\lambda_{\max}(P_c)} V_{(\mathcal{L})} = k_c V_{(\mathcal{L})}$, where $\lambda_{\min}(R_c)$ and $\lambda_{\max}(P_c)$ are mini-

minimum and maximum singular values of R_c and P_c , respectively; moreover, considering that $-\alpha_c \mathcal{L}^T C_c^T C_c \mathcal{L} < 0$; for $L_c(t) > 0$. Then,

$$\dot{V}_{(\mathcal{L}, L_c(t))} \leq -\alpha_c V_{(\mathcal{L})} - \frac{\dot{L}_c(t)}{L_c(t)} [k_c V_{(\mathcal{L})} - \gamma_c L_c^2(t)] + 2\alpha_c \mathcal{L}^T P_c \Phi_c \quad (3.1.22)$$

Now, from (3.1.22), the term

$$[k_c V_{(\mathcal{L})} - \gamma_c L_c^2(t)] = \left[k_c^{\frac{1}{2}} V_{(\mathcal{L})}^{\frac{1}{2}} + \gamma_c^{\frac{1}{2}} L_c(t) \right] \left[k_c^{\frac{1}{2}} V_{(\mathcal{L})}^{\frac{1}{2}} - \gamma_c^{\frac{1}{2}} L_c(t) \right]$$

and defining $f_{(V_{(\mathcal{L})}, L_c(t))} = \left[k_c^{\frac{1}{2}} V_{(\mathcal{L})}^{\frac{1}{2}} + \gamma_c^{\frac{1}{2}} L_c(t) \right] > 0$. It follows that

$$\dot{V}_{(\mathcal{L}, L_c(t))} \leq -\alpha_c V_{(\mathcal{L})} - f_{(V_{(\mathcal{L})}, L_c(t))} \frac{\dot{L}_c(t)}{L_c(t)} \left[k_c^{\frac{1}{2}} V_{(\mathcal{L})}^{\frac{1}{2}} - \gamma_c^{\frac{1}{2}} L_c(t) \right] + 2\alpha_c \mathcal{L}^T P_c \Phi_c \quad (3.1.23)$$

Consider that the following inequalities are satisfied,

$$|z_1| = |\mathcal{L}_1|^2 \leq \|\mathcal{L}\|^2 \quad (3.1.24)$$

and

$$\lambda_{\min}(P_c) \|\mathcal{L}\|^2 \leq V_{(\xi)} \leq \lambda_{\max}(P_c) \|\mathcal{L}\|^2 \quad (3.1.25)$$

where $\lambda_{\min}(P_c)$ and $\lambda_{\max}(P_c)$ are the minimum and maximum singular values of P_c . Then, it follows that the following inequality hold,

$$|z_1|^{\frac{1}{2}} \leq \|\mathcal{L}\| \leq \left(\frac{V_{(\xi)}}{\lambda_{\min}(P_c)} \right)^{\frac{1}{2}} \quad (3.1.26)$$

for $z_1 = \frac{\Upsilon_1}{L_c^2(t)} = \frac{S}{L_c^2(t)}$. Now, taking into account the above inequality, equation (3.1.23) can be expressed as

$$\dot{V}_{(\mathcal{L}, L_c(t))} \leq -\alpha_c V_{(\mathcal{L})} - f_{(V_{(\mathcal{L})}, L_c(t))} \frac{\dot{L}_c(t)}{L_c(t)} \left[k_c^{\frac{1}{2}} \left(\frac{|S|}{L_c^2(t)} \right)^{\frac{1}{2}} - \gamma_c^{\frac{1}{2}} L_c(t) \right] + 2\alpha_c \mathcal{L}^T P_c \Phi_c \quad (3.1.27)$$

Therefore, an adaptive law can be chosen as follows,

$$\dot{L}_c(t) = \left[k_c^{\frac{1}{2}} \left(\frac{|S|}{L_c^2(t)} \right)^{\frac{1}{2}} - \gamma_c^{\frac{1}{2}} L_c(t) \right] L_c(t) \quad (3.1.28)$$

Then, it follows that

$$\dot{V}_{(\mathcal{L}, L_c(t))} \leq -\alpha_c V_{(\mathcal{L})} - f_{(V_{(\mathcal{L})}, L_c(t))} \left[k_c^{\frac{1}{2}} \left(\frac{|S|}{L_c^2(t)} \right)^{\frac{1}{2}} - \gamma_c^{\frac{1}{2}} L_c(t) \right]^2 + 2\alpha_c \mathcal{L}^T P_c \Phi_c \quad (3.1.29)$$

Assuming that S tends to zero faster than $L_c(t)$. Then, (3.1.29) is given by

$$\dot{V}_{(\mathcal{L}, L_c(t))} \leq -\alpha_c V_{(\mathcal{L})} - f_{(V_{(\mathcal{L})}, L_c(t))} \gamma_c L_c^2(t) + 2\alpha_c \mathcal{L}^T P_c \Phi_c \quad (3.1.30)$$

Moreover, from Assumption 3.3 and taking into account the norm for the term $2\alpha_c \mathcal{L}^T P_c \Phi_c$, it follows that

$$\dot{V}_{(\mathcal{L}, L_c(t))} \leq -\alpha_c V_{(\mathcal{L})} + 2\alpha_c \varrho \|\mathcal{L}\|^2 \|P_c\| - f_{(V_{(\mathcal{L})}, L_c(t))} \gamma_c L_c^2(t) \quad (3.1.31)$$

and considering the inequality (3.1.25), it is obtained the following

$$\dot{V}_{(\mathcal{L}, L_c(t))} \leq -\frac{L_c(t)}{2|z_1|^{\frac{1}{2}}} [1 - \sigma_c] V_{(\mathcal{L})} - f_{(V_{(\mathcal{L})}, L_c(t))} \gamma_c L_c^2(t) \quad (3.1.32)$$

with $\sigma_c = \frac{2\varrho \|P_c\|}{\lambda_{\min}(P_c)}$. Moreover, taking into account (3.1.26), the above equation can be expressed as follows

$$\dot{V}_{(\mathcal{L}, L_c(t))} \leq -L_c(t) \Gamma_c V_{(\mathcal{L})}^{\frac{1}{2}} - f_{(V_{(\mathcal{L})}, L_c(t))} \gamma_c L_c^2(t) \quad (3.1.33)$$

with $\Gamma_c = \frac{[1 - \sigma_c] \lambda_{\min}^{\frac{1}{2}}(P_c)}{2}$. Now, equation (3.1.33) will be factored as follows

$$\dot{V}_{(\mathcal{L}, L_c(t))} \leq -L_c(t) \sqrt{2} \gamma_c^{\frac{1}{2}} \left[\frac{\Gamma_c}{\sqrt{2} \gamma_c^{\frac{1}{2}}} V_{(\mathcal{L})}^{\frac{1}{2}} + f_{(V_{(\mathcal{L})}, L_c(t))} \frac{\gamma_c^{\frac{1}{2}}}{\sqrt{2}} L_c(t) \right] \quad (3.1.34)$$

Thus, selecting $\eta_1 = \left[L_c(t) \sqrt{2} \gamma_c^{\frac{1}{2}} \right]$ and $\varphi_c = \min \left[\frac{\Gamma_c}{\sqrt{2} \gamma_c^{\frac{1}{2}}}, f_{(V_{(\mathcal{L})}, L_c(t))} \right]$, it is possible to

express the following equation

$$\dot{V}_{(\mathcal{L}, L_c(t))} \leq -\eta_2 \left[V_{(\mathcal{L})}^{\frac{1}{2}} + \frac{\gamma_c^{\frac{1}{2}}}{\sqrt{2}} L_c(t) \right] \quad (3.1.35)$$

with $\eta_2 = \eta_1 \varphi_c$. Then, from Jensen's inequality [83],

$$[|a_c|^m + |b_c|^m]^{\frac{1}{m}} \leq |a_c| + |b_c|, \quad (3.1.36)$$

defining $a_c = V_{(\mathcal{L})}^{\frac{1}{2}}$, $b_c = V_{(L_c)}^{\frac{1}{2}}$ and $m = 2$. Thus, the following inequality can be established

$$\left[|V_{(\mathcal{L})}^{\frac{1}{2}}|^2 + |V_{(L_c(t))}^{\frac{1}{2}}|^2 \right]^{\frac{1}{2}} \leq |V_{(\mathcal{L})}^{\frac{1}{2}}| + \frac{\gamma_c^{\frac{1}{2}}}{\sqrt{2}} |L_c(t)| \quad (3.1.37)$$

In this way

$$V_{(\mathcal{L}, L_c(t))}^{\frac{1}{2}} \leq |V_{(\mathcal{L})}^{\frac{1}{2}}| + \frac{\gamma_c^{\frac{1}{2}}}{\sqrt{2}} |L_c(t)| \quad (3.1.38)$$

Therefore, the dynamic of Lyapunov function can be expressed as

$$\dot{V}_{(\mathcal{L}, L_c(t))} \leq -\eta_2 V_{(\mathcal{L}, L_c(t))}^{\frac{1}{2}}. \quad (3.1.39)$$

Then, from the Lyapunov function, $\dot{V}_{(\mathcal{L}, L_c(t))}$ is negative definite and ensures convergence in finite-time, for $L_c(t)$ sufficiently large, satisfying $\eta_2 > 0$. Moreover, the comparison principle is taken into account to estimate the convergence time. Thus, considering the equation $\dot{v} = -\eta_2 v^{\frac{1}{2}}$ and its solution defined as $v(t) = (v(0)^{\frac{1}{2}} - \frac{1}{2}\eta_2 t)^2$. Then, $V_{(\mathcal{L}, L_c(t))} < v(t)$ when $V_{(\mathcal{L}(0), L_c(0))} < v(0)$, such that, \mathcal{L} has a convergence in finite-time in an estimated time given by $T_2 = \frac{2V_{(\mathcal{L}(0), L_c(0))}^{\frac{1}{2}}}{\eta_2}$. Therefore, \mathcal{L} tends to zero as well as S tends to zero in finite-time.

In this section, an ASTWC-1 has been presented. The gains have been reparameterized in order to reduce the tuning time, avoid the overestimation of gains during the tuning and the chattering in the control input. This adaptive controller will be applied in the IPMSM.

3.1.2 Control design for IPMSM

The design of controllers for the speed and the direct-axis current are presented by considering the adaptive law-1 given by Theorem 3.1.

Control loop for speed $-\Omega$

Consider a sliding surface given by

$$S_\Omega = \vartheta_{12}e_{1\Omega} + e_{2\Omega} \quad (3.1.40)$$

where $e_{1\Omega} = \Omega - \Omega^*$ is speed tracking error, $e_{2\Omega} = \dot{\Omega} - \dot{\Omega}^*$ and $\vartheta_{12} > 0$. Therefore, the dynamic of the sliding surface S_Ω is given by

$$\dot{S}_\Omega = \vartheta_{12}\dot{e}_{2\Omega} + a_1b_1 + a_2b_2 + a_3b_2 - b_3 + b_4 - \ddot{\Omega}^* + v_qc_1 \quad (3.1.41)$$

where $a_1 = \frac{p(L_d - L_q)i_q}{J}$, $a_2 = \frac{p(L_d - L_q)i_d}{J}$, $a_3 = \frac{p\psi_r}{J}$, $b_1 = \frac{v_d}{L_d} - \frac{R_s i_d}{L_d} + \frac{L_q p \Omega i_q}{L_d}$, $b_2 = -\frac{R_s i_q}{L_q} - \frac{L_d p \Omega i_d}{L_q} - \frac{\psi_r p \Omega}{L_q}$, $b_3 = \frac{f_v}{J} \left[\frac{p(L_d - L_q)i_d i_q}{J} + \frac{p\psi_r i_q}{J} - \frac{f_v \Omega}{J} \right]$, $b_4 = \frac{f_v T_l}{J^2}$ and $c_1 = \frac{p(L_d - L_q)i_d}{JL_q} + \frac{p\psi_r}{JL_q}$. Then, the control input v_q is given by

$$v_q = \frac{1}{c_1} \left[-\vartheta_{12}\dot{e}_{2\Omega} - a_1b_1 - a_2b_2 - a_3b_2 + b_3 + \ddot{\Omega}^* + \mathcal{V}_{st-\Omega} \right] \quad (3.1.42)$$

with

$$\mathcal{V}_{st-\Omega} = -\tilde{K}_{c1\Omega} |S_\Omega|^{\frac{1}{2}} \text{sign}(S_\Omega) - \int_0^t \tilde{K}_{c2\Omega} \text{sign}(S_\Omega) d\tau \quad (3.1.43)$$

where $\tilde{K}_{c1\Omega} = 2L_{c\Omega}^2(t)$, $\tilde{K}_{c2\Omega} = \frac{L_{c\Omega}^4(t)}{2}$ and according to Theorem 3.1, $L_{c\Omega}(t)$ is an adaptive parameter given by

$$\dot{L}_{c\Omega}(t) = k_{c\Omega}^{\frac{1}{2}} |S_\Omega|^{\frac{1}{2}} - \gamma_{c\Omega}^{\frac{1}{2}} L_{c\Omega}^2(t) \quad (3.1.44)$$

with $k_{c\Omega} > \gamma_{c\Omega} > 0$. Therefore, 3.1.42 is an ASTWC-1 for the speed of the IPMSM.

Control loop for current $-i_d$

A sliding surface is given by

$$S_{i_d} = \vartheta_{13}e_{i_d} + \int_0^t e_{i_d}d\tau \quad (3.1.45)$$

where $e_{i_d} = i_d - i_d^*$ is a current tracking error and $\vartheta_{13} > 0$. Moreover, the dynamic of the sliding surface S_{i_d} is given by

$$\dot{S}_{i_d} = -\frac{\vartheta_{13}R_s i_d}{L_d} + \frac{\vartheta_{13}p\Omega L_q i_q}{L_d} + \frac{\vartheta_{13}v_d}{L_d} - \vartheta_{13}\dot{i}_d^* + e_{i_d} \quad (3.1.46)$$

Then, the control input v_d can be chosen as follows

$$v_d = \frac{L_d}{\vartheta_{13}} \left(\frac{\vartheta_{13}R_s i_d}{L_d} - \frac{\vartheta_{13}p\Omega L_q i_q}{L_d} + \vartheta_{13}\dot{i}_d^* - e_{i_d} + \mathcal{V}_{st-i_d} \right) \quad (3.1.47)$$

with

$$\mathcal{V}_{st-i_d} = -\tilde{K}_{c1_{i_d}}|S_{i_d}|^{\frac{1}{2}}\text{sign}(S_{i_d}) - \int_0^t \tilde{K}_{c2_{i_d}}\text{sign}(S_{i_d})d\tau \quad (3.1.48)$$

where $\tilde{K}_{c1_{i_d}} = 2L_{c_{i_d}}^2(t)$ and $\tilde{K}_{c2_{i_d}} = \frac{L_{c_{i_d}}^4(t)}{2}$ and according to Theorem 3.1, $L_{c_{i_d}}(t)$ is an adaptive parameter given by

$$\dot{L}_{c_{i_d}}(t) = k_{c_{i_d}}^{\frac{1}{2}}|S_{i_d}|^{\frac{1}{2}} - \gamma_{c_{i_d}}^{\frac{1}{2}}L_{c_{i_d}}^2(t) \quad (3.1.49)$$

with $k_{c_{i_d}} > \gamma_{c_{i_d}} > 0$. Therefore, 3.1.47 is an ASTWC-1 for the current $-i_d$ of the IPMSM.

3.1.3 Simulation results

Consider the adaptive law-1 established by Theorem 3.1 and the system (1.3.30)-(1.3.31) in closed-loop with the controllers given by (3.1.42) and (3.1.47). Then, simulation result are introduced in this section in order to show the performance of the system under the action of adaptive controllers. The parameters of the adaptive control are given in Table 3.1.

Table 3.1: Parameters for the ASTWCs-1

Values							
$L_{c_\Omega}(0)$	ϑ_{12}	γ_{c_Ω}	k_{c_Ω}	$L_{c_{i_d}}(0)$	ϑ_{13}	$\gamma_{c_{i_d}}$	$k_{c_{i_d}}$
20	400	0.05	90	20	200	0.1	1

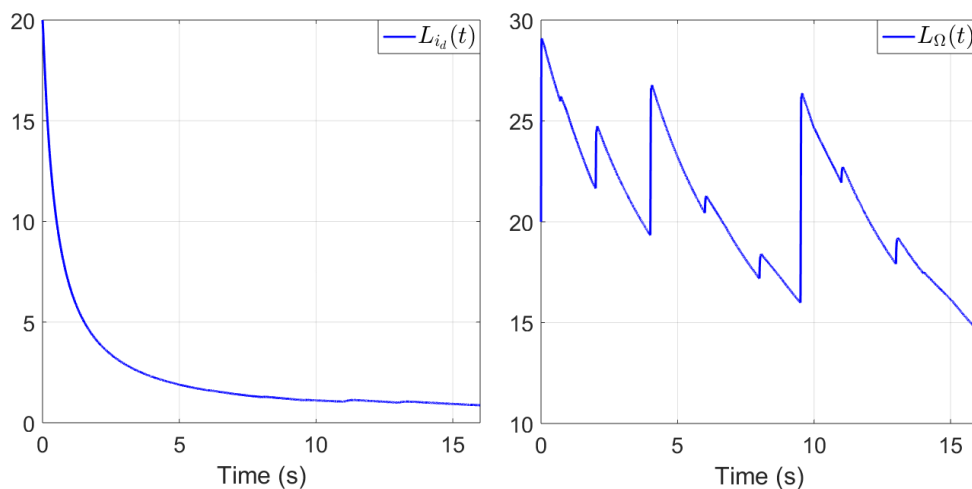


Figure 3.1: ASTWC-1. Behaviour of adaptive law for the speed and current- i_d controllers

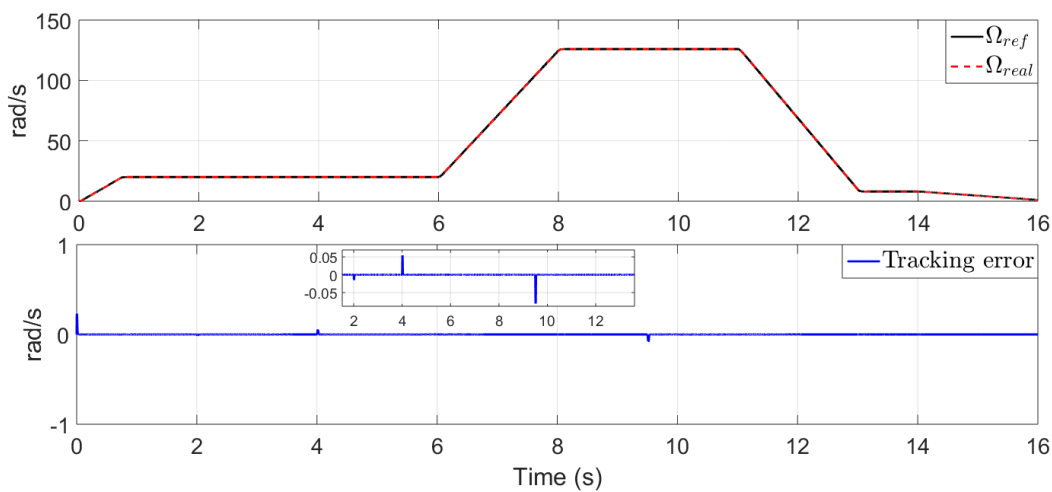


Figure 3.2: ASTWC-1. Speed tracking and speed tracking error

The profile given by the Figure 1.7 and the parameter variation given by Figure 1.8 are considered in this test. In the first instance, it is possible to see the behavior of the adaptive gains in Figure 3.1, $L_{i_d}(t)$ and $L_\Omega(t)$, respectively. Then, considering this adaptive laws, the

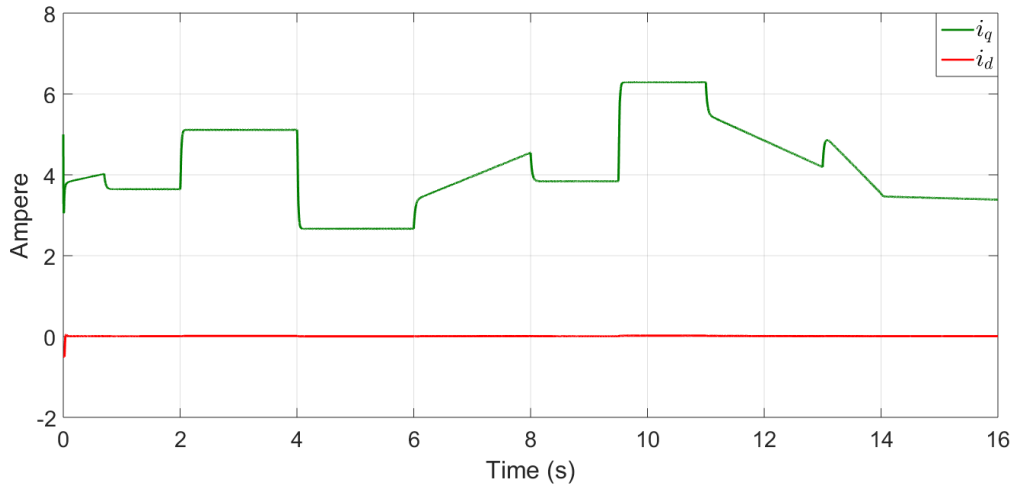


Figure 3.3: ASTWC-1. Behaviour of the currents i_{dq}

speed (see Figure 3.2) has been controlled. The tracking error can show a minimum error under the action of the load torque and parameters variations. In fact, in Figure 3.1, it is possible to see the reaction of the adaptive parameter in the controller when the load torque changes its value, so that the adaptive gains adjust their values in order to reject system disturbances. Moreover, in Figure 3.3, the currents i_{dq} are introduced. The current $-i_d$ tracks a reference current equal to zero and the current $-i_q$ takes different values according to the speed and load torque. A good performance of ASTWCs-1 can be seen in this simulation test.

In Chapter 4, the ASTWCs-1 of the IPMSM will be interconnected with the AHOSMO-1 presented in Chapter 2. From this, the sensorless scheme for the IPMSM will be introduced.

3.2 Control design based on Super-Twisting approach:

Proposal-2

In this section, a second adaptive control is designed for the system given by (3.1.1).

Consider that in [88], an adaptive super- twisting control was proposed with reparameterized gains, taking into account the following structure:

A sliding surface S_2 was defined by

$$S_2 = \vartheta_{21}e_{1_x} + e_{2_x} \quad (3.2.1)$$

where $e_{1_x} = \chi_1 - \chi_{ref}$ is a tracking error, $e_{2_x} = \dot{\chi}_1 - \dot{\chi}_{ref}$ and $\vartheta_{21} > 0$; whose dynamic is given by

$$\dot{S}_2 = \vartheta_{21}e_{2_x} + f(\chi) + g(\chi)u + \delta(t) - \ddot{\chi}_{ref} \quad (3.2.2)$$

Then, a control input was chosen as follows

$$u = \frac{1}{g(\chi)} \left(-\vartheta_{21}e_{2_x} - f(\chi) + \ddot{\chi}_{ref} - K_{G1}|S_2|^{\frac{1}{2}}\text{sign}(S_2) - \int_0^t K_{G2}\text{sign}(S_2)d\tau \right), \quad (3.2.3)$$

where $K_{G1} = 2L_G(t)$ and $K_{G2} = \frac{L_G^2(t)}{2}$ have been reparameterized based on a single parameter $L_G(t) > 0$. Then, for the above controller, the following adaptive law was proposed

$$\dot{L}_G(t) = \frac{-\frac{k_G}{\sqrt{2}}|L_G(t) - L_{G_{ref}}| + \frac{L_G(t)}{2}|S_2|^{\frac{1}{2}}}{(L_G(t) - L_{G_{ref}}) + \frac{2}{L_G(t)^2} \left(|S_2|^{\frac{1}{2}} + \frac{1}{L_G(t)} \int_0^t L_G^2(\tau)\text{sign}(S_2)d\tau \right) \left(-\int_0^t \frac{L_G^2(\tau)}{2}\text{sign}(S_2)d\tau \right)} \quad (3.2.4)$$

for $L_{G_{ref}}, k_G > 0$. In this section, an adaptive law will be designed by using the same reparameterized gains. However, the proposed adaptive law in this work has been simplified. Next, an adaptive law will be designed.

3.2.1 Adaptive super-twisting control design

Based on [88], in this section the design of one adaptive super-twisting control is introduced in order to simplify the adaptive law given by (3.2.4), which helps to simplify the calculations during the stability analysis.

Then, the following equation

$$u = \frac{1}{g(\chi)} \left(-\vartheta_{21}e_{2_x} - f(\chi) + \ddot{\chi}_{ref} + \mathcal{V}_{st} \right), \quad (3.2.5)$$

with

$$\mathcal{V}_{st} = -\tilde{K}_{c3}|S_2|^{\frac{1}{2}}\text{sign}(S_2) - \int_0^t \tilde{K}_{c4}\text{sign}(S_2)d\tau \quad (3.2.6)$$

is an Adaptive Super-Twisting Control (ASTWC-2) for the system (3.1.1) and the reparameterized gains, in terms of a single parameter, are given by

$$\tilde{K}_{c3} = 2L_{c2}(t) \quad \tilde{K}_{c4} = \frac{L_{c2}^2(t)}{2} \quad (3.2.7)$$

where $L_{c2}(t) > 0$ is an adaptive parameter.

Remark 3.2. *A demonstration to calculate the proposed gains has been introduced in the Appendix A (See A.2.2).*

A stability analysis and an adaptive law for the parameter $L_{c2}(t)$ will be presented in the sequel. Consider that the dynamic of the sliding surface (3.2.2) in closed-loop with the control (3.2.5) is given by

$$\dot{S}_2 = -\tilde{K}_{c3}|S_2|^{\frac{1}{2}}\text{sign}(S_2) - \int_0^t \tilde{K}_{c4}\text{sign}(S_2)d\tau + \delta(t) \quad (3.2.8)$$

where the super-twisting (STW) control (3.2.8) can be expressed as follows

$$\begin{cases} \dot{S}_2 = -\tilde{K}_{c3}|S_2|^{\frac{1}{2}}\text{sign}(S_2) + \nu_2 + \delta(t) \\ \dot{\nu}_2 = -\tilde{K}_{c4}\text{sign}(S_2) \end{cases} \quad (3.2.9)$$

Assumption 3.4. *The disturbance $\delta(t)$ and its time derivative $\dot{\delta}(t)$ are bounded for unknown positive constants δ_M, Δ_M , respectively, i.e., $|\delta(t)| < \delta_M, |\dot{\delta}(t)| \leq \Delta_M; \forall t \geq 0$ [87].*

Now, introducing the following change of variable $z_{12} = S_2$ and $z_{22} = \nu_2 + \delta(t)$. Then, system (3.2.9) is rewritten as

$$\Sigma_{STW_2} : \begin{cases} \dot{z}_{12} = -2L_{c2}(t)|z_{12}|^{\frac{1}{2}}\text{sign}(z_{12}) + z_{22} \\ \dot{z}_{22} = -\frac{L_{c2}^2(t)}{2}\text{sign}(z_{12}) + d(t) \end{cases} \quad (3.2.10)$$

with $d(t) = \dot{\delta}(t)$. Consider the following change of variable

$$\mathcal{L}_{12} = \frac{|z_{12}|^{\frac{1}{2}} \text{sign}(z_{12})}{L_{c2}(t)} \quad \mathcal{L}_{22} = \frac{z_{22}}{L_{c2}^2(t)} \quad (3.2.11)$$

then the dynamics, in terms of these new variables, are given by

$$\begin{aligned} \dot{\mathcal{L}}_{12} &= \frac{L_{c2}(t)}{2|z_{12}|^{\frac{1}{2}}} [-2\mathcal{L}_{12} + \mathcal{L}_{22}] - \mathcal{L}_{12} \frac{\dot{L}_{c2}(t)}{L_{c2}(t)} \\ \dot{\mathcal{L}}_{22} &= \frac{L_{c2}(t)}{2|z_{12}|^{\frac{1}{2}}} \left[-\mathcal{L}_{12} + \frac{2|z_{12}|^{\frac{1}{2}} d(t)}{L_{c2}^3(t)} \right] - 2\mathcal{L}_{22} \frac{\dot{L}_{c2}(t)}{L_{c2}(t)} \end{aligned} \quad (3.2.12)$$

To make some calculations easier, system (3.2.12) can be expressed in compact form as follows

$$\dot{\mathcal{L}}_{c2} = \alpha_{c2} [(A_c - P_c^{-1} C_c^T C_c) \mathcal{L}_{c2} + \Phi_{c2}] - D_{c2} \mathcal{L}_{c2} \frac{\dot{L}_{c2}(t)}{L_{c2}(t)} \quad (3.2.13)$$

with $\alpha_{c2} = \frac{L_{c2}(t)}{2|z_{12}|^{\frac{1}{2}}}$ and $\mathcal{L}_{c2} = [\mathcal{L}_{12} \quad \mathcal{L}_{22}]^T$, $C_c = [1 \quad 0]^T$

$$A_c = \begin{bmatrix} 0 & 1 \\ 0 & 0 \end{bmatrix} \quad P_c = \begin{bmatrix} 1 & -1 \\ -1 & 2 \end{bmatrix} \quad D_{c2} = \begin{bmatrix} 1 & 0 \\ 0 & 2 \end{bmatrix} \quad \Phi_{c2} = \begin{bmatrix} 0 \\ \frac{2|z_{12}|^{\frac{1}{2}}}{L_{c2}^3(t)} [d(t)] \end{bmatrix} \quad (3.2.14)$$

Furthermore, P_c is a symmetric positive-definite matrix, solution of the following algebraic Lyapunov equation

$$P_c + A_c^T P_c + P_c A_c - C_c^T C_c = 0 \quad (3.2.15)$$

Assumption 3.5. *The terms in the vector Φ_{c2} are uniformly bounded with respect to u and locally Lipschitz with respect to \mathcal{L}_{c2} , i.e., $\|\Phi_{c2}\| \leq \wp_2 \|\mathcal{L}_{c2}\|$, for $\wp_2 > 0$.*

Theorem 3.2. *Consider the system (3.2.10) and the Assumption 3.1, 3.4 and 3.5 are fulfilled. Furthermore,*

$$\dot{L}_{c2}(t) = k_{c2}^{\frac{1}{2}} |S_2|^{\frac{1}{2}} - \gamma_{c2}^{\frac{1}{2}} L_{c2}^2(t) \quad (3.2.16)$$

is an adaptive law-2 for $L_{c2}(t)$, with $k_{c2} > 0$ and $\gamma_{c2} > 0$ chosen appropriately, where $k_{c2} > \gamma_{c2} > 0$. Then, the trajectories of Σ_{STW_2} converge towards a vicinity of the origin in finite time.

Proof

A Lyapunov candidate function is introduced as follows

$$V_{(\mathcal{L}_{c_2}, L_{c_2}(t))} = V_{(\mathcal{L}_{c_2})} + V_{(L_{c_2}(t))} \quad (3.2.17)$$

with $V_{(\mathcal{L}_{c_2})} = \mathcal{L}_{c_2}^T P_c \mathcal{L}_{c_2}$ and $V_{(L_{c_2}(t))} = \frac{\gamma_{c_2}}{2} L_{c_2}^2(t)$, for $\gamma_{c_2} > 0$. Then, taking first time derivative of (3.2.17) and replacing the suitable expressions, it follows that

$$\begin{aligned} \dot{V}_{(\mathcal{L}_{c_2}, L_{c_2}(t))} = & \alpha_{c_2} \mathcal{L}_{c_2}^T [A_{c_2}^T P_c + P_c A_{c_2}] \mathcal{L}_{c_2} - 2\alpha_{c_2} \mathcal{L}_{c_2}^T C_c^T C_c \mathcal{L}_{c_2} \\ & - 2 \frac{\dot{L}_{c_2}(t)}{L_{c_2}(t)} \mathcal{L}_{c_2}^T P_c D_{c_2} \mathcal{L}_{c_2} + \gamma_{c_2} \dot{L}_{c_2}(t) L_{c_2}(t) + 2\alpha_{c_2} \mathcal{L}_{c_2}^T P_c \Phi_{c_2} \end{aligned} \quad (3.2.18)$$

From $A_c^T P_c + P_c A_c = -P_c + C_c^T C_c$, it follows that equation (3.2.18) can be rewritten as follows

$$\begin{aligned} \dot{V}_{(\mathcal{L}_{c_2}, L_{c_2}(t))} = & -\alpha_{c_2} \mathcal{L}_{c_2}^T P_c \mathcal{L}_{c_2} - \alpha_{c_2} \mathcal{L}_{c_2}^T C_c^T C_c \mathcal{L}_{c_2} - 2 \frac{\dot{L}_{c_2}(t)}{L_{c_2}(t)} \mathcal{L}_{c_2}^T P_c D_{c_2} \mathcal{L}_{c_2} \\ & + \gamma_{c_2} \dot{L}_{c_2}(t) L_{c_2}(t) + 2\alpha_{c_2} \mathcal{L}_{c_2}^T P_c \Phi_{c_2} \end{aligned} \quad (3.2.19)$$

Now, consider that the following inequalities are satisfied

$$\frac{|z_{1_2}|}{L_{c_2}^2(t)} = |\mathcal{L}_{1_2}|^2 \leq \|\mathcal{L}_{c_2}\|^2 \quad (3.2.20)$$

and

$$\lambda_{\min}(P_c) \|\mathcal{L}_{c_2}\|^2 \leq V_{(\mathcal{L}_{c_2})} \leq \lambda_{\max}(P_c) \|\mathcal{L}_{c_2}\|^2 \quad (3.2.21)$$

where $\lambda_{\min}(P_c)$ and $\lambda_{\max}(P_c)$ are the minimum and maximum singular values of P_c . Moreover,

$$\lambda_{\min}(P_c D_{c_2}) \|\mathcal{L}_{c_2}\|^2 \leq \mathcal{L}_{c_2}^T P_c D_{c_2} \mathcal{L}_{c_2} \leq \lambda_{\max}(P_c D_{c_2}) \|\mathcal{L}_{c_2}\|^2 \quad (3.2.22)$$

where $\lambda_{\min}(P_c D_{c_2})$ and $\lambda_{\max}(P_c D_{c_2})$ are the minimum and maximum singular values of $P_c D_{c_2}$.

Then,

$$\begin{aligned} \dot{V}_{(\mathcal{L}_{c_2}, L_{c_2}(t))} &\leq -\alpha_{c_2} \mathcal{L}_{c_2}^T P_c \mathcal{L}_{c_2} - \alpha_{c_2} \mathcal{L}_{c_2}^T C_c^T C_c \mathcal{L}_{c_2} - 2\lambda_{\min}(P_c D_{c_2}) \|\mathcal{L}_{c_2}\|^2 \frac{\dot{L}_{c_2}(t)}{L_{c_2}(t)} \\ &\quad + \gamma_{c_2} \dot{L}_{c_2}(t) L_{c_2}(t) + 2\alpha_{c_2} \mathcal{L}_{c_2}^T P_c \Phi_{c_2} \end{aligned} \quad (3.2.23)$$

such that,

$$\dot{V}_{(\mathcal{L}_{c_2}, L_{c_2}(t))} \leq -\alpha_{c_2} V_{(\mathcal{L}_{c_2})} - \alpha_{c_2} \mathcal{L}_{c_2}^T C_c^T C_c \mathcal{L}_{c_2} - \frac{\dot{L}_{c_2}(t)}{L_{c_2}(t)} \left[k_{c_2} \|\mathcal{L}_{c_2}\|^2 - \gamma_{c_2} L_{c_2}^2(t) \right] + 2\alpha_{c_2} \mathcal{L}_{c_2}^T P_c \Phi_{c_2} \quad (3.2.24)$$

where $k_{c_2} = 2\lambda_{\min}(P_c D_{c_2}) > 0$. Now, from (3.2.24), the term

$$\left[k_{c_2} \|\mathcal{L}_{c_2}\|^2 - \gamma_{c_2} L_{c_2}^2(t) \right] = \left[k_{c_2}^{\frac{1}{2}} \|\mathcal{L}_{c_2}\| + \gamma_{c_2}^{\frac{1}{2}} L_{c_2}(t) \right] \left[k_{c_2}^{\frac{1}{2}} \|\mathcal{L}_{c_2}\| - \gamma_{c_2}^{\frac{1}{2}} L_{c_2}(t) \right]$$

Moreover, since $f_{(\mathcal{L}_{c_2}, L_{c_2}(t))} = \left[k_{c_2}^{\frac{1}{2}} \|\mathcal{L}_{c_2}\| + \gamma_{c_2}^{\frac{1}{2}} L_{c_2}(t) \right] > 0$. Then, equation (3.2.24) can be expressed as follows

$$\begin{aligned} \dot{V}_{(\mathcal{L}_{c_2}, L_{c_2}(t))} &\leq -\alpha_{c_2} V_{(\mathcal{L}_{c_2})} - \alpha_{c_2} \mathcal{L}_{c_2}^T C_c^T C_c \mathcal{L}_{c_2} + 2\alpha_{c_2} \mathcal{L}_{c_2}^T P_c \Phi_{c_2} \\ &\quad - f_{(\mathcal{L}_{c_2}, L_{c_2}(t))} \frac{\dot{L}_{c_2}(t)}{L_{c_2}(t)} \left[k_{c_2}^{\frac{1}{2}} \|\mathcal{L}_{c_2}\| - \gamma_{c_2}^{\frac{1}{2}} L_{c_2}(t) \right] \end{aligned} \quad (3.2.25)$$

Now, considering the inequalities (3.2.20) and (3.2.21), it follows that the following inequalities hold

$$\|\mathcal{L}_{1_2}\| \leq \|\mathcal{L}_{c_2}\| \leq \left(\frac{V_{(\mathcal{L}_{c_2})}}{\lambda_{\min}(P_c)} \right)^{\frac{1}{2}} \quad (3.2.26)$$

for $|\mathcal{L}_{1_2}| = \frac{|z_{1_2}|^{\frac{1}{2}}}{L_{c_2}(t)} = \frac{|S_2|^{\frac{1}{2}}}{L_{c_2}(t)}$. Therefore, taking into account the inequality given by (3.2.26), equation (3.2.25) can be expressed as

$$\begin{aligned} \dot{V}_{(\mathcal{L}_{c_2}, L_{c_2}(t))} &\leq -\alpha_{c_2} V_{(\mathcal{L}_{c_2})} - \alpha_{c_2} \mathcal{L}_{c_2}^T C_c^T C_c \mathcal{L}_{c_2} + 2\alpha_{c_2} \mathcal{L}_{c_2}^T P_c \Phi_{c_2} \\ &\quad - f_{(\mathcal{L}_{c_2}, L_{c_2}(t))} \frac{\dot{L}_{c_2}(t)}{L_{c_2}(t)} \left[k_{c_2}^{\frac{1}{2}} \left(\frac{|S_2|^{\frac{1}{2}}}{L_{c_2}(t)} \right) - \gamma_{c_2}^{\frac{1}{2}} L_{c_2}(t) \right] \end{aligned} \quad (3.2.27)$$

Then, choosing an adaptive law as follows

$$\dot{L}_{c_2}(t) = \left[k_{c_2}^{\frac{1}{2}} \left(\frac{|S_2|^{\frac{1}{2}}}{L_{c_2}(t)} \right) - \gamma_{c_2}^{\frac{1}{2}} L_{c_2}(t) \right] L_{c_2}(t) \quad (3.2.28)$$

the following expression is obtained

$$\begin{aligned} \dot{V}_{(\mathcal{L}_{c_2}, L_{c_2}(t))} \leq & -\alpha_{c_2} V_{(\mathcal{L}_{c_2})} - \alpha_{c_2} \mathcal{L}_{c_2}^T C_c^T C_c \mathcal{L}_{c_2} + 2\alpha_{c_2} \mathcal{L}_{c_2}^T P_c \Phi_{c_2} \\ & - f_{(\mathcal{L}_{c_2}, L_{c_2}(t))} \left[k_{c_2}^{\frac{1}{2}} \left(\frac{|S_2|^{\frac{1}{2}}}{L_{c_2}(t)} \right) - \gamma_{c_2}^{\frac{1}{2}} L_{c_2}(t) \right]^2 \end{aligned} \quad (3.2.29)$$

Assuming that S_2 tends to zero faster than $L_{c_2}(t)$ and $-\alpha_{c_2} \mathcal{L}_{c_2}^T C_c^T C_c \mathcal{L}_{c_2} < 0$; for $L_{c_2}(t) > 0$.

Then, (3.2.29) is given by

$$\dot{V}_{(\mathcal{L}_{c_2}, L_{c_2}(t))} \leq -\alpha_{c_2} V_{(\mathcal{L}_{c_2})} - f_{(\mathcal{L}_{c_2}, L_{c_2}(t))} \gamma_{c_2} L_{c_2}^2(t) + 2\alpha_{c_2} \mathcal{L}_{c_2}^T P_c \Phi_{c_2} \quad (3.2.30)$$

Moreover, taking into account the norm for the term $2\alpha_{c_2} \mathcal{L}_{c_2}^T P_c \Phi_{c_2}$ and Assumption 3.5, it follows that

$$\dot{V}_{(\mathcal{L}_{c_2}, L_{c_2}(t))} \leq -\alpha_{c_2} V_{(\mathcal{L}_{c_2})} + 2\alpha_{c_2} \varrho_2 \|\mathcal{L}_{c_2}\|^2 \|P_c\| - f_{(\mathcal{L}_{c_2}, L_{c_2}(t))} \gamma_{c_2} L_{c_2}^2(t) \quad (3.2.31)$$

Now, consider the inequality (3.2.21), then,

$$\dot{V}_{(\mathcal{L}_{c_2}, L_{c_2}(t))} \leq -\frac{L_{c_2}(t)}{2|z_{12}|^{\frac{1}{2}}} [1 - \sigma_{c_2}] V_{(\mathcal{L}_{c_2})} - f_{(\mathcal{L}_{c_2}, L_{c_2}(t))} \gamma_{c_2} L_{c_2}^2(t) \quad (3.2.32)$$

with $\sigma_{c_2} = \frac{2\varrho_2 \|P_c\|}{\lambda_{\max}(P_c)}$. The above equation can be written as

$$\dot{V}_{(\mathcal{L}_{c_2}, L_{c_2}(t))} \leq -\frac{L_{c_2}(t)}{\frac{2|z_{12}|^{\frac{1}{2}} L_{c_2}(t)}{L_{c_2}(t)}} [1 - \sigma_{c_2}] V_{(\mathcal{L}_{c_2})} - f_{(\mathcal{L}_{c_2}, L_{c_2}(t))} \gamma_{c_2} L_{c_2}^2(t) \quad (3.2.33)$$

Therefore, from (3.2.26), the above equation can be expressed as follows

$$\dot{V}_{(\mathcal{L}_{c_2}, L_{c_2}(t))} \leq -\Gamma_{c_2} V_{(\mathcal{L}_{c_2})}^{\frac{1}{2}} - f_{(\mathcal{L}_{c_2}, L_{c_2}(t))} \gamma_{c_2} L_{c_2}^2(t) \quad (3.2.34)$$

with $\Gamma_{c_2} = \frac{[1 - \sigma_{c_2}] \lambda_{\min}^{\frac{1}{2}}(P_c)}{2}$. Now, equation (3.2.34) will be factorized

$$\dot{V}_{(\mathcal{L}_{c_2}, L_{c_2}(t))} \leq -L_{c_2}(t) \sqrt{2} \gamma_{c_2}^{\frac{1}{2}} \left[\frac{\Gamma_{c_2}}{L_{c_2}(t) \sqrt{2} \gamma_{c_2}^{\frac{1}{2}}} V_{(\mathcal{L}_{c_2})}^{\frac{1}{2}} + f_{(\mathcal{L}_{c_2}, L_{c_2}(t))} \frac{\gamma_{c_2}^{\frac{1}{2}}}{\sqrt{2}} L_{c_2}(t) \right] \quad (3.2.35)$$

Thus, selecting $\eta_{1_2} = [L_{c_2}(t) \sqrt{2} \gamma_{c_2}^{\frac{1}{2}}]$ and $\varphi_{c_2} = \min \left(\frac{\Gamma_{c_2}}{L_{c_2}(t) \sqrt{2} \gamma_{c_2}^{\frac{1}{2}}}, f_{(\mathcal{L}_{c_2}, L_{c_2}(t))} \right)$, it is possible to express the following equation

$$\dot{V}_{(\mathcal{L}_{c_2}, L_{c_2}(t))} \leq -\eta_{2_2} \left[V_{(\mathcal{L}_{c_2})}^{\frac{1}{2}} + \frac{\gamma_{c_2}^{\frac{1}{2}}}{\sqrt{2}} L_{c_2}(t) \right] \quad (3.2.36)$$

with $\eta_{2_2} = \eta_{1_2} \varphi_{c_2}$.

On the other side, Jensen's inequality [83] is given by

$$[|a_{c_2}|^m + |b_{c_2}|^m]^{\frac{1}{m}} \leq |a_{c_2}| + |b_{c_2}| \quad (3.2.37)$$

defining $a_{c_2} = V_{(\mathcal{L}_{c_2})}^{\frac{1}{2}}$, $b_{c_2} = \frac{\gamma_{c_2}^{\frac{1}{2}}}{\sqrt{2}} L_{c_2}(t)$ and $m = 2$. Thus, the following inequality can be established

$$\left[|V_{(\mathcal{L}_{c_2})}^{\frac{1}{2}}|^2 + \left| \frac{\gamma_{c_2}^{\frac{1}{2}}}{\sqrt{2}} L_{c_2}(t) \right|^2 \right]^{\frac{1}{2}} \leq |V_{(\mathcal{L}_{c_2})}^{\frac{1}{2}}| + \frac{\gamma_{c_2}^{\frac{1}{2}}}{\sqrt{2}} |L_{c_2}(t)| \quad (3.2.38)$$

and

$$V_{(\mathcal{L}_{c_2}, L_{c_2}(t))}^{\frac{1}{2}} \leq |V_{(\mathcal{L}_{c_2})}^{\frac{1}{2}}| + \frac{\gamma_{c_2}^{\frac{1}{2}}}{\sqrt{2}} |L_{c_2}(t)| \quad (3.2.39)$$

Finally, the dynamic of Lyapunov function can be expressed as follows

$$\dot{V}_{(\mathcal{L}_{c_2}, L_{c_2}(t))} \leq -\eta_{2_2} V_{(\mathcal{L}_{c_2}, L_{c_2}(t))}^{\frac{1}{2}} \quad (3.2.40)$$

Then, from the Lyapunov function, $\dot{V}_{(\mathcal{L}_{c_2}, L_{c_2}(t))}$ is negative definite and ensures convergence in finite-time, for $L_{c_2}(t)$ sufficiently large, satisfying $\eta_{2_2} > 0$. Moreover, the comparison principle is taken into account to estimate the convergence time. Thus, considering the equation $\dot{v} = -\eta_{2_2} v^{\frac{1}{2}}$ and its solution defined as $v(t) = (v(0)^{\frac{1}{2}} - \frac{1}{2}\eta_{2_2}t)^2$. Then, $V_{(\mathcal{L}_{c_2}, L_{c_2}(t))} < v(t)$ when $V_{(\mathcal{L}_{c_2}(0), L_{c_2}(0))} < v(0)$, such that, \mathcal{L}_{c_2} has a convergence in finite-time in an estimated time given by $T_{2_2} = \frac{2V_{(\mathcal{L}_{c_2}(0), L_{c_2}(0))}^{\frac{1}{2}}}{\eta_{2_2}}$. Therefore, \mathcal{L} tends to zero as well as S_2 tends to zero in finite-time.

In this section, an ASTWC-2 has been presented. The gains have been reparameterized in order to reduce the tuning time, avoid the overestimation of gains during the tuning and the chattering in the control input. In addition, compared to the previous adaptive controller (ASTWC-1), the number of coordinate changes has been reduced in this new design in order to reduce calculations during the proof. The ASTWC-2 will be applied in the IPMSM and a comparative study will be presented later.

3.2.2 Control design for IPMSM

In this section, the design of controllers for the speed and the direct-axis current are presented by considering the adaptive law-2 given by Theorem 3.2.

Control loop for Ω

Consider a sliding surface given by

$$S_{\Omega_2} = \vartheta_{22}e_{1\Omega} + e_{2\Omega} \quad (3.2.41)$$

where $e_{1\Omega} = \Omega - \Omega^*$ is speed tracking error, $e_{2\Omega} = \dot{\Omega} - \dot{\Omega}^*$ and $\vartheta_{22} > 0$. Therefore, the dynamic of the sliding surface S_{Ω} is given by

$$\dot{S}_{\Omega_2} = \vartheta_{22}e_{2\Omega} + a_1b_1 + a_2b_2 + a_3b_2 - b_3 + b_4 - \ddot{\Omega}^* + v_q c_1 \quad (3.2.42)$$

where $a_1 = \frac{p(L_d - L_q)i_q}{J}$, $a_2 = \frac{p(L_d - L_q)i_d}{J}$, $a_3 = \frac{p\psi_r}{J}$, $b_1 = \frac{v_d}{L_d} - \frac{R_s i_d}{L_d} + \frac{L_q p \Omega i_q}{L_d}$, $b_2 = -\frac{R_s i_q}{L_q} - \frac{L_d p \Omega i_d}{L_q} - \frac{\psi_r p \Omega}{L_q}$, $b_3 = \frac{f_v}{J} \left(\frac{p(L_d - L_q)i_d i_q}{J} + \frac{p\psi_r i_q}{J} - \frac{f_v \Omega}{J} - \frac{T_l}{J} \right)$, $b_4 = \frac{f_v T_l}{J^2}$ and $c_1 = \frac{p(L_d - L_q)i_d}{JL_q} + \frac{p\psi_r}{JL_q}$.

Then, the control input v_q is given by

$$v_q = \frac{1}{c_1} \left(-\vartheta_{22} e_{2\Omega} - a_1 b_1 - a_2 b_2 - a_3 b_2 + b_3 + \ddot{\Omega}^* + \mathcal{V}_{st-\Omega_2} \right) \quad (3.2.43)$$

with

$$\mathcal{V}_{st-\Omega_2} = -\tilde{K}_{c3\Omega} |S_{\Omega_2}|^{\frac{1}{2}} \text{sign}(S_{\Omega_2}) - \int_0^t \tilde{K}_{c4\Omega} \text{sign}(S_{\Omega_2}) d\tau \quad (3.2.44)$$

where $\tilde{K}_{c3\Omega} = 2L_{c\Omega_2}(t)$, $\tilde{K}_{c4\Omega} = \frac{L_{c\Omega_2}^2(t)}{2}$ and according to Theorem 3.2, $L_{c\Omega_2}(t)$ is an adaptive parameter given by

$$\dot{L}_{c\Omega_2}(t) = k_{c\Omega_2}^{\frac{1}{2}} |S_{\Omega}|^{\frac{1}{2}} - \gamma_{c\Omega_2}^{\frac{1}{2}} L_{c\Omega_2}^2(t) \quad (3.2.45)$$

with $k_{c\Omega_2} > \gamma_{c\Omega_2} > 0$. Therefore, 3.2.43 is an ASTWC-2 for the speed of the IPMSM.

Control loop for i_d

Now, a sliding surface is introduced

$$S_{i_{d_2}} = \vartheta_{23} e_{i_d} + \int_0^t e_{i_d} d\tau \quad (3.2.46)$$

where $e_{i_d} = i_d - i_d^*$ is a current tracking error and $\vartheta_{23} > 0$. Moreover, the dynamic of the sliding surface S_{i_d} is given by

$$\dot{S}_{i_{d_2}} = -\frac{\vartheta_{23} R_s i_d}{L_d} + \frac{\vartheta_{23} p \Omega L_q i_q}{L_d} + \frac{\vartheta_{23} v_d}{L_d} - \vartheta_{23} \dot{i}_d^* + e_{i_d} \quad (3.2.47)$$

Then, the control input v_d can be chosen as follows

$$v_d = \frac{L_d}{\vartheta_{23}} \left(\frac{\vartheta_{23} R_s i_d}{L_d} - \frac{\vartheta_{23} p \Omega L_q i_q}{L_d} + \vartheta_{23} \dot{i}_d^* - e_{i_d} + \mathcal{V}_{st-i_{d_2}} \right) \quad (3.2.48)$$

with

$$\mathcal{V}_{st-i_{d_2}} = -\tilde{K}_{c3i_d} |S_{i_{d_2}}|^{\frac{1}{2}} \text{sign}(S_{i_{d_2}}) - \int_0^t \tilde{K}_{c4i_d} \text{sign}(S_{i_{d_2}}) d\tau \quad (3.2.49)$$

where $\tilde{K}_{c3i_d} = 2L_{c_{i_{d_2}}}(t)$, $\tilde{K}_{c4i_d} = \frac{L_{c_{i_{d_2}}}(t)}{2}$ and according to Theorem 3.2, $L_{c_{i_{d_2}}}(t)$ is an adaptive parameter given by

$$\dot{L}_{c_{i_{d_2}}}(t) = k_{c_{i_{d_2}}}^{\frac{1}{2}} |S_{i_{d_2}}|^{\frac{1}{2}} - \gamma_{c_{i_{d_2}}}^{\frac{1}{2}} L_{c_{i_{d_2}}}(t) \quad (3.2.50)$$

with $k_{c_{i_{d_2}}} > \gamma_{c_{i_{d_2}}} > 0$. Therefore, 3.2.48 is an ASTWC-2 for the current $-i_d$ of the IPMSM.

3.2.3 Simulation results

Consider the adaptive law established by Theorem 3.2 and the system (1.3.30)-(1.3.31) in closed-loop with the controllers given by (3.2.43) and (3.2.48). Then, similarly to the previous adaptive law introduced in section 3.1.1, simulation results are illustrated in this section in order to show the performance of the system in closed-loop under the action of adaptive controllers. The parameters of the adaptive controllers (ASTWCs-2) are given in Table 3.2. In Figure 3.4,

Table 3.2: Parameters for ASTWCs-2

Values							
$L_{c_{\Omega_2}}(0)$	ϑ_{22}	$\gamma_{c_{\Omega_2}}$	$k_{c_{\Omega_2}}$	$L_{c_{i_{d_2}}}(0)$	ϑ_{23}	$\gamma_{c_{i_{d_2}}}$	$k_{c_{i_{d_2}}}$
100	400	0.001	300	500	200	0.06	100

the adaptive gains for the controllers (3.2.43) and (3.2.48) are shown, respectively. Moreover, considering the adaptive gain for the speed controller, in Figure 3.5 is illustrated the speed tracking and its tracking error. Then, according to the adaptive parameter $L_{\Omega_2}(t)$, the tracking error is minimized when there are changes in the load torque, such that, it is possible to see the value increase in adaptive gain in order to reduce the error.

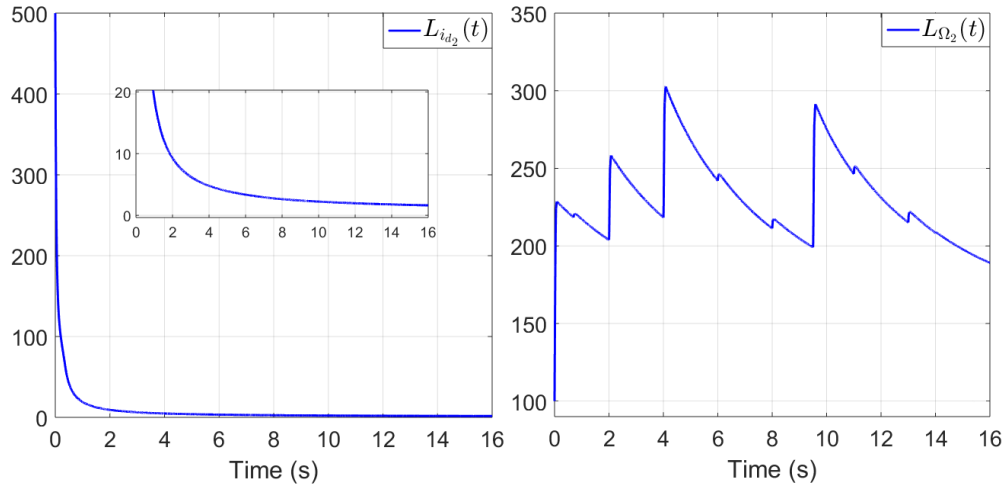


Figure 3.4: ASTWC-2. Behaviour of adaptive law for the speed and current- i_d controllers

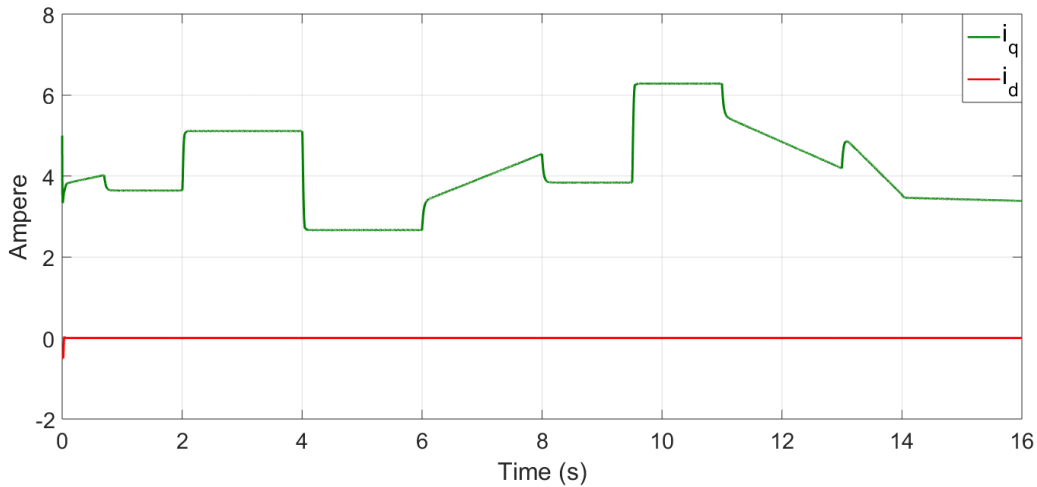


Figure 3.6: ASTWC-2. Behaviour of the currents- i_{dq}

On the other hand, the currents- i_{dq} are introduced in Figure 3.6. The behaviour of the adaptive parameter $L_{i_{d_2}}(t)$ for the current- i_d control can be seen in Figure 3.4, obtaining a good performance for a current- i_d reference equal to zero. Therefore, we can say that the controllers based on adaptive gains have had a satisfactory result in the presence of disturbances and parametric uncertainties. In addition, an evaluation of the proposed adaptive laws is given. The adaptive parameters $L_{c_{\Omega}}(t), L_{c_{i_d}}(t)$, whose solution is given by Theorem 3.1, are evaluated at a specific time (5s). Similarly, the adaptive parameters $L_{c_{\Omega_2}}(t), L_{c_{i_{d_2}}}(t)$, whose solution is given by Theorem 3.2, are evaluated at a specific time (5s), as can be seen in Table 3.3. The

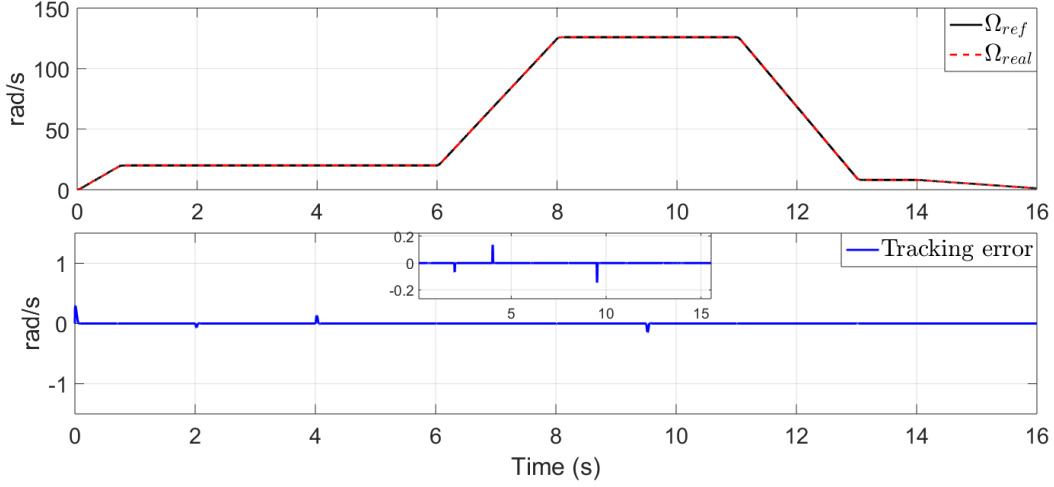


Figure 3.5: ASTWC-2. Speed tracking and speed tracking error

final value in each gain can show that the adaptive parameter ($L_{c\Omega_2}$) is more conservative for the speed controller. However, for the current controller, both strategies have achieved to adjust the gains with similar values. Therefore, it is possible to say that the adaptive law given by Theorem 3.1 provides more energy in the presence of disturbances (Load torque).

In Chapter 4, the ASTWCs-2 of the IPMSM will be interconnected with the AHOSMO-2 presented in Chapter 2. From this, the sensorless scheme for the IPMSM will be introduced.

Table 3.3: Value for the gains of both adaptive controllers at 5 seconds

ASTWCs-1					
$L_{c\Omega}(5)$	$\tilde{K}_{c1\Omega}$	$\tilde{K}_{c2\Omega}$	$L_{c_{i_d}}(5)$	$\tilde{K}_{c1_{i_d}}$	$\tilde{K}_{c2_{i_d}}$
24.9	1248	$1.9 e^5$	2.07	8.57	9.19
ASTWCs-2					
$L_{c\Omega_2}(5)$	$\tilde{K}_{c3\Omega}$	$\tilde{K}_{c4\Omega}$	$L_{c_{i_{d2}}}(5)$	$\tilde{K}_{c3_{i_d}}$	$\tilde{K}_{c4_{i_d}}$
285.4	570.7	$4.07e^4$	4.3	8.61	9.27

3.3 Comparative study

In this section, two comparative studies are addressed. First, considering constant gains, the proposed controllers based on reparameterized gains are compared with two similar strategies of

the literature. After that, the proposed adaptive controllers are compared with three adaptive strategies of the literature. The performance of each strategy will be shown by considering simulation tests.

3.3.1 Comparative study with constant gains

In this work has been proposed two strategies with parameterized gains in order to tune the gains in an easier way, *i.e.*, the gains are based on a single parameter. Then, a comparative study will be carried out by considering only constant gains, *i.e.*, the proposed adaptive laws are not considered. Therefore, considering that $(* = \Omega, i_d)$, the gains for the proposal 1 are given by $K_{c1*} = 2L_{c*}^2, K_{c2*} = \frac{L_{c*}^4}{2}$ where L_{c*} is positive constant. Similarly, the gains for the proposal 2 are given by $K_{c3*} = 2L_{c*2}, K_{c4*} = \frac{L_{c*2}^2}{2}$ where L_{c*2} is positive constant. Then, considering the proposed strategies in this work, two similar strategies have been taken from the literature to compare the performance of each of them.

Levant [89] *Super-twisting strategy was proposed in [39]. However, in [39], the super-twisting control has two gains, which results complex to tune, causing overestimation of gains. For this reason, in [89] was proposed an alternative to tune the gains as follows*

$$\begin{aligned}\sigma_L &= -k_{1L}|s|^{1/2}\text{sign}(s) + \nu_L \\ \dot{\nu}_L &= -k_{2L}\text{sign}(s)\end{aligned}\tag{3.3.1}$$

where s is the sliding surface, $k_{1L} = 1.5L_L^{1/2}$ and $k_{2L} = 1.1L_L$ where L_L is the parameter to be tuned.

Moreno [84] *A second alternative to tune the gains of the super twisting was proposed in [84]. In this strategy the super twisting is given by*

$$\begin{aligned}\sigma_M &= -k_{1M}|s|^{1/2}\text{sign}(s) + \nu_M \\ \dot{\nu}_M &= -k_{2M}\text{sign}(s)\end{aligned}\tag{3.3.2}$$

and its gains are defined by

$$k_{1M} = \mu_M \sqrt{\frac{2\gamma_M}{(1-\beta_M)\alpha_M}} \sqrt{L_M} \quad k_{2M} = \frac{(\beta_M + 1)}{(1-\beta_M)} L_M$$

where μ_M , α_M , β_M and γ_M are positive constants, such that $0 < \beta_M < 1$ and $\gamma_M > 1$, satisfying the following inequality

$$\mu_M - \frac{2}{\gamma_M} \alpha_M > \alpha_M^2 - \beta_M(1 + \mu_M)\alpha_M + \frac{1}{4}(1 + \mu_M)^2 \quad (3.3.3)$$

Now, the comparative study will be introduced by considering the best values of each strategy in order to make a fair comparison.

In this way, the parameter value L_{c^*} in the proposal-1 is given by $L_{c^*} = 16$ and the parameter value $L_{c^{*2}}$ in the proposal-2 is given by $L_{c^{*2}} = 254$.

Now, considering the strategy (3.3.1) and applying the strategy in the speed and current controller, a value of $L_L = 30000$ is chosen.

On the other hand, in (3.3.2), the chosen values are the following: $\mu_M = 3.5$, $\alpha_M = 2.8$, $\beta_M = 0.8$, $\gamma_M = 12$ and $L_M = 600$. Similar values are applied in the speed and current controller.

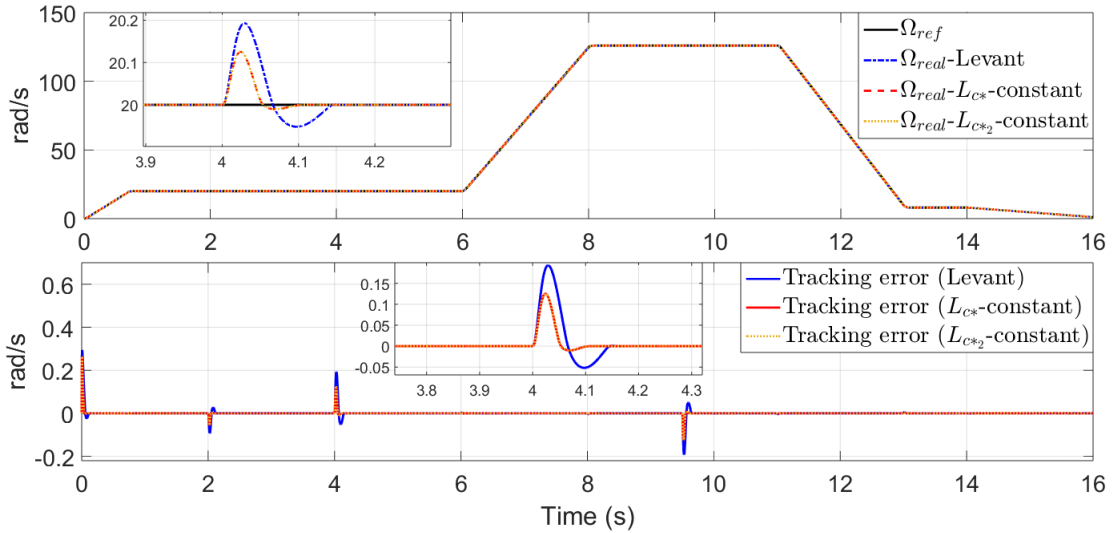


Figure 3.7: Speed tracking. Comparative study among Levant strategy and proposed strategies

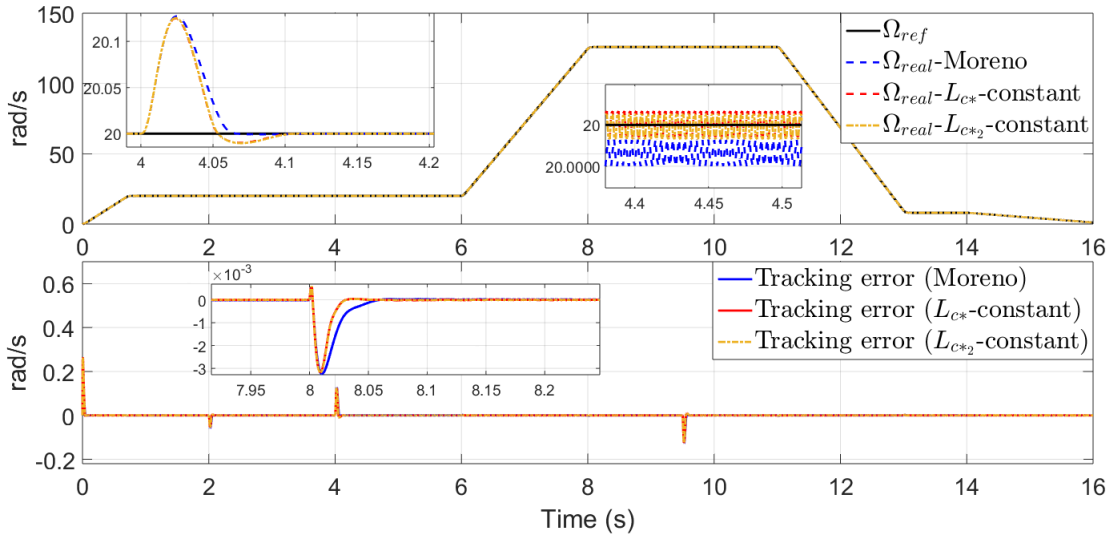


Figure 3.8: Speed tracking. Comparative study among Moreno strategy and proposed strategies

Then, taking into account the information for each strategy, a comparison for the speed tracking is illustrated. In Figure 3.7, the proposed strategies are compared with (3.3.1) and in Figure 3.8, the proposed strategies are compared with (3.3.2). Then, it is possible to show that the adjustment of gains of (3.3.1) is not enough to attenuate the disturbance, it can be seen at 4 s (see Figure 3.7). In Figure 3.8 is possible to illustrate a similar behaviour among the strategies. On the other side, the currents i_{dq} are illustrated in Figure 3.9 and Figure 3.10.

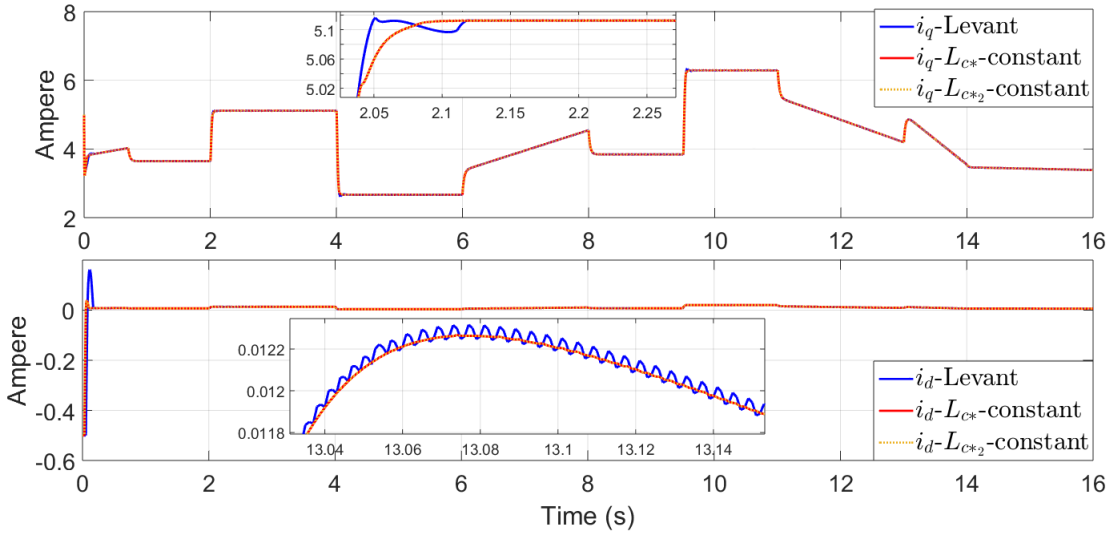


Figure 3.9: Currents— i_{dq} . Comparative study among Levant strategy and proposed strategies

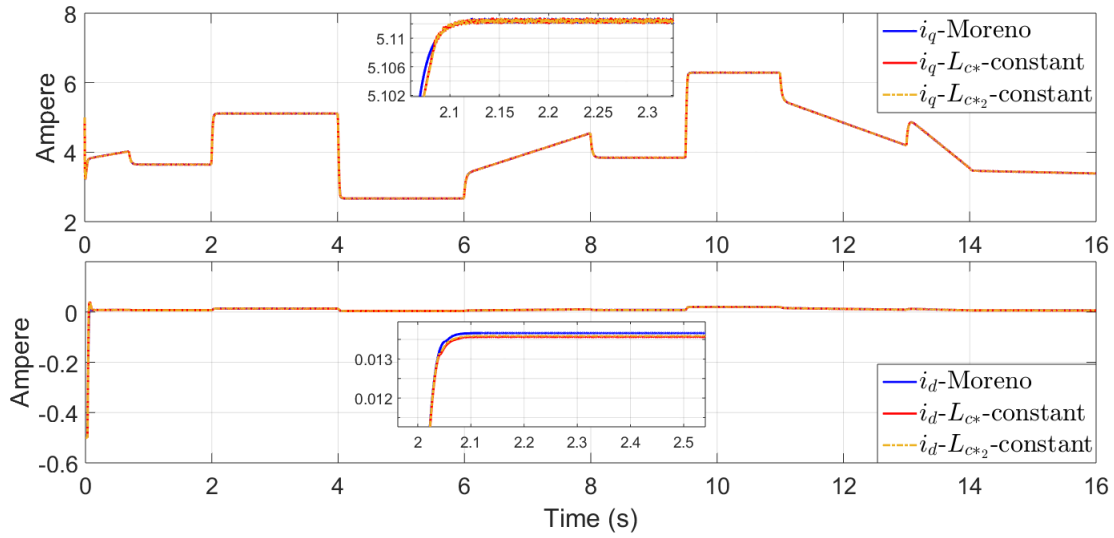


Figure 3.10: Currents $-i_{dq}$. Comparative study among Moreno strategy and proposed strategies

According to comparison, strategy (3.3.1) presents more chattering in the current $-i_d$, while the strategy (3.3.2) has a similar behaviour with the proposed strategies.

Similarly, in Figure 3.11 and Figure 3.12, the voltages $-dq$ are introduced. A behaviour with more chattering in the signal can be seen for the strategy (3.3.1) (See Figure 3.11). On the other side, considering the strategy (3.3.2), in Figure 3.12 can be seen a similar performance of the voltages with proposed strategies. In addition, a performance index (Integral Absolute

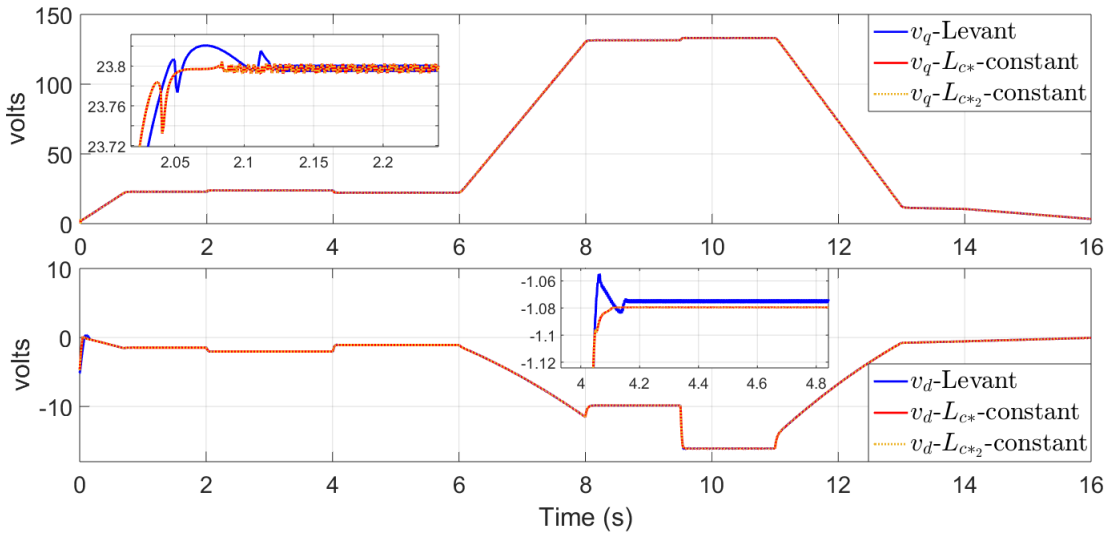


Figure 3.11: Voltages $-v_{dq}$. Comparative study among Levant strategy and proposed strategies

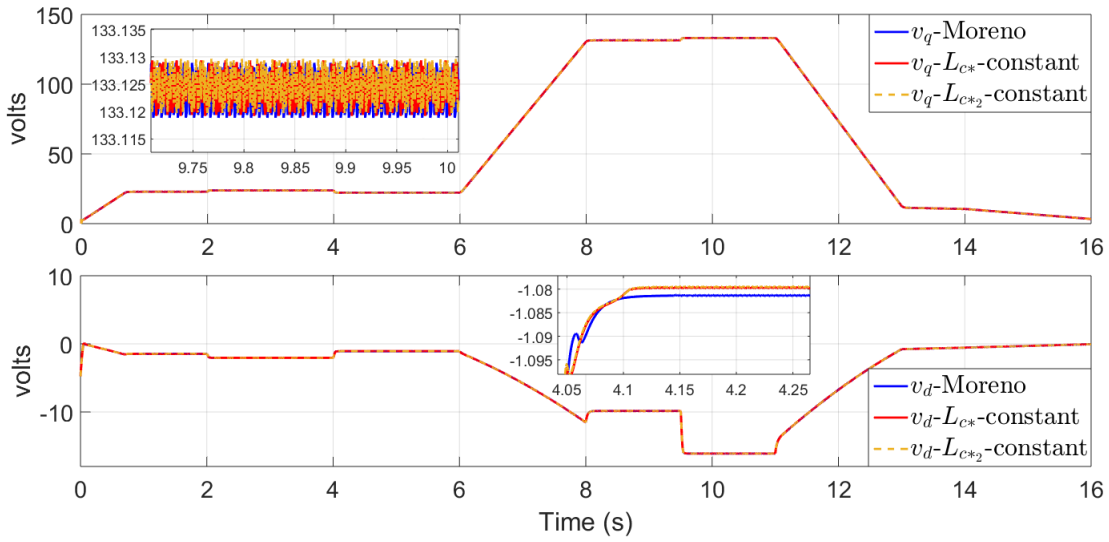


Figure 3.12: Voltages $-v_{dq}$. Comparative study among Moreno strategy and proposed strategies

Value-IAE) is considered. In Figure 3.13, it is possible to show that the strategy (3.3.2) and the proposed strategies have a similar performance, except (3.3.1). Finally, we can conclude that in

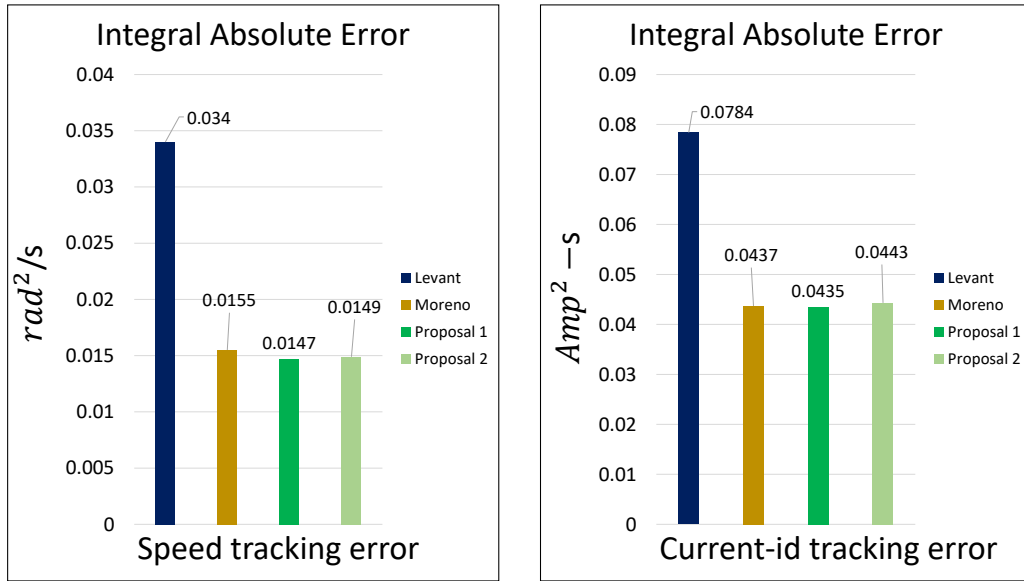


Figure 3.13: Performance index: Comparative study using constant gains

(3.3.1), the value for L_L needs to be very large, which turns out to be somewhat complex to find a more precise value. Moreover, the main disadvantage in (3.3.2) is that it is necessary to find and adjust different parameters for satisfying the inequality and after that, gain adjustment

can be done. However, the proposed strategies in this work only needs to adjust one parameter satisfying the tracking with a good performance, which has allowed the design of the proposed adaptive laws for the controller in sections 3.1.1 and 3.2.1.

It is worth mentioning that the choice of constant gains could generate an overestimation of the gains and cause chattering in the signals. A simulation test is shown in Figure 3.14, where the proposed strategy given in section 3.1.1 (Proposal 1) has been considered using constant gains. The parameter value L_{c^*} can be seen with different values, 10 at the beginning, 40 at 4.5 seconds and 70 at 10 seconds, respectively. In the beginning, the gain is small and the tracking is achieved with less precision, after that, at 4.5 seconds, the gains are increased achieving a correct estimation. However, at 10 seconds, it is possible to illustrate the chattering effect for a value of $L_{c^*} = 70$. Similarly, this can be illustrated by the voltages and currents.

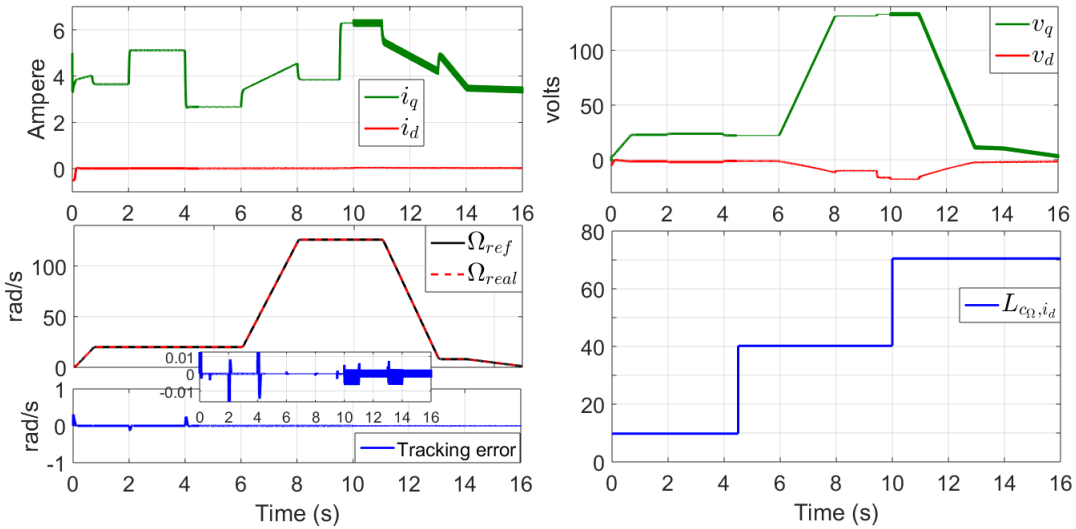


Figure 3.14: Proposal 1. Performance using different constant gain values

For this reason, the design of adaptive laws is necessary to avoid this issue. In Figure 3.15, the action of the adaptive parameters, L_{c_Ω} and $L_{c_{i_d}}$, are shown such that the gains are adjusted according to the need of the controller to achieve the minimum error, avoiding overestimation of gains and chattering in the signals.

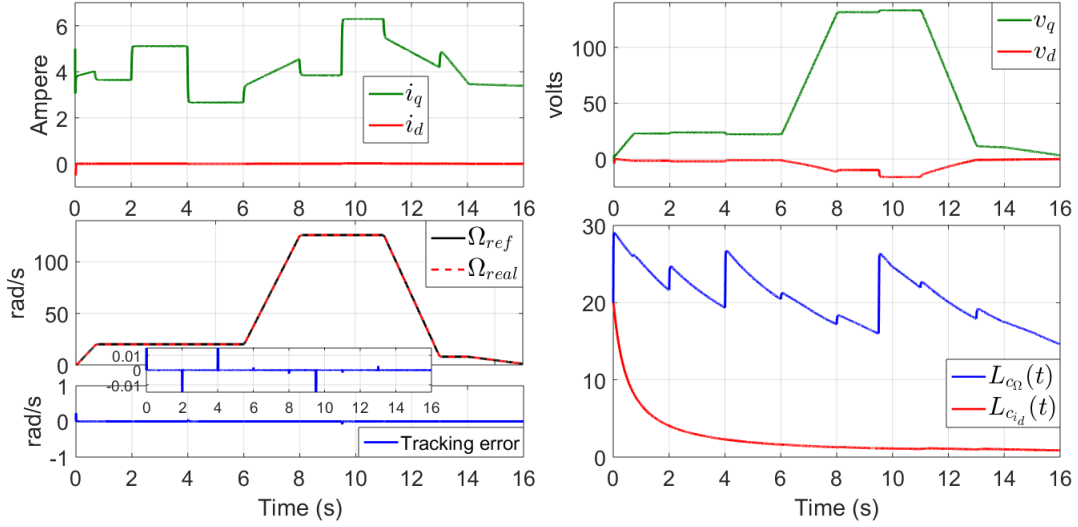


Figure 3.15: Proposal 1 (ASTWC-1). Performance using adaptive gains

3.3.2 Comparative study with adaptive strategies

The adaptive laws introduced in Theorem 3.1 and Theorem 3.2 are compared with three proposed strategies in the literature.

The term \mathcal{V}_{st-*} for $* = \Omega, i_d$ will be defined for each controller.

Firstly, an Adaptive Sliding mode Control (**ASMC**) has been introduced in [90], with the control input \mathcal{V}_{st-*} given by

$$\mathcal{V}_{st-*} = -K_*(t)\text{sign}(S_*) \quad (3.3.4)$$

where $K_*(t)$ is an adaptive law defined by

$$\dot{K}_*(t) \begin{cases} \bar{K}_* |S_*| \text{sign}(|S_*| - \epsilon_*) & \text{if } K_* > \mu_* \\ \mu_* & \text{if } K_* \leq \mu_* \end{cases} \quad (3.3.5)$$

where $K_*(0) > 0$, $\bar{K}_* > 0$, $\mu_* > 0$ and $\epsilon_* = 2K_*(t)T_e$ with T_e is the sampling time.

Secondly, an Adaptive Super twisting (**ASTW**) was introduced in [91], where the control input \mathcal{V}_{st-*} is given by

$$\mathcal{V}_{st-*} = -\alpha_*(t)|S_*|^{\frac{1}{2}}\text{sign}(S_*) - \int_0^t \frac{\beta_*(t)}{2}\text{sign}(S_*)d\tau \quad (3.3.6)$$

with $\alpha_*(t)$ and $\beta_*(t)$ defined by

$$\dot{\alpha}_*(t) = \begin{cases} \varpi \sqrt{\frac{\gamma_*}{2}} \text{sign}(|S_*| - \mu_*) & \text{if } \alpha_* > 0 \\ 0 & \text{if } \alpha_* = 0 \end{cases} \quad (3.3.7)$$

$$\beta_*(t) = 2\epsilon_*\alpha_*$$

where ϖ , γ_* , μ_* and ϵ_* are positive constants.

The third adaptive law was introduced in [88] and a simplified adaptive super twisting (**SAST**) was proposed, with the control input \mathcal{V}_{st-*} given by

$$\mathcal{V}_{st-*} = -K_{G1*}|S_*|^{\frac{1}{2}}\text{sign}(S_*) - \int_0^t K_{G2*}\text{sign}(S_*)dt \quad (3.3.8)$$

where $K_{G1*} = 2L_{G*}(t)$ and $K_{G2*} = \frac{L_{G*}(t)^2}{2}$ and $L_{G*}(t) > 0$ is an adaptive parameter, solution of

$$\dot{L}_{G*}(t) = \frac{-\frac{k_{G*}}{\sqrt{2}}|L_{G*}(t) - L_{ref}| + \frac{L_{G*}(t)}{2}|S_*|^{\frac{1}{2}}}{\left(L_{G*}(t) - L_{ref}\right) + \frac{2}{L_{G*}(t)^2}(|S_*|^{\frac{1}{2}} + \frac{1}{L_{G*}(t)} \int L_{G*}^2(\tau)\text{sign}(S_*)d\tau) \left(-\int \frac{L_{G*}^2(\tau)}{2}\text{sign}(S_*)d\tau\right)} \quad (3.3.9)$$

for $L_{ref} > 0$ and $k_{G*} > 0$.

The ASMC, ASTW and SAST are compared with the proposal 1 (ASTWC-1) given by Theorem 3.1 and the proposal 2 (ASTWC-2) given by Theorem 3.2 under the same conditions in order to evaluate the performance of each adaptive control in terms of tracking error and tuning process (number of parameters).

A simulation test has been carried out in Matlab-Simulink environment, using a sampling time of 1×10^{-3} with a fixed-step *ode4* solver. The profile for the speed and the disturbance (Load Torque) are given in Figure 1.7 and the parameters used in the adaptive strategies have been chosen in order to get the best results.

ASMC: $\bar{K}_{i_d} = 20$, $\mu_{i_d} = 0.5$, $\bar{K}_{\Omega} = 20$, $\mu_{\Omega} = 0.5$ $T_e = 1 \times 10^{-3}$.

ASTW: $\bar{\omega}_{i_d} = 5$, $\gamma_{i_d} = 2$, $\mu_{i_d} = 0.1$, $\epsilon_{i_d} = 2$, $\bar{\omega}_{\Omega} = 5$, $\gamma_{\Omega} = 2$, $\mu_{\Omega} = 0.1$, $\epsilon_{\Omega} = 2$.

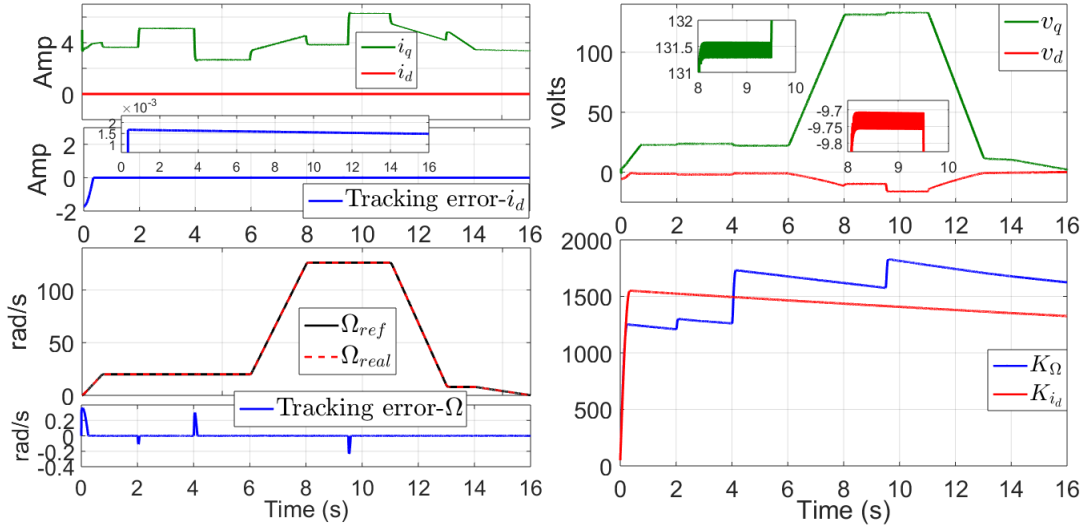


Figure 3.16: Control performance using ASMC strategy

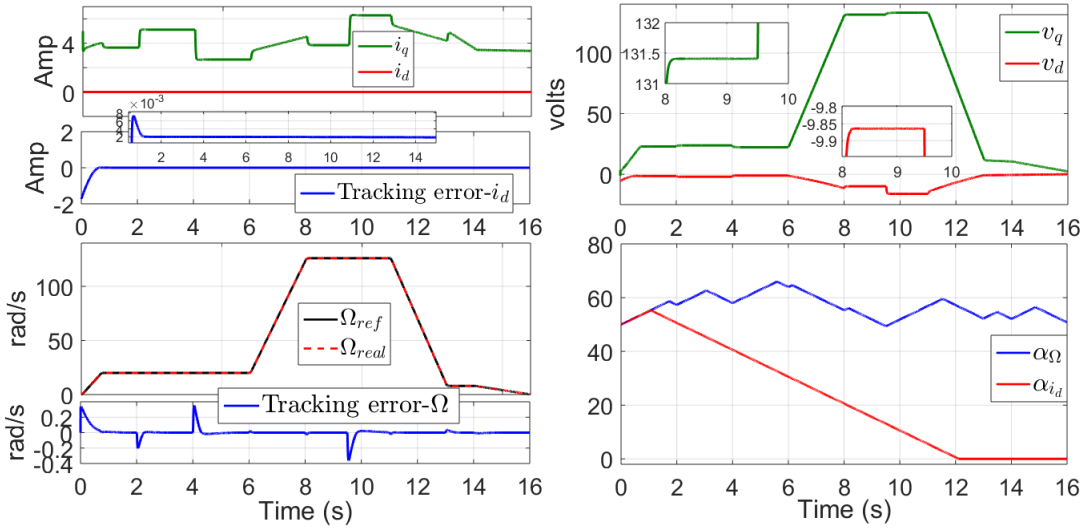


Figure 3.17: Control performance using ASTW strategy

SAST: $k_{G_{i_d}} = 15$, $k_{G_\Omega} = 10$, $L_{ref} = 0.1$.

ASTWC-1: $k_{c_{i_d}} = 1$, $\gamma_{c_{i_d}} = 0.1$, $k_{c_\Omega} = 90$, $\gamma_{c_\Omega} = 0.05$.

ASTWC-2: $k_{c_{i_{d_2}}} = 100$, $\gamma_{c_{i_{d_2}}} = 0.06$, $k_{c_{\Omega_2}} = 200$, $\gamma_{c_{\Omega_2}} = 0.001$.

In Figure 3.16, ASMC is addressed. An increase in the chattering can be seen in the voltages. It has been improved in the ASTW (See Figure 3.17). However, to get good results, it is necessary to adjust different parameters in the adaptive law. Then, in order to reduce the

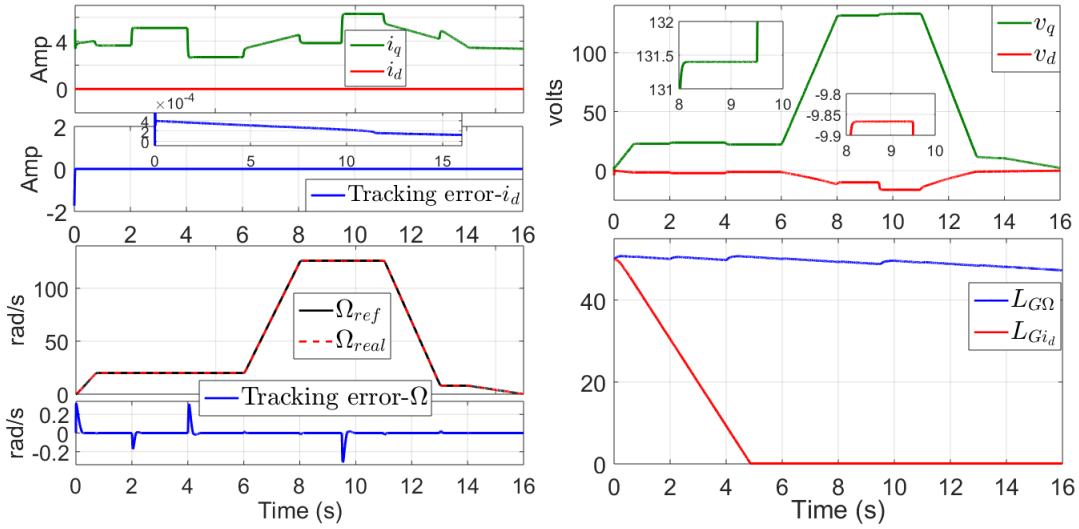


Figure 3.18: Control performance using SAST strategy

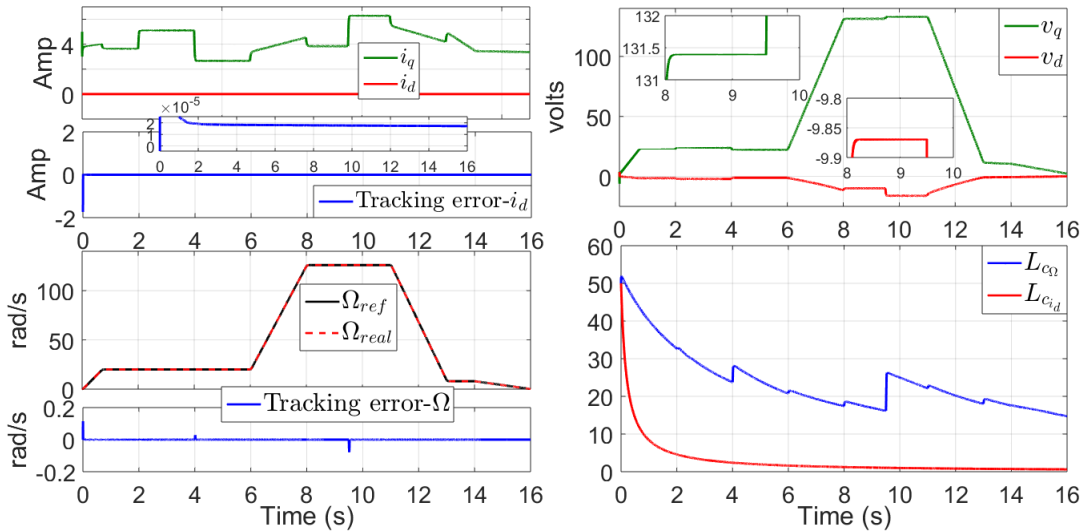


Figure 3.19: Control performance using proposed ASTWC-1 strategy

number of parameters for tuning the adaptive controller, a SAST is illustrated in Figure 3.18 achieving good results in the tracking errors. However, the structure of the adaptive law is complex. Therefore, considering a reparameterization of gains, similarly to SAST, in this work an effort has been made to simplify adaptive law, achieving better results, as shown in Figure 3.19 and Figure 3.20, ASTWC-1 and ASTWC-2, respectively. The tracking errors has been greatly decreased as well as the time of convergence. Moreover, the adaptive laws only need two

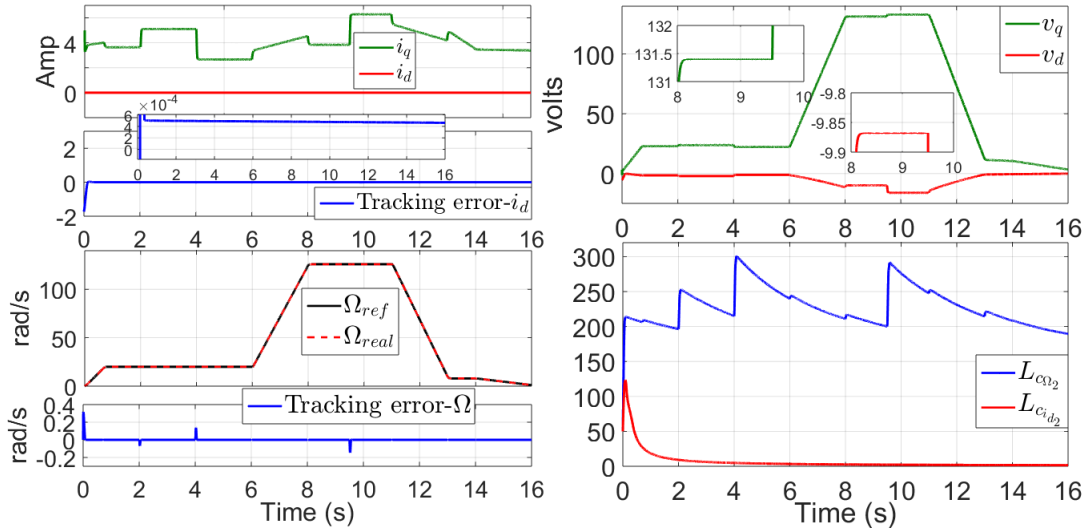


Figure 3.20: Control performance using proposed ASTWC-2 strategy

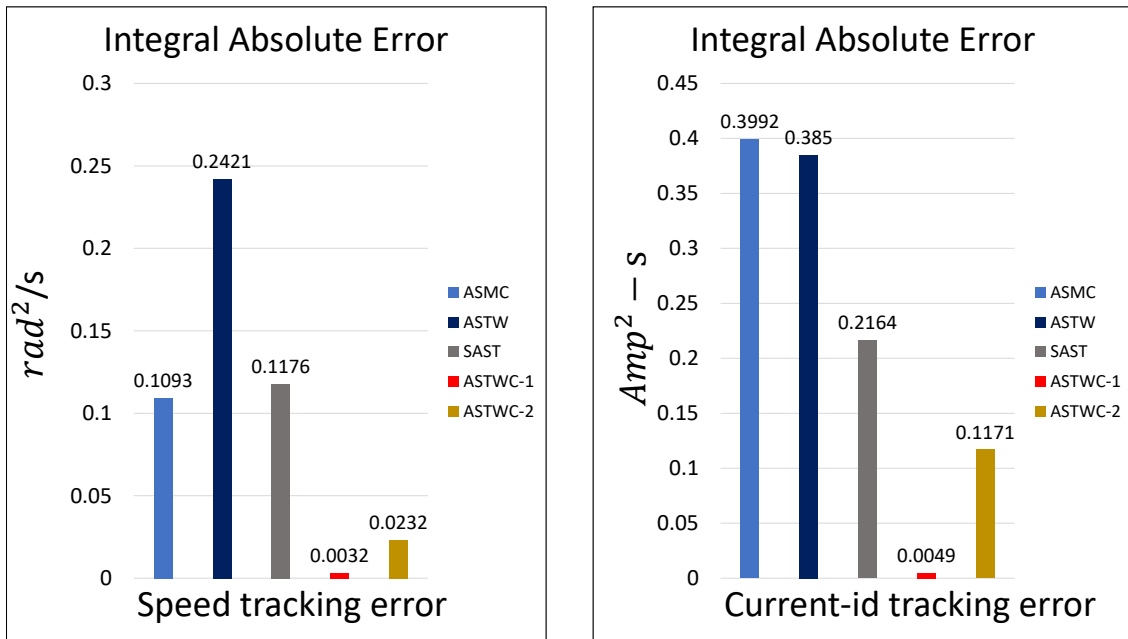


Figure 3.21: Performance index: Comparative study using adaptive gains

parameters to be adjusted, similarly as the SAST. Nevertheless, the structure is less complex.

In order to compare the strategies, a performance index, Integral Absolute Error (IAE), is considered. From Figure 3.21, it can be concluded that the two proposed strategies (ASTWC-1, ASTWC-2) can guarantee a high level of accuracy in the tracking error. Moreover, from the Figures 3.16-3.20, a reduced level of chattering can be illustrated in all strategies, except for

ASMC.

3.4 Conclusion

In this chapter, two adaptive controllers based on super-twisting approach have been introduced. The gains of the controllers have been reparameterized in terms of a single parameter to reduce the tuning time. From reparameterized gains, an adaptive law was designed for each controller in order to avoid overestimation of gains and the classical chattering. Simulation tests have been carried out in closed-loop. Some tests were performed to justify the use of adaptive laws. Moreover, considering constant and adaptive gains, a comparative study was carried out taking into account some results from the literature, to show the performance of each of them with respect to the proposed strategies, so that the proposed strategies can show a reduction in tuning time with good performance, effectiveness and a less complex structure.

Chapter 4

Sensorless control of the Interior Permanent Synchronous Motor

In this Chapter, two sensorless control schemes for the IPMSM are introduced, i.e., the proposed observers are interconnected with the proposed controllers in closed-loop. First, the stability analysis for the first scheme is addressed, interconnecting in closed-loop the adaptive observer given in section 2.2.1 (AHOSMO-1) with the adaptive control given in section 3.1.1 (ASTWC-1). Simulation and experimental results are introduced for this strategy. After that, the adaptive observer given in section 2.3.1 (AHOSMO-2) is interconnected in closed-loop with the adaptive control given in section 3.2.1 (ASTWC-2). A stability analysis is introduced and simulation and experimental results are illustrated for this strategy.

4.1 Closed-loop analysis: Scheme 1

Consider the proposed control in section 3.1.1 (ASTWC-1) using the estimates provided by the proposed observer in section 2.2.1 (AHOSMO-1). Then, the stability analysis of the system in closed-loop with the control-observer scheme is established as follows

Theorem 4.1. *Consider the dynamical model of the IPMSM (1.3.30)-(1.3.31) in closed-loop with the controllers (3.1.42) and (3.1.47) using the estimates provided by the observer (2.2.35). Then, tracking errors e_{1_Ω} and $e_{1_{i_d}}$; and estimation error e_{θ_e} converge to zero in finite time.*

Proof: Since the control input $v_q(\hat{x})$ depends on estimates $\hat{\Omega}$, \hat{i}_d and \hat{i}_q ; and taking into account the sliding surface given by (3.1.41), then the dynamic of the sliding surface is given by

$$\dot{S}_\Omega = \vartheta_{12}e_{2_\Omega} + a_1b_1 + a_2b_2 + a_3b_2 - b_3 + b_4 - \ddot{\Omega}^* + c_1v_q(\hat{x}). \quad (4.1.1)$$

Now, adding and subtracting the term $c_1v_q(x)$ in the sliding surface, it follows that

$$\dot{S}_\Omega = \vartheta_{12}e_{2_\Omega} + a_1b_1 + a_2b_2 + a_3b_2 - b_3 + b_4 - \ddot{\Omega}^* + c_1v_q(x) + c_1[v_q(\hat{x}) - v_q(x)] \quad (4.1.2)$$

Notice that the term $c_1[v_q(\hat{x}) - v_q(x)]$ is Lipschitz, *i. e.*, there exists a positive constant μ_{11} such that $\|c_1[v_q(\hat{x}) - v_q(x)]\| \leq \mu_{11}\|\hat{x} - x\|$. Then, applying the control input $v_q(x)$ given by (3.1.42) into (4.1.2), the dynamic of the sliding surface is given by

$$\dot{S}_\Omega = -2L_{c_\Omega}^2(t)|S_\Omega|^{\frac{1}{2}}\text{sign}(S_\Omega) - \int_0^t \frac{L_{c_\Omega}^4(t)}{2}\text{sign}(S_\Omega)d\tau + c_1[v_q(\hat{x}) - v_q(x)] + \delta_\Omega(t) \quad (4.1.3)$$

for $\delta_\Omega(t) = b_4 = \frac{f_v T_l}{J^2}$. The dynamic of S_Ω can be expressed as follows

$$\begin{cases} \dot{S}_\Omega = -2L_{c_\Omega}^2(t)|S_\Omega|^{1/2}\text{sign}(S_\Omega) + \nu_\Omega + \delta_\Omega(t) + c_1[v_q(\hat{x}) - v_q(x)] \\ \dot{\nu}_\Omega = -\frac{L_{c_\Omega}^4(t)}{2}\text{sign}(S_\Omega) \end{cases} \quad (4.1.4)$$

Now, defining the following change of coordinates $\Upsilon_{1_\Omega} = S_\Omega$ and $\Upsilon_{2_\Omega} = \nu_\Omega + \delta_\Omega(t)$. It follows that

$$\begin{cases} \dot{\Upsilon}_{1_\Omega} = -2L_{c_\Omega}^2(t)|\Upsilon_{1_\Omega}|^{1/2}\text{sign}(\Upsilon_{1_\Omega}) + \Upsilon_{2_\Omega} + c_1[v_q(\hat{x}) - v_q(x)] \\ \dot{\Upsilon}_{2_\Omega} = -\frac{L_{c_\Omega}^4(t)}{2}\text{sign}(\Upsilon_{1_\Omega}) + d_\Omega(t) \end{cases} \quad (4.1.5)$$

with $d_\Omega(t) = \dot{\delta}_\Omega(t)$. To analyze the stability of the system (4.1.5), consider the following change of coordinates as follows

$$z_{1\Omega} = \frac{\Upsilon_{1\Omega}}{L_{c\Omega}^2(t)} \quad z_{2\Omega} = \frac{\Upsilon_{2\Omega}}{L_{c\Omega}^2(t)}. \quad (4.1.6)$$

whose dynamics are given by

$$\begin{aligned} \dot{z}_{1\Omega} &= -2L_{c\Omega}(t)|z_{1\Omega}|^{\frac{1}{2}}\text{sign}(z_{1\Omega}) + z_{2\Omega} + \frac{c_1[v_q(\hat{x}) - v_q(x)]}{L_{c\Omega}^2(t)} - \frac{2z_{1\Omega}\dot{L}_{c\Omega}(t)}{L_{c\Omega}(t)} \\ \dot{z}_{2\Omega} &= -\frac{L_{c\Omega}^2(t)}{2}\text{sign}(z_{1\Omega}) + \frac{d_\Omega(t)}{L_{c\Omega}^2(t)} - \frac{2z_{2\Omega}\dot{L}_{c\Omega}(t)}{L_{c\Omega}(t)} \end{aligned} \quad (4.1.7)$$

After that, in order to represent the system in a simple form, a new change of variable is introduced as follows

$$\mathcal{L}_{1\Omega} = |z_{1\Omega}|^{\frac{1}{2}}\text{sign}(z_{1\Omega}) \quad \mathcal{L}_{2\Omega} = \frac{z_{2\Omega}}{L_{c\Omega}(t)} \quad (4.1.8)$$

then, the dynamical behavior, in the new coordinates, is given by

$$\begin{aligned} \dot{\mathcal{L}}_{1\Omega} &= \frac{L_{c\Omega}(t)}{2|z_{1\Omega}|^{\frac{1}{2}}} \left[-2\mathcal{L}_{1\Omega} + \mathcal{L}_{2\Omega} + \frac{c_1[v_q(\hat{x}) - v_q(x)]}{L_{c\Omega}^3(t)} \right] - \mathcal{L}_{1\Omega} \frac{\dot{L}_{c\Omega}(t)}{L_{c\Omega}(t)} \\ \dot{\mathcal{L}}_{2\Omega} &= \frac{L_{c\Omega}(t)}{2|z_{1\Omega}|^{\frac{1}{2}}} \left[-\mathcal{L}_{1\Omega} + \frac{2|z_{1\Omega}|^{\frac{1}{2}}d_\Omega(t)}{L_{c\Omega}^4(t)} \right] - 3\mathcal{L}_{2\Omega} \frac{\dot{L}_{c\Omega}(t)}{L_{c\Omega}(t)} \end{aligned} \quad (4.1.9)$$

which can be represented in a compact form as follows

$$\dot{\mathcal{L}}_\Omega = \alpha_\Omega [(A_\Omega - P_\Omega^{-1}C_\Omega^T C_\Omega) \mathcal{L}_\Omega + \Phi_\Omega] - N_\Omega \mathcal{L}_\Omega \frac{\dot{L}_{c\Omega}(t)}{L_{c\Omega}(t)} \quad (4.1.10)$$

with $\alpha_\Omega = \frac{L_{c\Omega}(t)}{2|z_{1\Omega}|^{\frac{1}{2}}}$, $\mathcal{L}_\Omega = [\mathcal{L}_{1\Omega} \quad \mathcal{L}_{2\Omega}]^T$, $C_\Omega = [1 \quad 0]$,

$$A_\Omega = \begin{bmatrix} 0 & 1 \\ 0 & 0 \end{bmatrix}, \quad P_\Omega = \begin{bmatrix} 1 & -1 \\ -1 & 2 \end{bmatrix}, \quad N_\Omega = \begin{bmatrix} 1 & 0 \\ 0 & 3 \end{bmatrix}, \quad \Phi_\Omega = \begin{bmatrix} \frac{c_1[v_q(\hat{x}) - v_q(x)]}{L_{c\Omega}^3(t)} \\ \frac{2|z_{1\Omega}|^{\frac{1}{2}}}{L_{c\Omega}^4(t)} [d_\Omega(t)] \end{bmatrix},$$

where, from Assumption 3.3, the nonlinear term Φ_Ω satisfies the following inequality, $\|\Phi_\Omega\| \leq \varsigma_{11}\|\mathcal{L}_\Omega\|$ for $\varsigma_{11} > 0$.

Following the same steps of the previous analysis, consider the control input v_d expressed in terms of the estimates as follows

$$v_d(\hat{x}) = \frac{L_d}{\vartheta_{13}} \left(\frac{\vartheta_{13} R_s \hat{i}_d}{L_d} - \frac{\vartheta_{13} p \hat{\Omega} L_q \hat{i}_q}{L_d} + \vartheta_{13} \dot{i}_d^* - e_{i_d} \right. \\ \left. - 2L_{c_{i_d}}^2(t) |S_{i_d}|^{\frac{1}{2}} \text{sign}(S_{i_d}) - \int_0^t \frac{L_{c_{i_d}}^4(\tau)}{2} \text{sign}(S_{i_d}) d\tau \right) \quad (4.1.11)$$

Then, from the sliding surface (3.1.46) and the control input (4.1.11) depending on the estimated states, the dynamic of the sliding surface is given by

$$\dot{S}_{i_d} = -\frac{\vartheta_{13} R_s i_d}{L_d} + \frac{\vartheta_{13} p \Omega L_q i_q}{L_d} + \frac{\vartheta_{13}}{L_d} v_d(\hat{x}) - \vartheta_{13} \dot{i}_d^* + e_{i_d} + \delta_{i_d}(t) \quad (4.1.12)$$

where $\delta_{i_d}(t)$ represents the uncertain/disturbance term.

Adding and subtracting the term $\frac{\vartheta_{13}}{L_d} v_d(x)$ in (4.1.12), it follows that

$$\dot{S}_{i_d} = -\frac{\vartheta_{13} R_s i_d}{L_d} + \frac{\vartheta_{13} p \Omega L_q i_q}{L_d} + \frac{\vartheta_{13}}{L_d} v_d(x) - \vartheta_{13} \dot{i}_d^* + e_{i_d} + \frac{\vartheta_{13}}{L_d} [v_d(\hat{x}) - v_d(x)] + \delta_{i_d}(t) \quad (4.1.13)$$

where the term $\frac{\vartheta_{13}}{L_d} [v_d(\hat{x}) - v_d(x)]$ is Lipschitz, *i.e.*, there exist a positive constant μ_{12} such that $\|\frac{\vartheta_{13}}{L_d} [v_d(\hat{x}) - v_d(x)]\| \leq \mu_{12} \|\hat{x} - x\|$. Moreover, applying the control input $v_d(x)$ given by (3.1.47) into the above system, the dynamic of the sliding surface is given by

$$\dot{S}_{i_d} = -2L_{c_{i_d}}^2(t) |S_{i_d}|^{\frac{1}{2}} \text{sign}(S_{i_d}) - \int_0^t \frac{L_{c_{i_d}}^4(\tau)}{2} \text{sign}(S_{i_d}) d\tau + \frac{\vartheta_2}{L_d} [v_d(\hat{x}) - v_d(x)] + \delta_{i_d}(t) \quad (4.1.14)$$

which can be represented as follows

$$\begin{cases} \dot{S}_{i_d} = -2L_{c_{i_d}}^2(t) |S_{i_d}|^{1/2} \text{sign}(S_{i_d}) + \nu_{i_d} + \delta_{i_d}(t) + \frac{\vartheta_2}{L_d} [v_d(\hat{x}) - v_d(x)] \\ \dot{\nu}_{i_d} = -\frac{L_{c_{i_d}}^4(t)}{2} \text{sign}(S_{i_d}) \end{cases} \quad (4.1.15)$$

Now, defining $\Upsilon_{1_{i_d}} = S_{i_d}$ and $\Upsilon_{2_{i_d}} = \nu_{i_d} + \delta_{i_d}(t)$. The system \dot{S}_{i_d} can be expressed as follows

$$\begin{aligned}\dot{\Upsilon}_{1_{i_d}} &= -2L_{c_{i_d}}^2(t)|\Upsilon_{1_{i_d}}|^{1/2}\text{sign}(\Upsilon_{1_{i_d}}) + \Upsilon_{2_{i_d}} + \frac{\vartheta_2}{L_d}[v_d(\hat{x}) - v_d(x)] \\ \dot{\Upsilon}_{2_{i_d}} &= -\frac{L_{c_{i_d}}^4(t)}{2}\text{sign}(\Upsilon_{1_{i_d}}) + d_{i_d}(t)\end{aligned}\quad (4.1.16)$$

with $d_{i_d}(t) = \delta_{i_d}(t)$. Then, from (4.1.16), consider the following change of coordinates, $z_{1_{i_d}} = \frac{\Upsilon_{1_{i_d}}}{L_{c_{i_d}}^2(t)}$ and $z_{2_{i_d}} = \frac{\Upsilon_{2_{i_d}}}{L_{c_{i_d}}^2(t)}$, whose dynamics are given by

$$\begin{aligned}\dot{z}_{1_{i_d}} &= -2L_{c_{i_d}}(t)|z_{1_{i_d}}|^{\frac{1}{2}}\text{sign}(z_{1_{i_d}}) + z_{2_{i_d}} + \frac{\frac{\vartheta_{13}}{L_d}[v_d(\hat{x}) - v_d(x)]}{L_{c_{i_d}}^2(t)} - \frac{2z_{1_{i_d}}\dot{L}_{c_{i_d}}}{L_{c_{i_d}}(t)} \\ \dot{z}_{2_{i_d}} &= -\frac{L_{c_{i_d}}^2(t)}{2}\text{sign}(z_{1_{i_d}}) + \frac{d_{i_d}(t)}{L_{c_{i_d}}^2(t)} - \frac{2z_{2_{i_d}}\dot{L}_{c_{i_d}}(t)}{L_{c_{i_d}}(t)}\end{aligned}\quad (4.1.17)$$

After that, a new change of variable is introduced as

$$\mathcal{L}_{1_{i_d}} = |z_{1_{i_d}}|^{\frac{1}{2}}\text{sign}(z_{1_{i_d}}) \quad \mathcal{L}_{2_{i_d}} = \frac{z_{2_{i_d}}}{L_{c_{i_d}}(t)}\quad (4.1.18)$$

whose dynamics are given by

$$\begin{aligned}\dot{\mathcal{L}}_{1_{i_d}} &= \frac{L_{c_{i_d}}(t)}{2|z_{1_{i_d}}|^{\frac{1}{2}}}\left[-2\mathcal{L}_{1_{i_d}} + \mathcal{L}_{2_{i_d}} + \frac{\frac{\vartheta_{13}}{L_d}[v_d(\hat{x}) - v_d(x)]}{L_{c_{i_d}}^3(t)}\right] - \mathcal{L}_{1_{i_d}}\frac{\dot{L}_{c_{i_d}}(t)}{L_{c_{i_d}}(t)} \\ \dot{\mathcal{L}}_{2_{i_d}} &= \frac{L_{c_{i_d}}(t)}{2|z_{1_{i_d}}|^{\frac{1}{2}}}\left[-\mathcal{L}_{1_{i_d}} + \frac{2|z_{1_{i_d}}|^{\frac{1}{2}}d_{i_d}(t)}{L_{c_{i_d}}^4(t)}\right] - 3\mathcal{L}_{2_{i_d}}\frac{\dot{L}_{c_{i_d}}(t)}{L_{c_{i_d}}(t)}\end{aligned}\quad (4.1.19)$$

Then, system (4.1.19) can be rewritten in a compact form as follows

$$\dot{\mathcal{L}}_{i_d} = \alpha_{i_d} [(A_{i_d} - P_{i_d}^{-1}C_{i_d}^T C_{i_d}) \mathcal{L}_{i_d} + \Phi_{i_d}] - N_{i_d} \mathcal{L}_{i_d} \frac{\dot{L}_{c_{i_d}}(t)}{L_{c_{i_d}}(t)}\quad (4.1.20)$$

with $\alpha_{i_d} = \frac{L_{c_{i_d}}(t)}{2|z_{1_{i_d}}|^{\frac{1}{2}}}$, $\mathcal{L}_{i_d} = [\mathcal{L}_{1_{i_d}} \quad \mathcal{L}_{2_{i_d}}]^T$, $C_{i_d} = [1 \quad 0]$,

$$A_{i_d} = \begin{bmatrix} 0 & 1 \\ 0 & 0 \end{bmatrix}, \quad P_{i_d} = \begin{bmatrix} 1 & -1 \\ -1 & 2 \end{bmatrix}, \quad N_{i_d} = \begin{bmatrix} 1 & 0 \\ 0 & 3 \end{bmatrix}, \quad \Phi_{i_d} = \begin{bmatrix} \frac{\vartheta_{13}}{L_d} [v_d(\hat{x}) - v_d(x)] \\ \frac{L_{c_{i_d}}^3(t)}{L_{c_{i_d}}^4(t)} [d_{i_d}(t)] \end{bmatrix}.$$

From Assumption 3.3, the term Φ_{i_d} is Lipschitz, i.e. there exists $\varsigma_{12} > 0$, such that $\|\Phi_{i_d}\| \leq \varsigma_{12} \|\mathcal{L}_{i_d}\|$.

Then, considering the adaptive observer-1 given in section 2.2.1 and the adaptive control-1 given in section 3.1.1, the dynamics in closed-loop, controller-observer, are established as follows

$$\begin{cases} \dot{\xi} = \alpha_o [(A_o - P_o^{-1} C_o^T C_o) \xi + \Phi_o] - N_o \xi \frac{\dot{L}_o(t)}{L_o(t)} \\ \dot{\mathcal{L}}_\Omega = \alpha_\Omega [(A_\Omega - P_\Omega^{-1} C_\Omega^T C_\Omega) \mathcal{L}_\Omega + \Phi_\Omega] - N_\Omega \mathcal{L}_\Omega \frac{\dot{L}_{c_\Omega}(t)}{L_{c_\Omega}(t)} \\ \dot{\mathcal{L}}_{i_d} = \alpha_{i_d} [(A_{i_d} - P_{i_d}^{-1} C_{i_d}^T C_{i_d}) \mathcal{L}_{i_d} + \Phi_{i_d}] - N_{i_d} \mathcal{L}_{i_d} \frac{\dot{L}_{c_{i_d}}(t)}{L_{c_{i_d}}(t)} \end{cases} \quad (4.1.21)$$

If $\forall t > T_1$, such that ξ tend to zero, then, e_i tend to zero. Therefore, from Theorem 2.1, the observer converges in finite time to zero, it follows that the terms $c_1[v_q(\hat{x}) - v_q(x)]$ and $\frac{\vartheta_{13}}{L_d}[v_d(\hat{x}) - v_d(x)]$ contained in Φ_Ω and Φ_{i_d} , respectively; tend to zero in finite time. Therefore, the system given by (3.1.16) is obtained. Finally, from the same procedure given in the proof of the Theorem 3.1, the stability of the closed-loop system is proved.

4.2 Simulation and experimental results: Scheme 1

In this section, simulation and experimental results have been evaluated in order to show the performance of the proposed strategy. The adaptive observer introduced in section 2.2.1 and the adaptive control introduced in section 3.1.1 have been interconnected to illustrate the performance of the control in closed-loop under the action of the observer estimates, *i.e.*, controller+observer (ASTWC-1 + AHOSMO-1). A scheme of the proposed sensorless control-1 is shown in Figure 4.1.

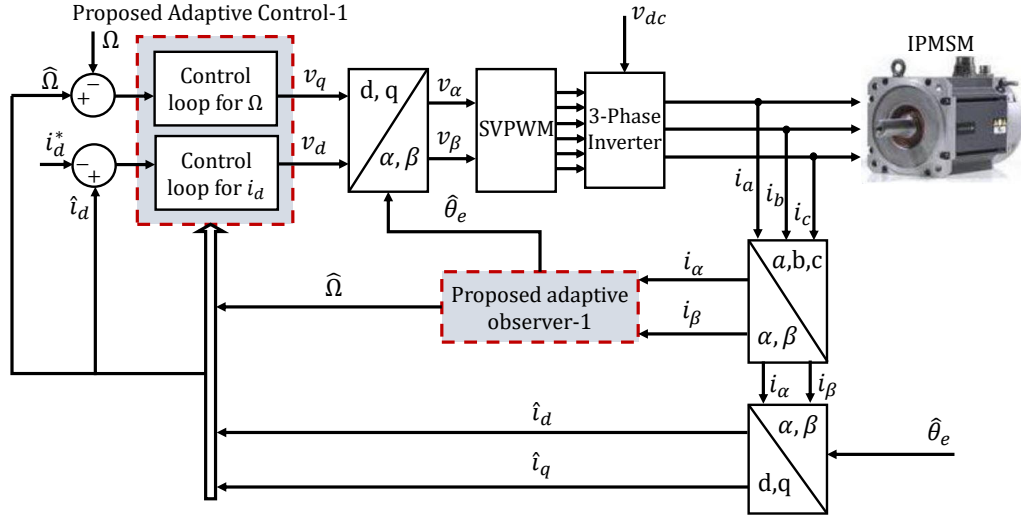


Figure 4.1: Proposed sensorless control: Scheme-1.

4.2.1 Simulation tests

A simulation test has been carried out in Matlab-Simulink environment, using a sampling time of 1×10^{-3} with a fixed-step *ode4* solver. White noise was added in the measurable currents $-i_{\alpha\beta}$ with a power noise of 1×10^{-7} in order to illustrate a realistic situation. The parameter variation given in Figure 1.8 and the profile given in Figure 1.7 are considered.

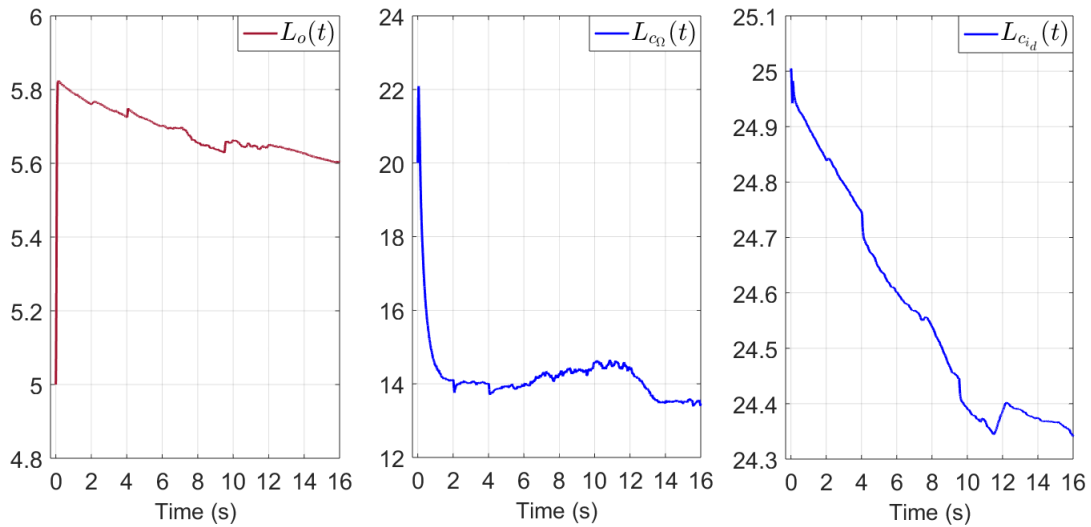


Figure 4.2: Simulation test: Behaviour of the adaptive gains, observer and control

From simulations, the behaviour of adaptive law L_o for the observer; and the adaptive laws L_{c_Ω} and $L_{c_{i_d}}$ for the speed and current- i_d controllers, respectively, are shown in Figure 4.2. The adaptive laws have been implemented by considering the parameters of the Table 4.1. Then,

Table 4.1: Parameters for the sensorless control-1 in simulation test.

AHOSMO-1		ASTWC-1					
γ_0	k_o	ϑ_{12}	γ_{c_Ω}	k_{c_Ω}	ϑ_{13}	$\gamma_{c_{i_d}}$	$k_{c_{i_d}}$
0.01	90	400	0.1	3	200	0.002	0.8

in Figure 4.3, the speed estimation and its estimation error are plotted. Small overshoots can be seen under the load torque variations. However, the performance of the adaptive observer is good under these variations. On the other hand, the estimated angular position compared with

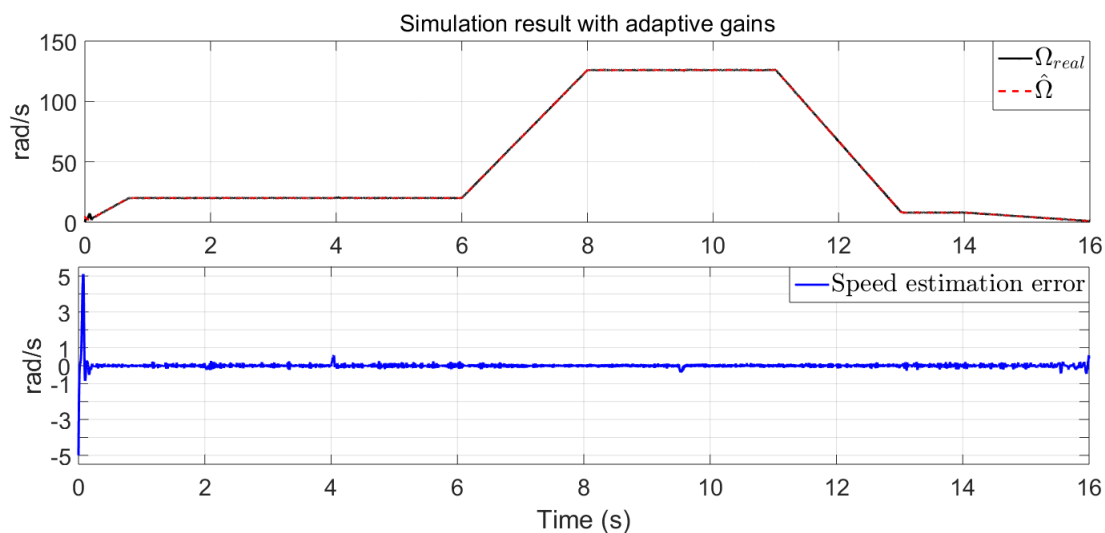


Figure 4.3: Simulation test: Speed estimation and estimation error

the real angular position is plotted in Figure 4.4. It is easy to see that the angular position error converges to zero ensuring observability for a wide speed range, *i.e.*, high, medium and close to zero. In Figure 4.5, the estimation of acceleration is plotted and an estimation with noise can be seen due to the application of the additive noise in the currents- $i_{\alpha\beta}$.

Now, taking into account the estimates of the observer, the controllers of speed and current- i_d are applied in the IPMSM. Therefore, IPMSM has been controlled and rotor speed tracking is

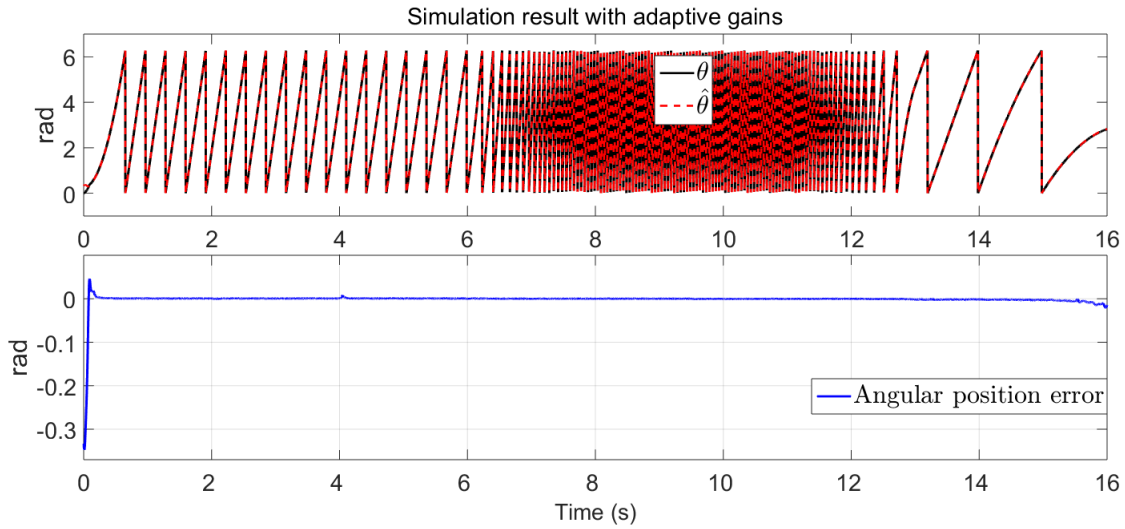


Figure 4.4: Simulation test: Angular position estimation and angular position error

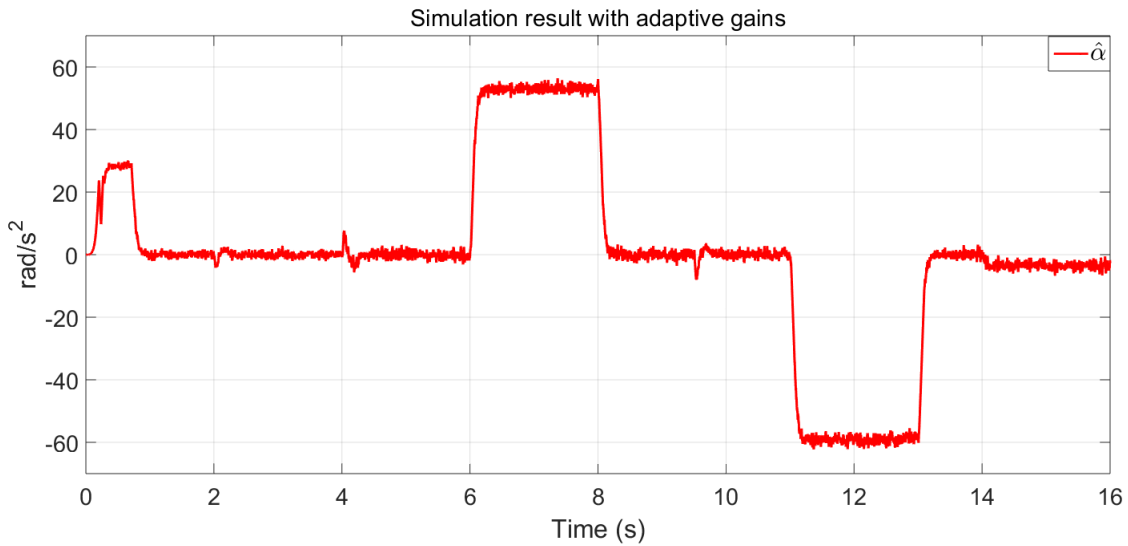


Figure 4.5: Simulation test: Estimation of acceleration

plotted in Figure 4.6 showing a tracking with good performance. Similarly, in Figure 4.7, the current- i_d tracks the desired reference $i_d^* = 0$ and the current i_q takes different values according to the speed and load torque profiles. Then, from these figures, the effectiveness of the proposed scheme based on sliding mode is shown by simulations under parameter and load torque variations. Finally, from simulations can be shown that the angular position estimation error e_{θ_e} has been extracted successfully showing good performance in closed loop.

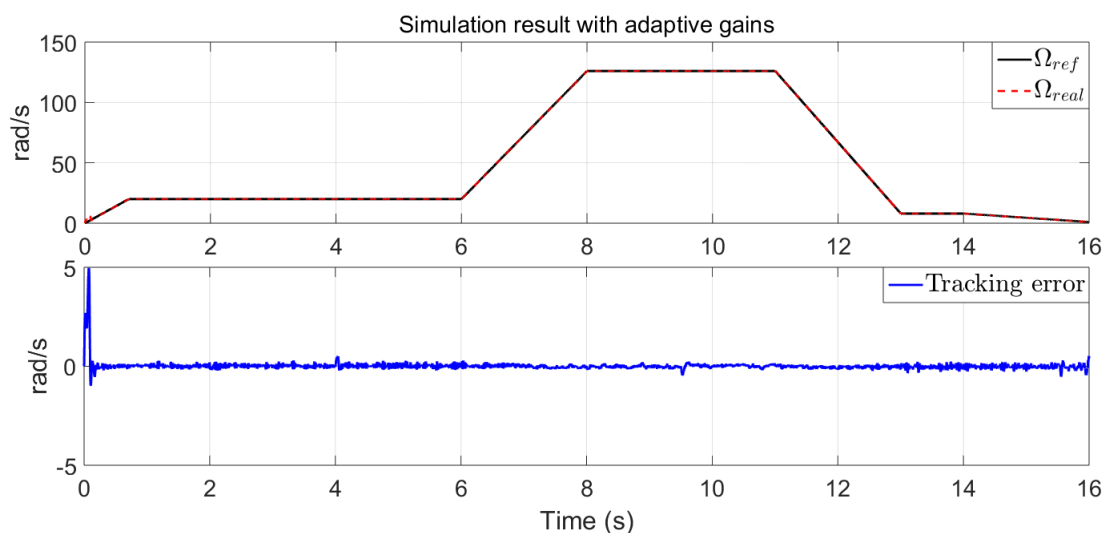
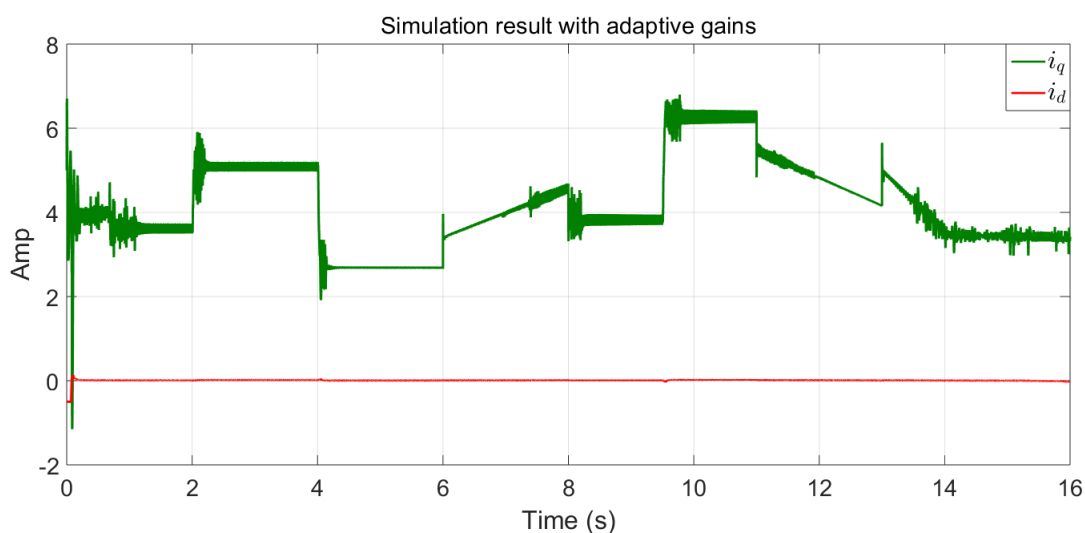


Figure 4.6: Simulation test: Speed tracking and tracking error

Figure 4.7: Simulation test: Behaviour of the currents— i_{dq}

4.2.2 Experimental test

The proposed strategy is implemented taking into account the profiles defined in Figure 1.7. Moreover, as previously mentioned, during the experiments an encoder is used to measure the real angular position. Then, considering measured position, a Kalman-filter is applied in order to calculate the rotor speed. Therefore, from this information, it is possible to know if the proposed observer does a correct estimation and the controller a correct reference tracking. Now,

Table 4.2: Parameters for the sensorless control-1 in experimental test.

AHOSMO-1		ASTWC-1					
γ_0	k_o	ϑ_{12}	γ_{c_Ω}	k_{c_Ω}	ϑ_{13}	$\gamma_{c_{i_d}}$	$k_{c_{i_d}}$
0.07	35	180	0.0003	0.1	20	0.0009	0.2

considering the proposed adaptive observer; the speed, angular position and acceleration are going to be estimated to control the speed and current $-i_d$ of IPMSM using adaptive controllers.

A comparison is carried out with the same proposed strategy using constant gains in order to see the improvement with the implementation of adaptive gains. It is worth mentioning that during the experiments with constant gains, the constant gains have been chosen in order to avoid damaging the hardware.

Experimental validation has been carried out considering the following parameters: for the case with constant gains, the observer is implemented with $L_o = 4.5$; $\vartheta_{12} = 180$ and $L_{c_\Omega} = 35$ in the speed controller; $\vartheta_{13} = 20$ and $L_{c_{i_d}} = 20$ in the current $-i_d$ controller. On the other hand, the adaptive observer and adaptive control parameters are given in Table 4.2.

The behaviour of the adaptive laws for the observer and controllers are illustrated in Figure 4.8. Then, the speed and the angular position have been estimated using constant gain and

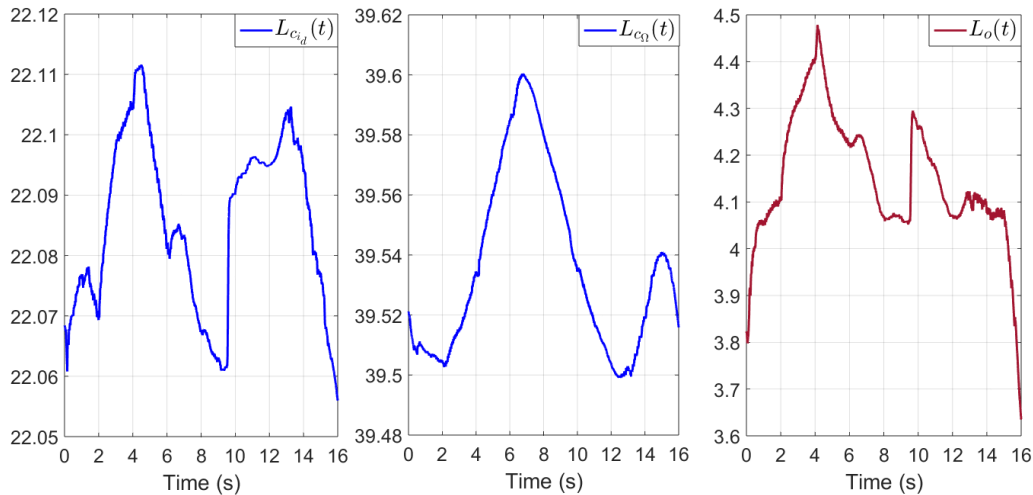


Figure 4.8: Experimental test. Adaptive laws: Control ($L_{c_{i_d}}(t)$, $L_{c_\Omega}(t)$) and observer ($L_o(t)$).

adaptive gain as can be shown in Figure 4.9 and Figure 4.10, respectively. At first glance, it is

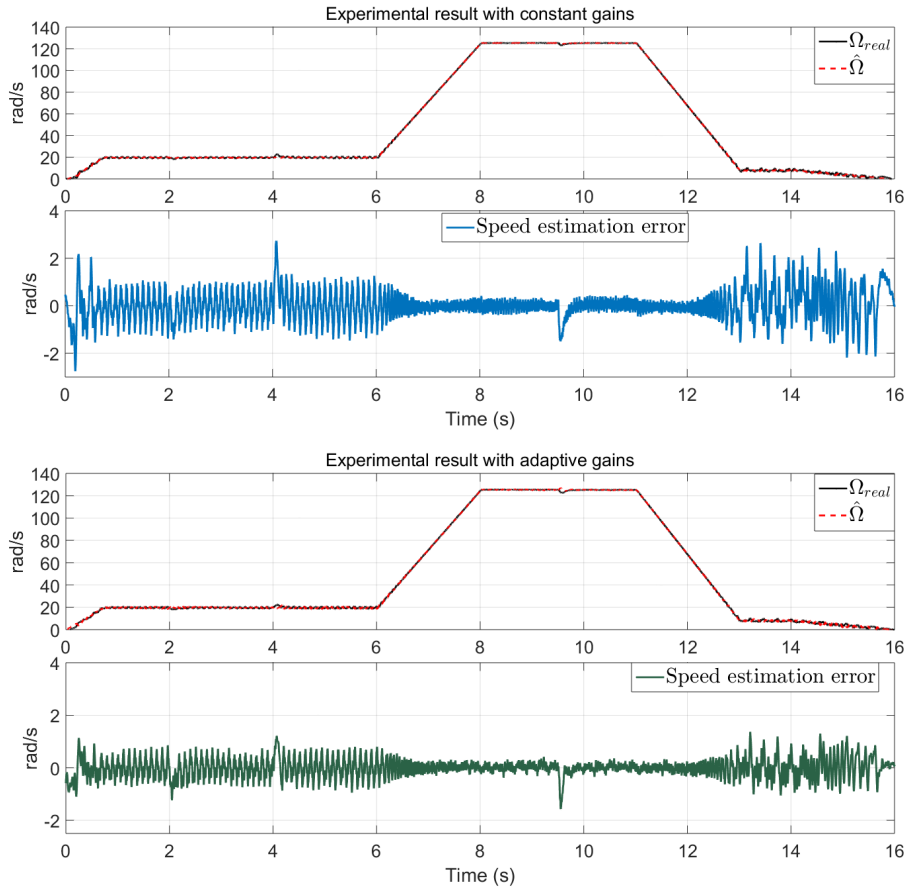


Figure 4.9: Experimental test: Speed estimation and estimation error.

not possible to see the improvement in detail through speed estimation error and angular error. However, in Figure 4.11, in order to show numerically the improvement, a performance index is computed: Integral Absolute Error (IAE). Therefore, it is possible to see that the proposed adaptive observer improves the estimation by adjusting the gains in order to obtain a minimum error. On the other side, the estimation of the acceleration is shown in Figure 4.12 using constant gains and adaptive gains. Then, the estimation with adaptive gains has an improvement by avoiding overestimation with large gains and reducing the chattering.

Now, the estimates of the observer have been used in the controllers to control the machine in closed-loop. In Figure 4.13, the speed tracking and its tracking error are shown. A comparative study using constant gains and adaptive gains is given. It is clear that an improvement can be seen numerically in Figure 4.11 using the adaptive gains in the scheme. On the other hand,

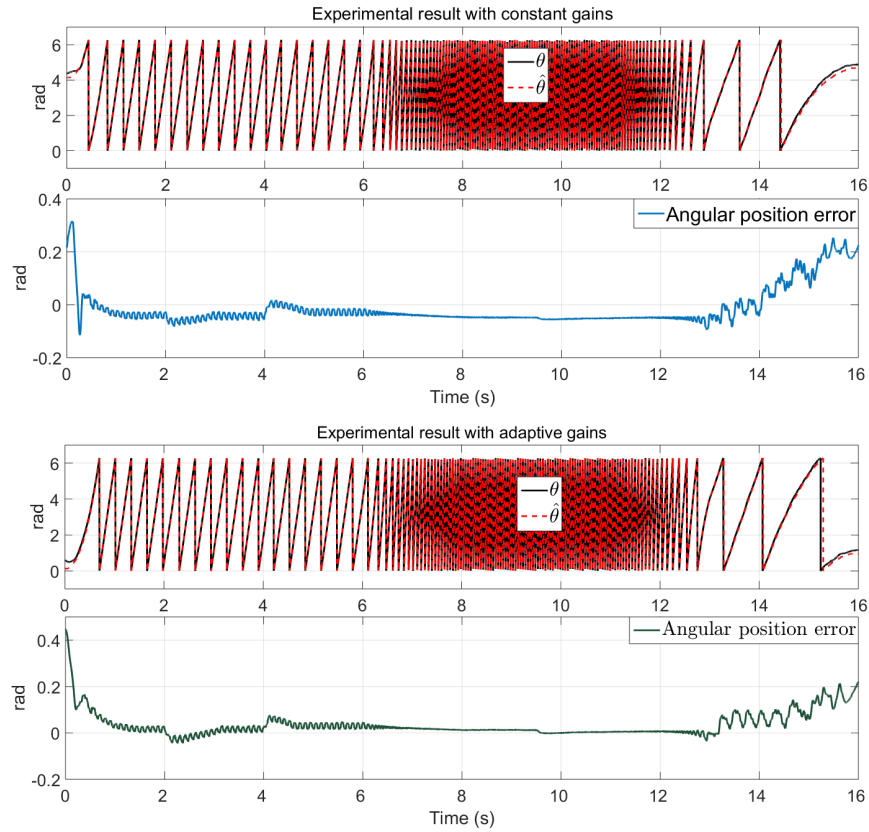


Figure 4.10: Experimental test: Angular position estimation and estimation error.

the currents $-i_{dq}$ are plotted in Figure 4.14 and the control inputs $-v_{dq}$ using adaptive laws are presented in Figure 4.15. Then, the closed-loop in IPMSM is achieved successfully.

Therefore, as can be seen the proposed strategy only requires the current $-i_{\alpha\beta}$ signals for extracting the angular position estimation error e_{θ_e} , directly, without any additional information or elements, then, e_{θ_e} can be used in the observer based on the virtual system to estimate angular position, speed and acceleration, such that the proposed strategy has been validated experimentally, with good effectiveness at low, medium and high speed in closed loop.

As can be seen in simulation, the tracking errors and estimation errors show the effect of adding white noise. It is clear that the chattering has been attenuated. However, the effects of white noise are present in the signals. On the other hand, during the experimental test, these errors are more important compared to those obtained in the simulation. It is well-known that in the experiments the effect caused by external disturbances (e.g. inverter) and the noise

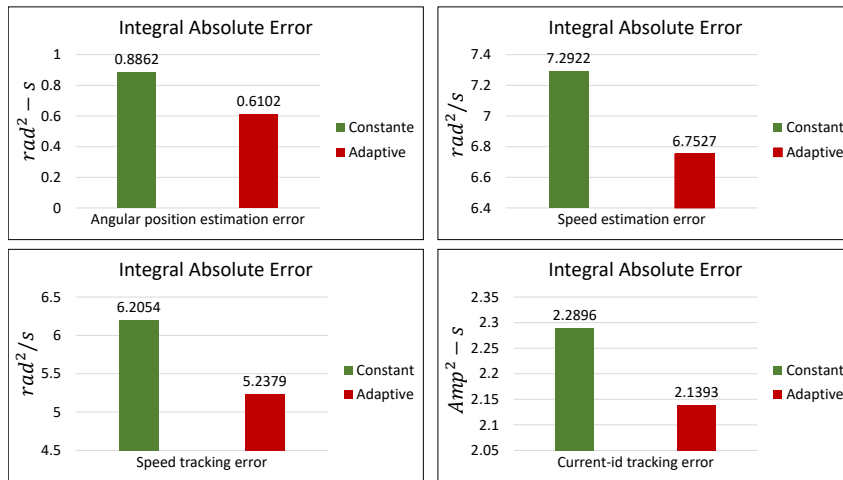


Figure 4.11: Performance index for the estimation and tracking of states during experiments

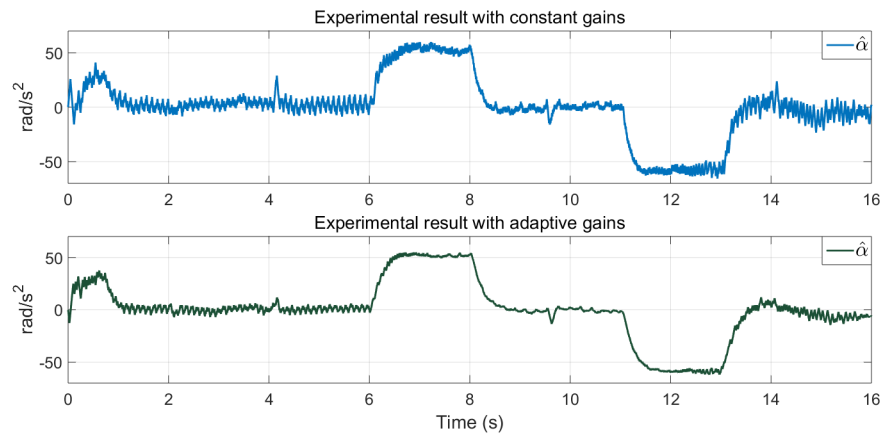


Figure 4.12: Experimental test: Estimation of the acceleration.

appears in the measured signals. However, the proposed strategy works well and attenuate the effects of chattering, uncertain parameters and unmodeled dynamics.

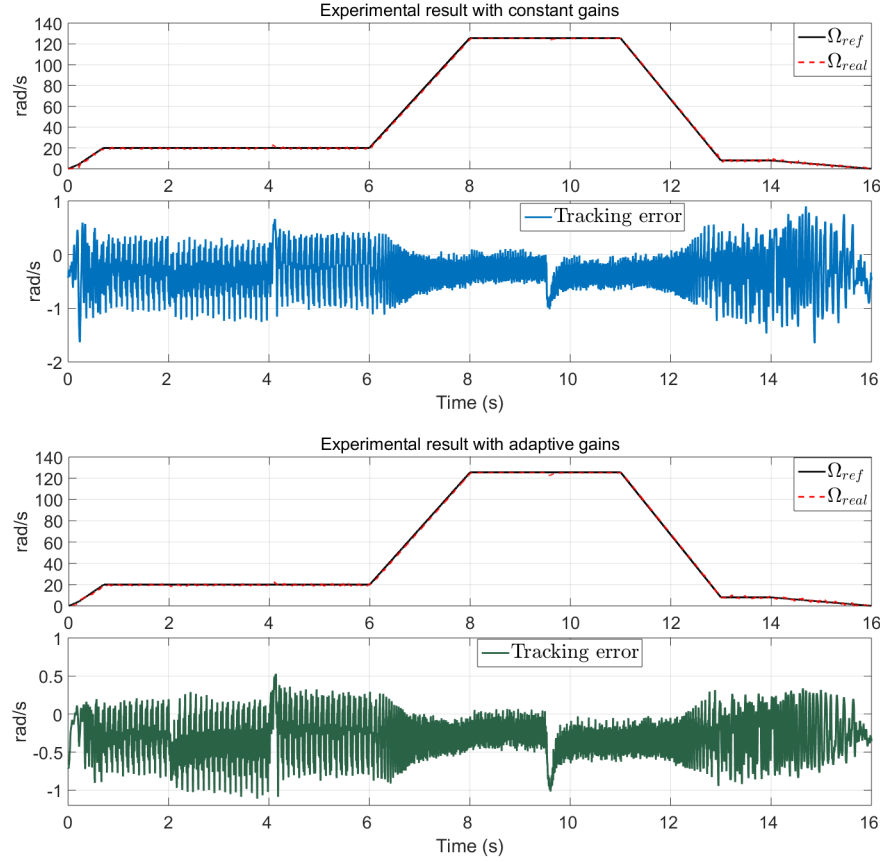


Figure 4.13: Experimental test: Speed tracking and tracking error

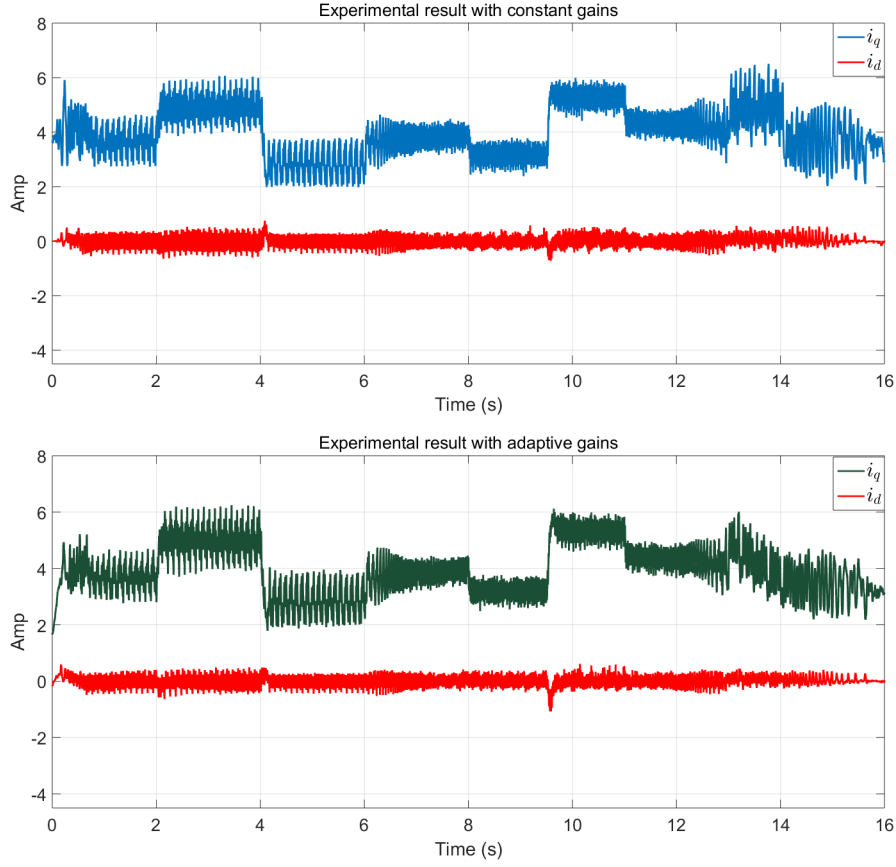
4.3 Closed-loop analysis: Scheme 2

Consider the proposed control given in the section 3.2.1 (ASTWC-2) using the estimates provided by the proposed observer given in section 2.3.1 (AHOSMO-2). Then, the stability analysis of the system in closed-loop, control-observer scheme, is established as follows

Theorem 4.2. *Consider the dynamical model of the IPMSM (1.3.30)-(1.3.31) in closed-loop with the controllers (3.2.43)-(3.2.48) using the estimates provided by the observer (2.3.42). Then, tracking errors e_{1_w} and $e_{1_{i_d}}$; and estimation error e_{θ_e} converge to zero in finite time.*

Proof: Since the control input $v_q(\hat{x})$ depends on estimates $\hat{\Omega}$, \hat{i}_d and \hat{i}_q ; and taking into account the sliding surface given by (3.2.42), then the dynamic of the sliding surface is given as follows

$$\dot{S}_{\Omega_2} = \vartheta_{22}e_{2_{\Omega}} + a_1b_1 + a_2b_2 + a_3b_2 - b_3 + b_4 - \ddot{\Omega}^* + c_1v_q(\hat{x}) \quad (4.3.1)$$


 Figure 4.14: Experimental test: Profiles of the currents— i_{dq}

Now, adding and subtracting the term $c_1 v_q(x)$ in the sliding surface, it follows that

$$\dot{S}_{\Omega_2} = \vartheta_{22} e_{2\Omega} + a_1 b_1 + a_2 b_2 + a_3 b_2 - b_3 + b_4 - \ddot{\Omega}^* + c_1 v_q(x) + c_1 [v_q(\hat{x}) - v_q(x)] \quad (4.3.2)$$

Notice that the term $c_1 [v_q(\hat{x}) - v_q(x)]$ is Lipschitz, *i.e.*, there exists a positive constant μ_{21} such that $\|c_1 [v_q(\hat{x}) - v_q(x)]\| \leq \mu_{21} \|\hat{x} - x\|$.

Applying the control input $v_q(x)$ given by (3.2.43) into the above system, the dynamic of the sliding surface is given by

$$\dot{S}_{\Omega_2} = -2L_{c_{\Omega_2}}(t) |S_{\Omega_2}|^{\frac{1}{2}} \text{sign}(S_{\Omega_2}) - \int_0^t \frac{L_{c_{\Omega_2}}^2(\tau)}{2} \text{sign}(S_{\Omega_2}) d\tau + c_1 [v_q(\hat{x}) - v_q(x)] + \delta_{\Omega}(t) \quad (4.3.3)$$

for $\delta_{\Omega}(t) = b_4 = \frac{f_v T_l}{J^2}$.

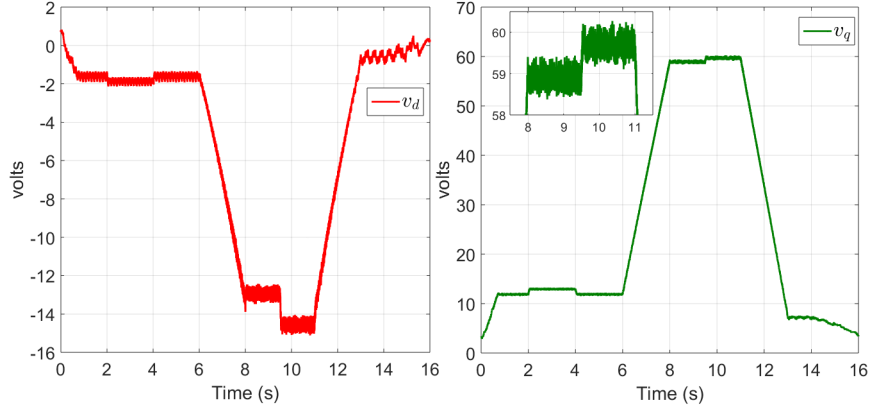


Figure 4.15: Experimental test: Profiles of the voltages $-v_{dq}$ with adaptive laws.

Then, the dynamic of S_{Ω_2} can be expressed as follows

$$\begin{cases} \dot{S}_{\Omega_2} = -2L_{c_{\Omega_2}}(t)|S_{\Omega_2}|^{\frac{1}{2}}\text{sign}(S_{\Omega_2}) + \nu_{\Omega_2} + \delta_{\Omega}(t) + c_1[v_q(\hat{x}) - v_q(x)] \\ \dot{\nu}_{\Omega_2} = -\frac{L_{c_{\Omega_2}}^2(t)}{2}\text{sign}(S_{\Omega_2}) \end{cases} \quad (4.3.4)$$

Now, defining the following change of coordinates $z_{1\Omega_2} = S_{\Omega_2}$ and $z_{2\Omega_2} = \nu_{\Omega_2} + \delta_{\Omega}(t)$. The system (4.3.4) is given by

$$\begin{cases} \dot{z}_{1\Omega_2} = -2L_{c_{\Omega_2}}(t)|z_{1\Omega_2}|^{\frac{1}{2}}\text{sign}(z_{1\Omega_2}) + z_{2\Omega_2} + c_1[v_q(\hat{x}) - v_q(x)] \\ \dot{z}_{2\Omega_2} = -\frac{L_{c_{\Omega_2}}^2(t)}{2}\text{sign}(z_{1\Omega_2}) + d_{\Omega}(t) \end{cases} \quad (4.3.5)$$

with $d_{\Omega}(t) = \dot{\delta}_{\Omega}(t)$. Now, a change of variable is introduced

$$\mathcal{L}_{1\Omega_2} = \frac{|z_{1\Omega_2}|^{\frac{1}{2}}\text{sign}(z_{1\Omega_2})}{L_{c_{\Omega_2}}(t)} \quad \mathcal{L}_{2\Omega_2} = \frac{z_{2\Omega_2}}{L_{c_{\Omega_2}}^2(t)} \quad (4.3.6)$$

then, the dynamical behavior of system (4.3.6), in the new coordinates, is given by

$$\begin{aligned}\dot{\mathcal{L}}_{1\Omega_2} &= \frac{L_{c\Omega_2}(t)}{2|z_{1\Omega_2}|^{\frac{1}{2}}} \left[-2\mathcal{L}_{1\Omega_2} + \mathcal{L}_{2\Omega_2} + \frac{c_1[v_q(\hat{x}) - v_q(x)]}{L_{c\Omega_2}^2(t)} \right] - \mathcal{L}_{1\Omega_2} \frac{\dot{L}_{c\Omega_2}(t)}{L_{c\Omega_2}(t)} \\ \dot{\mathcal{L}}_{2\Omega_2} &= \frac{L_{c\Omega_2}(t)}{2|z_{1\Omega_2}|^{\frac{1}{2}}} \left[-\mathcal{L}_{1\Omega_2} + \frac{2|z_{1\Omega_2}|^{\frac{1}{2}}d_\Omega(t)}{L_{c\Omega_2}^3(t)} \right] - 2\mathcal{L}_{2\Omega_2} \frac{\dot{L}_{c\Omega_2}(t)}{L_{c\Omega_2}(t)}\end{aligned}\quad (4.3.7)$$

which can be represented in a compact form as follows

$$\dot{\mathcal{L}}_{\Omega_2} = \alpha_{\Omega_2} \left[(A_{\Omega_2} - P_{\Omega_2}^{-1}C_{\Omega_2}^T C_{\Omega_2}) \mathcal{L}_{\Omega_2} + \Phi_{\Omega_2} \right] - D_{\Omega_2} \mathcal{L}_{\Omega_2} \frac{\dot{L}_{c\Omega_2}(t)}{L_{c\Omega_2}(t)} \quad (4.3.8)$$

with $\alpha_{\Omega_2} = \frac{L_{c\Omega_2}(t)}{2|z_{1\Omega_2}|^{\frac{1}{2}}}$ and

$$\mathcal{L}_{\Omega_2} = \begin{bmatrix} \mathcal{L}_{1\Omega_2} \\ \mathcal{L}_{2\Omega_2} \end{bmatrix} \quad A_{\Omega_2} = \begin{bmatrix} 0 & 1 \\ 0 & 0 \end{bmatrix} \quad C_{\Omega_2} = \begin{bmatrix} 1 & 0 \end{bmatrix} \quad (4.3.9)$$

$$P_{\Omega_2} = \begin{bmatrix} 1 & -1 \\ -1 & 2 \end{bmatrix} \quad D_{\Omega_2} = \begin{bmatrix} 1 & 0 \\ 0 & 2 \end{bmatrix} \quad \Phi_{\Omega_2} = \begin{bmatrix} \frac{c_1[v_q(\hat{x}) - v_q(x)]}{L_{c\Omega_2}^2(t)} \\ \frac{2|z_{1\Omega_2}|^{\frac{1}{2}}}{L_{c\Omega_2}^3(t)} [d_\Omega(t)] \end{bmatrix} \quad (4.3.10)$$

From Assumption 3.5, the nonlinear term Φ_{Ω_2} satisfies the following inequality, $\|\Phi_{\Omega_2}\| \leq \varsigma_{21}\|\mathcal{L}_{\Omega_2}\|$ for $\varsigma_{21} > 0$.

Following the same steps of the previous analysis, consider the control input v_d , expressed in terms of the estimates as follows

$$\begin{aligned}v_d(\hat{x}) &= \frac{L_d}{\vartheta_{23}} \left(\frac{\vartheta_{23}R_s\hat{i}_d}{L_d} - \frac{\vartheta_{23}p\hat{\Omega}L_q\hat{i}_q}{L_d} + \vartheta_{23}\dot{i}_d^* - e_{i_d} \right. \\ &\quad \left. - 2L_{c_{i_{d_2}}}(t)|S_{i_{d_2}}|^{\frac{1}{2}}\text{sign}(S_{i_{d_2}}) - \int_0^t \frac{L_{c_{i_{d_2}}}^2(\tau)}{2}\text{sign}(S_{i_{d_2}})d\tau \right)\end{aligned}\quad (4.3.11)$$

Then, from sliding surface (3.2.47) and the control input (4.3.11) depending on the estimated

states, the dynamic of the sliding surface is given by

$$\dot{S}_{i_{d_2}} = -\frac{\vartheta_{23}R_s i_d}{L_d} + \frac{\vartheta_{23}p\Omega L_q i_q}{L_d} + \frac{\vartheta_{23}}{L_d}v_d(\hat{x}) - \vartheta_{23}i_d^* + e_{i_d} + \delta_{i_d}(t) \quad (4.3.12)$$

where $\delta_{i_d}(t)$ represents the uncertain/disturbance term.

Adding and subtracting the term $\frac{\vartheta_{23}}{L_d}v_d(x)$ in (4.3.12), it follows that

$$\dot{S}_{i_{d_2}} = -\frac{\vartheta_{23}R_s i_d}{L_d} + \frac{\vartheta_{23}p\Omega L_q i_q}{L_d} + \frac{\vartheta_{23}}{L_d}v_d(x) - \vartheta_{23}i_d^* + e_{i_d} + \frac{\vartheta_{23}}{L_d}[v_d(\hat{x}) - v_d(x)] + \delta_{i_d}(t) \quad (4.3.13)$$

where the term $\frac{\vartheta_{23}}{L_d}[v_d(\hat{x}) - v_d(x)]$ is Lipschitz, i.e., there exist a positive constant μ_{22} such that

$$\left\| \frac{\vartheta_{23}}{L_d}[v_d(\hat{x}) - v_d(x)] \right\| \leq \mu_{22} \|\hat{x} - x\|.$$

Moreover, applying the control input $v_d(x)$ given by (3.2.48) into the above system, the dynamic of the sliding surface is given by

$$\dot{S}_{i_{d_2}} = -2L_{c_{i_{d_2}}}(t)|S_{i_{d_2}}|^{\frac{1}{2}}\text{sign}(S_{i_{d_2}}) - \int_0^t \frac{L_{c_{i_{d_2}}}^2(t)}{2}\text{sign}(S_{i_{d_2}})d\tau + \frac{\vartheta_{23}}{L_d}[v_d(\hat{x}) - v_d(x)] + \delta_{i_d}(t) \quad (4.3.14)$$

which can be represented as follows

$$\begin{cases} \dot{S}_{i_{d_2}} = -2L_{c_{i_{d_2}}}(t)|S_{i_{d_2}}|^{\frac{1}{2}}\text{sign}(S_{i_{d_2}}) + \nu_{i_{d_2}} + \delta_{i_d}(t) + \frac{\vartheta_{23}}{L_d}[v_d(\hat{x}) - v_d(x)] \\ \dot{\nu}_{i_{d_2}} = -\frac{L_{c_{i_{d_2}}}^2(t)}{2}\text{sign}(S_{i_{d_2}}) \end{cases} \quad (4.3.15)$$

Now, defining $z_{1_{i_{d_2}}} = S_{i_{d_2}}$ and $z_{2_{i_{d_2}}} = \nu_{i_{d_2}} + \delta_{i_d}(t)$. The system $\dot{S}_{i_{d_2}}$ can be expressed as follows

$$\begin{aligned} \dot{z}_{1_{i_{d_2}}} &= -2L_{c_{i_{d_2}}}(t)|z_{1_{i_{d_2}}}|^{\frac{1}{2}}\text{sign}(z_{1_{i_{d_2}}}) + z_{2_{i_{d_2}}} + \frac{\vartheta_{23}}{L_d}[v_d(\hat{x}) - v_d(x)] \\ \dot{z}_{2_{i_{d_2}}} &= -\frac{L_{c_{i_{d_2}}}^2(t)}{2}\text{sign}(z_{1_{i_{d_2}}}) + d_{i_d}(t) \end{aligned} \quad (4.3.16)$$

with $d_{i_d}(t) = \dot{\delta}_{i_d}(t)$. Now, a new change of variable is introduced

$$\mathcal{L}_{1_{i_{d_2}}} = \frac{|z_{1_{i_{d_2}}}|^{\frac{1}{2}} \text{sign}(z_{1_{i_{d_2}}})}{L_{c_{i_{d_2}}}(t)} \quad \mathcal{L}_{2_{i_{d_2}}} = \frac{z_{2_{i_{d_2}}}}{L_{c_{i_{d_2}}}^2(t)} \quad (4.3.17)$$

whose dynamics are given by

$$\begin{aligned} \dot{\mathcal{L}}_{1_{i_{d_2}}} &= \frac{L_{c_{i_{d_2}}}(t)}{2|z_{1_{i_{d_2}}}|^{\frac{1}{2}}} \left[-2\mathcal{L}_{1_{i_{d_2}}} + \mathcal{L}_{2_{i_{d_2}}} + \frac{\vartheta_{23}[v_d(\hat{x}) - v_d(x)]}{L_{c_{i_{d_2}}}^2(t)} \right] - \mathcal{L}_{1_{i_{d_2}}} \frac{\dot{L}_{c_{i_{d_2}}}(t)}{L_{c_{i_{d_2}}}(t)} \\ \dot{\mathcal{L}}_{2_{i_{d_2}}} &= \frac{L_{c_{i_{d_2}}}(t)}{2|z_{1_{i_{d_2}}}|^{\frac{1}{2}}} \left[-\mathcal{L}_{1_{i_{d_2}}} + \frac{2|z_{1_{i_{d_2}}}|^{\frac{1}{2}} d_{i_d}(t)}{L_{c_{i_{d_2}}}^3(t)} \right] - 2\mathcal{L}_{2_{i_{d_2}}} \frac{\dot{L}_{c_{i_{d_2}}}(t)}{L_{c_{i_{d_2}}}(t)} \end{aligned} \quad (4.3.18)$$

Then, system (4.3.18) can be rewritten in a compact form as follows

$$\dot{\mathcal{L}}_{i_{d_2}} = \alpha_{i_{d_2}} \left[\left(A_{i_{d_2}} - P_{i_{d_2}}^{-1} C_{i_{d_2}}^T C_{i_{d_2}} \right) \mathcal{L}_{i_{d_2}} + \Phi_{i_{d_2}} \right] - D_{i_{d_2}} \mathcal{L}_{i_{d_2}} \frac{\dot{L}_{c_{i_{d_2}}}(t)}{L_{c_{i_{d_2}}}(t)} \quad (4.3.19)$$

with $\alpha_{i_{d_2}} = \frac{L_{c_{i_{d_2}}}(t)}{2|z_{1_{i_{d_2}}}|^{\frac{1}{2}}}$ and

$$\mathcal{L}_{i_{d_2}} = \begin{bmatrix} \mathcal{L}_{1_{i_{d_2}}} \\ \mathcal{L}_{2_{i_{d_2}}} \end{bmatrix} \quad A_{i_{d_2}} = \begin{bmatrix} 0 & 1 \\ 0 & 0 \end{bmatrix} \quad C_{i_{d_2}} = \begin{bmatrix} 1 & 0 \end{bmatrix} \quad (4.3.20)$$

$$P_{i_{d_2}} = \begin{bmatrix} 1 & -1 \\ -1 & 2 \end{bmatrix} \quad D_{i_{d_2}} = \begin{bmatrix} 1 & 0 \\ 0 & 2 \end{bmatrix} \quad \Phi_{i_{d_2}} = \begin{bmatrix} \frac{\vartheta_{23}[v_d(\hat{x}) - v_d(x)]}{L_{c_{i_{d_2}}}^2(t)} \\ \frac{2|z_{1_{i_{d_2}}}|^{\frac{1}{2}}}{L_{c_{i_{d_2}}}^3(t)} [d_{i_d}(t)] \end{bmatrix} \quad (4.3.21)$$

From Assumption 3.5, the term $\Phi_{i_{d_2}}$ is Lipschitz, i.e. there exists $\varsigma_{22} > 0$, such that $\|\Phi_{i_{d_2}}\| \leq \varsigma_{22} \|\mathcal{L}_{i_{d_2}}\|$.

Then, considering the adaptive observer given in section 2.3.1 and the adaptive control given

in section 3.2.1, the dynamics in closed-loop, controller-observer, are established as follows

$$\begin{cases} \dot{\xi}_{o_2} = \alpha_{o_2} [(A_{o_2} - P_{o_2}^{-1}C_{o_2}^T C_{o_2}) \xi_{o_2} + \Phi_{o_2}] - D_{o_2} \xi_{o_2} \frac{\dot{L}_{o_2}(t)}{L_{o_2}(t)} \\ \dot{\mathcal{L}}_{\Omega_2} = \alpha_{\Omega_2} [(A_{\Omega_2} - P_{\Omega_2}^{-1}C_{\Omega_2}^T C_{\Omega_2}) \mathcal{L}_{\Omega_2} + \Phi_{\Omega_2}] - D_{\Omega_2} \mathcal{L}_{\Omega_2} \frac{\dot{L}_{c_{\Omega_2}}(t)}{L_{c_{\Omega_2}}(t)} \\ \dot{\mathcal{L}}_{i_{d_2}} = \alpha_{i_d} [(A_{i_{d_2}} - P_{i_{d_2}}^{-1}C_{i_{d_2}}^T C_{i_{d_2}}) \mathcal{L}_{i_{d_2}} + \Phi_{i_{d_2}}] - D_{i_{d_2}} \mathcal{L}_{i_{d_2}} \frac{\dot{L}_{c_{i_{d_2}}}(t)}{L_{c_{i_{d_2}}}(t)} \end{cases} \quad (4.3.22)$$

If $\forall t > T_{1_2}$, such that ξ_{o_2} tend to zero, then, e_{i_2} tend to zero. Therefore, from Theorem 2.2, the observer converges in finite time to zero, it follows that the terms $c_1[v_q(\hat{x}) - v_q(x)]$ and $\frac{\vartheta_{23}}{L_d}[v_d(\hat{x}) - v_d(x)]$ contained in Φ_{Ω_2} and $\Phi_{i_{d_2}}$, respectively; tend to zero in finite time. Therefore, the system given by (3.2.13) is obtained. Finally, from the same procedure given in the proof of the Theorem 3.2, the stability of the closed-loop system is proved.

4.4 Simulation and experimental results: Scheme 2

In this section, simulation and experimental results have been evaluated in order to show the performance of the proposed strategy. The adaptive observer introduced in section 2.3.1 (AHOSMO-2) and the adaptive control introduced in section 3.2.1 (ASTWC-2) have been interconnected to illustrate the performance of the control in closed-loop under the action of the observer estimates, *i.e.*, controller+observer (ASTWC-2 + AHOSMO-2). A scheme of the proposed sensorless control strategy-2 is shown in Figure 4.16.

4.4.1 Simulation test

A simulation test is carried out in Matlab-Simulink environment, using a sampling time of 1×10^{-3} with a fixed-step *ode4* solver. White noise was added in the measurable currents $-i_{\alpha\beta}$ with a power noise of 1×10^{-7} in order to illustrate a realistic situation. Moreover, the adaptive laws have been implemented by considering the parameters of the Table 4.3. The behaviour of adaptive law $L_{o_2}(t)$ for the observer; and the adaptive laws $L_{c_{\Omega_2}}(t)$ and $L_{c_{i_{d_2}}}(t)$ for speed and current $-i_d$ controllers are shown in the Figure 4.17, respectively.

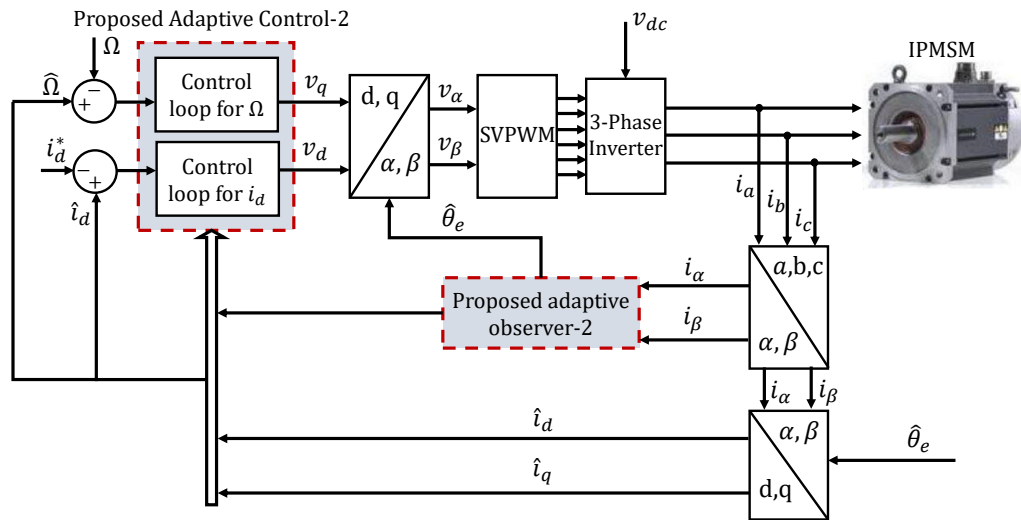


Figure 4.16: Proposed sensorless control: Scheme-2.

Table 4.3: Parameters for the sensorless control-2 in simulation test

AHOSMO-2		ASTWCS-2					
γ_{o_2}	k_{o_2}	ϑ_{22}	$\gamma_{c_{\Omega_2}}$	$k_{c_{\Omega_2}}$	ϑ_{23}	$\gamma_{c_{i_{d_2}}}$	$k_{c_{i_{d_2}}}$
0.016	200	400	0.008	120	200	0.0011	120

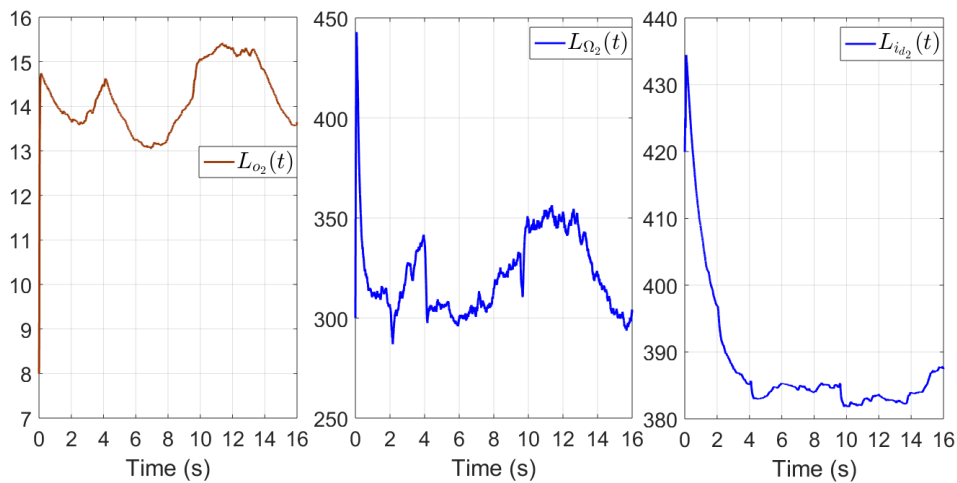


Figure 4.17: Simulation test: Behaviour of adaptive gains for the observer ($L_{o_2}(t)$) and controllers ($L_{\Omega_2}(t), L_{i_{d_2}}(t)$)

Considering the adaptive laws, in Figure 4.18, the speed estimation and its estimation error are introduced, showing a minimum error. In Figure 4.19, the angular position estimation and

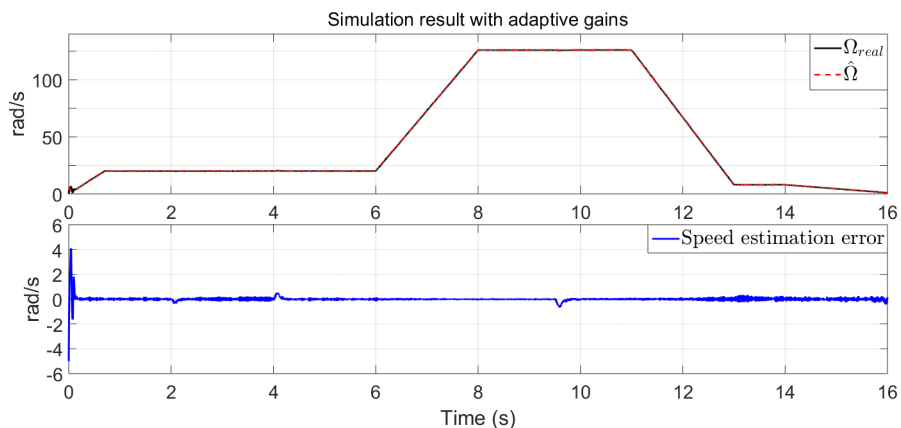


Figure 4.18: Simulation test: Speed estimation and estimation error

its angular position estimation error are plotted. As can be seen, the estimation is ensured over a wide speed range in presence of parametric uncertainties (see Figure 1.8). Moreover, in

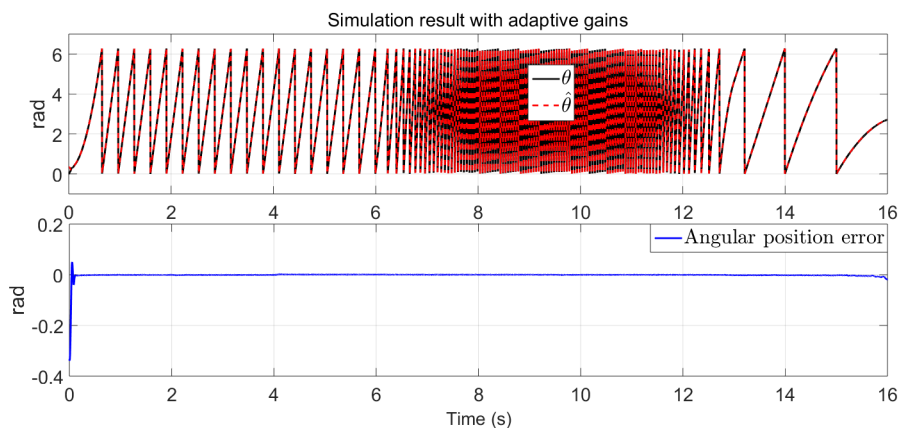


Figure 4.19: Simulation test: Angular position estimation and angular position error

Figure 4.20, acceleration has been estimated in order to compensate the fast dynamics in the system and reduce the estimation error in the speed and angular position.

Information from observer estimates has been interconnected with the controllers in closed-loop, as can be seen in the scheme 4.16. Then, in Figure 4.21, speed tracking and its tracking error are illustrated with a good performance.

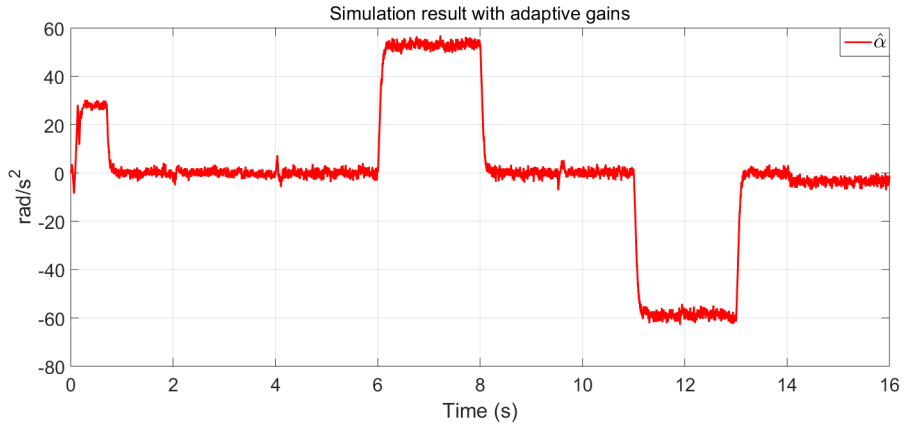


Figure 4.20: Simulation test: Estimation of acceleration

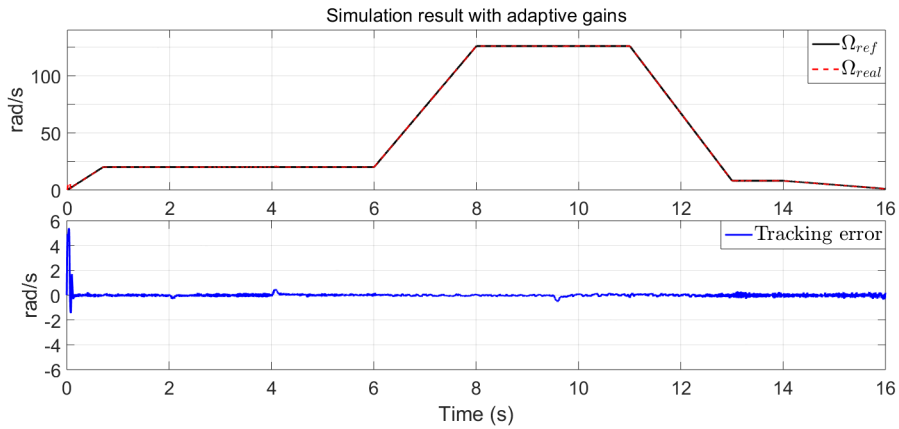


Figure 4.21: Simulation test: Speed tracking and tracking error

Moreover, the currents $-i_{dq}$ are plotted in Figure 4.22. Therefore, from the illustrations, it is possible to see that the behaviour of the adaptive laws with the system in closed loop (controller+observer) have a good performance. Moreover, the extraction of e_{θ_e} introduced in section 2.1 has been achieved successfully.

4.4.2 Experimental test

One experimental test is addressed to see in real time the performance of the strategy. The proposed strategy is implemented taking into account the profiles defined in Figure 1.7. Moreover, as previously mentioned, a sensor (encoder) has been used to measure the real angular position in the experiments. From this information, a Kalman-filter is applied to calculate the

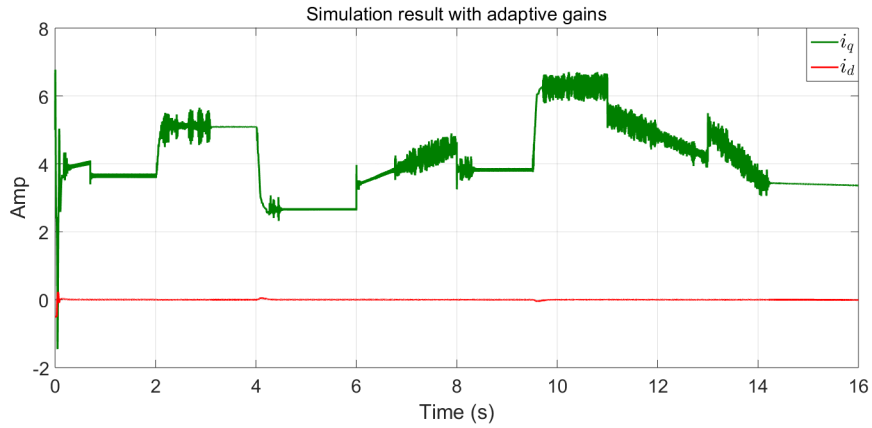


Figure 4.22: Simulation test: Behaviour of the currents— i_{dq}

rotor speed. Therefore, it is possible to know if the proposed observer does a correct estimation of the speed and angular position. Similarly, it possible to know if the controller does a correct reference tracking. The adaptive laws have been implemented by considering the parameters given in Table 4.4 and are shown in Figure 4.23.

Table 4.4: Parameters for the sensorless control-2 in experimental test

AHOSMO-2		ASTWCS-2					
γ_{o_2}	k_{o_2}	ϑ_{22}	$\gamma_{c_{\Omega_2}}$	$k_{c_{\Omega_2}}$	ϑ_{23}	$\gamma_{c_{i_{d_2}}}$	$k_{c_{i_{d_2}}}$
0.001	3	180	0.0001	35	20	0.0005	30

Then, in Figure 4.24, it possible to see the convergence of the estimated speed towards the real speed with good performance. In Figure 4.25, the estimation of the angular position and its angular error are plotted and a small error is obtained. It is possible to see a good performance over wide speed range, i.e., high, medium and low speed. However, the error increases when the speed is very close to zero. On the other hand, in Figure 4.26, the acceleration has been estimated in order to compensate the estimation error of angular position and speed.

The estimates of the observer are interconnected in the controllers to control the speed and the current of the IPMSM. In Figure 4.27, the tracking of the speed and the tracking error are showed. The tracking error shows that the performance of the proposed strategy is good and the tracking is ensured with good accuracy even close to zero.

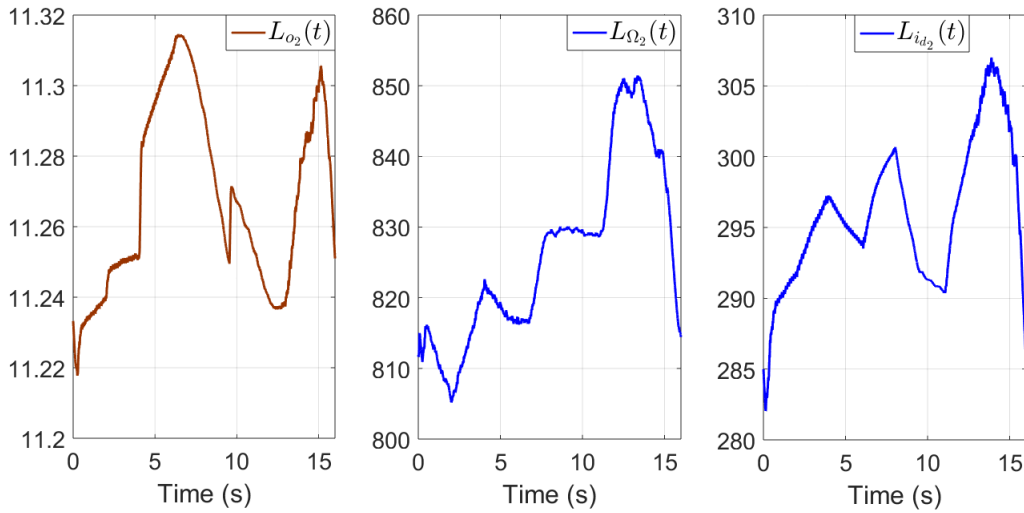


Figure 4.23: Experimental test: Behaviour of adaptive gains for the observer and controllers

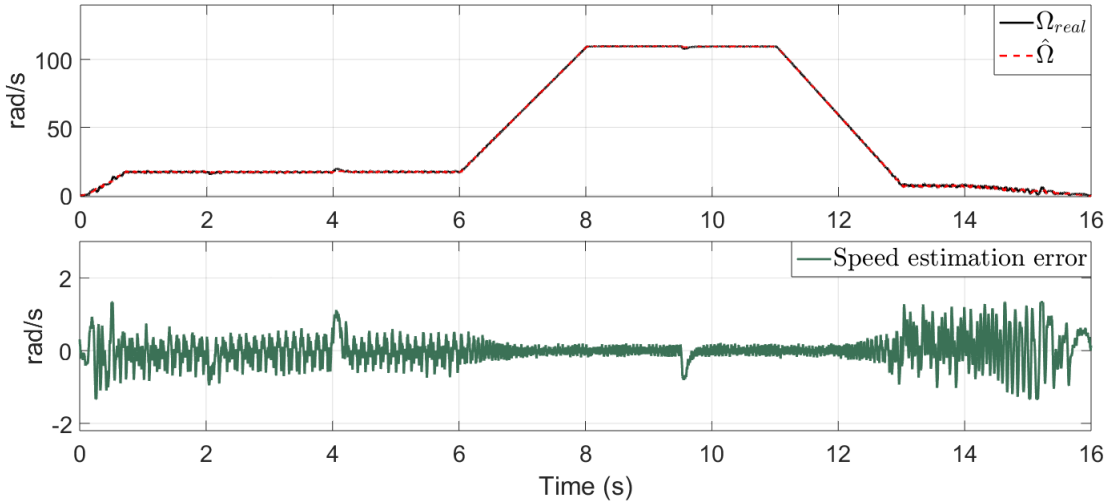


Figure 4.24: Experimental test: Speed estimation and estimation error

Moreover, the tracking of the current i_d and the behaviour of the current i_q are shown in Figure 4.28. The current i_d tracks a reference equal to 0, and the current i_q has a behaviour according to the load torque and the speed. In addition, the behaviour of the control inputs $-v_{dq}$ using adaptive laws are shown in the Figure 4.29.

As can be seen the proposed strategy only requires the angular position estimation error e_{θ_e} to estimate angular position, speed and acceleration using an observer based on a parameter

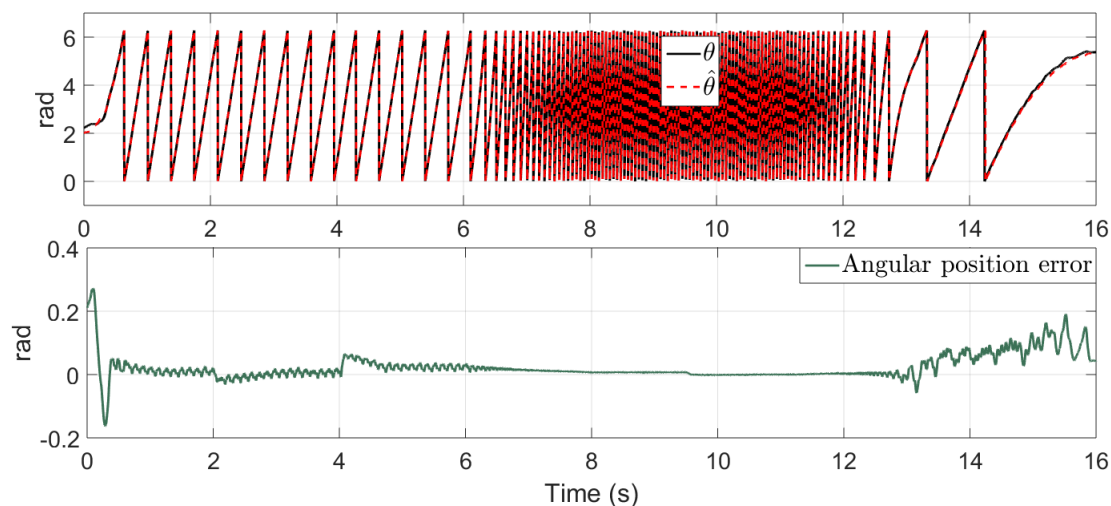


Figure 4.25: Experimental test: Angular position estimation and angular position estimation error

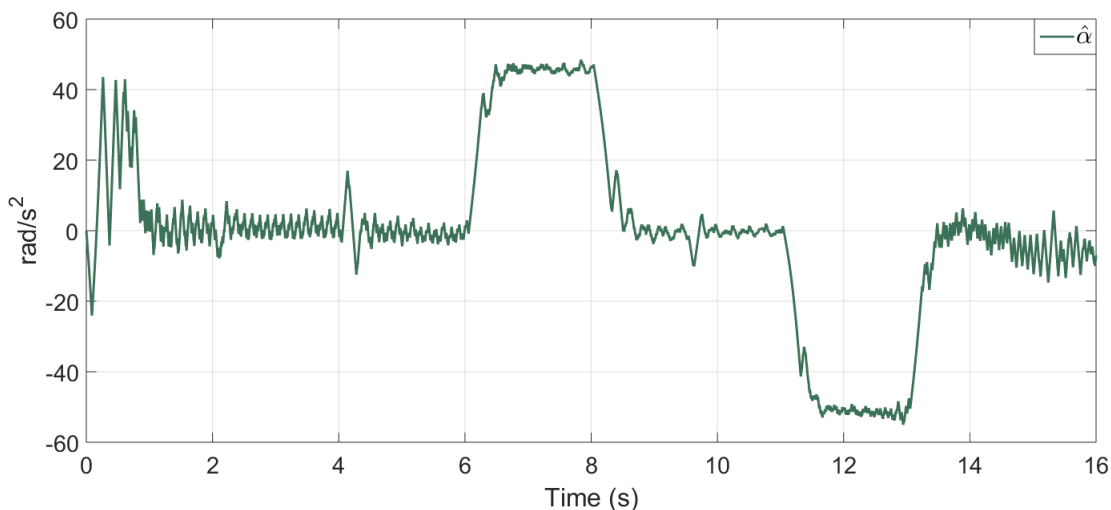


Figure 4.26: Experimental test: Estimation of acceleration

free virtual system. From this information, the sensorless scheme is possible. The proposed strategy has been validated experimentally, with good effectiveness at low, medium and high speed in closed loop.

On the other hand, it is possible to see in simulation that the tracking errors and estimation errors show the effect of adding white noise. It is clear that the chattering has been attenuated. However, the effects of white noise are present in the signals. On the other hand, during the

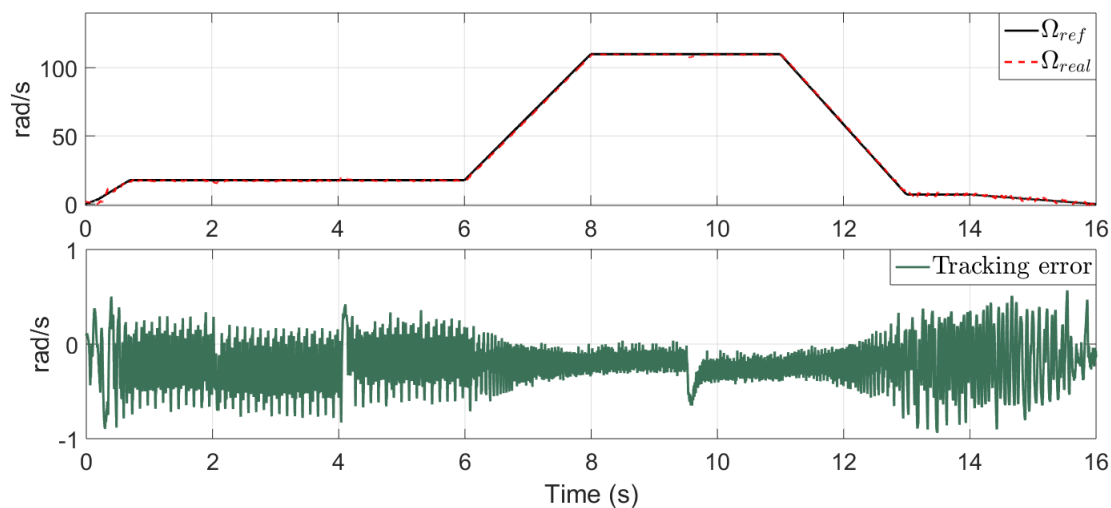
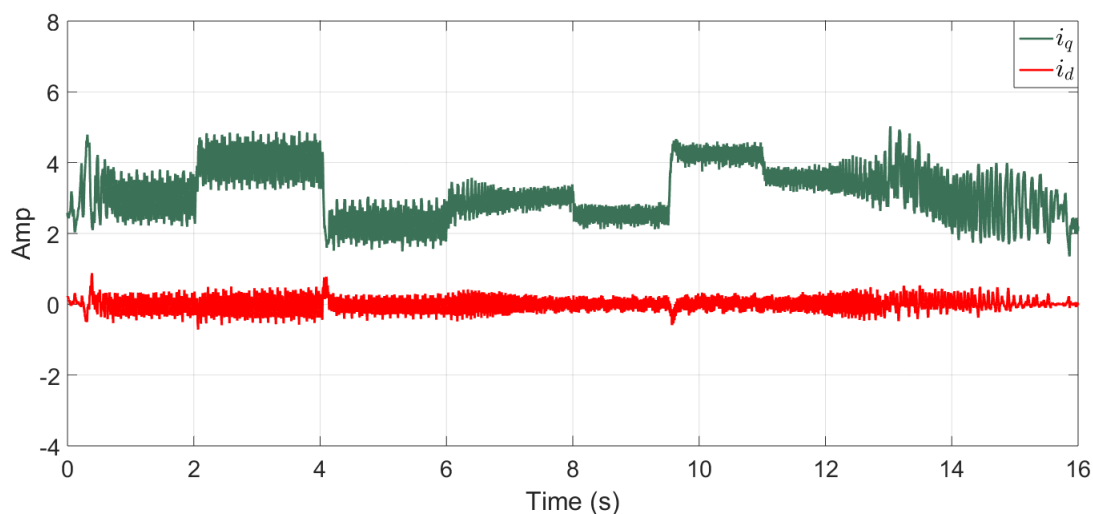


Figure 4.27: Experimental test: Speed tracking and tracking error

Figure 4.28: Experimental test: Behaviour of the currents— i_{dq}

experimental test, these errors are more important compared to those obtained in the simulation. It is well-known that in the experiments the effect caused by external disturbances (e.g. inverter) and the noise appears in the measured signals. However, the proposed strategy works well and attenuate the effects of chattering, uncertain parameters and unmodeled dynamics.

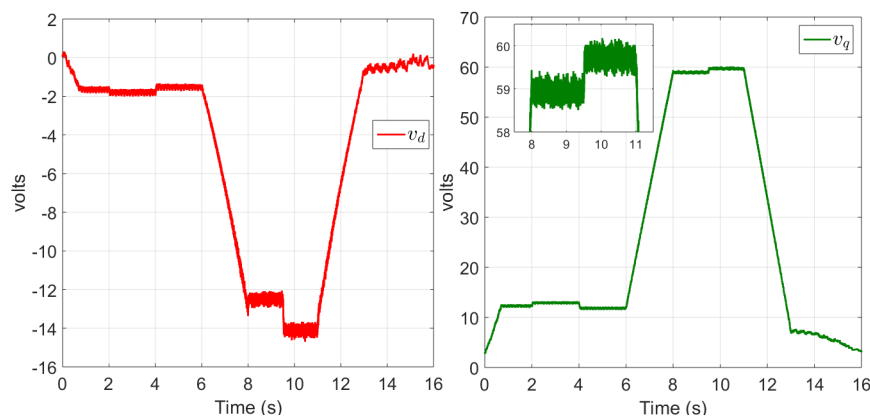


Figure 4.29: Experimental test: Profiles of the voltages $-v_{dq}$ with adaptive laws.

4.5 Conclusion

In this chapter, experimental and simulation tests were introduced to show the performance of the proposed sensorless control. The experimental tests have been carried out in Laboratoire des Sciences du Numérique de Nantes (LS2N) of the Ecole Centrale De Nantes, France. The extraction of the angular position estimation error has been successfully achieved from the measurable currents $i_{\alpha\beta}$ and the observers have been implemented obtaining good results. Then, angular position, speed and acceleration have been estimated. These estimates have been interconnected with the controller in closed-loop to control the electrical machine. In this way, the sensorless control applied in the experimental setup has shown a good performance under a wide speed range, even very close to zero.

An stability analysis under the action of the observer estimates has been introduced. This analysis is simpler due to that the separation principle holds.

Conclusion

In this work a new alternative for sensorless control of the IPMSM was proposed. The main contributions of this work have been the following:

- A strategy to extract the angular error e_{θ_e} was proposed, and based on a virtual system without parameters of the IPMSM, two Adaptive High-Order Sliding Mode Observers (AHOSMOs) were designed to estimate angular position, speed and acceleration over a wide speed range, and overcome the issues caused by parametric uncertainties. The angular position estimation error is independent of all machine parameters and high-frequency signal injection characteristics. Therefore, this can improve the feasibility of the design and reduces the cost of the implementation.
- Two Adaptive Super-Twisting Controllers (ASTWCs) were designed to track the desired speed reference and a desired d-axis current reference. These controllers were interconnected with the AHOSMOs achieving a sensorless control strategy.
- The gains for both, the control and observer, were reparameterized in terms of a single parameter to reduce the tuning time. The main advantage of this strategy is that adaptive laws were easy to implement, which has avoided overestimation of gains that increases chattering, reduced time to adjust gains, and reduced damage to the system.
- The closed-loop stability analysis under the action of the observer has been improved because the separation principle holds.

This work has been presented as follows:

In the first place, a state of the art of electrical machines and their main characteristics, as well as their applications were presented. After this, the two main classifications of sensorless control methods were presented, as well as their advantages and disadvantages. The problem statement, objectives and the contributions were included in this section. Then, the organization of the thesis was addressed. In addition, a list of publications in indexed journals and conferences has been presented.

In chapter one, a summary of the different types of PMSM was presented, as well as a brief introduction to the IPMSM. Considering that the dynamic model of the IPMSM is necessary for the design of control strategies, the modeling of the IPMSM was carried out. In addition, the parameter-free virtual system was presented in this section in order to design the observers without machine parameters. On the other hand, in order to test the performance of the different proposals of this thesis, the benchmark used in simulation and experimental tests was provided, as well as the description of the hardware of the experimental setup.

In chapter two, a new method to extract the angular position estimation error e_{θ_e} was introduced. The information of e_{θ_e} was extracted by considering the currents $i_{\alpha\beta}$ without machine model information. The extraction of e_{θ_e} has been used to design observers based on a virtual system without parameters of the IPMSM in order to overcome the issues caused by parametric uncertainties. Then, two adaptive observers have been designed. Both adaptive observers have been proposed with reparameterized gains, *i.e.*, the gains depend on a single parameter. Based on this reparametrization, an adaptive law was designed for each observer. The designed observers have been applied considering the extraction of the angular error to estimate the angular position, speed and acceleration. Simulation results and a comparative study were introduced.

In chapter three, two adaptive controllers based on super twisting were proposed. Both adaptive controllers have the reparameterized gains in terms of a single parameter such as the proposed adaptive observers in chapter two. This has allowed designing an adaptive law for each control in order to improve its performance, avoiding large gains and saving tuning time. Simulation results were presented to show the performance of this strategies. Moreover,

considering some results of the literature, a comparative study was introduced.

In chapter four, two schemes of sensorless control were introduced. The interconnection among the proposed observers and controllers was carried out to show the performance of the system under the action of observer estimates. Then, two sensorless controllers were applied to the IPMSM. Simulation and experimental results have been illustrated showing a good performance and effectiveness for a wide speed range, showing that the extraction of e_{θ_e} has been made successfully. Therefore, thanks to the virtual system without parameters of the IPMSM, greater precision has been achieved in the estimates. It is worth mentioning that thanks to the robustness of the sliding modes, good results have been obtained in the tracking of references despite uncertainties and disturbance.

In this work, a new alternative to sensorless control has been introduced. Therefore, based on the presented alternative, it is possible to show that to extract the angular error of the electrical motor, it is not always necessary to use dynamic equations of the motor, allowing to design observers without the use of a dynamic model of the machine.

Some perspectives are given below:

For the design of observers in the sensorless control of an electrical motor, it is necessary to know the initial condition of the motor rotor, which is an open problem that requires further study to improve the performance of the proposed schemes. In addition, when the electrical machine is stopped and it is desired to know the angular position for the control application, it is necessary to inject high-frequency signals to excite the system, which generates noise in the signals and the need to use filters. For this reason, it is necessary to investigate more about the elimination of filters and high-frequency injection to avoid phase shifts in the obtained signal as well as acoustic noise, so that the speed control at zero speed can be less complex.

Bibliography

- [1] M. J. Melfi, S. Evon, and R. McElveen, "Induction versus permanent magnet motors," *IEEE Industry Applications Magazine*, vol. 15, no. 6, pp. 28–35, 2009.
- [2] R. Menon, A. H. Kadam, N. A. Azeez, and S. S. Williamson, "A comprehensive survey on permanent magnet synchronous motor drive systems for electric transportation applications," in *IECON 2016-42nd Annual Conference of the IEEE Industrial Electronics Society*, pp. 6627–6632, IEEE, 2016.
- [3] P. Kakosimos, E. Tsampouris, A. Kladas, and C. Gerada, "Aerospace actuator design: A comparative analysis of permanent magnet and induction motor configurations," in *2012 XXth International Conference on Electrical Machines*, pp. 2538–2544, IEEE, 2012.
- [4] J. Puranen *et al.*, "Induction motor versus permanent magnet synchronous motor in motion control applications: a comparative study," 2006.
- [5] T. Noguchi, "Trends of permanent-magnet synchronous machine drives," *IEEJ Transactions on Electrical and Electronic Engineering*, vol. 2, no. 2, pp. 125–142, 2007.
- [6] T. Kabashima, Y. Arinaga, K. Uemura, I. Murokita, and M. Ohto, "A novel magnetic rotary encoder for servo motors," *IEEJ Transactions on Industry Applications*, vol. 126, no. 9, pp. 1202–1207, 2006.
- [7] M. M. I. Chy and M. N. Uddin, "Development and implementation of a new adaptive intelligent speed controller for ipmsm drive," *IEEE Transactions on Industry Applications*, vol. 45, no. 3, pp. 1106–1115, 2009.

- [8] M. N. Uddin and M. A. Rahman, "High-speed control of ipmsm drives using improved fuzzy logic algorithms," *IEEE transactions on industrial electronics*, vol. 54, no. 1, pp. 190–199, 2007.
- [9] L. Sheng, G. Xiaojie, and Z. Lanyong, "Robust adaptive backstepping sliding mode control for six-phase permanent magnet synchronous motor using recurrent wavelet fuzzy neural network," *IEEE Access*, vol. 5, pp. 14502–14515, 2017.
- [10] A. Ghafarri-Kashani, M. Yazdanpanah, and J. Faiz, "Robust speed control of pmsm using mixed nonlinear $h\infty$ /smc techniques," *IFAC Proceedings Volumes*, vol. 41, no. 2, pp. 8413–8418, 2008.
- [11] G. Wang, M. Valla, and J. Solsona, "Position sensorless permanent magnet synchronous machine drives—a review," *IEEE Transactions on Industrial Electronics*, vol. 67, no. 7, pp. 5830–5842, 2019.
- [12] S.-K. Sul and S. Kim, "Sensorless control of ipmsm: Past, present, and future," *IEEE Journal of Industry Applications*, vol. 1, no. 1, pp. 15–23, 2012.
- [13] S.-K. Sul, Y.-C. Kwon, and Y. Lee, "Sensorless control of ipmsm for last 10 years and next 5 years," *CES Transactions on Electrical Machines and Systems*, vol. 1, no. 2, pp. 91–99, 2017.
- [14] D. Liang, J. Li, and R. Qu, "Sensorless control of permanent magnet synchronous machine based on second-order sliding-mode observer with online resistance estimation," *IEEE Transactions on Industry Applications*, vol. 53, no. 4, pp. 3672–3682, 2017.
- [15] K.-W. Lee and J.-I. Ha, "Evaluation of back-emf estimators for sensorless control of permanent magnet synchronous motors," *Journal of Power Electronics*, vol. 12, no. 4, pp. 604–614, 2012.
- [16] F. Genduso, R. Miceli, C. Rando, and G. R. Galluzzo, "Back emf sensorless-control algorithm for high-dynamic performance pmsm," *IEEE Transactions on Industrial Electronics*, vol. 57, no. 6, pp. 2092–2100, 2009.

-
- [17] J. Liu and Z. Zhu, "Improved sensorless control of permanent-magnet synchronous machine based on third-harmonic back emf," *IEEE Transactions on Industry Applications*, vol. 50, no. 3, pp. 1861–1870, 2013.
- [18] M. Naidu and B. K. Bose, "Rotor position estimation scheme of a permanent magnet synchronous machine for high performance variable speed drive," in *Conference Record of the 1992 IEEE Industry Applications Society Annual Meeting*, pp. 48–53, IEEE, 1992.
- [19] C. Lascu and G.-D. Andreescu, "Pll position and speed observer with integrated current observer for sensorless pmsm drives," *IEEE Transactions on Industrial Electronics*, vol. 67, no. 7, pp. 5990–5999, 2020.
- [20] P. Bernard and L. Praly, "Estimation of position and resistance of a sensorless pmsm: a nonlinear luenberger approach for a nonobservable system," *IEEE Transactions on Automatic Control*, vol. 66, no. 2, pp. 481–496, 2020.
- [21] P. Niedermayr, L. Alberti, S. Bolognani, and R. Abl, "Implementation and experimental validation of ultra-high speed pmsm sensor-less control by means of extended kalman filter," *IEEE Journal of Emerging and Selected Topics in Power Electronics*, 2020.
- [22] H. Al-Ghossini, F. Locment, M. Sechilariu, L. Gagneur, and C. Forgez, "Adaptive-tuning of extended kalman filter used for small scale wind generator control," *Renewable Energy*, vol. 85, pp. 1237–1245, 2016.
- [23] A. Bist and S. V. Jadhav, "Sensorless control based on sliding mode observer for pmsm drive," in *2020 IEEE International Conference on Power Electronics, Drives and Energy Systems (PEDES)*, pp. 1–6, IEEE, 2020.
- [24] K. V. Tejan, R. M. Pindoriya, and B. S. Rajpurohit, "Rotor position sensorless technique using high-speed sliding mode observer for pmsm drive," in *2021 IEEE Industry Applications Society Annual Meeting (IAS)*, pp. 1–8, IEEE, 2021.

- [25] F. Sellschopp and M. Arjona, "Dc decay test for estimating d-axis synchronous machine parameters: a two-transfer-function approach," *IEE Proceedings-Electric Power Applications*, vol. 153, no. 1, pp. 123–128, 2006.
- [26] P. Turner, A. Reece, and D. Macdonald, "The dc decay test for determining synchronous machine parameters: measurement and simulation," *IEEE Transactions on Energy Conversion*, vol. 4, no. 4, pp. 616–623, 1989.
- [27] Y. Gao, R. Qu, and Y. Liu, "An improved ac standstill method for inductance measurement of interior permanent magnet synchronous motors," in *2013 International Conference on Electrical Machines and Systems (ICEMS)*, pp. 927–931, IEEE, 2013.
- [28] T. Sun, S.-O. Kwon, J.-J. Lee, and J.-P. Hong, "An improved ac standstill method for testing inductances of interior pm synchronous motor considering cross-magnetizing effect," in *2009 IEEE Energy Conversion Congress and Exposition*, pp. 2415–2422, IEEE, 2009.
- [29] S. J. Underwood and I. Husain, "Online parameter estimation and adaptive control of permanent-magnet synchronous machines," *IEEE Transactions on Industrial Electronics*, vol. 57, no. 7, pp. 2435–2443, 2009.
- [30] Y. Shi, K. Sun, L. Huang, and Y. Li, "Online identification of permanent magnet flux based on extended kalman filter for ipmsm drive with position sensorless control," *IEEE Transactions on Industrial Electronics*, vol. 59, no. 11, pp. 4169–4178, 2011.
- [31] M. A. Hamida, J. De Leon, A. Glumineau, and R. Boisliveau, "An adaptive interconnected observer for sensorless control of pm synchronous motors with online parameter identification," *IEEE Transactions on Industrial Electronics*, vol. 60, no. 2, pp. 739–748, 2012.
- [32] C. Wu, Y. Zhao, and M. Sun, "Enhancing low-speed sensorless control of pmsm using phase voltage measurements and online multiple parameter identification," *IEEE Transactions on Power Electronics*, vol. 35, no. 10, pp. 10700–10710, 2020.

- [33] M. S. Rifaq, F. Mwasilu, J. Kim, H. H. Choi, and J.-W. Jung, "Online parameter identification for model-based sensorless control of interior permanent magnet synchronous machine," *IEEE Transactions on Power Electronics*, vol. 32, no. 6, pp. 4631–4643, 2016.
- [34] V. Utkin, "Variable structure systems with sliding modes," *IEEE Transactions on Automatic control*, vol. 22, no. 2, pp. 212–222, 1977.
- [35] S. K. Spurgeon, "Sliding mode observers: a survey," *International Journal of Systems Science*, vol. 39, no. 8, pp. 751–764, 2008.
- [36] Y.-S. Jung and M.-G. Kim, "Sliding mode observer for sensorless control of ipmsm drives," *Journal of Power Electronics*, vol. 9, no. 1, pp. 117–123, 2009.
- [37] O. Saadaoui, A. Khlaief, M. Abassi, A. Chaari, and M. Boussak, "A sliding-mode observer for high-performance sensorless control of pmsm with initial rotor position detection," *International Journal of Control*, vol. 90, no. 2, pp. 377–392, 2017.
- [38] N. Ren, L. Fan, and Z. Zhang, "Sensorless pmsm control with sliding mode observer based on sigmoid function," *Journal of Electrical Engineering & Technology*, vol. 16, no. 2, pp. 933–939, 2021.
- [39] A. Levant, "Sliding order and sliding accuracy in sliding mode control," *International journal of control*, vol. 58, no. 6, pp. 1247–1263, 1993.
- [40] A. Ferreira de Loza, L. Fridman, L. Aguilar, and R. Iriarte, "High-order sliding-mode observer-based input-output linearization," *International Journal of Robust and Nonlinear Control*, vol. 29, no. 10, pp. 3183–3199, 2019.
- [41] B. Wang, Y. Shao, Y. Yu, Q. Dong, Z. Yun, and D. Xu, "High-order terminal sliding-mode observer for chattering suppression and finite-time convergence in sensorless spmsm drives," *IEEE Transactions on Power Electronics*, vol. 36, no. 10, pp. 11910–11920, 2021.

- [42] T. Zhang, Z. Xu, J. Li, H. Zhang, and C. Gerada, "A third-order super-twisting extended state observer for dynamic performance enhancement of sensorless ipmsm drives," *IEEE Transactions on Industrial Electronics*, vol. 67, no. 7, pp. 5948–5958, 2019.
- [43] D. Liang, J. Li, R. Qu, and W. Kong, "Adaptive second-order sliding-mode observer for pmsm sensorless control considering vsi nonlinearity," *IEEE Transactions on Power Electronics*, vol. 33, no. 10, pp. 8994–9004, 2017.
- [44] C. L. Baratieri and H. Pinheiro, "New variable gain super-twisting sliding mode observer for sensorless vector control of nonsinusoidal back-emf pmsm," *Control Engineering Practice*, vol. 52, pp. 59–69, 2016.
- [45] S. Wu, J. Zhang, and B. Chai, "Adaptive super-twisting sliding mode observer based robust backstepping sensorless speed control for ipmsm," *ISA transactions*, vol. 92, pp. 155–165, 2019.
- [46] Y. Zhan, J. Guan, and Y. Zhao, "An adaptive second-order sliding-mode observer for permanent magnet synchronous motor with an improved phase-locked loop structure considering speed reverse," *Transactions of the Institute of Measurement and Control*, vol. 42, no. 5, pp. 1008–1021, 2020.
- [47] P. L. Jansen and R. D. Lorenz, "Transducerless position and velocity estimation in induction and salient ac machines," *IEEE transactions on industry applications*, vol. 31, no. 2, pp. 240–247, 1995.
- [48] X. Zhao, C. Wang, W. Duan, and J. Jiang, "Research on sensorless control system of low speed and high power pmsm based on improved high frequency signal injection," *Energy Reports*, vol. 7, pp. 499–504, 2021.
- [49] S. Wang, K. Yang, and K. Chen, "An improved position-sensorless control method at low speed for pmsm based on high-frequency signal injection into a rotating reference frame," *IEEE Access*, vol. 7, pp. 86510–86521, 2019.

- [50] A. Messali, M. Ghanes, M. A. Hamida, and M. Koteich, "A resilient adaptive sliding mode observer for sensorless ac salient pole machine drives based on an improved hf injection method," *Control Engineering Practice*, vol. 93, p. 104163, 2019.
- [51] Y. Zhang, Z. Yin, J. Liu, R. Zhang, and X. Sun, "Ipmsm sensorless control using high-frequency voltage injection method with random switching frequency for audible noise improvement," *IEEE Transactions on Industrial Electronics*, vol. 67, no. 7, pp. 6019–6030, 2019.
- [52] S.-I. Kim, J.-H. Im, E.-Y. Song, and R.-Y. Kim, "A new rotor position estimation method of ipmsm using all-pass filter on high-frequency rotating voltage signal injection," *IEEE Transactions on Industrial Electronics*, vol. 63, no. 10, pp. 6499–6509, 2016.
- [53] B. Shuang, Z. Zhu, and X. Wu, "Improved cross-coupling effect compensation method for sensorless control of ipmsm with high frequency voltage injection," *IEEE Transactions on Energy Conversion*, vol. 37, no. 1, pp. 347–358, 2021.
- [54] Y. Tauchi and H. Kubota, "Audible noise reduction method in ipmsm position sensorless control based on high-frequency current injection," *IEEJ Journal of Industry Applications*, vol. 4, no. 3, pp. 180–186, 2015.
- [55] G. Wang, D. Xiao, N. Zhao, X. Zhang, W. Wang, and D. Xu, "Low-frequency pulse voltage injection scheme-based sensorless control of ipmsm drives for audible noise reduction," *IEEE Transactions on Industrial Electronics*, vol. 64, no. 11, pp. 8415–8426, 2017.
- [56] Z. Yang, K. Wang, and X. Sun, "Novel random square-wave voltage injection method based on markov chain for ipmsm sensorless control," *IEEE Transactions on Power Electronics*, 2022.
- [57] G. Wang, L. Yang, B. Yuan, B. Wang, G. Zhang, and D. Xu, "Pseudo-random high-frequency square-wave voltage injection based sensorless control of ipmsm drives for audible noise reduction," *IEEE Transactions on Industrial Electronics*, vol. 63, no. 12, pp. 7423–7433, 2016.

- [58] Z. Lin, X. Li, Z. Wang, T. Shi, and C. Xia, "Minimization of additional high-frequency torque ripple for square-wave voltage injection ipmsm sensorless drives," *IEEE Transactions on Power Electronics*, vol. 35, no. 12, pp. 13345–13355, 2020.
- [59] X. Wu, Y. Feng, X. Liu, S. Huang, X. Yuan, J. Gao, and J. Zheng, "Initial rotor position detection for sensorless interior pmsm with square-wave voltage injection," *IEEE Transactions on Magnetics*, vol. 53, no. 11, pp. 1–4, 2017.
- [60] C.-E. Hwang, Y. Lee, and S.-K. Sul, "Analysis on position estimation error in position-sensorless operation of ipmsm using pulsating square wave signal injection," *IEEE Transactions on Industry Applications*, vol. 55, no. 1, pp. 458–470, 2018.
- [61] R. Ni, D. Xu, F. Blaabjerg, K. Lu, G. Wang, and G. Zhang, "Square-wave voltage injection algorithm for pmsm position sensorless control with high robustness to voltage errors," *IEEE Transactions on Power Electronics*, vol. 32, no. 7, pp. 5425–5437, 2016.
- [62] S. Wu and J. Zhang, "A terminal sliding mode observer based robust backstepping sensorless speed control for interior permanent magnet synchronous motor," *International Journal of Control, Automation and Systems*, vol. 16, no. 6, pp. 2743–2753, 2018.
- [63] R. Cai, R. Zheng, M. Liu, and M. Li, "Robust control of pmsm using geometric model reduction and μ -synthesis," *IEEE Transactions on Industrial Electronics*, vol. 65, no. 1, pp. 498–509, 2017.
- [64] F. M. Zaihidee, S. Mekhilef, and M. Mubin, "Application of fractional order sliding mode control for speed control of permanent magnet synchronous motor," *IEEE Access*, vol. 7, no. 1, pp. 101765–101774, 2019.
- [65] X. Zhang, L. Sun, K. Zhao, and L. Sun, "Nonlinear speed control for pmsm system using sliding-mode control and disturbance compensation techniques," *IEEE transactions on power electronics*, vol. 28, no. 3, pp. 1358–1365, 2012.

- [66] C. Xia, X. Wang, S. Li, and X. Chen, “Improved integral sliding mode control methods for speed control of pmsm system,” *International Journal of Innovative Computing, Information and Control*, vol. 7, no. 4, pp. 1971–1982, 2011.
- [67] A. K. Junejo, W. Xu, C. Mu, M. M. Ismail, and Y. Liu, “Adaptive speed control of pmsm drive system based a new sliding-mode reaching law,” *IEEE Transactions on Power Electronics*, vol. 35, no. 11, pp. 12110–12121, 2020.
- [68] Z. Li, F. Wang, D. Ke, J. Li, and W. Zhang, “Robust continuous model predictive speed and current control for pmsm with adaptive integral sliding-mode approach,” *IEEE Transactions on Power Electronics*, vol. 36, no. 12, pp. 14398–14408, 2021.
- [69] X. Liu and H. Yu, “Continuous adaptive integral-type sliding mode control based on disturbance observer for pmsm drives,” *Nonlinear dynamics*, vol. 104, no. 2, pp. 1429–1441, 2021.
- [70] D. A. Haghighi and S. Mobayen, “Design of an adaptive super-twisting decoupled terminal sliding mode control scheme for a class of fourth-order systems,” *ISA transactions*, vol. 75, pp. 216–225, 2018.
- [71] V. I. Utkin and A. S. Poznyak, “Adaptive sliding mode control with application to super-twist algorithm: Equivalent control method,” *Automatica*, vol. 49, no. 1, pp. 39–47, 2013.
- [72] Y. Shtessel, M. Taleb, and F. Plestan, “A novel adaptive-gain supertwisting sliding mode controller: Methodology and application,” *Automatica*, vol. 48, no. 5, pp. 759–769, 2012.
- [73] C. Edwards and Y. Shtessel, “Adaptive dual-layer super-twisting control and observation,” *International Journal of Control*, vol. 89, no. 9, pp. 1759–1766, 2016.
- [74] M. A. Hamida, J. De Leon, and A. Glumineau, “High-order sliding mode observers and integral backstepping sensorless control of ipms motor,” *International Journal of Control*, vol. 87, no. 10, pp. 2176–2193, 2014.

- [75] G. Wang, H. Zhan, G. Zhang, X. Gui, and D. Xu, "Adaptive compensation method of position estimation harmonic error for emf-based observer in sensorless ipmsm drives," *IEEE Transactions on Power Electronics*, vol. 29, no. 6, pp. 3055–3064, 2013.
- [76] S. Ichikawa, Z. Chen, M. Tomita, S. Doki, and S. Okuma, "Sensorless control of an interior permanent magnet synchronous motor on the rotating coordinate using an extended electromotive force," in *IECON'01. 27th Annual Conference of the IEEE Industrial Electronics Society (Cat. No. 37243)*, vol. 3, pp. 1667–1672, IEEE, 2001.
- [77] S. Singh and A. Tiwari, "Various techniques of sensorless speed control of pmsm: A review," in *2017 Second International Conference on Electrical, Computer and Communication Technologies (ICECCT)*, pp. 1–6, IEEE, 2017.
- [78] S. Zheng, X. Tang, B. Song, S. Lu, and B. Ye, "Stable adaptive pi control for permanent magnet synchronous motor drive based on improved jitl technique," *Isa Transactions*, vol. 52, no. 4, pp. 539–549, 2013.
- [79] M. C. Harke, D. Raca, and R. Lorenz, "Implementation issues for fast initial position and magnet polarity identification of pm synchronous machines with near zero saliency," in *2005 European Conference on Power Electronics and Applications*, pp. 10–pp, IEEE, 2005.
- [80] H. Kim, K.-K. Huh, R. D. Lorenz, and T. M. Jahns, "A novel method for initial rotor position estimation for ipm synchronous machine drives," *IEEE Transactions on Industry Applications*, vol. 40, no. 5, pp. 1369–1378, 2004.
- [81] M. C. Harke, D. Raca, and R. D. Lorenz, "Fast and smooth initial position and magnet polarity estimation of salient and near zero saliency pm synchronous machines," in *IEEE International Conference on Electric Machines and Drives, 2005.*, pp. 1037–1044, IEEE, 2005.

- [82] F. Deutsch, W. Li, and S.-H. Park, “Characterizations of continuous and lipschitz continuous metric selections in normed linear spaces,” *Journal of Approximation Theory*, vol. 58, no. 3, pp. 297–314, 1989.
- [83] J. L. W. V. Jensen, “Sur les fonctions convexes et les inégalités entre les valeurs moyennes,” *Acta mathematica*, vol. 30, no. 1, pp. 175–193, 1906.
- [84] J. A. Moreno and M. Osorio, “Strict Lyapunov functions for the super-twisting algorithm,” *IEEE transactions on automatic control*, vol. 57, no. 4, pp. 1035–1040, 2012.
- [85] H. Liu and H. K. Khalil, “Output feedback stabilization using super-twisting control and high-gain observer,” *International Journal of Robust and Nonlinear Control*, vol. 29, no. 3, pp. 601–617, 2019.
- [86] G. Bornard and H. Hammouri, “A high gain observer for a class of uniformly observable systems,” in *[1991] Proceedings of the 30th IEEE Conference on Decision and Control*, pp. 1494–1496, IEEE, 1991.
- [87] Y. B. Shtessel, J. A. Moreno, F. Plestan, L. M. Fridman, and A. S. Poznyak, “Super-twisting adaptive sliding mode control: A Lyapunov design,” in *49th IEEE conference on decision and control (CDC)*, pp. 5109–5113, IEEE, 2010.
- [88] S. V. Gutierrez, J. De León-Morales, F. Plestan, and O. Salas-Peña, “A simplified version of adaptive super-twisting control,” *International Journal of Robust and Nonlinear Control*, vol. 29, no. 16, pp. 5704–5719, 2019.
- [89] A. Levant, “Principles of 2-sliding mode design,” *automatica*, vol. 43, no. 4, pp. 576–586, 2007.
- [90] F. Plestan, Y. Shtessel, V. Bregeault, and A. Poznyak, “New methodologies for adaptive sliding mode control,” *International journal of control*, vol. 83, no. 9, pp. 1907–1919, 2010.

-
- [91] Y. Shtessel, F. Plestan, and M. Taleb, “Lyapunov design of adaptive super-twisting controller applied to a pneumatic actuator,” *IFAC Proceedings Volumes*, vol. 44, no. 1, pp. 3051–3056, 2011.

Appendix A

Reparameterized gains

A.1 Reparameterized gains for the proposed observers

Consider the following algebraic Lyapunov equation in order to compute the observer gains

$$P_o + A_o^T P_o + P_o A_o - C_o^T C_o = 0 \quad (\text{A.1.1})$$

where P_o is a symmetric positive-definite matrix,

$$A_o = \begin{bmatrix} 0 & 1 & 0 \\ 0 & 0 & 1 \\ 0 & 0 & 0 \end{bmatrix}, \quad C_o = \begin{bmatrix} 1 & 0 & 0 \end{bmatrix}, \quad (\text{A.1.2})$$

then the solution of P_o for (A.1.1) is given by

$$P_o = \begin{bmatrix} 1 & -1 & 1 \\ -1 & 2 & -3 \\ 1 & -3 & 6 \end{bmatrix} \quad (\text{A.1.3})$$

Now, consider the following LTI system

$$\begin{aligned}\dot{\mathbf{x}} &= A_o \mathbf{x} \\ \mathbf{y} &= C_o \mathbf{x}\end{aligned}\tag{A.1.4}$$

where $\mathbf{x} \in \mathfrak{R}^3$ is a state vector and $\mathbf{y} \in \mathfrak{R}$ the output. Then, an observer for the system (A.1.4) is given by

$$\begin{aligned}\dot{\hat{\mathbf{x}}} &= A_o \hat{\mathbf{x}} + K_o(\mathbf{y} - \hat{\mathbf{y}}) \\ \hat{\mathbf{y}} &= C_o \hat{\mathbf{x}}\end{aligned}\tag{A.1.5}$$

where K_o is the gain. Then, the estimation error is given by $e = \mathbf{x} - \hat{\mathbf{x}}$ and its dynamics can be expressed by

$$\dot{e} = (A_o - K_o C_o)e\tag{A.1.6}$$

Then, the gain K_o has the following values

$$K_o = \begin{bmatrix} K_{o1} \\ K_{o2} \\ K_{o3} \end{bmatrix} = P_o^{-1} C_o^T = \begin{bmatrix} 3 \\ 3 \\ 1 \end{bmatrix}\tag{A.1.7}$$

A.1.1 Adaptive observer: Proposal 1

In this section, the gains of the proposed observer will be determined and computed in terms of a single parameter.

Consider the following class of nonlinear system given by

$$\begin{aligned}\dot{x}_1 &= x_2 \\ \dot{x}_2 &= x_3 \\ \dot{x}_3 &= \rho(t) \\ y &= x_1\end{aligned}\tag{A.1.8}$$

where x_1 , x_2 and x_3 are the states, $\rho(t)$ is bounded function whose bound is unknown, and $y \in \mathfrak{R}$ the output of the system.

Now, a sliding mode observers for the system (A.1.8) is given by

$$\begin{aligned}
\dot{\hat{x}}_1 &= \hat{x}_2 + \tilde{K}_{1,1}|e_1|^{\frac{2}{3}}\text{sign}(e_1) \\
\dot{\hat{x}}_2 &= \hat{x}_3 + \tilde{K}_{2,1}|e_1|^{\frac{1}{3}}\text{sign}(e_1) \\
\dot{\hat{x}}_3 &= \tilde{K}_{3,1}\text{sign}(e_1) \\
\hat{y} &= \hat{x}_1
\end{aligned} \tag{A.1.9}$$

where \hat{x}_1 , \hat{x}_2 , and \hat{x}_3 are the estimated states, \hat{y} is the estimated output and $\tilde{K}_{1,1}$, $\tilde{K}_{2,1}$ and $\tilde{K}_{3,1}$ are the gains. Then, defining the following estimation errors $e_i = x_i - \hat{x}_i$, for $i = 1, 2, 3$; the dynamics are given by

$$\begin{aligned}
\dot{e}_1 &= e_2 - \tilde{K}_{1,1}|e_1|^{\frac{2}{3}}\text{sign}(e_1) \\
\dot{e}_2 &= e_3 - \tilde{K}_{2,1}|e_1|^{\frac{1}{3}}\text{sign}(e_1) \\
\dot{e}_3 &= \rho(t) - \tilde{K}_{3,1}\text{sign}(e_1)
\end{aligned} \tag{A.1.10}$$

and taking into account the dynamics of the estimation errors, the following change of variable is established as follows

$$\zeta_1 = \frac{e_1}{L_o^2(t)}, \quad \zeta_2 = \frac{e_2}{L_o^2(t)}, \quad \zeta_3 = \frac{e_3}{L_o^2(t)} \tag{A.1.11}$$

where $L_o(t) > 0$ is the single adaptive parameter. The dynamical system in terms of the new variables is given by

$$\begin{aligned}
\dot{\zeta}_1 &= -\frac{\tilde{K}_{1,1}}{L_o^{\frac{2}{3}}(t)}|\zeta_1|^{\frac{2}{3}}\text{sign}(\zeta_1) + \zeta_2 - 2\zeta_1\frac{\dot{L}_o(t)}{L_o(t)} \\
\dot{\zeta}_2 &= -\frac{\tilde{K}_{2,1}}{L_o^{\frac{4}{3}}(t)}|\zeta_1|^{\frac{1}{3}}\text{sign}(\zeta_1) + \zeta_3 - 2\zeta_2\frac{\dot{L}_o(t)}{L_o(t)} \\
\dot{\zeta}_3 &= -\frac{\tilde{K}_{3,1}}{L_o^2(t)}\text{sign}(\zeta_1) + \frac{\rho(t)}{L_o^2(t)} - 2\zeta_3\frac{\dot{L}_o(t)}{L_o(t)}
\end{aligned} \tag{A.1.12}$$

Moreover, in order to simplify the state space representation, the following new change of variable is introduced

$$\xi_1 = |\zeta_1|^{\frac{2}{3}}\text{sign}(\zeta_1), \quad \xi_2 = \frac{\zeta_2}{L_o(t)}, \quad \xi_3 = \frac{3\zeta_3|\zeta_1|^{\frac{1}{3}}}{2L_o^2(t)} \tag{A.1.13}$$

and the dynamical system can be expressed by using the new variables as follows

$$\begin{aligned}
\dot{\xi}_1 &= \frac{2L_o(t)}{3|\zeta_1|^{\frac{1}{3}}} \left[-\frac{\tilde{K}_{1,1}}{L_o^{\frac{5}{3}}(t)} \xi_1 + \xi_2 \right] - \frac{4\dot{L}_o(t)}{3L_o(t)} \xi_1 \\
\dot{\xi}_2 &= \frac{2L_o(t)}{3|\zeta_1|^{\frac{1}{3}}} \left[-\frac{3\tilde{K}_{2,1}}{2L_o^{\frac{10}{3}}(t)} \xi_1 + \xi_3 \right] - \frac{3\dot{L}_o(t)}{L_o(t)} \xi_2 \\
\dot{\xi}_3 &= \frac{2L_o(t)}{3|\zeta_1|^{\frac{1}{3}}} \left[-\left(\frac{3}{2}\right)^2 \frac{\tilde{K}_{3,1}}{L_o^5(t)} \xi_1 + \left(\frac{3}{2}\right)^2 \frac{|\zeta_1|^{\frac{2}{3}} \rho(t)}{L_o^5(t)} + \frac{\xi_3}{2|\zeta_1|^{\frac{2}{3}}} (-3\xi_1 + \xi_2) \right] - \frac{14\dot{L}_o(t)}{3L_o(t)} \xi_3
\end{aligned} \tag{A.1.14}$$

The resulting system (A.1.14) can be expressed in the following compact form

$$\dot{\xi} = \alpha_o \left[\left(A_o - \tilde{G}_o C_o \right) \xi + \Phi_o \right] - N_o \xi \frac{\dot{L}_o(t)}{L_o(t)} \tag{A.1.15}$$

where $\alpha_o = \frac{2L_o(t)}{3|\zeta_1|^{\frac{1}{3}}}$, $\xi = \begin{bmatrix} \xi_1 & \xi_2 & \xi_3 \end{bmatrix}^T$ and

$$\tilde{G}_o = \begin{bmatrix} \frac{\tilde{K}_{1,1}}{L_o^{\frac{5}{3}}(t)} \\ \frac{3\tilde{K}_{2,1}}{2L_o^{\frac{10}{3}}(t)} \\ \left(\frac{3}{2}\right)^2 \frac{\tilde{K}_{3,1}}{L_o^5(t)} \end{bmatrix}, N_o = \begin{bmatrix} \frac{4}{3} & 0 & 0 \\ 0 & 3 & 0 \\ 0 & 0 & \frac{14}{3} \end{bmatrix}, \Phi_o = \begin{bmatrix} 0 \\ 0 \\ \left(\frac{3}{2}\right)^2 \frac{|\zeta_1|^{\frac{2}{3}} \rho(t)}{L_o^5(t)} + \frac{\xi_3}{2|\zeta_1|^{\frac{2}{3}}} \left(-\frac{\tilde{K}_{1,1}}{L_o^{\frac{5}{3}}(t)} \xi_1 + \xi_2 \right) \end{bmatrix}. \tag{A.1.16}$$

Then, from (A.1.6), it is obtained that $\tilde{G}_o = P_o^{-1} C_o^T$. Then, setting \tilde{G}_o equal to (A.1.7), it follows that

$$\begin{bmatrix} \frac{\tilde{K}_{1,1}}{L_o^{\frac{5}{3}}(t)} \\ \frac{3\tilde{K}_{2,1}}{2L_o^{\frac{10}{3}}(t)} \\ \left(\frac{3}{2}\right)^2 \frac{\tilde{K}_{3,1}}{L_o^5(t)} \end{bmatrix} = \begin{bmatrix} 3 \\ 3 \\ 1 \end{bmatrix} \tag{A.1.17}$$

Therefore, the gains for the observer are computed and reparameterized in terms of $L_o(t)$

as follows

$$\tilde{K}_{1,1} = 3L_o^{\frac{5}{3}}(t) \quad \tilde{K}_{2,1} = 2L_o^{\frac{10}{3}}(t) \quad \tilde{K}_{3,1} = \left(\frac{4}{9}\right) L_o^5(t) \quad (\text{A.1.18})$$

such that, the compact system (A.1.15) can be rewritten as

$$\dot{\xi} = \alpha_o [(A_o - P_o^{-1}C_o^T C_o) \xi + \Phi_o] - N_o \xi \frac{\dot{L}_o(t)}{L_o(t)} \quad (\text{A.1.19})$$

A.1.2 Adaptive observer: Proposal 2

In this section, a second observer is designed for a class of nonlinear system given by (A.1.8). The gains of the proposed observer will be determined and computed in terms of a single parameter.

Consider the following sliding mode observer for the system (A.1.8),

$$\begin{aligned} \dot{\hat{x}}_{1_2} &= \hat{x}_2 + \tilde{K}_{1,2}|e_{1_2}|^{\frac{2}{3}} \text{sign}(e_{1_2}) \\ \dot{\hat{x}}_{2_2} &= \hat{x}_3 + \tilde{K}_{2,2}|e_{1_2}|^{\frac{1}{3}} \text{sign}(e_{1_2}) \\ \dot{\hat{x}}_{3_2} &= \tilde{K}_{3,2} \text{sign}(e_{1_2}) \\ \hat{y} &= \hat{x}_{1_2} \end{aligned} \quad (\text{A.1.20})$$

where \hat{x}_{1_2} , \hat{x}_{2_2} and \hat{x}_{3_2} are the estimated states, \hat{y} is the output of the system and $\tilde{K}_{1,2}$, $\tilde{K}_{2,2}$ and $\tilde{K}_{3,2}$ are the gains of the observer.

Consider the following estimation errors $e_{i_2} = x_i - \hat{x}_{i_2}$, for $i = 1, 2, 3$; and their dynamics as follows

$$\begin{aligned} \dot{e}_{1_2} &= e_{2_2} - \tilde{K}_{1,2}|e_{1_2}|^{\frac{2}{3}} \text{sign}(e_{1_2}) \\ \dot{e}_{2_2} &= e_{3_2} - \tilde{K}_{2,2}|e_{1_2}|^{\frac{1}{3}} \text{sign}(e_{1_2}) \\ \dot{e}_{3_2} &= \rho(t) - \tilde{K}_{3,2} \text{sign}(e_{1_2}) \end{aligned} \quad (\text{A.1.21})$$

Taking into account the dynamics of the estimation errors, the following change of variable is established as follows

$$\xi_{1_2} = \frac{|e_{1_2}|^{\frac{2}{3}} \text{sign}(e_{1_2})}{L_{o_2}(t)} \quad \xi_{2_2} = \frac{e_{2_2}}{L_{o_2}^2(t)} \quad \xi_{3_2} = \frac{3e_{3_2}|e_{1_2}|^{\frac{1}{3}}}{2L_{o_2}^3(t)} \quad (\text{A.1.22})$$

where $L_{o_2}(t)$ is the single adaptive parameter. The dynamical system in terms of the new variables is given by

$$\begin{aligned} \dot{\xi}_{1_2} &= \frac{2L_{o_2}(t)}{3|e_{1_2}|^{\frac{1}{3}}} \left[-\frac{\tilde{K}_{1,2}}{L_{o_2}(t)} \xi_{1_2} + \xi_{2_2} \right] - \frac{\dot{L}_{o_2}(t)}{L_{o_2}(t)} \xi_{1_2} \\ \dot{\xi}_{2_2} &= \frac{2L_{o_2}(t)}{3|e_{1_2}|^{\frac{1}{3}}} \left[-\frac{3\tilde{K}_{2,2}}{2L_{o_2}^2(t)} \xi_{1_2} + \xi_{3_2} \right] - \frac{2\dot{L}_{o_2}(t)}{L_{o_2}(t)} \xi_{2_2} \\ \dot{\xi}_{3_2} &= \frac{2L_{o_2}(t)}{3|e_{1_2}|^{\frac{1}{3}}} \left[-\left(\frac{3}{2}\right)^2 \frac{\tilde{K}_{3,2}}{L_{o_2}^3(t)} \xi_{1_2} + \left(\frac{3}{2}\right)^2 \frac{|e_{1_2}|^{\frac{2}{3}} \rho(t)}{L_{o_2}^4(t)} + \frac{\xi_{3_2}}{2|e_{1_2}|^{\frac{2}{3}}} \left[-\tilde{K}_{1,2} \xi_{1_2} + L_{o_2}(t) \xi_{2_2} \right] \right] \\ &\quad - \frac{3\dot{L}_{o_2}(t)}{L_{o_2}(t)} \xi_{3_2} \end{aligned} \quad (\text{A.1.23})$$

and can be written in a compact form as follows

$$\dot{\xi}_{o_2} = \alpha_{o_2} \left[\left(A_o - \tilde{G}_{o_2} C_o \right) \xi_{o_2} + \Phi_{o_2} \right] - D_{o_2} \xi_{o_2} \frac{\dot{L}_{o_2}(t)}{L_{o_2}(t)} \quad (\text{A.1.24})$$

where $\alpha_{o_2} = \frac{2L_{o_2}(t)}{3|e_{1_2}|^{\frac{1}{3}}}$, $\xi_{o_2} = \left[\xi_{1_2} \quad \xi_{2_2} \quad \xi_{3_2} \right]^T$ and

$$\tilde{G}_{o_2} = \begin{bmatrix} \frac{\tilde{K}_{1,2}}{L_{o_2}(t)} \\ \frac{3\tilde{K}_{2,2}}{2L_{o_2}^2(t)} \\ \left(\frac{3}{2}\right)^2 \frac{\tilde{K}_{3,2}}{L_{o_2}^3(t)} \end{bmatrix}, \quad D_{o_2} = \begin{bmatrix} 1 & 0 & 0 \\ 0 & 2 & 0 \\ 0 & 0 & 3 \end{bmatrix}, \quad (\text{A.1.25})$$

$$\Phi_{o_2} = \begin{bmatrix} 0 \\ 0 \\ \left(\frac{3}{2}\right)^2 \frac{|e_{1_2}|^{\frac{2}{3}} \rho(t)}{L_{o_2}^4(t)} + \frac{\xi_{3_2}}{2|e_{1_2}|^{\frac{2}{3}}} \left[-\tilde{K}_{1,2} \xi_{1_2} + L_{o_2}(t) \xi_{2_2} \right] \end{bmatrix}. \quad (\text{A.1.26})$$

Then, from (A.1.6), it is obtained that $\tilde{G}_{o_2} = P_o^{-1} C_o^T$. Then, setting \tilde{G}_{o_2} equal to (A.1.7), it

follows that

$$\begin{bmatrix} \frac{\tilde{K}_{1,2}}{L_{o_2}(t)} \\ \frac{3\tilde{K}_{2,2}}{2L_{o_2}^2(t)} \\ \left(\frac{3}{2}\right)^2 \frac{\tilde{K}_{3,2}}{L_{o_2}^3(t)} \end{bmatrix} = \begin{bmatrix} 3 \\ 3 \\ 1 \end{bmatrix} \quad (\text{A.1.27})$$

Therefore, the gains for the observer (A.1.20) are computed and reparameterized in terms of $L_{o_2}(t)$ as follows

$$\tilde{K}_{1,2} = 3L_{o_2}(t) \quad \tilde{K}_{2,2} = 2L_{o_2}^2(t) \quad \tilde{K}_{3,2} = \left(\frac{2}{3}\right)^2 L_{o_2}^3(t) \quad (\text{A.1.28})$$

such that, the compact system (A.1.24) can be rewritten as

$$\dot{\xi}_{o_2} = \alpha_{o_2} [(A_o - P_o^{-1}C_o^T C_o) \xi_{o_2} + \Phi_{o_2}] - D_{o_2} \xi_{o_2} \frac{\dot{L}_{o_2}(t)}{L_{o_2}(t)} \quad (\text{A.1.29})$$

A.2 Reparameterized gains for the proposed controllers

Consider the following algebraic Lyapunov equation in order to compute the control gains

$$P_c + A_c^T P_c + P_c A_c - C_c^T C_c = 0 \quad (\text{A.2.1})$$

where P_c is a symmetric positive-definite matrix,

$$A_c = \begin{bmatrix} 0 & 1 \\ 0 & 0 \end{bmatrix}, \quad C_c = \begin{bmatrix} 1 & 0 \end{bmatrix}. \quad (\text{A.2.2})$$

Then the solution of P_c for A.2.1 is given by

$$P_c = \begin{bmatrix} 1 & -1 \\ -1 & 2 \end{bmatrix}. \quad (\text{A.2.3})$$

Similarly, as the previous section A.1, consider the following LTI system

$$\begin{aligned}\dot{\mathbf{x}}_c &= A_c \mathbf{x}_c \\ \mathbf{y}_c &= C_c \mathbf{x}_c\end{aligned}\tag{A.2.4}$$

where $\mathbf{x}_c \in \mathfrak{R}^2$ is a state vector and $\mathbf{y}_c \in \mathfrak{R}$ the output. Then, an observer for the system (A.2.4) is given by

$$\begin{aligned}\dot{\hat{\mathbf{x}}}_c &= A_c \hat{\mathbf{x}}_c + K_c (\mathbf{y}_c - \hat{\mathbf{y}}_c) \\ \hat{\mathbf{y}}_c &= C_c \hat{\mathbf{x}}_c\end{aligned}\tag{A.2.5}$$

where K_c are the gains. Then, the estimation error is given by $e_c = \mathbf{x}_c - \hat{\mathbf{x}}_c$ and its dynamics can be expressed by

$$\dot{e}_c = (A_c - K_c C_c) e_c = (A_c - P_c^{-1} C_c^T C_c) e_c\tag{A.2.6}$$

Then, the gain K_c has the following values

$$K_c = \begin{bmatrix} K_{c1} \\ K_{c2} \end{bmatrix} = P_c^{-1} C_c^T = \begin{bmatrix} 2 \\ 1 \end{bmatrix}\tag{A.2.7}$$

A.2.1 Adaptive control: Proposal 1

In this section, the gains of the proposed controller (3.1.6) will be determined and computed in terms of a single parameter.

Consider the following system

$$\Sigma_{STW} : \begin{cases} \dot{\Upsilon}_1 = -\tilde{K}_{c1} |\Upsilon_1|^{1/2} \text{sign}(\Upsilon_1) + \Upsilon_2, \\ \dot{\Upsilon}_2 = -\tilde{K}_{c2} \text{sign}(\Upsilon_1) + d(t) \end{cases}\tag{A.2.8}$$

with $d(t) = \dot{\delta}(t)$. Now, consider the following change of coordinates

$$z_1 = \frac{\Upsilon_1}{L_c^2(t)} \quad z_2 = \frac{\Upsilon_2}{L_c^2(t)}\tag{A.2.9}$$

where $L_c(t)$ is the single adaptive parameter. The dynamical system in terms of the new

variables is given by

$$\begin{aligned} \dot{z}_1 &= -\frac{\tilde{K}_{c1}}{L_c(t)} |z_1|^{\frac{1}{2}} \text{sign}(z_1) + z_2 - \frac{2z_1 \dot{L}_c(t)}{L_c(t)} \\ \dot{z}_2 &= -\frac{\tilde{K}_{c2}}{L_c^2(t)} \text{sign}(z_1) + \frac{d(t)}{L_c^2(t)} - \frac{2z_2 \dot{L}_c(t)}{L_c(t)} \end{aligned} \quad (\text{A.2.10})$$

Moreover, in order to simplify the state space representation, the following new change of variable is introduced

$$\mathcal{L}_1 = |z_1|^{\frac{1}{2}} \text{sign}(z_1) \quad \mathcal{L}_2 = \frac{z_2}{L_c(t)} \quad (\text{A.2.11})$$

and the dynamical system can be expressed by using the new variables as follows

$$\begin{aligned} \dot{\mathcal{L}}_1 &= \frac{L_c(t)}{2|z_1|^{\frac{1}{2}}} \left[-\frac{\tilde{K}_{c1}}{L_c^2(t)} \mathcal{L}_1 + \mathcal{L}_2 \right] - \mathcal{L}_1 \frac{\dot{L}_c(t)}{L_c(t)} \\ \dot{\mathcal{L}}_2 &= \frac{L_c(t)}{2|z_1|^{\frac{1}{2}}} \left[-\frac{2\tilde{K}_{c2}}{L_c^4(t)} \mathcal{L}_1 + \frac{2|z_1|^{\frac{1}{2}} d(t)}{L_c^4(t)} \right] - 3\mathcal{L}_2 \frac{\dot{L}_c(t)}{L_c(t)} \end{aligned} \quad (\text{A.2.12})$$

System (A.2.12) can be expressed in compact form as follows

$$\dot{\mathcal{L}} = \alpha_c \left[\left(A_c - \tilde{G}_c C_c \right) \mathcal{L} + \Phi_c \right] - N_c \mathcal{L} \frac{\dot{L}_c(t)}{L_c(t)} \quad (\text{A.2.13})$$

with $\alpha_c = \frac{L_c(t)}{2|z_1|^{\frac{1}{2}}}$, $\mathcal{L} = \begin{bmatrix} \mathcal{L}_1 & \mathcal{L}_2 \end{bmatrix}^T$ and

$$\tilde{G}_c = \begin{bmatrix} \frac{\tilde{K}_{c1}}{L_c^2(t)} \\ \frac{2\tilde{K}_{c2}}{L_c^4(t)} \end{bmatrix}, \quad N_c = \begin{bmatrix} 1 & 0 \\ 0 & 3 \end{bmatrix}, \quad \Phi_c = \begin{bmatrix} 0 \\ \frac{2|z_1|^{\frac{1}{2}}}{L_c^4(t)} (d(t)) \end{bmatrix}. \quad (\text{A.2.14})$$

Then, from (A.2.6), it is obtained that $\tilde{G}_c = P_c^{-1} C_c^T$. Then, setting \tilde{G}_c equal to (A.2.7), it follows that

$$\begin{bmatrix} \frac{\tilde{K}_{c1}}{L_c^2(t)} \\ \frac{2\tilde{K}_{c2}}{L_c^4(t)} \end{bmatrix} = \begin{bmatrix} 2 \\ 1 \end{bmatrix} \quad (\text{A.2.15})$$

Therefore, the gains for the controller (3.1.6) are computed and reparameterized in terms of

$L_c(t)$ as follows

$$\tilde{K}_{c1} = 2L_c^2(t) \quad \tilde{K}_{c2} = \frac{L_c^4(t)}{2} \quad (\text{A.2.16})$$

Finally, the compact system (A.2.13) can be expressed as follows

$$\dot{\mathcal{L}} = \alpha_c [(A_c - P_c^{-1}C_c^T C_c) \mathcal{L} + \Phi_c] - N_c \mathcal{L} \frac{\dot{L}_c(t)}{L_c(t)} \quad (\text{A.2.17})$$

A.2.2 Adaptive control: Proposal 2

In this section, the gains of the proposed controller (3.2.5) will be determined and computed in terms of a single parameter.

Consider the following system as follows

$$\Sigma_{STW_2} : \begin{cases} \dot{z}_{1_2} = -\tilde{K}_{c3}|z_{1_2}|^{\frac{1}{2}} \text{sign}(z_{1_2}) + z_{2_2} \\ \dot{z}_{2_2} = -\tilde{K}_{c4} \text{sign}(z_{1_2}) + d(t) \end{cases} \quad (\text{A.2.18})$$

with $d(t) = \dot{\delta}(t)$. Now, introducing the following change of variable

$$\mathcal{L}_{1_2} = \frac{|z_{1_2}|^{\frac{1}{2}} \text{sign}(z_{1_2})}{L_{c2}(t)} \quad \mathcal{L}_{2_2} = \frac{z_{2_2}}{L_{c2}^2(t)} \quad (\text{A.2.19})$$

where $L_{c2}(t)$ is the single adaptive parameter. Then the dynamics of the system, in terms of these new variables, are given by

$$\begin{aligned} \dot{\mathcal{L}}_{1_2} &= \frac{L_{c2}(t)}{2|z_{1_2}|^{\frac{1}{2}}} \left[-\frac{\tilde{K}_{c3}}{L_{c2}(t)} \mathcal{L}_{1_2} + \mathcal{L}_{2_2} \right] - \mathcal{L}_{1_2} \frac{\dot{L}_{c2}(t)}{L_{c2}(t)} \\ \dot{\mathcal{L}}_{2_2} &= \frac{L_{c2}(t)}{2|z_{1_2}|^{\frac{1}{2}}} \left[-\frac{2\tilde{K}_{c4}}{L_{c2}^2(t)} \mathcal{L}_{1_2} + \frac{2|z_{1_2}|^{\frac{1}{2}} d(t)}{L_{c2}^3(t)} \right] - 2\mathcal{L}_{2_2} \frac{\dot{L}_{c2}(t)}{L_{c2}(t)} \end{aligned} \quad (\text{A.2.20})$$

System (A.2.20) can be expressed in compact form as follows

$$\dot{\mathcal{L}}_{c2} = \alpha_{c2} \left[(A_c - \tilde{G}_{c2} C_c) \mathcal{L}_{c2} + \Phi_{c2} \right] - D_{c2} \mathcal{L}_{c2} \frac{\dot{L}_{c2}(t)}{L_{c2}(t)} \quad (\text{A.2.21})$$

with $\alpha_{c_2} = \frac{L_{c_2}(t)}{2|z_{1_2}|^{\frac{1}{2}}}$, $\mathcal{L}_{c_2} = [\mathcal{L}_{1_2} \quad \mathcal{L}_{2_2}]^T$

$$\tilde{G}_{c_2} = \begin{bmatrix} \frac{\tilde{K}_{c_3}}{L_{c_2}(t)} \\ \frac{2\tilde{K}_{c_4}}{L_{c_2}^2(t)} \end{bmatrix} \quad D_{c_2} = \begin{bmatrix} 1 & 0 \\ 0 & 2 \end{bmatrix} \quad \Phi_{c_2} = \begin{bmatrix} 0 \\ \frac{2|z_{1_2}|^{\frac{1}{2}}}{L_{c_2}^3(t)} [d(t)] \end{bmatrix} \quad (\text{A.2.22})$$

Then, from (A.2.6), it is obtained that $\tilde{G}_{c_2} = P_c^{-1}C_c^T$. Then, setting \tilde{G}_{c_2} equal to (A.2.7), it follows that

$$\begin{bmatrix} \frac{\tilde{K}_{c_3}}{L_{c_2}(t)} \\ \frac{2\tilde{K}_{c_4}}{L_{c_2}^2(t)} \end{bmatrix} = \begin{bmatrix} 2 \\ 1 \end{bmatrix} \quad (\text{A.2.23})$$

Therefore, the gains for the controller (3.2.5) are computed and reparameterized in terms of $L_{c_2}(t)$ as follows

$$\tilde{K}_{c_3} = 2L_{c_2}(t) \quad \tilde{K}_{c_4} = \frac{L_{c_2}^2(t)}{2} \quad (\text{A.2.24})$$

Finally, the system (A.2.21) can be expressed as follows

$$\dot{\mathcal{L}}_{c_2} = \alpha_{c_2} [(A_c - P_c^{-1}C_c^T C_c) \mathcal{L}_{c_2} + \Phi_{c_2}] - D_{c_2} \mathcal{L}_{c_2} \frac{\dot{L}_{c_2}(t)}{L_{c_2}(t)} \quad (\text{A.2.25})$$